

# ULRR

## The influence of solvent on the nucleation of medium-sized flexible organic molecules from solution

Item Type	Thesis
Authors	Kuhs, Manuel
Download date	2026-05-20 13:27:08
Item License	<a href="https://creativecommons.org/licenses/by-nc-sa/1.0/">https://creativecommons.org/licenses/by-nc-sa/1.0/</a>
Link to Item	<a href="https://hdl.handle.net/10344/4800">https://hdl.handle.net/10344/4800</a>



UNIVERSITY of LIMERICK

OLLSCOIL LUIMNIGH

The Influence of Solvent on the Nucleation of  
Medium-Sized Flexible Organic Molecules from  
Solution

*Ph.D. Thesis*

Manuel Kuhs B.Sc.

Supervisor: Prof. Å. C. Rasmuson

Submitted to the Faculty of Science and Engineering, University of  
Limerick, Ireland, May 2015.

This page is intentionally left blank.

# DECLARATION

I declare that this thesis is entirely my own work and has not been previously submitted to this or any other university. Where the work of others is utilised, this is acknowledged and cited in the proper manner.

---

Manuel Kuhs

# Abstract

In this thesis the influence of solvents on crystal nucleation is probed to progress understanding of crystal nucleation from solution.

Induction times of two solutes in different solvents and at different thermodynamic driving forces were measured using a custom 20 mL multireactor system. To account for the wide distribution of induction times under identical conditions, around 2,000 induction times were collected, covering 25 combinations of solute, solvent and thermodynamic driving force. Both the thermodynamic driving force required to achieve median induction times of 2 hours, and the interfacial energies calculated using the Classical Nucleation Theory, were found to decrease in the order ethanol > isopropanol > toluene > ethyl acetate for fenoxycarb, and [n-propanol & toluene] > ethyl acetate > acetonitrile for tolbutamide. Thus both solutes nucleate more easily in ethyl acetate than in either toluene or the alcohols. Absolute values of interfacial energies ranged from 0.5 to 5 mJ/m<sup>2</sup> in line with results of similar experiments in the literature. For fenoxycarb these correlated quite well with solvent-solute interaction enthalpies (with the exception of toluene) such that stronger binding of the solute by the solvent corresponded to more difficult nucleation. This trend has recently also been reported for salicylic acid and risperidone. In the case of tolbutamide the same relationship appeared to be complicated by a second mechanism, whereby tolbutamide assumes different solvent-dependent conformers in solution that hinder nucleation relative to the energy barrier of rotating to the conformer found in the crystal.

While collecting induction times for fenoxycarb in isopropanol, a history of solution effect on the nucleation rate was discovered whereby nucleation becomes more difficult with increasing pretreatment temperature and time. Such an effect has been sporadically reported for the past 100 years, but its cause remains unsolved. In order to quantify this effect, the influence of solution pretreatment on the nucleation was measured by collecting 1,800 induction times spanning 17 combinations of pretreatment time and temperature. The influence of pretreatment time and temperature on the induction time was found to follow a first order rate reaction with an activation energy of over 260 kJ mol<sup>-1</sup>. On the basis of modelling it has previously been suggested for this system that the molecular packing in the crystal lattice is not the thermodynamically stable configuration at the level of simple dimers in solution, and that solute aggregation must exist in solution due to the low solvent-to-solute molecular ratio. It is thus hypothesized that the dissolution of crystalline material at first leaves molecular assemblies in solution that retain features of the crystalline structure, which facilitates subsequent nucleation. However, the longer the solution is kept at a temperature above the saturation temperature and the higher the temperature, the more these assemblies disintegrate and transform into molecular structures less suited to form critical nuclei. Thus a third mechanism affecting nucleation from solution may exist, involving the structure of solute clusters.

Solubilities, required to estimate thermodynamic driving forces and interfacial energies, were experimentally determined in several organic solvents using a gravimetric method. Temperature ranges of 2-8 °C for tolbutamide and 5-45 °C for fenoxycarb were investigated, with resulting solubilities ranging from 0.002 to 0.05 g tolbutamide / g solvent, and from 0.06 to 29 g fenoxycarb / g solvent. As solubility is a function of the solid-state structure, the latter was carefully identified using powder XRD, SEM, NMR and DSC. Deviations from linearity in a solubility van't Hoff plot were observed for fenoxycarb, and demonstrated to arise from the van't Hoff enthalpy of solution containing temperature-dependent heat capacity and activity coefficient terms.

## Publications

The following peer-reviewed journal publications have resulted from this thesis, or are in preparation. As the work of co-authors in papers I and II is referenced in this thesis even though both manuscripts are still in preparation, the current drafts are attached as Appendices (A and B, respectively).

- I. Kuhs, M.; Kumar, K.; Zeglinski, J.; Rasmuson, Å. C., Solvent Effects on Nucleation Kinetics and Thermodynamics of Fenoxycarb, **in preparation**. [Draft in Appendix A]
- II. Kuhs, M.; Zeglinski, J.; Kumar, K.; Rasmuson, Å. C., Tolbutamide nucleation dependence on solvent, **in preparation**. [Draft in Appendix B]
- III. Kuhs, M.; Rasmuson, Å. C., Measuring Nucleation Kinetics in Microfluidic Droplets: Complications and Limitations, **in preparation**.
- IV. Valavi, M.; Svärd, M.; Kuhs, M.; Rasmuson, Å. C., Thermodynamics of Tolbutamide in Solution, **in preparation**.
- V. Kuhs, M.; Zeglinski, J.; Rasmuson, Å. C., Influence of History of Solution in Crystal Nucleation of Fenoxycarb: Kinetics and Mechanisms. *Crystal Growth & Design* **2014**.
- VI. Zeglinski, J.; Svärd, M.; Karpinska, J.; Kuhs, M.; Rasmuson, Å. C., Analysis of the structure and morphology of Fenoxycarb crystals, *J Molecular Graphics and Modelling* **2014**, 53, 92-99.
- VII. Kuhs, M.; Svärd, M.; Rasmuson, Å. C., Thermodynamics of Fenoxycarb in solution. *J Chemical Thermodynamics* **2013**, 66, (0), 50-58.
- VIII. Karpinska, J.; Kuhs, M.; Rasmuson, Å. C.; Erxleben, A.; McArdle, P., ethyl N-[2-(4-phenoxyphenoxy)ethyl]carbamate. *Acta Crystallographica Section E* **2012**, 68, (10), o2834-o2835.

Conference contributions based on this thesis:

- IX. Kuhs, M.; Zeglinski, J.; Rasmuson, Å. C., Kinetics and Mechanism of a Solution History Effect on Nucleation. In *45th Annual BACG Conference*, ed.; Leeds, UK, **2014**, **oral presentation**.
- X. Rasmuson, Å. C.; Zeglinski, J.; Kumar, K.; Kuhs, M.; Cheuk, D.; Watterson, S., Crystal nucleation of organic compounds – early observations and new findings. In *44th Annual BACG Conference*, ed.; Manchester, UK, **2013**, **plenary lecture**.
- XI. Svärd, M.; Kuhs, M.; Watterson, S.; Hudson, S.; Rasmuson, Å. C., Thermodynamic Investigation into the Origin of Linearity and Non-Linearity in van't Hoff Plots. In *44th Annual BACG Conference*, ed.; Manchester, UK, **2013**, **poster**.
- XII. Kuhs, M.; Zeglinski, J.; Rasmuson, Å. C., Influence of History of Solution in Crystal Nucleation of Fenoxycarb: Kinetics and Mechanisms. In *44th Annual BACG Conference*, ed.; Manchester, UK, **2013**, **poster**.
- XIII. Kuhs, M.; Zeglinski, J.; Karpinska, J.; Rasmuson, Å. C., Crystallization Properties of Fenoxycarb. In *10th International Workshop on Crystal Growth of Organic Materials*, ed.; Limerick, Ireland, **2012**, **poster**.
- XIV. Mealey, D.; Kuhs, M.; Croker, D.; Hodnett, B. K.; Rasmuson, Å. C., High throughput methods for the study of nucleation processes. In *41st Annual BACG Conference*, ed.; Manchester, UK, **2010**, **poster**.

# Acknowledgements

This thesis could not have happened without the help of many people.

First, my supervisor, Prof Ake Rasmuson. Ake, thank you for the years of discussion, guidance, and help. From you I learnt what it is to “shoot from the hip”. I will miss your Swedish “imports”. Thank you for always being there, and for your patience with my often silly “theories” and getting too excited about “straight line fits”.

Next, thank you to all my colleagues in the nucleation group; Donal, who helped me a lot when I got started – thank you for your patience and willingness to explain even basic things to me; Denise, for some extra supervision at the beginning; Sam, for being a close friend; Jacek & Kumar, for being helpful co-authors; Dominic, Marcus, Anthony, who were always helpful; Frederik Nordstrom, for helpful discussion, and Miche for stimulating conversations.

Thank you also to my friends Marco, Martyn, Eric and George.

Thank you to my church, the Limerick Reformed Fellowship, where I was continuously refreshed spiritually, and taught to “work as unto the Lord”, and that “I can do all things through Him who strengtheneth me”.

The great joy of my life: My wife, Emily-Kate, and our two children, Sebastian & Penelope. I looked forward every day to coming home to you all. Emily-Kate, thank you for being my companion and best friend through my PhD. I look forward to sharing my life with you “until death do us part”.

Above all, to my heavenly Father, Who gave me the ability to do this PhD, Who patiently bears with my many sins, Who sent His Son to die for me upon the cross, Who sent His Spirit to live in me and makes me holy.

*Soli deo gloria*

# Contents

<b>DECLARATION</b> .....	<b>I</b>
<b>ABSTRACT</b> .....	<b>II</b>
<b>PUBLICATIONS</b> .....	<b>III</b>
<b>ACKNOWLEDGEMENTS</b> .....	<b>IV</b>
<b>LIST OF TABLES</b> .....	<b>VII</b>
<b>LIST OF FIGURES</b> .....	<b>VIII</b>
<b>LIST OF ABBREVIATIONS</b> .....	<b>XI</b>
<b>1 INTRODUCTION &amp; THEORY</b> .....	<b>1</b>
<b>1.1 INTRODUCTION</b> .....	<b>2</b>
1.1.1 OBJECTIVES & EXPERIMENTAL PLAN.....	3
<b>1.2 THEORY</b> .....	<b>5</b>
1.2.1 SUPERSATURATION, THE DRIVING FORCE OF NUCLEATION.....	5
1.2.2 CLASSICAL NUCLEATION THEORY.....	6
1.2.3 POLYMORPHISM.....	16
1.2.4 STOCHASTICITY.....	17
1.2.5 INFLUENCE OF SOLVENT.....	18
1.2.6 SOLUTION HISTORY EFFECT ON NUCLEATION.....	19
<b>2 MATERIALS &amp; EXPERIMENTAL METHODOLOGIES</b> .....	<b>21</b>
<b>2.1 MATERIALS</b> .....	<b>22</b>
2.1.1 FENOXYCARB.....	22
2.1.2 TOLBUTAMIDE.....	23
<b>2.2 EXPERIMENTAL METHODOLOGIES</b> .....	<b>23</b>
2.2.1 SOLUBILITIES.....	23
2.2.2 INDUCTION TIMES.....	25
2.2.3 TOLBUTAMIDE SOLID PHASE CHARACTERISATION.....	29
<b>2.3 ANALYTICAL TECHNIQUES</b> .....	<b>31</b>
2.3.1 X-RAY DIFFRACTION (XRD).....	31
2.3.2 NUCLEAR MAGNETIC RESONANCE (NMR).....	32
2.3.3 RAMAN SPECTROSCOPY.....	32
2.3.4 SCANNING ELECTRON MICROSCOPY (SEM).....	33
2.3.5 DIFFERENTIAL SCANNING CALORIMETER (DSC).....	33

<b>3</b>	<b><u>SOLUBILITIES</u></b>	<b><u>34</u></b>
3.1	TOLBUTAMIDE	35
3.2	FENOXYCARB	37
3.2.1	SOLID PHASE IDENTIFICATION	37
3.2.2	SOLUBILITIES	42
3.3	DISCUSSION	44
3.3.1	METHOD	44
3.3.2	NON-LINEAR VAN'T HOFF PLOTS	45
3.3.3	A MOLECULAR ANALYSIS OF THE MEASURED SOLUBILITIES	47
<b>4</b>	<b><u>INFLUENCE OF SOLVENT ON NUCLEATION OF TOLBUTAMIDE AND FENOXYCARB</u></b>	<b><u>51</u></b>
4.1	FENOXYCARB INDUCTION TIMES	52
4.2	TOLBUTAMIDE INDUCTION TIMES	56
4.3	DISCUSSION	59
4.3.1	INDUCTION TIME DISTRIBUTIONS	59
4.3.2	SHORT INDUCTION TIMES	61
4.3.3	SUPERSATURATION	62
4.3.4	INTERFACIAL ENERGIES AND PRE-EXPONENTIAL FACTORS	63
4.3.5	SOLVENT INFLUENCE ON EASE OF NUCLEATION	65
<b>5</b>	<b><u>INFLUENCE OF HISTORY OF SOLUTION IN CRYSTAL NUCLEATION OF FENOXYCARB</u></b>	<b><u>73</u></b>
5.1	VALIDATION	74
5.2	INDUCTION TIMES	78
5.3	DISCUSSION	82
5.3.1	FIRST NUCLEATION	82
5.3.2	RATE OF CHANGE OF SOLUTION STATE	84
5.3.3	HYPOTHESISED MECHANISM	88
<b>6</b>	<b><u>CONCLUSION</u></b>	<b><u>91</u></b>
	<b><u>BIBLIOGRAPHY</u></b>	<b><u>95</u></b>
	<b><u>APPENDIX A – PAPER DRAFT: SOLVENT EFFECTS ON NUCLEATION KINETICS AND THERMODYNAMICS OF FENOXYCARB</u></b>	<b><u>106</u></b>
	<b><u>APPENDIX B – PAPER DRAFT: TOLBUTAMIDE NUCLEATION DEPENDENCE ON SOLVENT</u></b>	<b><u>135</u></b>
	<b><u>APPENDIX C – DROPLET MICROFLUIDICS</u></b>	<b><u>170</u></b>

# List of Tables

TABLE 1: TYPES OF NUCLEATION EXPLAINED BY CONTACT ANGLE $\theta$ VIA EQUATION (11) AND ITS EFFECT ON THE CRITICAL FREE ENERGY CHANGE VIA EQUATION (10).....	10
TABLE 2. SOURCE AND MASS FRACTION PURITY OF CHEMICALS.....	22
TABLE 3: MOLE FRACTION SOLUBILITIES ( $x_{eq}$ ) OF TOLBUTAMIDE AT TEMPERATURE $T$ IN VARIOUS SOLVENTS, ALONG WITH STANDARD DEVIATIONS (SD). $x_{eq}$ AND SD UNITS ARE $10^{-4}$ . .....	35
TABLE 4: DSC MELTING DATA (EXTRAPOLATED ONSET TEMPERATURES AND ASSOCIATED HEATS OF FUSION, WITH 95% CONFIDENCE INTERVALS) FOR CRYSTALS OF TYPES 1 AND 2 BEFORE AND AFTER A MELTING-RECRYSTALLIZATION CYCLE.....	41
TABLE 5: MOLE FRACTION SOLUBILITY ( $x_{eq}$ ) OF FENOXYCARB AT TEMPERATURE $T$ IN VARIOUS SOLVENTS, ALONG WITH STANDARD DEVIATIONS (SD). .....	42
TABLE 6: SOLUTIONS AND INDUCTION TIME RESULTS FOR FENOXYCARB. $S = x/x_{eq}$ , WHERE $x$ IS THE ACTUAL MOLE FRACTION OF FENOXYCARB IN THE SOLUTION, AND $x_{eq}$ THE EQUILIBRIUM MOLE FRACTION AT $T_{CRY}$ (KUHS ET AL. 2013); $N$ IS THE NUMBER OF INDUCTION TIMES MEASURED FOR EACH CONDITION; LOGN. $T_{IND}$ IS THE MEDIAN OF THE LOGNORMAL FIT TO THE EXPERIMENTAL $T_{IND}$ DISTRIBUTIONS. ....	53
TABLE 7: CNT PARAMETERS CALCULATED FROM EQUATIONS (9), (16), AND (24) FOR FENOXYCARB.....	55
TABLE 8: SOLUTIONS AND INDUCTION TIME RESULTS FOR TOLBUTAMIDE FORM I <sup>L</sup> .....	57
TABLE 9: CALCULATED PARAMETERS OF THE CNT FOR TOLBUTAMIDE FORM I <sup>L</sup> ACCORDING TO EQUATIONS (9), (16), AND (24).....	59
TABLE 10: DEMONSTRATION OF THE EFFECT OF ERROR IN ESTIMATING $S$ ON THE SUBSEQUENT MAGNITUDE OF ERROR IN THE CALCULATION OF $(RT)\ln S$ AND INTERFACIAL ENERGY, SHOWN FOR SMALLEST AND LARGEST VALUES OF $S$ USED AND USING THE APPROXIMATE AVERAGE COEFFICIENT OF VARIATION (1.5%) OF THE SOLUBILITY VALUES AS THE ERROR IN $S$ .....	63
TABLE 11: RANKING (1 = LOWEST/EASIEST, 4 = HIGHEST/MOST DIFFICULT) FOR FENOXYCARB AND TOLBUTAMIDE OF INTERFACIAL ENERGIES FROM CNT AND THERMODYNAMIC DRIVING FORCES $(RT)\ln S$ REQUIRED TO ACHIEVE INDUCTION TIMES OF 2.06 (FENOXYCARB) AND 2 H (TOLBUTAMIDE). .....	66
TABLE 12: RESULTS OF 2 SAMPLE KOLMOGOROV-SMIRNOV TESTS OF THE RANK DISTRIBUTION OF EACH VIAL AGAINST THE UNIFORM DISCRETE DISTRIBUTION WHICH IS EXPECTED IF ALL VIALS ARE IDENTICAL. ....	76
TABLE 13: RELATIONSHIP BETWEEN INDUCTION TIME AND IMMEDIATELY PRECEDING INDUCTION TIME. ....	78
TABLE 14: RATE OF CHANGE OF SOLUTION STRUCTURE AT DIFFERENT PRETREATMENT TEMPERATURES. ....	85

# List of Figures

FIGURE 1: THE FREE ENERGY CHANGE INVOLVED IN THE FORMATION OF A CRYSTAL FROM SOLUTION. SEE TEXT FOR DETAIL. SOURCE: (VEKILOV 2010A) .....	8
FIGURE 2: THE INTERFACIAL TENSIONS AT THE BOUNDARIES BETWEEN 2 SOLIDS AND A LIQUID. ....	9
FIGURE 3: INDUCTION TIME MEASUREMENT IN WHICH SUPERSATURATION IS CONTROLLED USING TEMPERATURE. T IS ACTUAL SOLUTION TEMPERATURE, T <sub>SP</sub> IS SET POINT TEMPERATURE, C IS THE SOLUTION CONCENTRATION, T = 0 IS POINT IN TIME WHEN SUPERSATURATION IS FIRST ACHIEVED, T <sub>1</sub> IS TIME TAKEN FOR T <sub>SP</sub> TO ACTUALLY BE REACHED, AND T <sub>2</sub> THE APPEARANCE OF THE FIRST CRYSTAL. ....	14
FIGURE 4: THE PRINCIPLE OF THE DOUBLE PULSE TECHNIQUE. ON THE LEFT IS SHOWN THE REACTION PROFILE IN THE PHASE DIAGRAM, AND ON THE RIGHT A TEMPERATURE PROFILE. THE METASTABLE ZONE LIMIT IS THE LIMIT AT WHICH NUCLEATION WILL NOT OCCUR DURING THE EXPERIMENTAL TIME-FRAME, EVEN THOUGH THE SOLUTION IS SUPERSATURATED. SOURCE: (REVALOR <i>ET AL.</i> 2010).....	15
FIGURE 5: MOLECULAR STRUCTURE OF FENOXYCARB. ....	22
FIGURE 6: MOLECULAR STRUCTURE OF TOLBUTAMIDE. ....	23
FIGURE 7: RAMAN SHIFTS DISTINGUISHING BETWEEN TOLBUTAMIDE FORMS I <sup>L</sup> AND II AS POWDERS (SOLID LINES) AND SLURRIES OF N-PROPANOL (DASHED LINES). VERTICAL LINES INDICATE PEAKS UNIQUE TO FORMS I <sup>L</sup> (BLUE) AND II (RED).....	31
FIGURE 8: APPROACH TO EQUILIBRIUM FOR TOLBUTAMIDE FORM I <sup>L</sup> AT 1.92 °C. FOR EACH POINT THE POLYMORPHIC IDENTITY WAS CONFIRMED TO BE PURE FORM I <sup>L</sup> BY PXRD. THE FLUCTUATIONS ARE OF THE SAME MAGNITUDE AS THE SD VALUES OF THE CONCENTRATION MEASUREMENTS (SEE TABLE 3).....	35
FIGURE 9: TOLBUTAMIDE FORM I <sup>L</sup> SOLUBILITIES IN VARIOUS SOLVENTS AS G/G (BOTTOM) AND VAN'T HOFF (TOP). LINES ARE GUIDES FOR THE EYE ONLY. ....	36
FIGURE 10: VAN'T HOFF PLOT OF TOLBUTAMIDE ETHANOL SOLUBILITY COMPARED WITH LITERATURE VALUES (THIRUNAHARI <i>ET AL.</i> 2010).....	37
FIGURE 11: SOLUBILITY OF FENOXYCARB IN FIVE ORGANIC SOLVENTS (TOP) WITH VALUES FROM APPROACHING VIA SUPERSATURATION OVERLAID (BOTTOM). LINES ARE GUIDES FOR THE EYES ONLY. ....	43
FIGURE 12: MOLECULAR PACKING IN CRYSTALS OF FENOXYCARB (LEFT) AND TOLBUTAMIDE FORM 1 <sup>L</sup> (RIGHT). SOURCES: (THIRUNAHARI <i>ET AL.</i> 2010, ZEGLINSKI <i>ET AL.</i> 2014) .....	49
FIGURE 13: INDUCTION TIME DISTRIBUTIONS OF FENOXYCARB IN DIFFERENT SOLVENTS. TEMPERATURES ARE T <sub>CRY</sub> . ....	52
FIGURE 14: THE RELATIONSHIP BETWEEN MEDIAN INDUCTION TIME AND THERMODYNAMIC DRIVING FORCE, RTlnS, OF NUCLEATION OF FENOXYCARB IN DIFFERENT SOLVENTS. LINES ARE GUIDES FOR THE EYES ONLY.....	54
FIGURE 15: THE RELATIONSHIP BETWEEN T <sub>CRY</sub> , S AND T <sub>IND</sub> OF FENOXYCARB PLOTTED ACCORDING TO CNT. LINES ARE EXPONENTIAL FITS. A AND f IN TABLE 6 ARE CALCULATED FROM THE INTERCEPTS AND SLOPES, RESPECTIVELY, ACCORDING TO EQUATIONS (16) AND (24). ....	55
FIGURE 16: INDUCTION TIME DISTRIBUTIONS OF TOLBUTAMIDE IN DIFFERENT SOLVENTS. TEMPERATURES ARE T <sub>CRY</sub> AND STARS INDICATE SAMPLING OF SLURRY FOR PXRD ANALYSIS, WHICH ALWAYS GAVE A FORM I <sup>L</sup> DIFFRACTION PATTERN. ....	56

FIGURE 17: THE RELATIONSHIP BETWEEN MEDIAN INDUCTION TIME AND THERMODYNAMIC DRIVING FORCE OF NUCLEATION OF TOLBUTAMIDE IN DIFFERENT SOLVENTS. LINES ARE EXPONENTIAL FITS. ....	57
FIGURE 18: THE RELATIONSHIP BETWEEN $T_{CRY}$ , $S$ AND $T_{IND}$ OF TOLBUTAMIDE PLOTTED ACCORDING TO THE CLASSICAL NUCLEATION THEORY. LINES ARE EXPONENTIAL FITS FROM WHICH $A$ AND $f$ IN TABLE 9 ARE CALCULATED ACCORDING TO EQUATIONS (19) AND (27). ....	58
FIGURE 19: INTERFACIAL ENERGY COMPARED TO MOLE FRACTION SOLUBILITY FOR BOTH FENOXYCARB AND TOLBUTAMIDE (TOP AND BOTTOM LEFT, RESPECTIVELY), TO SOLVENT DENSITY FOR FENOXYCARB (TOP RIGHT), AND TO SOLVENT BOILING POINT FOR TOLBUTAMIDE (BOTTOM RIGHT). LINES ARE LINEAR FITS FOR CHECKING DIRECT PROPORTIONALITY. ....	67
FIGURE 20: FENOXYCARB THERMODYNAMIC DRIVING FORCE, $RT\ln S$ , REQUIRED TO REACH MEDIAN INDUCTION TIMES OF 2.06 H, CORRELATED TO CALORIMETRIC (LEFT) AND MOLECULAR DYNAMICS (MD, RIGHT) SOLVENT-SOLUTE INTERACTION ENTHALPIES DETERMINED BY CO-AUTHORS. SOURCE OF ENTHALPIES: APPENDIX A. ....	69
FIGURE 21: TOLBUTAMIDE NUCLEATION DIFFICULTY AS DRIVING FORCE REQUIRED TO REACH $T_{IND} = 2$ H CORRELATED TO CALORIMETRIC (LEFT) AND MOLECULAR DYNAMICS (RIGHT) SOLVENT-SOLUTE INTERACTION ENTHALPIES AS DETERMINED BY CO-AUTHORS. SOURCE OF ENTHALPIES: APPENDIX B. ....	69
FIGURE 22: REPRESENTATIVE CONFORMATIONS OF TOLBUTAMIDE IN N-PROPANOL (A AND B), AND IN TOLUENE (C), FOR WHICH CO-AUTHORS HAVE CALCULATED RADIAL DISTRIBUTION FUNCTIONS (RDF) TO ILLUSTRATE HOW DIFFERENT SOLVENTS INFLUENCE CONFORMATIONAL CHANGES. SOURCE: APPENDIX B. ....	70
FIGURE 23: SOLUTION CONCENTRATION IN G FENOXYCARB / G ISOPROPANOL OVER VIAL AGE DETERMINED BY SOLUTION $^1H$ NMR. SOLID LINE IS THE BEST STRAIGHT LINE FIT, FOR WHICH PEARSON'S CORRELATION PARAMETERS $R^2$ AND $P$ ARE SHOWN. ....	77
FIGURE 24: EFFECT OF PRETREATMENT TIME ON INDUCTION TIME AT (A) 25 °C, (B) 30 °C, (C) 35 °C AND (D) 45 °C PRETREATMENT TEMPERATURE. LEFT: CUMULATIVE DISTRIBUTION CURVES; RIGHT: POINT ESTIMATES OF EACH DISTRIBUTION AS GEOMETRIC MEAN. PRETREATMENT CONDITIONS MARKED WITH *, † AND ‡ WERE ITERATED 1, 5 AND 4 TIMES, RESPECTIVELY, COMPARED TO THE NORMAL 3 TIMES, WITH THE SET OF 25 VALIDATED SOLUTIONS. ....	80
FIGURE 25: EFFECT OF PRETREATMENT TEMPERATURE ON INDUCTION TIME FOR A PRETREATMENT TIME OF 2 H. (A) IS RAW DATA FOR ALL 3 RUNS PER PRETREATMENT CONDITION SET; (B) INDUCTION TIME GEOMETRIC MEAN VS PRETREATMENT TEMPERATURE. ....	81
FIGURE 26: NUCLEATION INDUCTION TIME DISTRIBUTION OF THE "FIRST NUCLEATION" COMPARED TO THE DISTRIBUTIONS OBTAINED AT SUBSEQUENT EXPERIMENTS AT THE SAME PREHEATING TIME OF 24 H. PRETREATMENT CONDITIONS MARKED WITH * ONLY HAVE 25 DATA POINTS (FROM A SINGLE ITERATION OF 25 SOLUTIONS), COMPARED TO THE NORMAL 75 (FROM 3 ITERATIONS). ....	82
FIGURE 27: RATE OF CHANGE OF $1/T_{IND}$ AGAINST $1/T$ ACCORDING TO THE ARRHENIUS PLOT. ....	86
FIGURE 28: RELATIONSHIP BETWEEN INFERRED INITIAL INDUCTION TIME AND PRETREATMENT TEMPERATURE. ....	87
FIGURE 29: OPTIMIZED STRUCTURES OF FENOXYCARB DIMERS: (1) FENOXYCARB DIMER IN GEOMETRY CLOSE TO THAT IN THE CRYSTAL, (2) FENOXYCARB DIMER WITH ALIPHATIC-TO-AROMATIC ORIENTATION OF END-GROUPS. NUMERIC VALUES ARE HYDROGEN BOND DISTANCES IN Å. WORK DONE BY A CO-AUTHOR (KUHS <i>ET AL.</i> 2014). ....	89

FIGURE 30: SCHEMATIC DESCRIPTION OF THE HYPOTHESIZED HISTORY OF SOLUTION MECHANISM..... 90

# List of Abbreviations

$A$	Pre-exponential factor
$a$	Activity
$A_s$	Cluster surface area
$b$	Molecular size
$c$	Concentration
$CDCl_3$	Deuterated Chloroform (0.03% TMS)
CV	Coefficient of Variation (mean / standard deviation)
DSC	Differential scanning calorimeter
$E_A$	Activation energy
$G$	Gibbs free energy
$H$	Enthalpy
h	Hours
$J$	Nucleation rate
$k$	Rate constant
$k_B$	Boltzman constant
$n$	Number
NMR	Nuclear magnetic resonance
$\rho$	Pearson's correlation coefficient
$R$	Universal gas constant
$R^2$	Coefficient of determination
rpm	Rotations per minute
$S$	Supersaturation Ratio
SEM	Scanning electron microscope
$T$	Temperature
$T_{cry}$	Crystallisation temperature
$T_{diss}$	Dissolution temperature
$t_g$	Growth time
$t_{ind}$	Induction time
$t_n$	Nucleation time
$T_{PT}$	Pretreatment temperature
$t_{PT}$	Pretreatment time
$t_r$	Relaxation time
$x$	Mole fraction
XRD	X-ray diffraction
$\gamma$	Interfacial energy

$\gamma_k$	Activity coefficient (where k is c, x or m)
$\mu$	Chemical potential
$\Omega$	Volume occupied by a molecule in the crystal

# I

## **1 Introduction & Theory**

### **1.1 Introduction**

Crystallization is the process whereby solid crystals precipitate from a melt, solution or gas to form material with long-distance order (Mullin 2001). Common natural examples include snowflake formation, honey crystallization and stalactite and stalagmite formation.

Crystallization is also a process heavily utilised in various manufacturing industries. Large-scale examples include the production of salt, silicon crystal wafer and sucrose from sugar beet. The process is also used in the pharmaceutical industry; in fact, over 90% of all pharmaceutical products contain crystalline ingredients (Valder and Merrifield 1996). It is even considered by some to be the single most important unit operation in the pharmaceutical industry (Bernstein 2002) because crystallization and the crystalline state are more suited to purification, reproducibility and stability than other common states such as amorphous solids and solutions (Munroe 2010).

In Ireland, over 50% of exports by value are pharmaceutical products, and Ireland is now the world's largest net exporter of pharmaceuticals (McKinley 2012). Thus the pharmaceutical industry is of great importance to Ireland.

There is insufficient understanding of crystallization, and the fundamental theory is not sufficiently developed to replace empirical approaches (Leng and Salmon 2009). This lack of knowledge poses significant problems in crystallizations. Poor yields and the presence of undesirable or unpredictable polymorphs continue to plague pharmaceutical crystallization processes at both lab and industrial scale (Rodríguez-Hornedo and Murphy 1999).

The process of crystallization is traditionally divided into two steps. In the first step, *nucleation*, the new phase is created in the form of the smallest cluster of molecules with the thermodynamic tendency to grow further. In the second step, *crystal growth*, this nucleus grows (Mullin 2001). Kashchiev (2000) defines nucleation as “the process of random generation of those nanoscopically small formations of the new phase that have the ability for irreversible overgrowth to macroscopic sizes”.

## Introduction & Theory

Much less is known about nucleation than crystal growth. Indeed, it is in particular the nucleation step that makes crystallization such a difficult process to study. The difficulty arises from a combination of the stochastic nature of nucleation, the miniscule size of the smallest stable nuclei (which are typically in the order of 10 to 1,000 molecules), and the great speed at which nuclei often form. Thus, it is very difficult to observe nucleation, both from a temporal and a spatial perspective (Revalor *et al.* 2010).

Nucleation has a significant influence on all crystallization processes. For example, the nucleation step is one of the main uncertainties in global climate modelling of the radiative forcing of aerosol particles, 30% of which are estimated to be produced by atmospheric nucleation (Spracklen *et al.* 2006). Nucleation is also of special importance in the pharmaceutical industry, where tight parameter control is necessary. Nucleation has a considerable effect on the morphology, size, size distribution and polymorphic form of crystals (Laval *et al.* 2007), as well as other factors such as “the concentration threshold above which crystallization is observed at times shorter than the desired product shelf life, or dilution rates and concentrations above which precipitation occurs upon injection” (Rodríguez-Hornedo and Murphy 1999). The lack of understanding of the nucleation phenomenon has led to many problems, including “disappearing or elusive polymorphs” (Dunitz and Bernstein 1995), such as the famous shortage of the HIV protease inhibitor Norvir in the 1990s due to the sudden formation of a different polymorph than the one produced for months (Rodríguez-Hornedo and Murphy 1999).

### **1.1.1 Objectives & Experimental Plan**

This PhD is focussed on the influence of solution structure (chiefly solvent choice) and solution history on the nucleation of medium-sized flexible organic molecules used industrially. By probing the influence of these factors on the measured nucleation rate, it was hoped to elucidate the interaction between solvent and solute as this interaction affects the nucleation process. This was expected to further increase understanding of the nucleation process itself, especially as it relates to molecules of industrial significance.

Since measuring solution activities is too time-consuming and fraught with practical difficulties, it was decided to use solubility to estimate thermodynamic driving forces of

## Introduction & Theory

nucleation (see 1.2.1). Since solubilities were not available for the investigated solute and solvent combinations, they had to be measured experimentally at several temperatures. As solubility is a function of the polymorphic form of the solute, solid-state characterisation was in turn necessary to verify that the measured solubilities corresponded to the polymorph whose nucleation was studied. For one of the molecules, it proved necessary to carry out quite extensive characterisation, involving numerous analytical methods. Conveniently, solubility also represents another invaluable source of information on solvent-solute interaction and solution structuring leading up to and possibly influencing nucleation.

Due to the inherently stochastic nature of nucleation, it was desirable to carry out crystallisation experiments at the low volumes at which this stochasticity is directly observed as distributions of induction times under identical conditions. To this end, droplet microfluidics was initially chosen as a promising technique for collecting large amounts of crystallisation data for statistical analysis. However, it proved unfeasible due to the long induction times (several weeks in the best cases) of medium-sized molecules at such small volumes. This work is reported in Appendix C. We then decided to scale up to 20 mL reactors with more traditional lab equipment to reduce the induction times to more reasonable levels.

Nucleation rates of two molecules in different solvents were collected at this scale. From this the relative ease of nucleation in the different solvents was evaluated, both directly from the experimental results as the thermodynamic driving force ( $RT\ln S$ ) required to achieve similar induction times, and using the interfacial energy from the Classical Nucleation Theory (CNT). Reported spectroscopic, calorimetric and modelled data relating to the solvent-solute interactions for the systems of interest were correlated with the nucleation rate dependence in an attempt to elucidate the mechanism(s) whereby solvents influence nucleation.

Finally, a history of solution effect on the nucleation rate of one of the compounds was observed and consequently studied systematically. For the first time, quantitative data on the kinetics of this effect were published. Based on published modelling data a mechanism of solution restructuring was hypothesised to explain this phenomenon.

## 1.2 Theory

### 1.2.1 Supersaturation, the Driving Force of Nucleation

Before discussing nucleation, the fundamental thermodynamic driving force of nucleation in solution must be discussed.

The fundamental driving force is the difference between the chemical potential ( $\mu$ ) of the substance in solution and in the crystal (Mullin 2001):

$$\Delta\mu = \mu_{\text{solute}} - \mu_{\text{crystal}} \quad (1)$$

For a supersaturated solution,  $\mu_{\text{solute}}$  is greater than  $\mu_{\text{crystal}}$ , such that a positive thermodynamic driving force exists for the formation of the new phase.

The fundamental supersaturation  $S$  is related to  $\Delta\mu$  as follows (Mullin 2001):

$$\Delta\mu = \ln(a/a^*)RT = \mathbf{RT}\ln S \quad (2)$$

Where  $a$  and  $a^*$  are the activities of the solution at supersaturation and equilibrium, respectively,  $\mathbf{R}$  is the Universal Gas Constant and  $T$  the temperature.

Because it is very difficult to directly measure solution activities, supersaturations are normally reported as solution *concentration* ratios, either in terms of molarity ( $c$ ), molality ( $m$ ) or mole fraction ( $x$ ):

$$S_c = \frac{c}{c^*}, \quad S_m = \frac{m}{m^*}, \quad S_x = \frac{x}{x^*} \quad (3)$$

The relationship between the real supersaturation  $S$  and the concentration ones depends on the relevant concentration-dependent activity coefficient ratio:

$$S = \frac{\gamma_k}{\gamma_k^*} S_k \quad (4)$$

Where  $k$  is the subscript  $c$ ,  $m$ , or  $x$  found in Equation (3).

From this equation it can be seen that if  $\frac{\gamma_k}{\gamma_k^*} \approx 1$ , the relevant concentration-dependent supersaturation is close to the real supersaturation.

## Introduction & Theory

In case the activity coefficient ratios are unknown, Mullins (2001) recommends the usage of molality, that is, measuring the solvent by mass, not volume or mole fraction, due to its temperature independence.

Since  $\gamma$  is a function of concentration, the assumption that  $\frac{\gamma_k}{\gamma_k^*} \approx 1$  is unjustified for large supersaturations (i.e.  $c \gg c^*$  or  $m \gg m^*$  etc.) (Vekilov 2010d). In such cases, activity must either be experimentally determined or a valid approximation must be found.

### **1.2.2 Classical Nucleation Theory**

The classical nucleation theory (CNT) was developed by Gibbs, Volmer and others (Mullin 2001) between the late 19<sup>th</sup> century and the first half of the 20<sup>th</sup>, based on the condensation of a vapour to a liquid. Since in this review we are concerned with nucleation of a solute into a solid crystal, we will follow the presentation of the CNT by Vekilov (2010a) in his summary of CNT, in which he considers the formation of a crystal instead of a liquid droplet, and accordingly considers the initial shape of the nucleus to be cubic instead of spherical.

#### **1.2.2.1 Thermodynamics**

The thermodynamic aspect of nucleation will be discussed first; that is, clusters of a given size that are in internal thermodynamic equilibrium and in complete or partial equilibrium with the solution will be analyzed. How these clusters achieved their current state, or what changes they will undergo in the future, will not be analysed here (Kashchiev 2000). This will be done in the following section.

It was Gibbs who first formulated the thermodynamic foundation of CNT in two papers (1876, 1878), which theory we will present with the previously-mentioned modifications.

For a supersaturated solution, the chemical potential,  $\mu$ , of the solute in solution is higher than in a crystal:

$$\Delta\mu = \mu_{\text{solute}} - \mu_{\text{crystal}} > 0 \quad (5)$$

## Introduction & Theory

Thus, the formation of such a cluster involving  $n$  molecules would lead to a reduction in free energy of  $-n\Delta\mu$ . However, the new phase boundary created by the cluster also leads to an increase in free energy due to the surface energy between the new and old phases:

$$A_S\gamma = 6a^2n^{2/3}\gamma \quad (6)$$

where  $A_S$  is the cluster surface area,  $n$  the number of molecules in the cluster,  $\gamma$  the surface free energy between cluster and solution, and  $a$  the width of the (cubic) cluster. Since the different faces of a crystal can have different surface energies,  $\gamma$  is an average value over the whole crystal.

Overall, the following free energy change results as a function of the number of molecules in the cluster:

$$\Delta G(n) = -n\Delta\mu + 6a^2n^{2/3}\gamma \quad (7)$$

It can be seen from a plot of this (Fig. 1) that the total free energy change passes through a maximum,  $\Delta G^*$ , corresponding to a certain number of molecules,  $n^*$ . Transient clusters of various sizes continuously form in solution due to localised fluctuations and collisions from Brownian motion and other perturbations. Any cluster smaller than  $n^*$  will have a tendency to reduce its free energy by dissolving. Thus it is evident that in order to grow spontaneously, a cluster must exceed the “critical size” of  $n^*$ . A cluster of size  $n^*$  is called a “critical nucleus” or just “nucleus”.

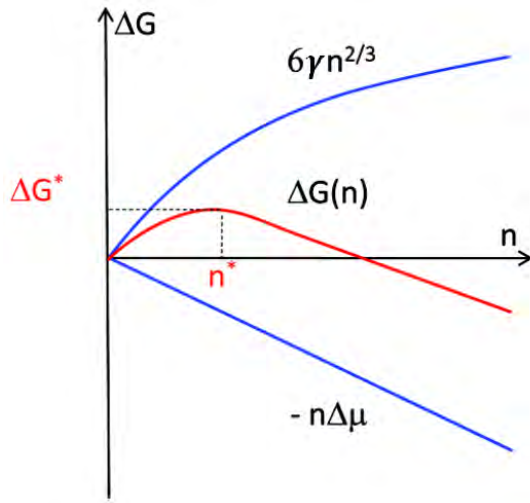


Figure 1: The free energy change involved in the formation of a crystal from solution. See text for detail. Source: (Vekilov 2010a)

By differentiating  $\Delta G(n)$ , the critical nucleus size and the critical free energy difference can be determined:

$$n^* = \frac{64\Omega^2\gamma^3}{\Delta\mu^3} \quad (8)$$

$$\Delta G^* = \frac{32\Omega^2\gamma^3}{\Delta\mu^2} = \frac{1}{2}n^*\Delta\mu \quad (9)$$

where  $\Omega$  is the volume occupied by a molecule in the crystal.

Thus it can be seen that since  $\Delta\mu$  is a function of both  $S$  and  $T$  (see Equation (2)),  $\Delta G^*$  itself is also a function of the external parameters  $S$  and  $T$ .

#### 1.2.2.1.1 Homogeneous and Heterogeneous Nucleation

A complicating factor is that impurities or additional components in a system can significantly affect nucleation. Generally speaking, the presence of foreign particles or such things as cavities in the container wall, or even already-formed crystals, drastically increase the nucleation rate. A decrease (i.e. inhibition) is also possible.

Impurities are so ubiquitous that it is considered extremely unlikely to observe true homogeneous nucleation unless experimental conditions are tightly controlled (Mullin 2001). Even then this is difficult to achieve, especially in crystallization from solution

## Introduction & Theory

(e.g. (Laval *et al.* 2007)). Studies suggest that an impurity as miniscule as a single molecule can cause heterogeneous nucleation with rates higher than the homogeneous equivalent by four or five orders of magnitude (Sear 2006).

This can be understood by considering the impact of these impurities and other factors on the interfacial energy or tension,  $\gamma$ , which, according to CNT, is one of the fundamental parameters determining the magnitude of the “activation energy”,  $\Delta G^*$  (see Figure 1) and thus affecting also  $n^*$  and the nucleation rate  $J$  (see Section 1.2.2.2).

Consider Figure 2, which shows the interfacial tensions at the boundaries between 3 phases. Instead of the solid-liquid-gas interaction that is conventionally represented in such a diagram, this represents two solids and a liquid, namely, the new crystal nucleus, the existing solid (foreign particle, etc.) and the solvent.

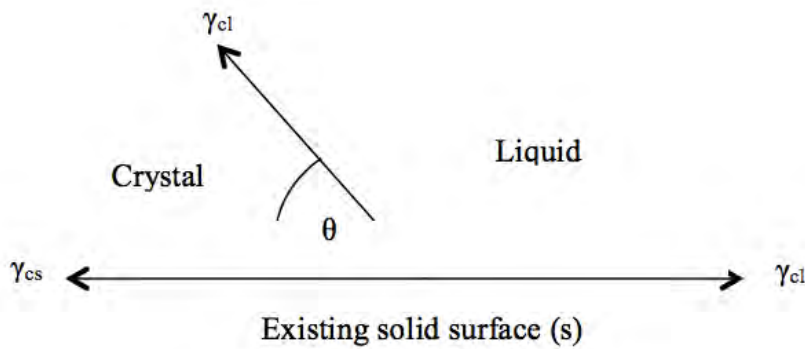


**Figure 2: The interfacial tensions at the boundaries between 2 solids and a liquid.**

The effective critical free energy change  $\Delta G_{ef}^*$  can be related to  $\Delta G^*$  by a factor  $\phi$ :

$$\Delta G_{ef}^* = \phi \Delta G^* \quad (10)$$

Volmer (1939) derived an expression for  $\phi$  in terms of  $\theta$ :

$$\phi = \frac{(2 + \cos\theta)(1 - \cos\theta)^2}{4} \quad (11)$$

The different possible values of  $\theta$ , the corresponding values of  $\phi$  and the effect on  $\Delta G_{ef}^*$  according to Equation (10) are summarised in Table 1.

**Table 1: Types of nucleation explained by contact angle  $\theta$  via Equation (11) and its effect on the critical free energy change via Equation (10).**

<b>Type of Nucleation</b>	<b>Cause</b>	<b>Effect</b>	<b>Eqn.</b>
<b>Homogeneous</b>	$\theta = 180^\circ, \therefore \phi = 1$	$\Delta G_{ef}^* = \Delta G^*$	(12)
<b>Heterogeneous</b>	$0 < \theta < 180^\circ, \therefore \phi < 1$	$\Delta G_{ef}^* < \Delta G^*$	(13)
<b>Secondary</b>	$\theta = 0, \therefore \phi = 0$	$\Delta G_{ef}^* = 0$	(14)

This can be understood as follows.  $\theta = 180^\circ$  means there is no affinity (i.e. complete non-wetting) between crystal and solid surface (or simply that there is no solid surface), so that the interfacial energy between the crystal and the liquid ( $\gamma$ ), and thus  $\Delta G^*$  (and  $n^*$ ), remains unaffected. This is known as *homogeneous nucleation*.

The second case represents partial wetting, which reduces  $\gamma_{ef}$  and thus  $\Delta G_{ef}^*$  (and  $n^*$ ). The pre-exponent in the rate law expression is also affected (Laval *et al.* 2007). This nucleation induced by foreign particles is known as *heterogeneous nucleation*. It must be noted that heterogeneous nucleation can also occur when wetting is “better” than complete, in which case  $\theta$  becomes meaningless (Kashchiev and Rosmalen 2003).

When there is complete wetting (i.e.  $\theta = 0$ ), no energy is required to nucleate (at least in the vicinity of the surface). This can occur when a crystal has already been formed or the solution is “seeded” with crystals. Although terminology sometimes differs in this case, we will use Mullin’s nomenclature, who terms this *secondary nucleation* (Mullin 2001).

### **1.2.2.2 Kinetics**

The first kinetic analysis of the cluster approach to nucleation was made by Farkas (Farkas 1927). The principles developed by him form the approach of the CNT, and are as follows.

We consider again the free energy change that occurs in the formation of a cluster from solution as depicted in Figure 1. Since the critical size cannot be reached spontaneously through a decrease in free energy, it must be achieved another way. According to the CNT this occurs through random localized fluctuations of solute concentration causing molecular collisions, eventually leading to a combination of collisions creating a cluster

## Introduction & Theory

larger than  $n^*$ . Considering that any clusters smaller than  $n^*$  will almost immediately redissolve, and considering that  $n^*$  can be several thousand molecules, it becomes apparent that the formation of a critical nucleus is statistically a very rare occurrence.

Volmer postulated (1939) that the nucleation rate  $J$  (the number of nuclei formed per unit volume of solution per unit time) is analogous to the Arrhenius equation as follows:

$$J = A \exp\left(-\frac{\Delta G^*}{RT}\right) \quad (15)$$

Where  $A$  is the pre-exponential factor and  $T$  the temperature.

The exponential factor represents the free energy barrier, while  $A$  accounts for the kinetics of the barrier crossing. External parameters such as temperature, concentration, pressure and supersaturation affect both  $A$  and  $\Delta G^*$ , but the effect on the former is far weaker (Vekilov 2010a).

If we insert Equation (9) into Equation (15) we get

$$J = A \exp\left(-\frac{32\Omega^2\gamma_{ef}^3}{R^3 T^3 \ln^2 S}\right) \quad (16)$$

This suggests that a plot of the natural log of the induction time  $t_{ind}$  (which is an approximation of  $J$ , see Section 1.2.2.2.1) against  $\ln^2 S$  should yield a straight line whose slope will allow calculation of  $\gamma$  (Mullin 2001).

For nucleation of crystals in solutions this is generally expressed, with the exception of a special type of heterogeneous nucleation, as follows (Kashchiev 2000, Kashchiev and Rosmalen 2003):

$$J = A' S \exp\left(-\frac{B}{\ln^2 S}\right) \quad (17)$$

where

$$A' = A / \exp\left(\frac{\Delta\mu}{RT}\right) = A/S \quad (18)$$

and

## Introduction & Theory

$$B = \frac{4c^3 \Omega^2 \gamma_{ef}^3}{27R^3 T^3} \quad (19)$$

where  $c = 6$  for cubes,  $c = (36\pi)^{1/3}$  for spheres, etc.

Equation (16) represents the simplest equation relating supersaturation to nucleation rate. Its main assumption is that  $A$  is a constant. This, though perhaps in practice sometimes valid, is not actually the case (Kashchiev 2000). For that reason, Equation (17), which uses  $A'$ , can be used when  $A$  is not approximately constant under the experimental conditions.

$A'$  is either strictly or practically independent of  $\Delta\mu$  (and thence of  $S$ ) if  $T$  is kept constant (Kashchiev 2000). Therefore, a plot of  $\ln(J/S)$  against  $1/\ln^2 S$  should yield a straight line at constant temperature and pressure, with the slope yielding  $B$  (and thence  $\gamma_{ef}$ ) and the intercept  $\ln A'$ , according to Equation (17). If  $T$  is not constant (most commonly when  $S$  is varied through  $T$ ), then  $A'$  is not, strictly speaking, a constant either, since it varies with  $T$ . This dependence is very complicated and changes with the type of nucleation occurring (see (Kashchiev 2000) for some examples). In practice, however, the dependence of  $A'$  on  $T$  can be negligible also (e.g. (Laval *et al.* 2007)).

Furthermore, the interfacial tension  $\gamma$  can also depend on  $T$ , thus further complicating analysis when  $T$  is a variable (Mullin 2001). However, in practice the temperature-dependence is often neglected (e.g. (Laval *et al.* 2007)).

The effects of other internal parameters on the nucleation rate can be derived from Equation (16) to lead to this (Vekilov *et al.* 1996):

$$J = v^* Z C_0 \exp\left(-\frac{\Delta G^*}{RT}\right) \quad (20)$$

Where  $v^*$  is the rate of attachment of monomers to the nucleus,  $Z$  the Zeldovich factor that accounts for the width of the free energy profile near  $\Delta G^*$  (see Fig. 1), and  $C_0$  the concentration of nucleation sites.

## Introduction & Theory

The difficulty in measuring nucleation kinetics is that it requires determining the frequency of formation of nuclei, which current technology is not able to detect directly (Mullin 2001). Broadly speaking, there are 2 ways in which this is indirectly estimated.

### 1.2.2.2.1 Induction Time

Perhaps the simplest method according to working principle is measuring the induction time,  $t_{ind}$ , that is, the time between achievement of supersaturation and first appearance of crystals. Thus, this technique involves creating supersaturation in a solution (by changing temperature, evaporating solvent, adding another solvent, etc.) and then measuring the time elapsed between reaching supersaturation and the first appearance of crystals.

The induction time consists of a relaxation time,  $t_r$ , the time taken for the system to achieve dynamic equilibrium; the nucleation time,  $t_n$ , the time taken for the formation of the first stable nucleus; and the growth time,  $t_g$ , the time it takes for the crystal to grow to a detectable size:

$$t_{ind} = t_r + t_n + t_g \quad (21)$$

Thus  $t_{ind}$  is not a fundamental property of the system since its value depends on the technique used to measure it (Boistelle and Astier 1988). It is merely an approximation of the real fundamental property,  $t_n$ .

The nucleation rate is related to the nucleation time as follows (Kashchiev and Rosmalen 2003):

$$J = 1/Vt_n \quad (22)$$

Where  $V$  is the reactor volume.

In non-viscous systems such as most solutions,  $t_r$  is negligible (Mullin 2001), and if  $t_g$  is known or can be estimated, then  $t_n$  can in turn be estimated from the induction time. The growth time is usually estimated by measuring the growth rate of the visible crystal (e.g. (Laval *et al.* 2007)). However, this is not necessarily valid since micromolecular growth

## Introduction & Theory

might occur at a different rate (and even different mechanism) than macromolecular growth (Mullin 2001). Thus we can say that for non-viscous systems:

$$J \approx 1/V(t_{ind} - t_g) \quad (23)$$

Inaccuracy can occur in the creation of supersaturation, see Figure 3; the supersaturation should be achieved as fast as possible, such that the time from achieving supersaturation to the first appearance of nuclei ( $t_2$ ) is far greater than the time taken to achieve the supersaturation of interest ( $t_1$ ).

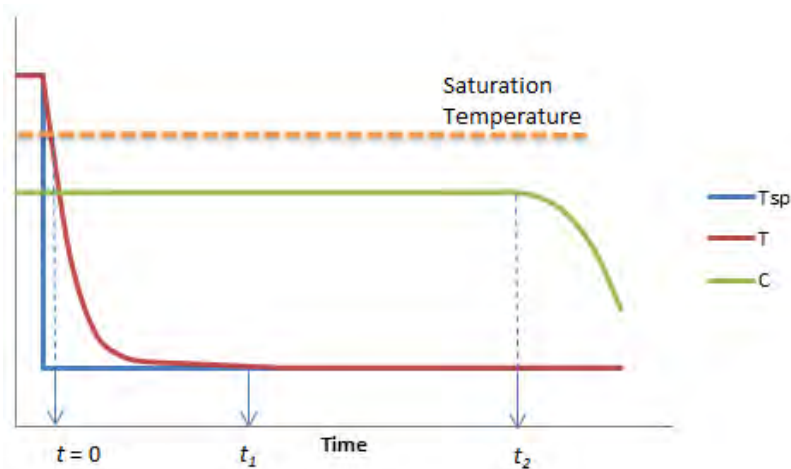


**Figure 3: Induction time measurement in which supersaturation is controlled using temperature. T is actual solution temperature, Tsp is set point temperature, C is the solution concentration,  $t = 0$  is point in time when supersaturation is first achieved,  $t_1$  is time taken for Tsp to actually be reached, and  $t_2$  the appearance of the first crystal.**

There are several techniques used to detect nucleation, such as microscopy (Dombrowski *et al.* 2007, Laval *et al.* 2008, Ildefonso *et al.* 2011), IR (Lindenberg and Mazzotti 2009), UV (Judge *et al.* 1995), Raman (Schwartz and Berglund 1999), static and dynamic light scattering (Muschol and Rosenberger 1995) to monitor solution concentration, as well as FBRM (Lindenberg and Mazzotti 2009, Mitchell *et al.* 2011), electrical conductivity (Graber *et al.* 1999), turbidity (Boistelle and Astier 1988), visually (Nordström *et al.* 2012), and ultrasonic velocity (Hodate *et al.* 1997).

1.2.2.2.2 Double-Pulse

The second technique, known as the “double pulse” method (Tsekova *et al.* 1999), aims to eliminate the problem of estimating  $t_g$  and  $t_n$  by decoupling nucleation and growth. It also has the significant advantage of being able to easily distinguish between homogeneous and heterogeneous nucleation (Galkin and Vekilov 1999).

A saturated solution is brought to a temperature  $T_1$  (the first “pulse”) at which nucleation will occur within the experimental time-frame, and is kept there for a certain time  $\Delta t_1$ . Then the temperature is changed to  $T_2$  *inside* the metastable zone (the second “pulse”) where no nucleation will occur, but the nuclei that have already formed will grow to a detectable size (see Figure 4). The nucleation rate can then be determined from the number of crystals (which are counted using a microscope) and  $\Delta t_1$ , presuming that the supersaturation is not significantly reduced by the crystallization occurring during  $\Delta t_1$ . An alternative to controlling supersaturation for this technique is to change the supersaturation by changing reactor volume instead of changing temperature, which is done using custom-built reactors (Gerdtts *et al.* 2004, Gerdtts *et al.* 2006).

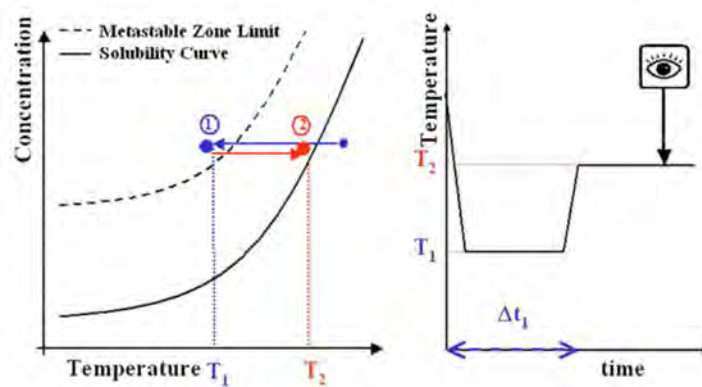


**Figure 4: The principle of the double pulse technique. On the left is shown the reaction profile in the phase diagram, and on the right a temperature profile. The metastable zone limit is the limit at which nucleation will not occur during the experimental time-frame, even though the solution is supersaturated. Source: (Revalor *et al.* 2010)**

The main problem with this technique is that it can drastically underestimate the number of nuclei formed during the first “pulse” (Dixit *et al.* 2001). Consider what happens during the second pulse: the temperature is raised, thus reducing supersaturation, with the aim of preventing further nucleation but allowing growth of existing crystals. If we

define  $n_1^*$  and  $n_2^*$  as the critical nucleus sizes during the first and second pulse, respectively, it follows from Equation (8) that  $n_1^* < n_2^*$ . This means that any nuclei formed during the first pulse which are smaller than  $n_2^*$  when the second pulse is applied will shrink and dissolve, since the critical nucleus size is the minimum size for a stable nucleus and any nuclei below this are unstable and will dissolve (see Sections 1.2.2.1 and 1.2.2.2).

### **1.2.3 Polymorphism**

Further complicating matters is the fact that compounds can form different crystal structures (known as *polymorphs*) which have the same chemical formula but differ in crystal packing, conformers, or a combination of both (Chen and Trout 2008). They have different physical properties, such as melting point, solubility, rheology, crystal shape (morphology), etc. (Mullin 2001).

In terms of thermodynamics and kinetics, differences are seen in that different polymorphs have different solubilities, and hence different supersaturations at the same conditions. But more importantly, different polymorphs will have different  $\gamma$  and through this different  $\Delta G^*$  and  $n^*$ , and thus different  $J$ .

Polymorphism can greatly complicate crystallisation processes. From a pharmaceutical perspective, the difference in solubility will affect bioavailability, while differences in crystal shape and rheology will affect processing such as filtration. Patents are granted for a specific polymorph, such that a competitor who discovers a new polymorph could bring it to market before the original patent expires.

It is not always the most stable form that nucleates first; in fact, it is often (though not always) the case that a metastable form preferentially nucleates. First discovered in the early part of the 19<sup>th</sup> century (Mullin 2001), it was Ostwald who generalised this behaviour several decades later (Ostwald 1897). He postulated a “rule of stages”, whereby a system doesn’t transform to the most stable state but to the one with the least free energy difference. However, the phenomenon is much more complicated, having now been shown to include competing nucleation rates (i.e. kinetics) as well as structural relationships between the solution and the nucleating form (Mullin 2001).

## Introduction & Theory

Seeding a solution with a specific polymorph will almost always result in the preferential crystallisation of that polymorph from solution (Mullin 2001). The famous shortage of the HIV protease inhibitor Norvir in the 1990s was traced to this phenomenon (Rodríguez-Hornedo and Murphy 1999). After multiple crystallisation cycles a new polymorph had nucleated, which, despite routine cleaning, always seeded subsequent crystallisation batches, thus preventing the licenced polymorph from forming.

Relative polymorph stability can also be quite complicated, since it is temperature-dependent. Polymorphs whose stability order reverses at a certain temperature are *enantiotropic*; otherwise they are *monotropic*. Ammonium nitrate's five known polymorphs, for example, exhibit four different enantiotropic changes at different temperatures (Mullin 2001). Identifying the stability relationship can be a complicated and time-consuming matter. For example, the (commercial) form I<sup>L</sup> of tolbutamide was for many years considered to be more stable than form II, but has recently been shown to be less stable (Thirunahari *et al.* 2010).

Further adding to the complexity, solvent molecules can be incorporated into the crystal lattice to form solvates (sometimes known as *pseudopolymorphs*).

Finally, it has been generally observed that the number of polymorphs discovered for a compound is a function of the time spent investigating the compound. Thus, it is technically more correct to speak of the “most stable *known* polymorph” rather than of the “stable polymorph”.

### **1.2.4 Stochasticity**

Nucleation is usually considered to be a stochastic process, which becomes visible at small volume scales by giving a distribution of induction times for identical experiments (Izmailov *et al.* 1999, Goh *et al.* 2010). The accepted theory for how nucleation occurs as detailed in Section 1.2.2.2 explains this stochasticity: Nucleation occurs through *random localized fluctuations* in solute concentration leading to a cluster sufficiently-large to overcome the free energy barrier (Izmailov *et al.* 1999).

Distributions of induction times under identical conditions have also been reported with reactor volumes up to 20 mL (Gracin and Rasmuson 2004, Jiang and ter Horst 2010, Yang and Rasmuson 2013, Yang *et al.* 2014, Mealey *et al.* 2015a, Mealey *et al.* 2015f). These distributions have been modelled with Poission (Galkin and Vekilov 1999, Dombrowski *et al.* 2007) and Gamma (Izmailov *et al.* 1999) distributions, a Master equation (Goh *et al.* 2010) and the probability that crystallization will have occurred in a droplet after a certain time (Laval *et al.* 2007). Some have found lognormal distributions to give the best fit to the data (Mealey *et al.* 2015a, Mealey *et al.* 2015f).

### **1.2.5 Influence of Solvent**

One promising approach to understanding nucleation is studying its dependence on the solute/solvent interaction in the case of crystallisation from solution. The sensitivity of nucleation to solution chemistry has been known over 100 years (Ostwald 1897), and is perhaps best demonstrated in the decisive influence that the choice of solvent can have on the nucleating polymorphic form (Teychené and Biscans 2008).

A general inverse proportionality between solubility and interfacial energy has been observed for inorganic molecules in aqueous solutions and can be deduced from general solution theory (Mullin 2001). It has also been reported for paracetamol in different organic solvents (Omar *et al.* 2006). For other organic systems interfacial energies in different solvents have been correlated with intrinsic solvent properties such as solvent boiling points (Yang and Rasmuson 2013) and solvent-solute interaction properties such as solvation and deformation energies (Yang *et al.* 2014) as well as strength of solvent-solute binding and subsequent desolvation (Khamar *et al.* 2014, Mealey *et al.* 2015f).

Furthermore, evidence is growing that the structural arrangement of clusters of solute molecules in solution affects the subsequent nucleation. This is known as the “link” hypothesis, whereby synthons formed in solution (such as dimers) are hypothesised to lead to polymorphs with the same synthons preferentially nucleating. The first direct evidence was reported for concentrated solutions of tetrolic acid, where FTIR analysis found dissolved tetrolic acid to exhibit hydrogen bonding motifs similar to those found in the nucleating polymorph (Parveen *et al.* 2005). Further investigation found a similar relationship between the synthons of benzoic acid in solution and in the nucleated

## Introduction & Theory

polymorph, though such a relationship was not found for mandelic acid (Davey *et al.* 2006). It was also demonstrated for nicotinamide that different solvents consistently nucleate different polymorphs, with FTIR and Raman spectroscopy suggesting that solvents in which nicotinamide exists as chain-like clusters nucleate chain-like polymorphs, whereas solutions in which nicotinamide forms dimers nucleate the dimer polymorph (Kulkarni *et al.* 2012). Molecular dynamics simulations corroborate the influence of solvent on the solute synthon formation (Chen and Trout 2008).

Related to the “link” theory is the influence of the solute conformation on the polymorphic form and rate of the nucleating crystals, for which the literature is vast and has recently been reviewed (Derdour and Skliar 2014). In general, it is found that the closer the conformational population in solution is to the conformer(s) in the nucleating crystal structure, the faster the nucleation will be (Petit *et al.* 1994). Different solvents can cause solute molecules to assume vastly different conformations, with the result that different solvents can nucleate different conformational polymorphs (Kitamura *et al.* 2012).

Finally, the solvent can also influence nucleation through its effect on the frequency of collisions. According to the CNT, this is accounted for in the pre-exponential factor (Eqn. 16 and 20) using different models, and strong correlations with experimental nucleation data have in some cases been found (Nordstrom *et al.* 2013).

### **1.2.6 Solution History Effect on Nucleation**

Thermal history of solution effects refer to the observation that the thermal pretreatment of a solution, i.e. prior to being brought into a state of supersaturation, may influence the nucleation behaviour of the solute. First reported in 1902 (Schaum and Schoenbeck 1902), an effect on crystallization of thermal solution history has been demonstrated for melts of organic compounds (Hinshelwood and Hartley 1922). Metals (Webster 1933) and polymers (Boon *et al.* 1968), as well as for aqueous and organic solutions of inorganic salts (Nakai 1972) and organic molecules (Nyvlt 1963) including proteins (Burke *et al.* 2001). Interesting results on this effect have also been presented for the nucleation of clathrate hydrates (Buchanan *et al.* 2005). In general, it is reported that increased preheating temperature and preheating time lead to slower crystallization

## Introduction & Theory

kinetics. Recently, Nordström *et al* (Nordström *et al.* 2012) gave a comprehensive summary of previous work in this area, as well as additional experimental evidence demonstrating that not only the rate of nucleation but also the polymorphic outcome in crystallization of m-hydroxy benzoic acid was influenced by the temperature and time of solution preheating. That solution pretreatment affects the polymorphic outcome has also been demonstrated in the case of aluminium hydroxide (Gerson *et al.* 1996).

The exact mechanism(s) behind thermal history effects has not yet been determined. Three different principles have been hypothesized (Buchanan *et al.* 2005, Nordström *et al.* 2012):

1. Even after the solid phase has completely dissolved, the solution temporarily contains locally higher concentrations, and/or the molecules in the dissolved state retain, for some time, structural features from the solid and/or the dissolution process.
2. Trace amounts of crystalline solids become very difficult to dissolve or are even thermodynamically stabilized by adhering to flat surfaces or being trapped in capillary cavities on the crystallizer walls.
3. Heterogeneous solid particles that promote nucleation dissolve, melt very slowly or are gradually deactivated at higher temperatures.

The analysis of Nordström *et al* (Nordström *et al.* 2012) suggests that the first mechanism is most likely to be relevant. Regardless of the precise mechanism responsible, history of solution effects can contribute to make industrial processes less reproducible. However, perhaps the most important aspect of history of solution is that this phenomenon most likely carries information about clustering of molecules in solution.

# II

## **2 Materials & Experimental Methodologies**

## 2.1 Materials

All materials were used as-received without further purification.

Table 2. Source and mass fraction purity of chemicals.

Chemical Name	Source	Purity
Fenoxycarb	Syngenta Switzerland	0.986
Tolbutamide	Sigma-Aldrich	0.997
Isopropanol	VWR	0.997
N-propanol	VWR	0.995
Methanol	Sigma-Aldrich	0.999
Ethanol	Sigma-Aldrich	0.998
Ethyl acetate	Sigma-Aldrich	0.997
Toluene	Sigma-Aldrich	0.999
Acetonitrile	VWR	0.999
Acetone	VWR	0.999
Acetic Acid	Sigma-Aldrich	0.997
Deuterated Chloroform (0.03% TMS)	VWR	0.998

### 2.1.1 Fenoxycarb

Fenoxycarb has chemical formula  $C_{17}H_{19}NO_4$  and systematic name *2-(p-phenoxyphenoxy)ethylcarbamate* and is shown in Figure 1. It is a flexible organic molecule that exhibits conformational isomerism in its single reported crystal form. (Karpinska *et al.* 2012) It is produced industrially as an insect growth regulator with juvenile hormone activity (Masner *et al.* 1987). Its melting temperature and enthalpy are reported as  $53.16 \pm 0.14$  °C and  $26.98 \pm 0.04$  kJ mol<sup>-1</sup>, respectively (Xiao-Hong *et al.* 2005). It is practically insoluble in water.

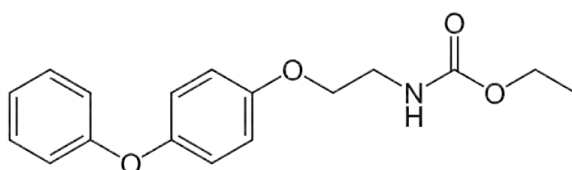
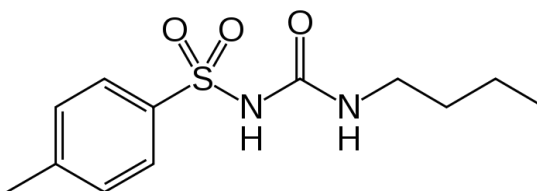


Figure 5: Molecular structure of fenoxycarb.

### 2.1.2 Tolbutamide

Tolbutamide is a first-generation oral anti-diabetic drug that stimulates the secretion of insulin in the pancreas and is used in managing type II diabetes (Thirunahari *et al.* 2010). It has chemical formula  $C_{12}H_{18}N_2O_3S$ , systematic name *n*-[(*Butylamino*)carbonyl]-4-methylbenzenesulfonamide, and is shown in Figure 6. A flexible organic molecule, it has six reported crystal forms, with a known stability order below 38 °C of Form II > I<sup>L</sup> > III > IV, where II is most stable and melts at 117 °C (Thirunahari *et al.* 2010, Nath and Nangia 2011); form I<sup>H</sup> is inaccessible below 38 °C (Hasegawa *et al.* 2009); and the exact relative stability of form V has not yet been determined, although it is highly unstable at room temperature, transforming to form I within several hours (Nath and Nangia 2011). Cooling crystallisation from pure solvents has only been reported in ethanol, where forms II, I<sup>L</sup> and III can all nucleate as follows (Thirunahari *et al.* 2011): for long induction times form II nucleates, otherwise forms I<sup>L</sup> and III nucleate at low and high cooling rates and supersaturations, respectively. Though poorly water-soluble (Forster *et al.* 2001), solubilities for pure non-aqueous solvents are only reported for ethanol and above 15 °C (Thirunahari *et al.* 2010).



**Figure 6: Molecular structure of tolbutamide.**

## 2.2 Experimental Methodologies

### 2.2.1 Solubilities

Solubilities were measured for all solute/solvent combinations that had previously been identified as suitable for induction time work (see section 2.2.2.1).

The solubility reflects the equilibrium between two different phases: the solute as a solid phase and the solute in solution. At least one third of all organic compounds are polymorphic, i.e. they can form different crystals structures. Since the physical

## Materials & Experimental Methodologies

properties differ for polymorphs of the same compound, the solubility of a compound depends on the polymorph, and it is vital that solubility measurements are associated with a proper identification and control of the solid phase (Maher *et al.* 2010, Maher *et al.* 2012). Accordingly, we also performed an investigation of the solid phase for which the solubility data is determined.

Solubility was determined using a modification of a published gravimetric technique (Nordström and Rasmuson 2006b, Maher *et al.* 2010) which is considered to be one of the most accurate methods for measuring solubility (Threlfall 2009). Solutions saturated at predetermined temperatures were created by adding an excess of solid to a solvent in a sealed vial (30 ml, PTFE/EDPM screw cap), equipped with a magnetic stirring bar (0.5 x 0.128 in), placed on top of a submersible magnetic stirring plate (2Mag) in a temperature-controlled water bath (Grant GR150, stability  $\pm 0.005$  C° and uniformity  $\pm 0.02$  C° at 37 °C). The temperature of the water bath was measured with a calibrated digital thermometer (Dostmann P650, accuracy  $\pm 0.03$  C°).

In the case of fenoxycarb, the solutions were stirred for 12 hours at 400 rpm, followed by a 6 hour settling period during which the stirring was turned off. Syringes (5 ml) and syringe filters (0.2  $\mu$ m PTFE) were pre-heated/cooled to the same temperature as the water bath. These were then used to filter ~0.5 ml of the supernatant into pre-weighed glass vials, which were quickly sealed to prevent evaporation. The vials were weighed, uncovered and placed in a fume hood for solvent evaporation, weighed regularly until fully dried ( $< 0.1\%$  mass loss over 48 hours) and the solubility calculated. The balance used had an accuracy of  $\pm 0.0001$  g. To test the repeatability of achieving an equilibrated solution, the solubility at 5, 10 and 15 °C was determined in duplicate. The repeatability of the filtration and drying processes was tested by filtering and drying the 20, 30 and 40 °C supernatants in duplicate. The concentration of a known solution of fenoxycarb in isopropanol was also determined by the same gravimetric method and differed only 0.25% from the known concentration. To verify that 12 hours of equilibration is sufficient to achieve equilibrium, saturation was also approached from supersaturation as follows. The solutions were heated 10 C° *above* the desired temperature and stirred for 12 hours, allowing most of the excess solid to dissolve. The water bath was then set

## Materials & Experimental Methodologies

to the desired temperature, and the solutions left stirring at this temperature for 12 hours. The solids were allowed to settle for 6 hours and the supernatant analysed as above. This was done only for the lowest temperature analysed (i.e. 5 °C) since it was presumed that reaching equilibrium would be slowest at this temperature. The solubility slurries were analysed using PXRD and NMR to verify that no polymorphic conversion had occurred.

Since induction times for tolbutamide were measured for the nucleation of the metastable form I<sup>L</sup>, solubilities had to be measured for the same metastable form of tolbutamide. The measurement of the solubility of any polymorph other than that considered stable becomes significantly more complex, as it is necessary to verify the solid phase for which solubility is being measured with much greater detail. Furthermore, it must be proven that equilibrium can be reached before the transformation to the more stable form begins. Thus, tolbutamide solubilities for the as-received metastable form I<sup>L</sup> were measured with several modifications to the technique used for fenoxycarb above. Vials were duplicated instead of duplicating samples from vials, and slurries were allowed to equilibrate for only 1 h. For each solvent, the time to reach equilibrium concentration was measured at 2 °C, corresponding to the lowest  $T_{cry}$ , where this process is presumably the slowest, by taking samples after 3 successive 1 h equilibration cycles following an initial 0.5 h cycle, and after a final 12 h equilibration. In all cases there was no significant variation in concentration after the first measurement (i.e. after 0.5 h), and the crystal form of the slurry was verified to still be pure form I<sup>L</sup> by PXRD. This is in keeping with literature reports of transformation times in ethanol of around 2-3 h at room temperature (Thirunahari *et al.* 2010, Thirunahari *et al.* 2011). The absence of transformation was also confirmed by PXRD for slurries of each solvent at their respective highest  $T_{cry}$  after a 1 h equilibration.

### **2.2.2 Induction Times**

#### **2.2.2.1 Exploratory Work**

The transition from identifying a solute/solvent combination of interest, to collecting useful induction time data, is quite lengthy and complex. In the process, several solute/solvent combinations, or even entire solutes, are usually discarded as unsuitable

## Materials & Experimental Methodologies

for induction time experiments. The following conditions must be met before induction times can be collected for further analysis:

- The crystallising polymorph must be identified.
- No significant degradation may occur during the course of the induction time experiments, as this would reduce the concentration of the crystallising species to an unknown amount, and the resultant impurities could influence the nucleation.
- Crystallisation must be detectable by the chosen detection method. In our case, visual detection was chosen due to its simplicity. Thus, crystallisation of very low solubility solute/solvent systems had to be avoided.
- Induction times must be within reasonable time frames. They should be significantly greater than the time taken to reach the equilibrium temperature, which in our case was less than 10 minutes (see below). And they should not exceed two to three days.

In practice, this requires several weeks of exploratory induction time work, in which many solute/solvent/concentration/crystallisation temperature combinations are tested for the above criteria. The result of this work was identification of the combinations for which induction time data was then collected as outlined below.

### **2.2.2.2 Final Induction Time Measurement**

A procedure published previously was followed closely (Nordström *et al.* 2012). For each solute/solvent combination, a stock solution of known concentration, identified as suitable according to the preceding section, was prepared by adding the powder to the solvent in a bottle. This was dissolved for at least 12 h in a sealed vessel with a large magnetic stir bar spinning at 400 rpm, and the vessel submersed in a water bath (same specifications as water bath used in solubility work) set to a certain dissolution temperature,  $T_{diss}$ . This temperature was above the saturation temperature for the given concentrations, namely 25 °C for fenoxycarb in isopropanol and all tolbutamide solutions, and 45 °C for the other fenoxycarb solutions. 20 mL portions were aliquoted into glass vials (30 mL) using syringes (20 mL) equipped with 0.2 µm PTFE filters and pre-heated or pre-cooled to  $T_{diss}$  to prevent crystallisation during filtration. The number

## Materials & Experimental Methodologies

of 20 mL vials prepared this way was as follows: 29 for fenoxycarb in isopropanol, 6 for fenoxycarb in each of the other solvents, and 30 for each of the tolbutamide solutions. Magnetic stir bars (1.27 x 0.325 cm) were added to these vials, which were then closed using PTFE-sealed screw caps, placed into a cold water bath set to  $T_{cry}$ , and the time to first appearance of crystals in each vial, the induction time ( $t_{ind}$ ), recorded with a video camera. The time to reach a temperature deviating by 1 C° from the final value was measured to be approximately 1 minute (Dostmann P750 with Pt100 immersion probe, accuracy 0.03 C°). It took about 7 minutes to reach the nucleation temperature within 0.03 C°.

A distribution of induction times is obtained similar to studies reported in the literature (Izmailov *et al.* 1999, Goh *et al.* 2010, Jiang and ter Horst 2010). For fenoxycarb, a lognormal function was fitted to each distribution to smooth the data, giving a reasonable fit. Lognormal distributions are seen in many data sets from different scientific disciplines, and are indicative of random variation resulting from multiple independent factors which have a multiplicative effect on the measured quantity (Limpert *et al.* 2001). For each distribution of fenoxycarb induction times, the geometric mean of the lognormal fit, which corresponds to the median of the distribution, is taken as the best point estimate of the central tendency of the induction time. For tolbutamide, the median of the experimental data was employed without fitting.

For any distribution of induction times, both  $t_g$  and  $t_r$  can be assumed not to vary on the assumption that  $t_g$  and  $t_r$  themselves are deterministic, since the solutions are identical in terms of supersaturation, concentration, etc. It should be noted that recent modelling has suggested that  $t_g$  may be stochastic (Maggioni and Mazzotti 2015). Nevertheless, proceeding on the assumption that it is not,  $t_g + t_r$  must as a consequence be less than the smallest  $t_{ind}$  recorded for each distribution, which in our experiments is negligible (at most a few minutes) compared to the median  $t_{ind}$  (at least 40 minutes) values. Thus, equation 23 becomes:

$$J \approx 1/Vt_{ind} \tag{24}$$

## Materials & Experimental Methodologies

Due to the lognormal shape of the  $t_{ind}$  distributions, the last vials can take excessively long to nucleate. Hence, it becomes unfeasible to wait for all vials to nucleate before starting the next experimental iteration. Accordingly, experiments were often stopped once more than 50% of vials had nucleated, and the remaining vials were shaken vigorously to induce crystallization prior to the next induction time experiment.

Regarding tolbutamide, relevant solubility data for tolbutamide has not been reported, and due to time constraints saturation temperatures ( $T_{sat}$ ) were not measured. Thus, the following steps were taken to ensure complete dissolution prior to creating supersaturation, despite precise  $T_{sat}$  for the solutions not being known. Approximate solubility measurements (not reported) indicated all  $T_{sat}$  were less than 20 °C. After mixing of solute powder and solvent, stock solutions were dissolved with stirring at 25 °C for at least 12 h (visual homogeneity was achieved after several minutes). After aliquoting and filtering as outlined previously, vials were heated to 35 °C prior to crystallisation at  $T_{cry}$ , and were subsequently kept at 35 °C for at least 3 h between successive crystallisation cycles. This filtration at 25 °C followed by heating to 35 °C ensured complete dissolution despite the absence of precise  $T_{sat}$  data.

To investigate the fenoxycarb thermal history of solution effect on nucleation, the contents of 29 aliquoted vials were redissolved, without opening, at certain pretreatment temperatures,  $T_{PT}$ , for different pretreatment times,  $t_{PT}$ . After this pretreatment, the vials were returned to the 5 °C water bath, and the induction times again recorded as previously. This procedure was repeated to investigate the effect of different combinations of  $T_{PT}$  and  $t_{PT}$  on the induction times. Each set of conditions was usually repeated three times to give a total of 75 data points per condition set (4 out of the 29 vials are ignored in the analysis for reasons outlined in section 5.1) in order to capture stochastic variation. The experiments were carried out in a more or less random order such that the same conditions were never directly repeated. Some sets of conditions were repeated a different number of times and are identified as such. Crystallization was induced in the remaining homogeneous solutions by vigorous manual shaking to ensure all solutions had crystallised prior to redissolving.

## Materials & Experimental Methodologies

To investigate the influence of solvent on the nucleation of fenoxycarb and tolbutamide, it was necessary to measure  $t_{ind}$  corresponding to at least three different thermodynamic driving forces for each solvent/solute combination. To this end,  $T_{PT}$  and  $t_{PT}$  were kept constant (45 °C for 24 h in the case of fenoxycarb to preclude the possibility of solution history; 35 °C for at least 3 h in the case of tolbutamide) while  $T_{cry}$  was varied to scan different combinations of  $S$  and  $T_{cry}$ .

### **2.2.3 Tolbutamide Solid Phase Characterisation**

Tolbutamide is reported to nucleate during cooling crystallisations in pure ethanol as either form II, I<sup>L</sup> or III, depending on  $t_{ind}$ ,  $S$  and cooling rate (Thirunahari *et al.* 2011). Absolute values of these conditions, however, cannot be compared to our work, since our work was carried out at 20 mL compared to over 400 mL in the literature, and we did not measure meta-stable zone widths but  $t_{ind}$ . We performed preliminary induction time experiments under experimental conditions and analysed the crystallised form using transmission PXRD. This was done within several minutes of crystallisation to minimise polymorphic transformation. In these exploratory experiments, all recrystallised tolbutamide was found to be form I<sup>L</sup>. We decided to carry out spot-checks on the final  $t_{ind}$  experiments to verify the crystallisation of only form I<sup>L</sup> by similarly analysing the crystal form of a vial with a short and a long  $t_{ind}$  of each of the lowest and highest  $S$  experiment performed last for each solvent (see stars in Figure 13). This was done during the last iteration of the respective crystallising conditions because extraction of slurry renders a vial unusable (the concentration, and thus  $S$ , having changed). In acetonitrile, ethyl acetate and toluene, form I<sup>L</sup> was found in each case. However, in n-propanol two vials were found to contain pure form I<sup>L</sup> and the other two pure form II. Repeating the n-propanol experiments and checking more vials found that both forms could nucleate non-concomitantly at either short or long  $t_{ind}$  and at either low or high  $S$ .

The nucleation of multiple forms of tolbutamide in n-propanol renders the  $t_{ind}$  data collected for this solvent unusable for calculating  $\gamma$  since it is impossible to know which form nucleated for the majority of induction times collected. Thus it was necessary to repeat tolbutamide n-propanol induction time experiments while monitoring the crystal

## Materials & Experimental Methodologies

form nucleating in each case using Raman spectroscopy *without opening the vials to allow re-using them* as follows.

Raman spectra of n-propanol slurries and pure powders of both pure form II and pure form I<sup>L</sup> tolbutamide (as determined by PXRD) were obtained. Comparing the four spectra (Figure 7), the peaks at 1160 and 1165 cm<sup>-1</sup> were found to be unique to forms I<sup>L</sup> and II in tolbutamide n-propanol slurries, respectively. In the repeat n-propanol  $t_{ind}$  experiments, the Raman spectrum for each vial was obtained less than 8 h after crystallisation in the same manner as for the slurries of known polymorphic form (under experimental conditions no trace of form II was detected by either PXRD or Raman in slurries of form I<sup>L</sup> after 8 h). About 60% of vials at each condition were found to be form I<sup>L</sup> without a form II peak and 30% form II without a form I<sup>L</sup> peak, both types of Raman spectra being identical to those of their respective slurries of known, pure forms. The remaining 10% were inconclusive. Only the induction times corresponding to the 60% of confirmed form I<sup>L</sup> were kept for subsequent analysis. Interestingly, a vial usually nucleated the same form in successive experiments (i.e. either only form I<sup>L</sup> or form II), and the  $t_{ind}$  distributions at each  $T_{cry}$  for both forms I<sup>L</sup> and II were mostly indistinguishable (Figure 13), though insufficient data for form II at 6 and 7 °C were collected for these conclusions to be statistically significant.

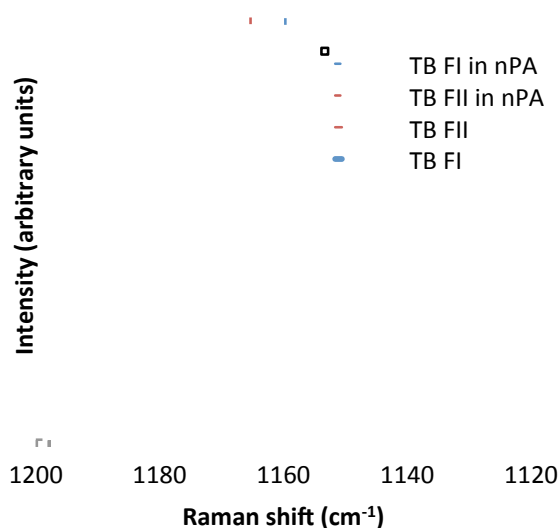


Figure 7: Raman shifts distinguishing between tolbutamide forms I<sup>L</sup> and II as powders (solid lines) and slurries of n-propanol (dashed lines). Vertical lines indicate peaks unique to forms I<sup>L</sup> (blue) and II (red).

## 2.3 Analytical Techniques

Several techniques were used to analyse the identity, purity and solid form of crystals, and the concentration of solutions.

### 2.3.1 X-Ray Diffraction (XRD)

For fenoxycarb, reflection XRD was performed by placing the ground powder sample on a silicon crystal zero-background disc, smoothed with a glass slide, and analysed using a Phillips PANalytical X'Pert MPD Pro with a PW3064 sample spinner, Cu K $\alpha$  source ( $\lambda = 1.5418 \text{ \AA}$ ), nickel filter, fixed divergence slit of  $1/2^\circ$ , and accelerating voltage and anode current of 40 kV and 35 mA, respectively. Data was collected from  $5 - 70^\circ 2\theta$  in steps of  $0.0167^\circ$  at a rate of 19.685 s/step and a sample rotation of 15 rpm using PANalytical Data Collector, version 2.0.

For tolbutamide an XRD instrument capable of transmission was available. Transmission significantly reduces preferred orientation effects, and thus sample preparation such as grinding is often not needed. Combined with the increased speed at which diffraction patterns could be collected with this instrument in transmission mode, all subsequent XRD work was performed with this instrument as follows. An Empyrean

## Materials & Experimental Methodologies

diffractometer (PANalytical, Phillips) with Cu K $\alpha$  radiation ( $\lambda = 1.5406 \text{ \AA}$ ) at room temperature was used to record data at a vial voltage and current of 40 kV and 35 mA, respectively, applying a step size of  $0.0131^\circ$  ( $2\theta$ ) and a scan speed of  $0.164^\circ$  ( $2\theta \text{ s}^{-1}$ ) in the angular range of 5 to  $35^\circ$  in  $2\theta$  and a sample rotation of 4 rpm.

Experimental PXRD spectra were compared to theoretical PXRD spectra calculated using the software package Mercury (CSD System) from the crystal structures found in the Cambridge Crystal Structure Database (CCSD). For both tolbutamide and fenoxycarb all relevant polymorphs have their structures reported in CCSD.

### **2.3.2 Nuclear Magnetic Resonance (NMR)**

In this thesis only molecules of known identity were studied. Therefore, NMR was used only for fast purity checks and concentration measurements. For the former, it is expected that impurities of more than 2-5% mole fraction would be observable in the NMR spectrum if they contain  $^1\text{H}$  isotopes (since only  $^1\text{H}$  NMR was done). Concentration measurements of roughly the same accuracy can be made by measuring the ratio between the integrals of a peak without interference from other peaks for each species divided by the number of protons responsible for the peak. This gives the molar ratio.

$^1\text{H}$  was the isotope chosen to be studied due to its prevalence in all chemicals used and the speed at which its NMR spectrum can be measured. NMR spectra were collected as follows. For powders, an amount fitting on the tip of a spatula was dissolved in 0.7 mL of deuterated chloroform (99.8% deuteration, 0.03% TMS, VWR BDH Prolabo), while for solutions 10  $\mu\text{L}$  were added.  $^1\text{H}$  solution NMR spectra were obtained at 270 MHz using a JEOL JNM-GSX 270 FT NMR.

### **2.3.3 Raman Spectroscopy**

A non-contact probe attached to a Kaiser RamanRxn2 Analyzer with an Invictus 785 nm NIR laser set to 200 mW was used to obtain Raman spectra. iC Raman software, version 4.1, was used to collect the spectra from  $150 - 3,400 \text{ cm}^{-1}$  with an exposure time of 15 s, 3 accumulations, a resampling interval of  $1 \text{ cm}^{-1}$ , cosmic ray removal, and intensity correction.

#### **2.3.4 Scanning Electron Microscopy (SEM)**

Dried samples both before and after grinding were spin-coated with gold and analysed using a JEOL CarryScope Scanning Electron Microscope JCM-5700.

#### **2.3.5 Differential Scanning Calorimeter (DSC)**

Using a PerkinElmer Pyris 1 Differential Scanning Calorimetry (DSC) instrument, the thermal properties of the dried, ground fenoxycarb samples in the solubility work were measured by placing around 5 mg of a sample into a 40 uL aluminium pan without holes, which was then sealed by a 30 uL aluminium lid with holes and placed into the sample holder. The reference pan consisted of the same two aluminium pans without sample. The sample was heated from 15 to 70 °C at a rate of 1 C° min<sup>-1</sup> (the first cycle), cooled back to 15 °C at 100 C° min<sup>-1</sup>, held at that temperature for 10 minutes and then reheated to 70 °C at 1 C° min<sup>-1</sup> (the second cycle). After baseline subtraction, the melting point (extrapolated onset temperature) and enthalpy of fusion were calculated.

# III

## 3 Solubilities

## Solubilities

### 3.1 Tolbutamide

The solubilities of tolbutamide metastable form I<sup>L</sup> were measured for each combination of solvent and  $T_{cry}$  used in the induction time experiments (Table 3). Due to time constraint, solubilities were not determined at any other temperatures. Approach to equilibrium results show that, within the rather large uncertainties of the final results (see sd values in Table 3) the solutions reached saturation after 0.5 h (Figure 8), which is faster than the equilibration time used for the solubility values (1 h).

**Table 3: Mole fraction solubilities ( $x_{eq}$ ) of tolbutamide at temperature  $T$  in various solvents, along with standard deviations (sd).  $x_{eq}$  and  $sd$  units are  $10^{-4}$ .**

$T$ (°C)*	Toluene		Acetonitrile		Ethyl acetate		N-propanol		Ethanol	
	$x_{eq}$	$sd$	$x_{eq}$	$sd$	$x_{eq}$	$sd$	$x_{eq}$	$sd$	$x_{eq}$	$sd$
2	6.57	0.41	51.52	0.01	80.72	0.17	55.82	3.15	64.11	6.03
3					82.91	0.24			69.95	0.15
4	7.35	0.42	59.09	0.69	88.72	0.38	63.69	5.70	75.45	0.52
5			63.63	0.03	91.08	0.94				
6	8.09	0.59					66.69	3.73		
7			70.18	0.28	99.72	0.48	68.84	0.90	86.77	0.28

\* Standard uncertainty  $u(T) = 0.2$  C°.

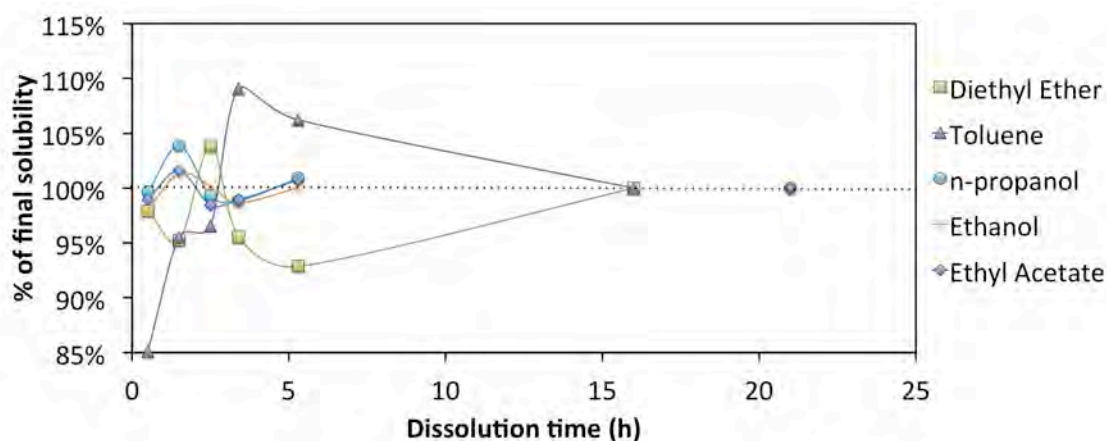


**Figure 8: Approach to equilibrium for tolbutamide form I<sup>L</sup> at 1.92 °C. For each data point, the polymorphic identity was confirmed to be pure form I<sup>L</sup> by PXRD. The fluctuations are of the same magnitude as the sd values of the concentration measurements (see Table 3).**

At the low temperatures and small temperature ranges for which solubilities were measured, the solubilities are highly linear (Figure 9), which is not unusual far from the melting point. The mole fraction order of solubilities decreases in the order ethyl acetate

## Solubilities

> ethanol > [n-propanol & acetonitrile] >> toluene, where the difference between n-propanol and acetonitrile is not significant, and tolbutamide is an entire order of magnitude less soluble in toluene than in the other solvents.

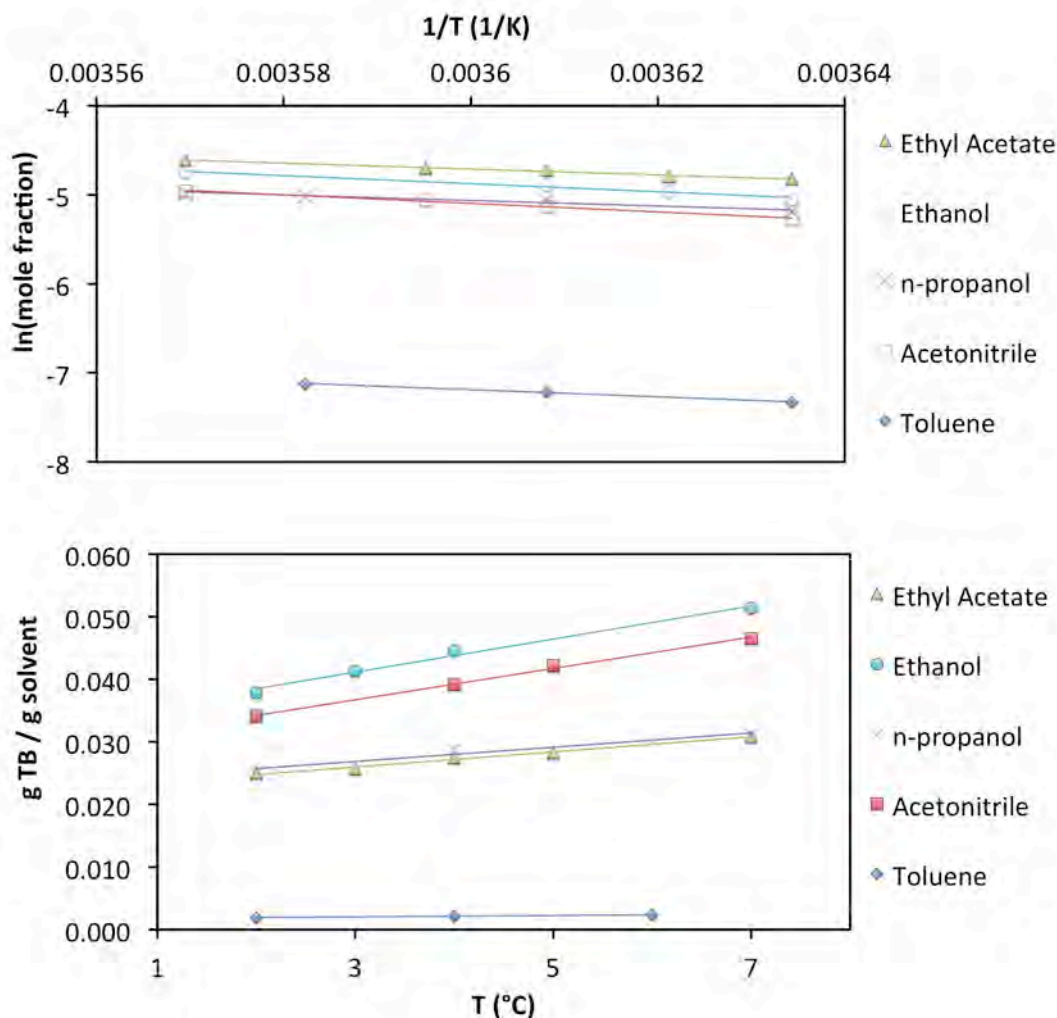


Figure 9: Tolbutamide form I<sup>L</sup> solubilities in various solvents as g/g (bottom) and van't Hoff (top). Lines are guides for the eye only.

Solubilities in ethanol at similar temperatures were measured to allow some comparison to published solubility data for this solvent (Thirunahari *et al.* 2010). Looking at the van't Hoff plot (Figure 10), our solubility data for ethanol seems to be somewhat higher than expected from the literature data, though it is well within the possible deviations from linearity as discussed in 3.3.2.

## Solubilities

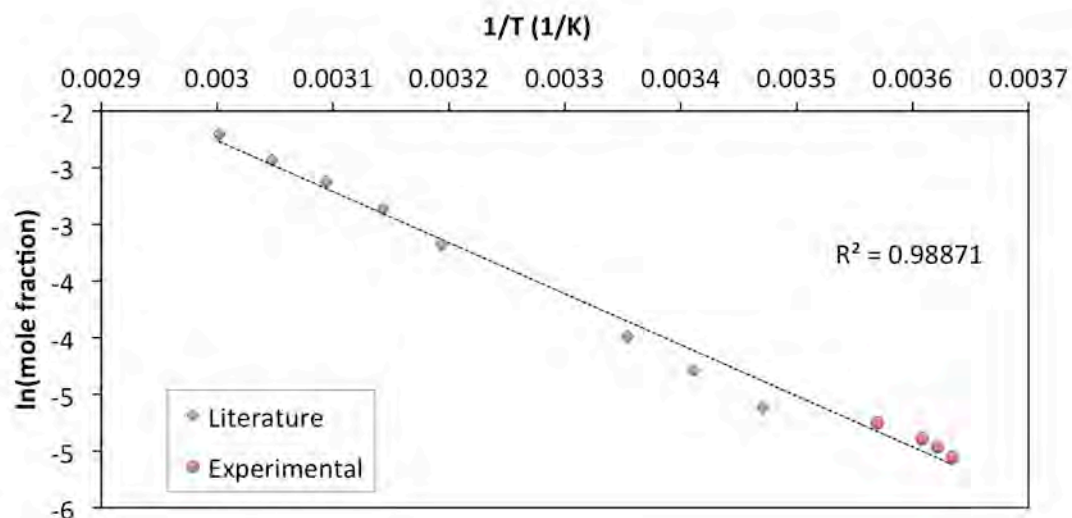


Figure 10: van't Hoff plot of tolbutamide solubility in ethanol compared with literature values (Thirunahari *et al.* 2010).

## 3.2 Fenoxycarb

The fenoxycarb solubility work presented below has been published in modified form in a peer-reviewed journal (Kuks *et al.* 2013).

### 3.2.1 Solid Phase Identification

To our knowledge only one crystal form of fenoxycarb has been discovered, and recently we reported its structure for the first time (Karpinska *et al.* 2012). However, during the solubility work, crystals appearing to the naked eye to be quite dissimilar in size and shape have been obtained. Three distinct types of crystals have been found, without any apparent preference, in all solvents and at all temperatures, as shown in Figure 9. Type 1 consists of large (up to 2 mm in the largest dimension), translucent crystals, visibly plate-like in habit, while types 2 and 3 consists of smaller crystals.

## Solubilities

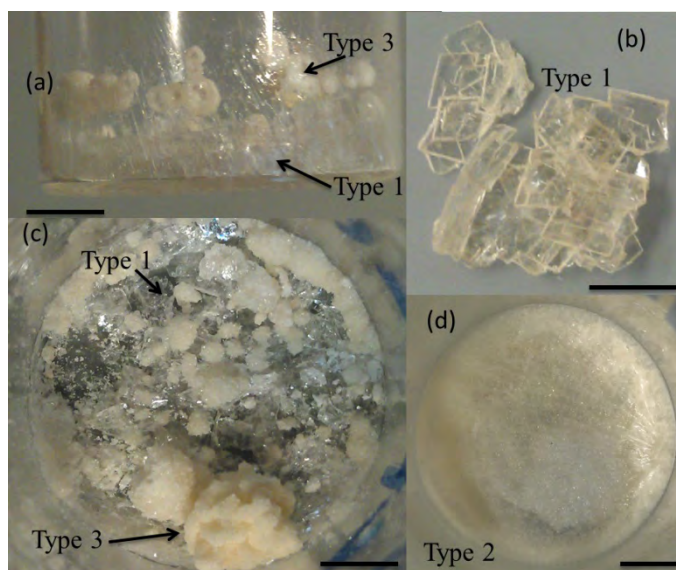


**Figure 9. Side (a) and top (c) views of type 1 and 3 crystals, with close-up of type 1 crystals (b), and type 2 crystals (d). Scale bar represents 0.6 mm.**

SEM microscopy revealed all three types to be of the same basic habit (thin platelets) of different sizes and orientation (Figure 10). Type 1 is indeed large platelets (a, b), while crystals of types 2 (c, d) and 3 (e, f) also consist of thin platelets, but tightly packed and with less defined edges.

## Solubilities

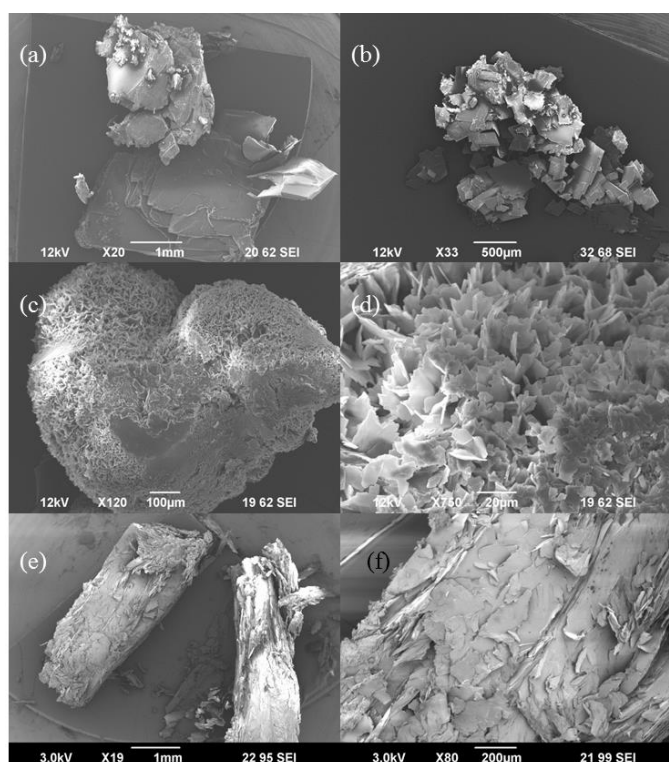


**Figure 10.** SEM images of crystals appearing as large translucent platelets (a, b), small yellow granules (c, d) and a congealed yellow mass (e, f).

*Ex-situ* ATR-FTIR analysis of slurries and dried crystals was carried out in all solvents between and inclusive of the temperatures at which solubilities were determined. The same was done *in-situ* in isopropanol using Raman spectroscopy. However, in no cases were differences in spectra observed after solvent subtraction. This suggests that all crystals were of a single polymorph. Pressure induced polymorph conversion during IR measurement (Nordström and Rasmuson 2006a) is unlikely as the Raman results, which involve no pressure application, also show no evidence of polymorphism.

Powder XRD analysis resulted in two slightly different diffraction patterns, one for type 1 and the other for both 2 and 3 (Figure 11). There are apparent differences in peak position which occur only between about 18 and 25 °2 $\theta$ , in which region peaks overlap and the signal does not return to the baseline. The small differences observed in the powder XRD data are typical of the effects of preferred orientation occurring due to slight differences in habits of the same polymorph, which can change peak intensity by up to 100% (Nangia and R. Desiraju 1999). Although the habit of both types appears to

## Solubilities

be identical, it is plausible that the differences in crystal size, aggregation and orientation could lead to preferred orientation effects. Powder XRD spectra of ground crystals of all types (not shown) show no clear difference in preferred orientation.

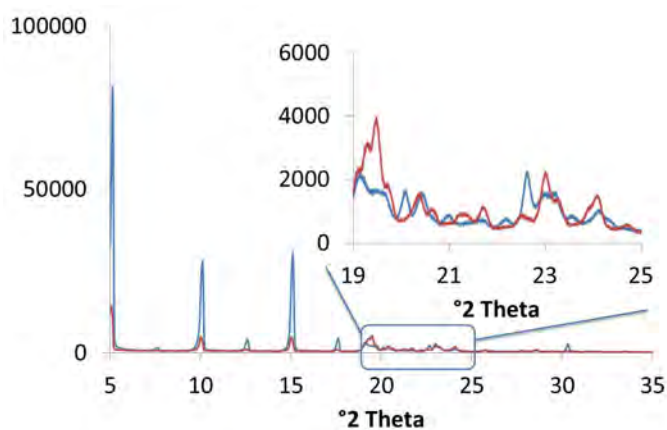


**Figure 11. Powder XRD diffraction patterns observed for fenoxy carb, representative of type 1 (blue) and type 2 (red), with Y axis showing intensity in arbitrary units. Differences in peak position only occur between 18 and 25 ° 2 $\theta$  (shown magnified in insert).**

The samples analysed by powder XRD were also analysed on the same day by solution  $^1\text{H}$  NMR in deuterated chloroform. In all cases only peaks corresponding to pure fenoxy carb, trace water from solvents and undeuterated chloroform were detected, i.e. no evidence of solid-state solvation was found. Although the  $^1\text{H}$  NMR water peaks could conceivably hide a water peak from hydrated fenoxy carb, DSC runs up to 80 °C (above the melting point of fenoxy carb) show no thermal events characteristic of dehydration.

Analysis of the different solid materials by DSC again yielded two slightly different sets of results (Figure 12). In all cases only a single melting endotherm was observed, with a slightly different onset temperature for the different types, given in Table 4. This difference partly remains after a melting-recrystallization cycle. The slight reduction in melting point for the second cycle in both cases is expected since complete melting and recrystallization in the sample pan should improve heat transfer.

Due partly to the small number of scans (4 and 2, respectively), 95% confidence intervals for the extrapolated onset melting temperatures of types 1 and 2 overlap;

## Solubilities

nevertheless, the averages of all four type 1 values are higher than both type 2 values and closer to the literature value (Xiao-Hong *et al.* 2005). Values of the enthalpy of fusion for the second cycle were also higher for type 1 than 2/3, but again with overlapping confidence intervals. Since the second DSC heat cycle is preceded by complete melting, the minor but significant difference in melting points and enthalpies of fusion between types 1 and 2/3 is most likely caused by a difference in impurity content, rather than differences in crystal size, shape or structure, as melting should remove all solid-state information. As higher impurity content is expected to decrease the melting point (Di *et al.* 2000), type 2/3 is hypothesized to be less pure than type 1.

**Table 4: DSC melting data (extrapolated onset temperatures and associated heats of fusion, with 95% confidence intervals) for crystals of types 1 and 2 before and after a melting-recrystallization cycle.**

	Type 1		Types 2 & 3		Lit.*
	1 <sup>st</sup> cycle	2 <sup>nd</sup> cycle	1 <sup>st</sup> cycle	2 <sup>nd</sup> cycle	
$T_m$ [K]	326.72	326.51	325.90	325.79	326.31
95% C.I. [K]	325.86 – 327.57	326.06 – 326.92	324 – 327.52	322.82 – 328.75	
$\Delta H_f$ [kJ mol <sup>-1</sup> ]	28.46	28.02	26.81	26.69	26.98
95% C.I. [kJ mol <sup>-1</sup> ]	26.87 – 30.06	27.03 – 29.01	24.49 – 29.13	24.80 – 28.57	

\* (Xiao-Hong *et al.* 2005)

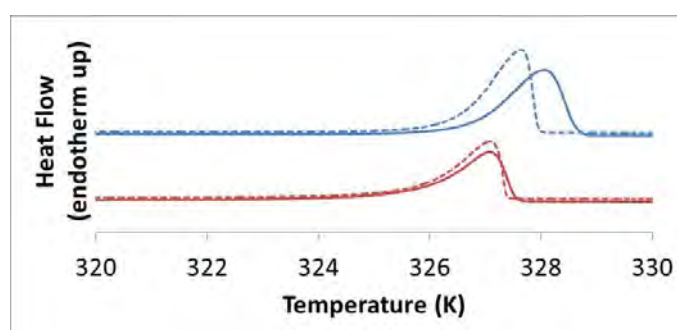


**Figure 12. Two DSC plots representative of the two different sets of results observed in the DSC analysis. Blue: type 1; red: type 2/3; solid: first cycle; dotted: second cycle.**

Our conclusion is that the observed crystal differences are due only to differences in impurities, crystal size, orientation and agglomeration. Probably, type 1 crystals are formed in the bulk of the solution under low nucleation rates, while the smaller crystals nucleate later, at the air-solution interface at higher nucleation rates, incorporating a larger share of the impurities.

## Solubilities

### 3.2.2 Solubilities

The solubility of fenoxycarb in various organic solvents at different temperatures is presented in Table 5 (as mole fraction) and shown graphically in Figure 11 top (as g/g solvent). Values obtained by approaching saturation from supersaturation were obtained at a slightly different temperature (Figure 11 bottom), but did not show any significant difference, confirming that the values in Table 5 represent the true equilibrium solubility at the given temperatures. The low CVs for the 5, 10 and 15 °C data confirm that achieving equilibrium is reproducible, while the low CVs at 20, 30 and 40 °C verify the repeatability of the drying process (see Section 2.2.1). Clearly the solubility is very high in all these solvents, partly reflecting that the temperature range is close to the melting point of fenoxycarb.

**Table 5: Mole fraction solubility ( $x_{eq}$ ) of fenoxycarb at temperature  $T$  in various solvents, along with standard deviations (sd).**

$T$ (°C) <sup>†</sup>	Methanol		Ethanol		Isopropanol		Ethyl acetate*		Toluene*	
	$x_{eq}$	sd	$x_{eq}$	sd	$x_{eq}$	sd	$x_{eq}$	sd	$x_{eq}$	sd
5.02	0.0188	0.00026	0.0195**	0.00003	0.0121**	0.00001	0.1820	0.00121	0.1242	0.00063
9.99	0.0298	0.00004	0.0287	0.00037	0.0175	0.00002	0.2195	0.00100	0.1648	0.00023
15.02	0.0551	0.00032	0.0440	0.00025	0.0288	0.00004	0.2694	0.00014	0.2143	0.00301
20.00	0.1196	0.00027	0.0798	0.00004	0.0504	0.00003	0.3272	0.00029	0.2735 <sup>‡</sup>	0.00051
24.99	0.2151	0.00104	0.1578	0.00012	0.1081	0.00006				
29.95	0.3693	0.01123	0.2969	0.00077	0.2612	0.00038	0.4682	0.00065	0.4416	0.00486
34.91	0.4654	0.00168	0.4354	0.00088	0.4242	0.00012				
40.00	0.6426	0.00677	0.6151	0.00835	0.6054	0.00264	0.6587	0.00158	0.6495	0.00227
44.65	0.7548	0.01690	0.7348	0.01234	0.7409	0.01819				

\* Solubilities at 24.99, 34.91 and 44.65 °C were only determined for the alcohols as the temperature dependence is most marked in these solvents.

\*\* At 5.1 °C

<sup>†</sup> Standard uncertainty  $u(T) = 0.055$  °C.

<sup>‡</sup> At 19.84 °C.

## Solubilities

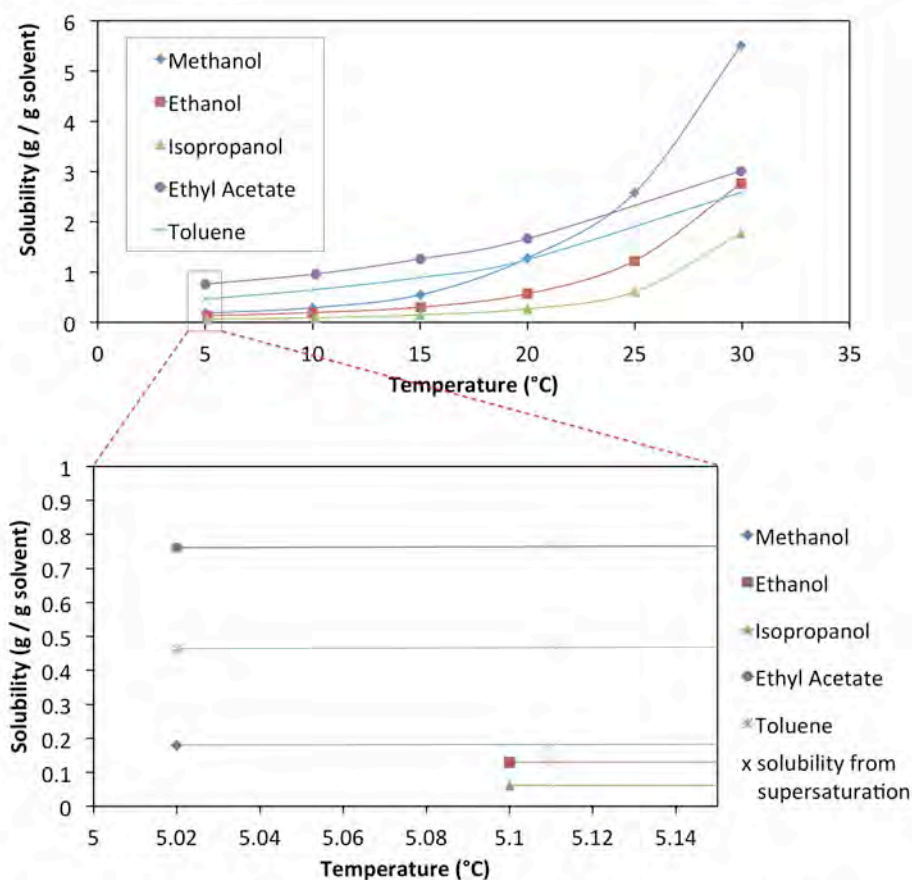


**Figure 11: Solubility of fenoxycarb in five organic solvents (top) with values from approaching via supersaturation overlaid (bottom). Lines are guides for the eyes only.**

Though the g / g solubility order depends on temperature, the mole fraction order does not, and this is merely a consequence of the difference in molecular weight between the solvents. The mole fraction solubility decreases in the order: ethyl acetate > toluene > methanol > ethanol > isopropanol. Also, although not quantitatively measured in this work, it was observed that fenoxycarb has by far the lowest solubility in water. In the lower temperature range the solubility is clearly lower in all the alcohols.

### **3.3 Discussion**

#### **3.3.1 Method**

All methods of measuring solubility depend on creating a solution that is fully saturated with regards to solute concentration, i.e. neither over- nor under-saturated. As the time taken to reach this equilibrium can vary widely, some evidence must be given to demonstrate equilibrium has been achieved. In the case of tolbutamide this was done by measuring the solution concentration over time, which was found not to vary significantly between the first and last measurement within the uncertainty of the measurements (Figure 8). For fenoxycarb full equilibration was confirmed by approaching saturation from both supersaturation and undersaturation, which gave almost identical values (Figure 11 bottom). Both these were done only at the lowest temperatures for which solubilities were measured, since dissolution is usually slowest at the lowest temperature.

The accuracy of the measured solubilities varies somewhat between tolbutamide and fenoxycarb. In general, fenoxycarb solubilities are more accurate: temperature uncertainties are lower (0.055 versus 0.2 C° for tolbutamide), and the average coefficient of variation (CV = mean / sd, excluding tolbutamide solubilities in toluene) of the measured concentration is 1.7% for tolbutamide compared to a mere 0.3% for fenoxycarb. The lower accuracy in measuring the solubility of tolbutamide most likely has the same cause as the highly uncertain measurements of tolbutamide in toluene (average CV = 10.2%), namely smaller absolute concentrations. When concentrations are low, the final mass measured by the balance will be very small, especially compared to the mass of the solution prior to drying, such that inaccuracies in the balance or the presence of dust particles invisible to the naked eye will have a greater influence on the measured concentration. Whereas for fenoxycarb the water bath temperature was checked with a calibrated external thermometer, this was neglected for tolbutamide. As a result, the uncertainty in the temperature for tolbutamide solubilities is greater (0.2 compared to 0.055 C°).

However, both average accuracies are similar or better than many reported in the literature, which range from 0.5% to over 5% (Liang *et al.* 2012, Yang *et al.* 2012,

## Solubilities

Bowen *et al.* 2013, Yang *et al.* 2015). In particular, measuring the concentration gravometrically avoids errors introduced by the dilution that is usually necessary for spectroscopic concentration measurements.

A further possible source of error is impurities in solute and/or solvent. Their effect on the measured solubility is complex. Both solute and solvent impurities will affect the equilibration position, either increasing or decreasing the effective solubility. Furthermore, any impurities that do not evaporate during the drying step will increase the measured solubility. Quantifying all these factors in order to determine the true solubility is not feasible, and thus solubilities are usually reported along with the % mass purities of all components used. For publishing solubility data for thermodynamic analysis, component purities above 99% are usually accepted, and are also usually considered sufficient for most practical applications such as estimating supersaturations for crystallisation experiments (this latter assumption is discussed in section 4.3.3).

### **3.3.2 Non-linear van't Hoff Plots**

The temperature dependence of the solubility yields the so-called van't Hoff or apparent enthalpy of solution,  $\Delta H_{SoIn}^{vH}$  (Nordström and Rasmuson 2009):

$$\left( \frac{\partial \ln x}{\partial T} \right)_{eq} = \frac{\Delta H_{SoIn}^{vH}}{RT^2} \quad (25)$$

where  $R$  is the universal gas constant and  $\Delta H_{SoIn}^{vH}$  at a given temperature is equal to the slope in a van't Hoff plot multiplied by  $-R$ . If  $\Delta H_{SoIn}^{vH}$  is constant, integration of Eqn. 10 yields:

$$\ln x = -\frac{\Delta H_{SoIn}^{vH}}{RT} + const \quad (26)$$

Figure 5 shows the solubility data of fenoxycarb in a van't Hoff plot. While the curves for fenoxycarb solubility in ethyl acetate and toluene are very linear, the curves for the solubility in the alcohols are strongly non-linear.

## Solubilities

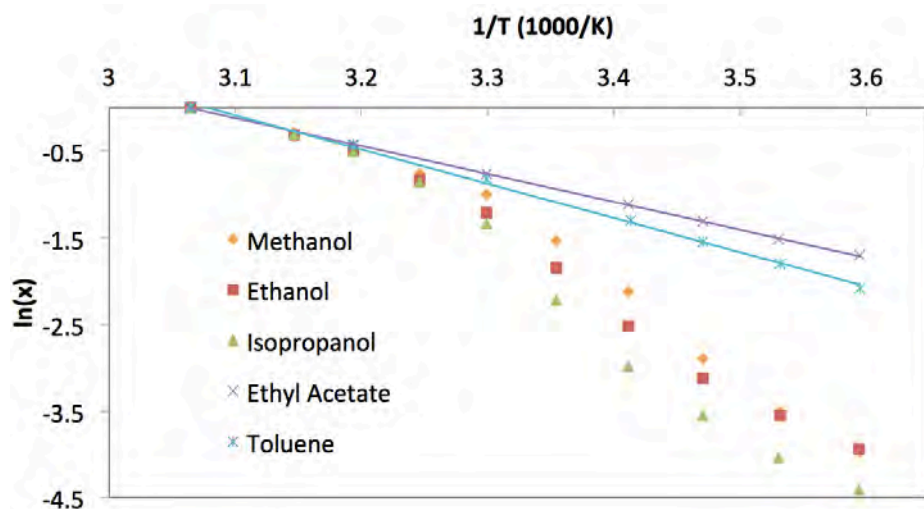


Figure 5. van't Hoff plot of fenoxycarb solubilities in various organic solvents. Points are experimental solubility except points on the x axis which is the melting point of fenoxycarb (Xiao-Hong *et al.* 2005). Lines are guides for the eyes only.

In most reported solubility data, a van't Hoff plot is presented as a straight or almost-straight line, and it is not uncommon to find implicit or explicit statements that a van't Hoff plot *should* yield a straight line, i.e. that the van't Hoff enthalpy of solution is independent of temperature (Mirmehrabi *et al.* 2004). However, it can be shown (Nordström and Rasmuson 2009) that the full thermodynamic interpretation of the van't Hoff enthalpy of solution is given by:

$$\Delta H_{Soln}^{vH} = \Delta H_f(T_m) + \int_{T_m}^T \Delta C_p dT - RT^2 \left( \frac{\partial \ln \gamma}{\partial T} \right)_{eq} \quad (27)$$

The first two terms on the right-hand side in Eqn. 12 together represent the enthalpy of fusion at  $T$ , while the third term contains the temperature derivative of the activity coefficient at equilibrium,  $\gamma_{eq}$ , in a saturated solution defined within a Raoult's law framework. It is to be noted that this term is not equal to the enthalpy of mixing, which explains why the van't Hoff enthalpy of solution differs from the thermodynamic enthalpy of solution (Hollenbeck 1980). It follows from equation (26) that non-linearity of the van't Hoff curve can occur because the heat capacity term cannot be neglected, and/or because of the temperature dependence of the activity coefficient. The temperature derivative of the activity coefficient includes the effect of the strongly increasing concentration of the saturated solution with increasing temperature. The

## Solubilities

behaviour shown in Figure 5 agrees with that predicted by Nordström and Rasmuson (2009). For positive deviations from Raoult's law significant non-linearity may occur, leading to van't Hoff plots quite similar to those experimentally observed in the present work. It has also been shown (Nordström and Rasmuson 2009) that all solubility curves should converge to the melting temperature/enthalpy of fusion at increasing temperature, which again is observed in our data.

As was demonstrated in our paper (Kuhs *et al.* 2013), the heat capacity term has a relatively weak influence on the van't Hoff enthalpy of solution. Thus, it is chiefly the third term in Eqn. 12, the enthalpy change related to dissolving the solute into the solvent, that governs the shape of the van't Hoff curves, in particular for the alcohols.

The van't Hoff plot in ethyl acetate forms a straight line ( $R^2$  value of the linear fit is 0.9999) reaching  $\ln x = 1$  at the melting point of 53.16 °C. The resulting constant van't Hoff enthalpy of solution in ethyl acetate is essentially identical to the reported enthalpy of fusion at the melting point, 26.98 kJ mol<sup>-1</sup> (Xiao-Hong *et al.* 2005). Accordingly, the ethyl acetate solution could easily have been mistaken for a perfect ideal solution. However, in our paper (Kuhs *et al.* 2013) it was demonstrated that the heat capacity term is far from negligible but is very well compensated for by the activity coefficient derivative term in ethyl acetate. In toluene, the van't Hoff enthalpy of solution becomes somewhat higher as the activity coefficient term is larger (i.e. the temperature derivative is more negative). In the alcohols, the activity coefficient term dominates completely, and depends significantly on temperature.

### **3.3.3 A molecular analysis of the measured solubilities**

Solubility is a combination of three interactions: Solvent-solvent and solute-solute, which hinder solubility, and solvent-solute, which promotes it. These same interactions could also influence crystal nucleation from solution, so it is of interest to rationalise the measured solubilities in order to increase our understanding of the solution structure leading up to, and possibly influencing, nucleation.

fenoxycarb can donate its amine proton for hydrogen bonding, and can accept protons from other molecules at its carbonyl and ether oxygens (four in total). Multiple

## Solubilities

fenoxycarb molecules can thus hydrogen bond to each other. As has been analysed in the literature (Zeglinski *et al.* 2014), the sole reported crystal structure of fenoxycarb consists of elongated fenoxycarb molecules arranged in parallel chains (see Figure 12 left). Hydrogen bonds between the carbonyl oxygen and the amide hydrogen have the effect of binding parallel chains of fenoxycarb together perpendicular to the chains, though there is also a weak interaction between the parallel-displaced benzene rings. There is, however, no strong interaction between adjacent fenoxycarb molecules in the same chain (i.e. in line with the chain). Altogether, each fenoxycarb molecule in the crystal is held together by two hydrogen bonds.

Tolbutamide can also both donate and accept hydrogen bonds. Compared to fenoxycarb, it has an additional proton (two amines in total) to donate, but can accept one less (two from the sulfone and one from the carbonyl group), which nevertheless could lead to stronger intermolecular bonding. The crystal structure of Form I<sup>L</sup> of tolbutamide has also been analysed (Thirunahari *et al.* 2010). Though slightly less elongated, the tolbutamide molecules form chains in the Form I<sup>L</sup> crystal (see Figure 12 right) similar to fenoxycarb. Each tolbutamide molecule is held in place by six hydrogen bonds perpendicular to the chain, which is significantly more than fenoxycarb's two, and may be a chief contributing factor to tolbutamide's higher melting point (by around 50 C°). Thus, tolbutamide may be more dependent on the hydrogen bonding ability of a solvent in order to be dissolved.

## Solubilities

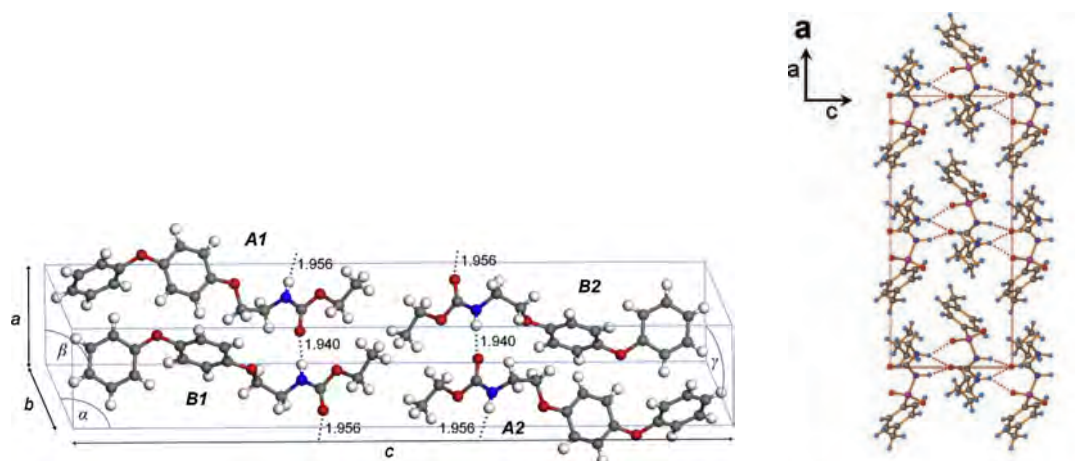


**Figure 12: Molecular packing in crystals of fenoxycarb (left) and tolbutamide Form 1<sup>L</sup> (right).** Sources: (Thirunahari *et al.* 2010, Zeglinski *et al.* 2014)

All utilised solvents except acetonitrile have hydrogen accepting functionality, though the  $\pi$ -electron system of toluene's aromatic ring can only act as a weak hydrogen bond acceptor (Reichardt and Welton 2011). Ethyl acetate and toluene are incapable of hydrogen bond donation, while the alcohols can both donate and accept. Hence, neither ethyl acetate nor toluene can hydrogen bond internally, which may indicate that they have weaker solvent-solvent interaction than the alcohols. However, it also implies that hydrogen bonding with molecules that both donate and accept hydrogen bonds, such as tolbutamide and fenoxycarb, would be weaker. Though toluene is the weakest in terms of hydrogen bonding, it is the only solvent that has an aromatic ring. Since both tolbutamide and fenoxycarb have aromatic rings, this may help toluene to solvate both tolbutamide and fenoxycarb. Indeed, it has been shown for a similar medium-sized organic molecule with an aromatic ring, risperidone, that toluene's aromatic ring can allow it to solvate a protic solute despite its lack of hydrogen bonding ability (Mealey *et al.* 2014). Ethyl acetate also has a unique structural similarity to tolbutamide and fenoxycarb, in that its polar group is in the centre, surrounded by non-polar regions. The only difference between the alcohols is the length of the aliphatic chain, whereby a longer chain decreases the solvent's polarity.

## Solubilities

For fenoxycarb, the mole fraction solubility decreases in the order: ethyl acetate > toluene > methanol > ethanol > isopropanol. For tolbutamide, the solubility order is: ethyl acetate > ethanol > [n-propanol & acetonitrile] >> toluene, where tolbutamide is almost an order of magnitude less soluble in toluene than in the other solvents.

Both tolbutamide and fenoxycarb have the highest solubility in ethyl acetate. This may suggest that ethyl acetate's structural similarity to tolbutamide and fenoxycarb, with polarity in the center surrounded by non-polar groups, is more significant than the alcohols' greater ability to form hydrogen bonds with tolbutamide and fenoxycarb, at least when offset against the alcohols' greater solvent-solvent interaction due to their internal hydrogen bonding ability. Also for both tolbutamide and fenoxycarb, the solubility in the alcohols decreases with increasing alkyl chain length.

Toluene, however, dissolves tolbutamide and fenoxycarb very differently. For fenoxycarb its solubility is in the same range as the other solvents, indeed is more soluble than the alcohols, while in tolbutamide it is almost an entire order of magnitude less soluble than all other solvents. Tolbutamide, fenoxycarb and toluene all have aromatic rings, so the explanation is unlikely to be there. However, toluene is unique among the solvents in that it is the only non-polar molecule, incapable of strong hydrogen bonding. Since tolbutamide is internally bonded with 6 hydrogen bonds in the crystal, while fenoxycarb only has two, it seems that toluene is unable to compete with the comparatively-strong solute-solute interaction of tolbutamide while it can compete with the weaker fenoxycarb solute-solute interaction.

That the absolute values, expressed both as mass and molecular ratios, of tolbutamide solubilities are significantly lower than those of fenoxycarb is probably a reflection of tolbutamide's greater solid state stability as reflected in its far higher melting point (over 100 °C compared to 53 °C).

# IV

## **4 Influence of Solvent on Nucleation of Tolbutamide and Fenoxycarb**

#### 4.1 Fenoxycarb Induction Times

Induction times were recorded at a combination of different  $S$  and  $T_{cry}$  for four different organic solvents (ethyl acetate, toluene, isopropanol and ethanol, Figure 13). Distributions of induction times resulted from identical crystallisation conditions at the small volume reactors we were using (20mL), and as expected, these distributions systematically decrease in induction times as the thermodynamic driving force,  $RT \ln S$ , increases.

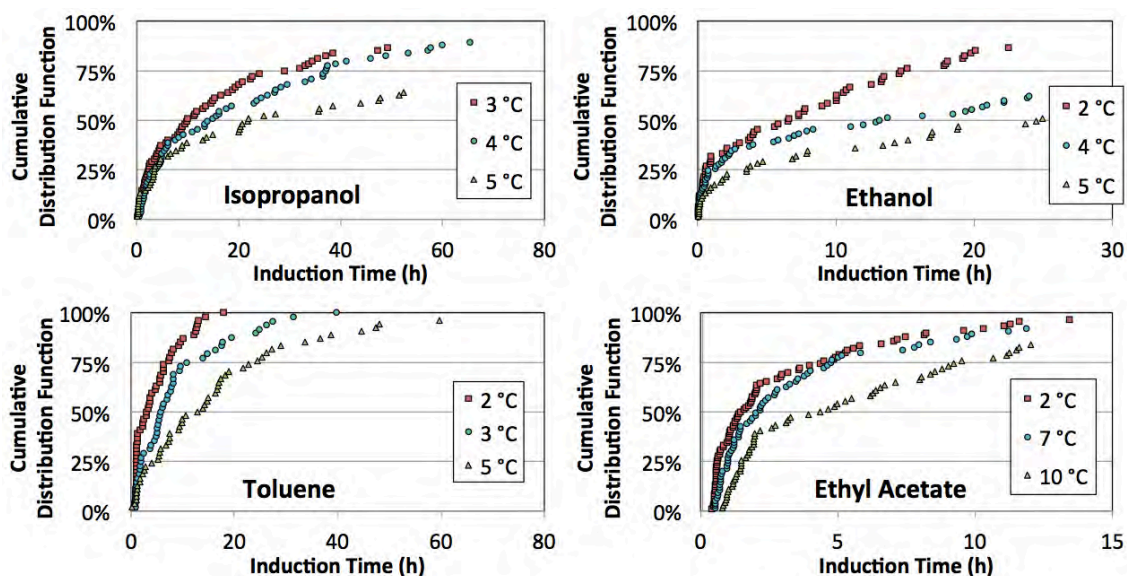


Figure 13: Induction time distributions of fenoxycarb in different solvents. Temperatures are  $T_{cry}$ .

## Influence of Solvent on Nucleation of Tolbutamide and Fenoxycarb

**Table 6: Solutions and induction time results for fenoxycarb.**  $S = x/x_{eq}$ , where  $x$  is the actual mole fraction of fenoxycarb in the solution, and  $x_{eq}$  the equilibrium mole fraction at  $T_{cry}$  (Kuhns *et al.* 2013);  $n$  is the number of induction times measured for each condition; *Logn.  $t_{ind}$*  is the median of the lognormal fit to the experimental  $t_{ind}$  distributions.

Solvent	Approx. $T_{sat}$ (°C)	Mass ratio (g fenoxycarb/g solvent)	# 20mL vials	$T_{cry}$ (°C)	S	RTlnS (kJ/mol)	n	Logn. $t_{ind}$ (h)
Ethyl acetate	15	1.2307	15	8.0	1.33	1.32	41	2.1
				7.0	1.38	1.49	55	2.0
				2.1	1.68	2.36	74	1.4
Toluene	20	1.2295	6	5.1	2.19	3.59	51	10.5
				3.1	2.44	4.08	48	5.5
				2.1	2.59	4.33	54	2.8
Isopropanol	20	0.2633	30	5.1	4.58	6.98	65	23.5
				4.0	5.19	7.53	65	12.1
				3.1	5.74	7.98	65	8.9
Ethanol	20	0.5706	15	5.1	4.18	6.56	38	31.7
				4.0	4.66	7.04	56	11.8
				2.1	5.64	7.88	65	4.3

The medians of the lognormal fits are plotted directly against the thermodynamic driving force of nucleation,  $RTlnS$ , in Figure 14. The relationship can be described as the induction time exponentially decaying with increased driving force. It is clear that the nucleation rate strongly depends on the choice of solvent, as vastly different thermodynamic driving forces are required to achieve similar induction times.

## Influence of Solvent on Nucleation of Tolbutamide and Fenoxycarb

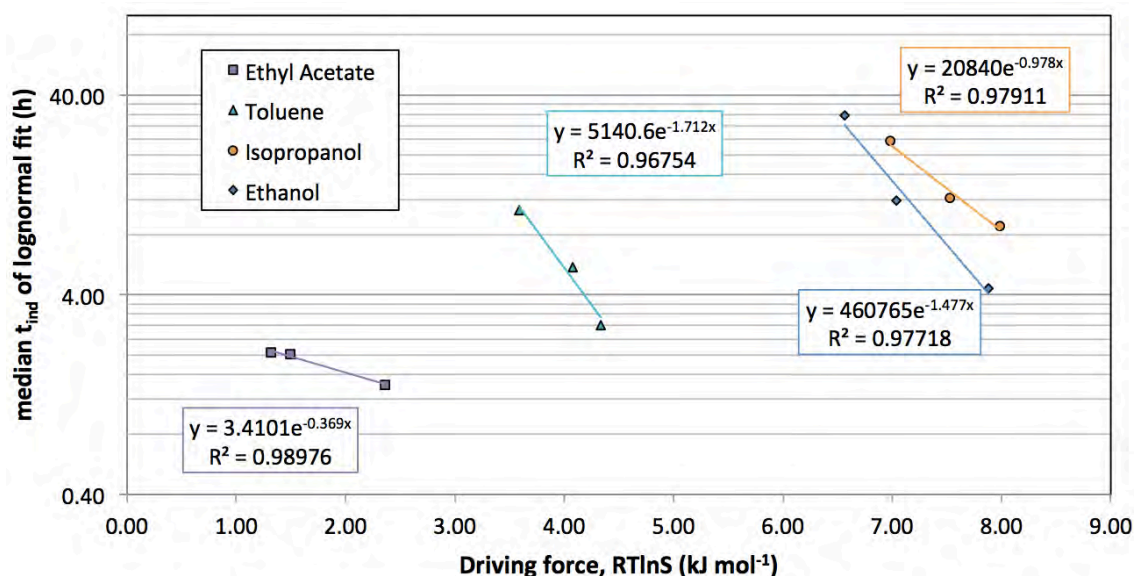


**Figure 14:** The relationship between median induction time and thermodynamic driving force,  $RT\ln S$ , of nucleation of fenoxycarb in different solvents. Lines are guides for the eyes only.

From this plot an approximate order of ease of nucleation can be established in the range of the examined  $RT\ln S$  (extrapolation of exponential fits suggests this order changes at higher and lower  $RT\ln S$ , especially for the alcohols). Nucleation in ethyl acetate clearly requires the lowest thermodynamic driving force for nucleation, toluene is an intermediate, and the alcohols are similar, requiring the highest, with isopropanol being slightly higher.

In order to compare the ease of nucleation at the same driving force, the fits from Figure 14 were extrapolated to  $t_{ind}$  of 2.06 h (the highest recorded  $t_{ind}$  for ethyl acetate). This gives the following required values for  $RT\ln S$ : 1.4 (ethyl acetate), 4.6 (toluene), 9.4 (isopropanol) and 8.3 (ethanol)  $\text{kJ mol}^{-1}$ . This matches the order previously mentioned.

For further evaluation, the results are plotted according to the CNT using equations (16) and (24) in Figure 18. The strength of the exponential fits ( $R^2$  ranging from 0.93 to 0.99) means the CNT is able to describe the relationship between induction time and  $S$  and  $T_{cry}$ .

## Influence of Solvent on Nucleation of Tolbutamide and Fenoxycarb

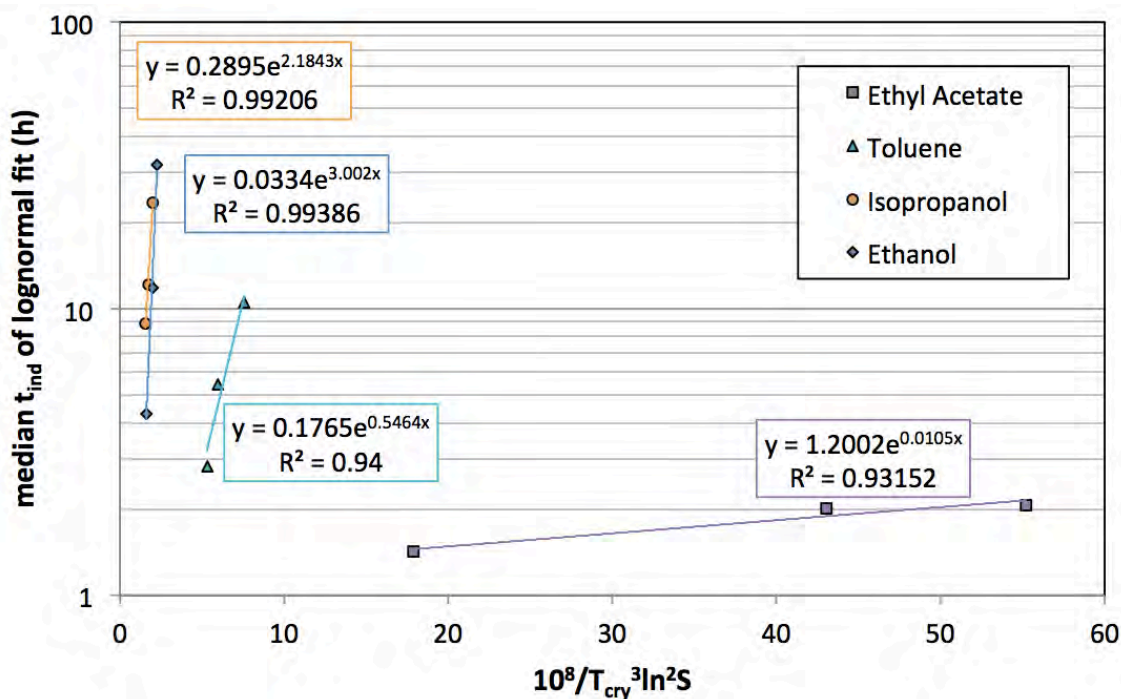


Figure 15: The relationship between  $T_{cry}$ ,  $S$  and  $t_{ind}$  of fenoxycarb plotted according to CNT. Lines are exponential fits.  $A$  and  $\gamma$  in Table 6 are calculated from the intercepts and slopes, respectively, according to equations (16) and (24).

From this,  $\gamma$  and  $A$  were calculated for each solvent (Table 7) from the slopes and intercepts, respectively, of the exponential fits of Figure 15 using equations (9), (16), and (24).

Table 7: CNT parameters calculated from equations (9), (16), and (24) for fenoxycarb.

Solvent	$A$ ( $\text{m}^{-3} \text{s}^{-1}$ )	$\gamma$ ( $\text{mJ m}^{-2}$ )	$n^*$	$\Delta G^*$ ( $\text{kJ mol}^{-1}$ )
Ethyl acetate	16.67	0.82	4.1	2.68
			2.8	2.09
			0.7	0.86
Toluene	2.45	3.06	10.6	19.0
			7.3	14.9
			6.1	13.2
Isopropanol	4.02	4.86	5.7	20.1
			4.6	17.3
			3.9	15.5
Ethanol	0.46	5.40	9.5	31.2
			7.7	27.3
			5.6	22.0

## Influence of Solvent on Nucleation of Tolbutamide and Fenoxycarb

As can be seen from the similarity of their slopes in Figure 15, the difference between  $\gamma$  of fenoxycarb in ethanol and isopropanol may not be significant. The ease of nucleation according to  $\gamma$  follows the general order of ease of nucleation from Figure 14, and decreases from ethanol > isopropanol > toluene > ethyl acetate. Only the order of the alcohols is switched. In both cases the differences between the alcohols is not very significant, and may simply be due to inaccuracies in the measurement techniques employed. Alternatively they could be due to the absence of any direct proportionality between  $RT_{cry}\ln S$  and  $\ln t_{ind}$ .

### 4.2 Tolbutamide Induction Times

Tolbutamide induction times were recorded at a combination of different  $S$  and  $T_{cry}$  for four different organic solvents (n-propanol, acetonitrile, ethyl acetate and toluene, Figure 13). Again, distributions of increasing induction times with decreasing driving force result.

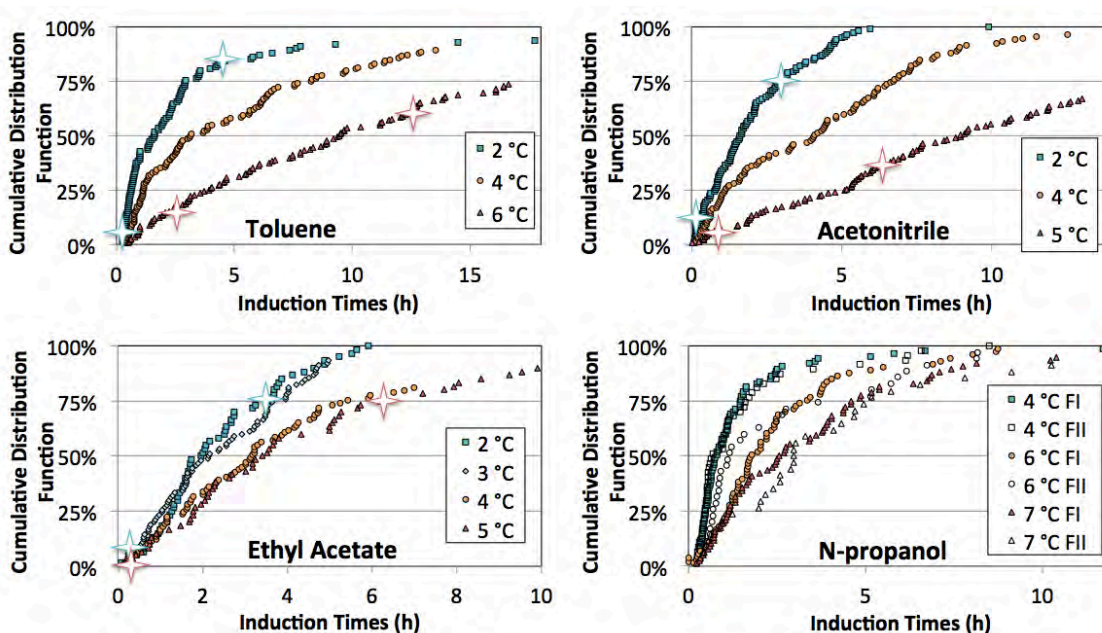


Figure 16: Induction time distributions of tolbutamide in different solvents. Temperatures are  $T_{cry}$  and stars indicate sampling of slurry for PXR analysis, which always gave a form I<sup>L</sup> diffraction pattern.

## Influence of Solvent on Nucleation of Tolbutamide and Fenoxycarb

**Table 8: Solutions and induction time results for tolbutamide form I<sup>L</sup>.**

Solvent	$c$ (g tolbutamide / g solvent)	$T_{cry}$ (°C)	$S$	$RT\ln S$ (kJ $mol^{-1}$ )	$n$	median $t_{ind}$ (h)
Toluene	0.0050	2	2.60	2.19	104	1.60
		4	2.33	1.95	130	3.15
		6	2.12	1.74	106	9.45
Acetonitrile	0.0534	2	1.57	1.03	118	1.62
		4	1.36	0.72	113	4.08
		5	1.27	0.55	97	8.97
Ethyl acetate	0.0471	2	1.89	1.45	60	1.97
		3	1.83	1.39	84	2.15
		4	1.71	1.24	72	3.15
		5	1.67	1.18	60	3.42
N-propanol (Form I <sup>L</sup> only)	0.0655	4	2.27	1.89	87	0.78
		6	2.17	1.80	73	1.78
		7	2.10	1.73	76	2.55

The medians of the lognormal fits are plotted against the thermodynamic driving force of nucleation,  $RT_{cry}\ln S$ , in Figure 6.

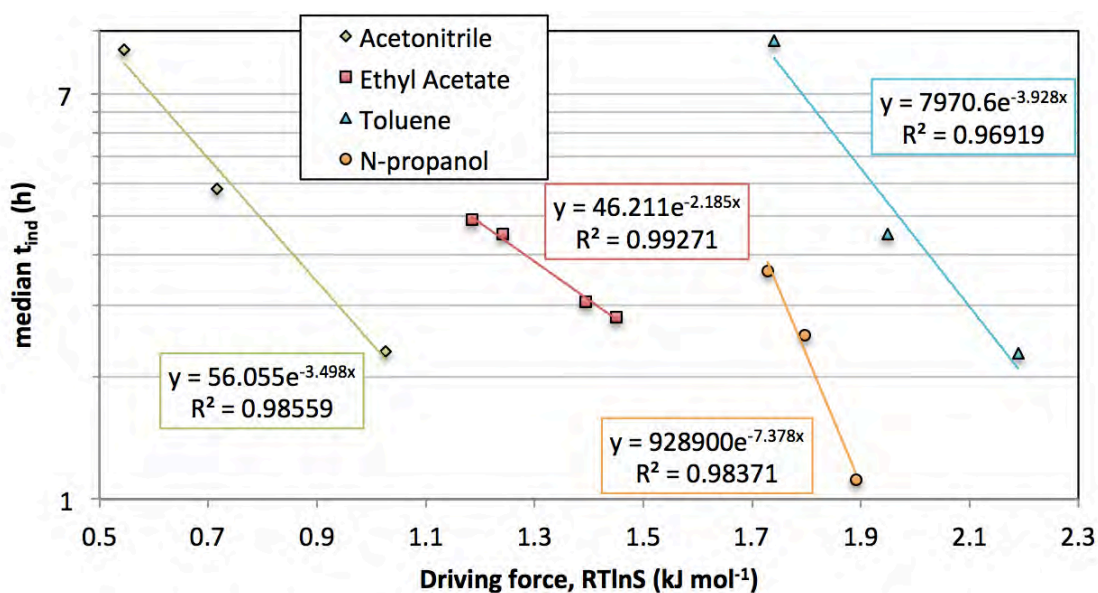


**Figure 17: The relationship between median induction time and thermodynamic driving force of nucleation of tolbutamide in different solvents. Lines are exponential fits.**

## Influence of Solvent on Nucleation of Tolbutamide and Fenoxycarb

$t_{ind}$  seems to exponentially decay with increasing driving force. From this plot an approximate order of ease of nucleation can be established without assuming a particular theory of nucleation. However, this order is only valid at the examined  $RT\ln S$  (extrapolation of exponential fits suggests this order changes at higher and lower  $RT\ln S$ , especially reversing the order between n-propanol and toluene). Comparing similar  $t_{ind}$  values, acetonitrile clearly requires the lowest thermodynamic driving force for nucleation, followed by ethyl acetate, n-propanol, and finally toluene as requiring the highest driving force.

In order to compare the ease of nucleation at the same driving force, the fits from Figure 17 were extrapolated to  $t_{ind}$  of 2 h. This gives the following values for  $RT\ln S$ : 0.95 (acetonitrile), 1.44 (ethyl acetate), 1.77 (n-propanol), and 2.11 (toluene) kJ/mol. This matches the order previously mentioned.

For further evaluation, the results are plotted according to the CNT by combining Equations (19) and (27).

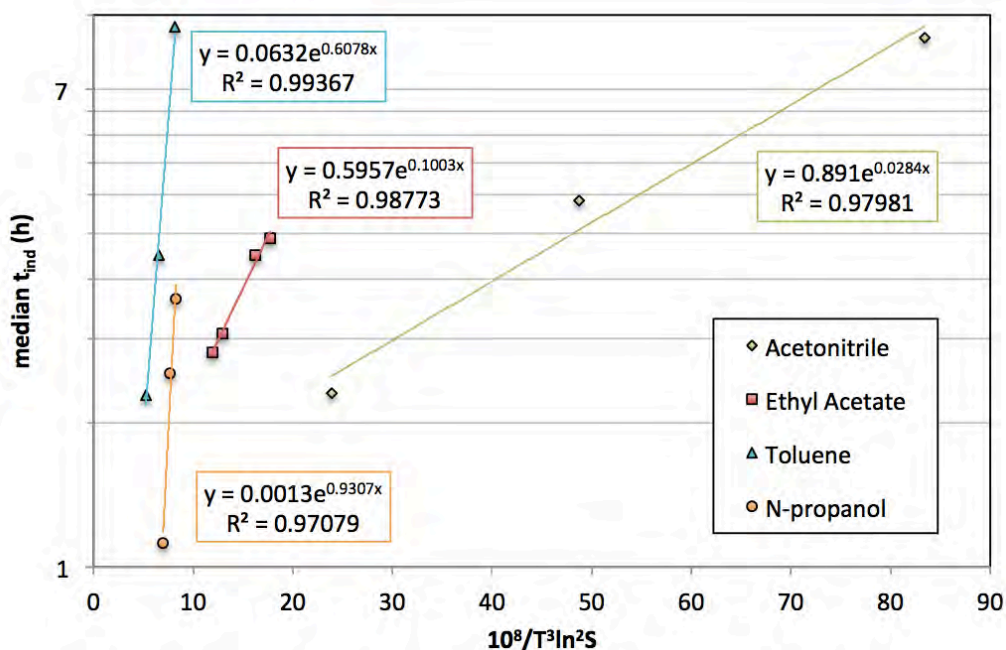


**Figure 18:** The relationship between  $T_{cry}$ ,  $S$  and  $t_{ind}$  of tolbutamide plotted according to the Classical Nucleation Theory. Lines are exponential fits from which  $A$  and  $\gamma$  in Table 9 are calculated according to Equations (19) and (27).

## Influence of Solvent on Nucleation of Tolbutamide and Fenoxycarb

From this,  $\gamma$  and  $A$  were calculated for each solvent (Table 9). For similar reasons as for fenoxycarb, the temperature dependence of  $\gamma$  and  $A$  appears to be negligible under the present conditions. Similarly, the absolute values of  $\gamma$  are the same order of magnitude as reported in the previous section.

**Table 9:** Calculated parameters of the CNT for tolbutamide form I<sup>L</sup> according to equations (9), (16), and (24).

<i>Solvent</i>	$\gamma$ ( $mJ\ m^{-2}$ )	$A$ ( $m^{-3}\ s^{-1}$ )	$\Delta G^*$ ( $kJ\ mol^{-1}$ )	$n^*$
<b>Toluene</b>	3.46	0.88	7.29	6.7
			9.20	9.4
			11.54	13.3
<b>Acetonitrile</b>	1.25	12.38	1.55	3.0
			3.19	8.9
			5.48	20.1
<b>Ethyl acetate</b>	1.90	8.27	2.74	3.8
			3.74	6.0
			4.11	6.9
<b>N-propanol (Form I<sup>L</sup> only)</b>	3.99	0.02	14.97	15.8
			16.57	18.4
			17.90	20.7

As can be seen from their slopes in Figure 18,  $\gamma$  of n-propanol and toluene are not sufficiently different to be distinguished (similarly, their pre-exponents, derived from the intercepts, are likely not significantly different). As expected, the order of  $\gamma$  follows the order of driving force required to reach similar induction times from Figure 14, and decreases in the order [n-propanol & toluene] > ethyl acetate > acetonitrile.

## 4.3 Discussion

### 4.3.1 Induction Time Distributions

Our method of measuring induction times using a custom 20 mL multireactor system has been published multiple times (Liu and Rasmuson 2013, Yang and Rasmuson 2013, Kuhs *et al.* 2014, Liu *et al.* 2014, Mealey *et al.* 2015a, Mealey *et al.* 2015f). The studies involved numerous small to medium-sized organic molecules nucleating from various

## Influence of Solvent on Nucleation of Tolbutamide and Fenoxycarb

organic solvents, and in all cases wide induction time distributions resulted. Distributions of induction times are also reported for experiments at a slightly smaller scale of around 1 mL using the commercial Crystal16 multireactor system (Jiang and ter Horst 2010, Kulkarni *et al.* 2013, Sullivan *et al.* 2014). That distributions of induction times for identical experiments occur at even smaller volumes has been well-known for several decades due to attempts at measuring true homogeneous nucleation rates using the “droplet method” (Wood and Walton 1970), in which pure homogeneous liquids are attained by dividing a small volume of liquid into more “droplets” than there are impurities in the original volume. These droplets usually have volumes in or below the nanolitre range.

The cause of these distributions is that nucleation appears to be an inherently stochastic process. This stochastic component is well known at a theoretical level, since nucleation is usually explained as occurring through *random localized fluctuations* in solute concentration leading to a cluster sufficiently-large to overcome the free energy barrier (Izmailov *et al.* 1999), see Section 1.2.2.2. However, induction times and metastable zone widths (MSZW) are often assumed to be deterministic, because at larger scales, especially in the industry, induction times and MSZW do not exhibit distributions. It is a general principle that a microscopic stochastic process may become deterministic at the macro scale: this makes casinos and the insurance industry profitable, even though the outcome of an individual game in the former case, or the occurrence of a claim by a particular client in the latter, are stochastic and could lead to losses for the business. Indeed, a recent study of the effect of volume on the width of the induction time distribution finds a consistent decrease in the width of the distribution with reactor volume increasing from 1 mL to 1 L (Kadam *et al.* 2012). More recently, modelling of nucleation as a stochastic process has confirmed this trend (Maggioni and Mazzotti 2015).

Let us assume a certain distribution of induction times occurring at, say, 20 mL, and a single induction time resulting at a 1000 L scale. Now we divide the 1000 L volume into 20 mL sections. For argument’s sake, we will assume that these 20 mL sections are isolated from each other. The sections will then exhibit a distribution of induction times,

## Influence of Solvent on Nucleation of Tolbutamide and Fenoxycarb

the same as repeatedly measuring the induction time of a single 20 mL system. However, the induction time of the entire 1000 L volume will, by definition, be the induction time of the 20 mL section with the shortest induction time. The higher the number of individual 20 mL sections, the more deterministic, or less random, the value of the lowest induction time will become.

### **4.3.2 Short Induction Times**

Crystallization induction time is defined as the time taken for the first appearance of crystals in a solution of constant supersaturation (Mullin 2001). Therefore, in cases where supersaturation is achieved by cooling, as is the case in this study, the time to reach the steady-state crystallization temperature must be negligible compared to the induction time. The former was experimentally estimated to be around 7 minutes by measuring, with a thermocouple, the time taken for the solution in a vial to reach the same temperature as the water bath within 0.01 C°. This value is negligible compared to nearly all median  $t_{ind}$  values.

However, often the first induction times in an experiment occur within a few minutes and hence before the vial contents have reached the desired crystallization temperature completely. This is far from ideal, but is almost unavoidable due to the broad spread of the induction time distributions. In the evaluation, we have the choice to either omit these early induction times or to include them. We believe that the second option is more correct. The error in these data points is that the recorded induction times are longer than they would have been if the nucleation temperature had been reached instantaneously, since the anticipated supersaturation hasn't been fully reached at the moment of nucleation. Accordingly, if these values are included in the calculation of the average induction time, the average time will be *somewhat* longer than the true value. However, if all these early values are removed completely, the calculated average induction time will be *much longer*, and accordingly more deviating from the "true average value". In addition, by using the median value (equal to the geometric mean of the log-normal distribution function) to represent the central tendency of the induction time distribution, this particular problem is significantly reduced, since the median of a distribution by definition does not depend on the exact values of the earlier data points.

## Influence of Solvent on Nucleation of Tolbutamide and Fenoxycarb

However, as will be shown further on, there are experimental conditions where the geometric mean/median induction time is in the same range as the time to cool to the nucleation temperature. This problem can be dealt with by trying to reduce either the cooling time or the supersaturation. The first approach requires more specialized techniques that are difficult to implement in experiments with large sample numbers, while the second would force the whole study into longer induction times. Accordingly, the supersaturation range used throughout the study is a compromise, and for the cases where a larger fraction of the induction times appear within the first 5-7 minutes, the specific geometric mean/median value should be interpreted as having a greater uncertainty, and being higher than the true value. Thus, for the purpose of this work and the conclusions drawn, we conclude that the effect of a limited cooling rate in establishing the nucleation conditions has no significant influence, partly because the approach to the nucleation temperature is highly non-linear and after only 1 minute (0.0167 h) the deviation is only 1 C°.

### **4.3.3 Supersaturation**

It is important to acknowledge that the thermodynamic driving force,  $RT\ln S$ , and consequently the interfacial energy, are highly sensitive to the accuracy of the supersaturation values,  $S$ , employed. Due to the prohibitive complexity of measuring activities to directly calculate  $S$ , it was necessary to use the concentration ratio as an approximation, and this estimation is accurate to the extent that the relevant activity coefficient ratio approaches unity (see equation (4)). Activity coefficients are a function of both concentration and temperature. Equilibrium activity coefficient values are available in the literature for fenoxycarb for the solvents and concentrations of interest (Kuhs *et al.* 2013); non-equilibrium activity coefficients, however, are lacking, and as the relationship between activity coefficient and concentration can be nonmonotonic (Vincze *et al.* 2010), are non-trivial to estimate with a sufficient degree of certainty.

Further uncertainty in the estimation of  $S$  arises from the uncertainties in solubility and concentration values. The average coefficient of variation for solubility and concentration values for both fenoxycarb and tolbutamide in this work is around 1.5% (see Table 3 and Table 5), which can cause even greater error in the calculation of

## Influence of Solvent on Nucleation of Tolbutamide and Fenoxycarb

$RT\ln S$  and the interfacial energy due to their non-linear relationship. The resultant error is greater in  $RT\ln S$  than in the interfacial energy (since calculation of the latter from nucleation experiments depends on  $\ln^2 S$ , see equation (16), while the former depends on  $\ln S$ ), and the magnitude of the resultant error in both increases the closer  $S$  is to unity as a result of the logarithmic function. Example values are shown in Table 10 for the smallest and largest values of  $S$  used in our experiments, as well as the effect on the resultant interfacial energy assuming there are no other errors. As can be seen, an average 1.5% error in  $S$  leads in the worst case (i.e. at the lowest  $S$ ) to an error of around 5% in both thermodynamic driving force,  $RT\ln S$ , and interfacial energy. This is unlikely to change the trends among solvents for either solute, except perhaps in the cases of the alcohols for fenoxycarb and toluene and n-propanol for tolbutamide, where the differences are not significant.

**Table 10: Demonstration of the effect of error in estimating  $S$  on the subsequent magnitude of error in the calculation of  $(RT)\ln S$  and interfacial energy, shown for smallest and largest values of  $S$  used and using the approximate average coefficient of variation (1.5%) of the solubility values as the error in  $S$ .**

	$S$	$\ln S$	$\ln^2 S$	Interfacial energy ( $\text{mJ m}^{-2}$ , assuming no other errors)
<b>Fenoxycarb in ethyl acetate</b>	1.33	0.285	0.0813	0.82
<b>1.5% error</b>	1.35	0.300	0.0900	0.86
	<i>resultant error:</i>	<i>5.2%</i>	<i>10.7%</i>	<i>4.9%</i>
<b>Fenoxycarb in isopropanol</b>	5.74	1.75	3.05	4.86
<b>1.5% error</b>	5.83	1.76	3.11	4.77
	<i>resultant error:</i>	<i>0.9%</i>	<i>1.7%</i>	<i>-1.9%</i>

### 4.3.4 Interfacial Energies and Pre-exponential Factors

Although  $\gamma$  and  $A$  are temperature and concentration dependent (Kashchiev 2000, Mullin 2001), the variation in  $T_{cry}$  is quite low for both fenoxycarb and tolbutamide ( $\sim 5$  C°), and more importantly, the ability of the CNT to account for the data (see goodness of fits in Figure 15 and Figure 18) suggests the effect of  $T_{cry}$  and concentration on  $\gamma$  and

## Influence of Solvent on Nucleation of Tolbutamide and Fenoxycarb

$A$  is negligible under the narrow investigated temperature range. A negligible variance in  $\gamma$  over temperature ranges of 65 C° has in fact been reported (Lancia *et al.* 1999).

It is regrettable that for all solute-solvent combinations except one induction times were only obtained at three thermodynamic driving forces. When collecting induction time distributions for different solvents at different thermodynamic driving forces, a balance must be found between the time requirement of a single iteration (which is not the median but the longest induction time), the number of iterations required to achieve a representative number of data points, and the number of different solute/solvent combinations of interest. Particularly due to the length of a single iteration (up to 1 day), it was not feasible to probe more than three thermodynamic driving forces per solvent-solute combination unless we were willing to investigate less solvents. It was decided that a minimum of four solvents should be probed per solute even if only three driving forces could be investigated for each. Nevertheless, the good fits of the CNT to the data, expressed as the coefficient of determination,  $R^2$  (ranging from 0.93 to 0.999, see Figure 13 and Figure 16), gives confidence in the validity of the CNT parameters,  $\gamma$  and  $A$ , derived from these fits. In the case of tolbutamide in ethyl acetate, induction times were measured at 4 thermodynamic driving forces, and the CNT gave a satisfactory fit with  $R^2 = 0.987$ . Finally, it is to be noted that in order to analyse our data we do not only use the interfacial energies, which admittedly depend on regression of only three data points, but also the thermodynamic driving force required to reach the same induction times, which is directly obtained from experimental parameters.

The absolute values of  $\gamma$  are of the same order of magnitude as similar studies for similar compounds, namely between 0.5 and 10 mJ m<sup>-2</sup> (Yang and Rasmuson 2013, Yang *et al.* 2014). In the case of  $A$ , Kashchiev (2003) claims this is usually between 10<sup>15</sup> and 10<sup>25</sup> m<sup>3</sup> s<sup>-1</sup> for heterogeneous nucleation. However, our values for  $A$  are over 15 orders of magnitude lower, ranging from 10<sup>-2</sup> to 10 m<sup>3</sup> s<sup>-1</sup>. On the other hand, experimental results from studies of similar organic systems range from 10<sup>2</sup> to 10<sup>6</sup> m<sup>3</sup> s<sup>-1</sup> (Jiang and ter Horst 2010, Mealey *et al.* 2015f). It is to be noted that some of these studies report  $A'$  instead of  $A$  (see equation (18)); however, as values of  $S$  are close to unity in these cases,  $A'$  and  $A$  are of the same order of magnitude.

## Influence of Solvent on Nucleation of Tolbutamide and Fenoxycarb

According to equation (20),  $A$  depends in part on the attachment frequency ( $\nu^*$ ) and the concentration of nucleation sites ( $C_0$ ). Though possible, it is difficult to imagine a difference in  $C_0$  of many orders of magnitude between similar organic systems with the same solute at similar concentrations, etc. A difference of several orders of magnitude in  $\nu^*$  seems somewhat more likely, as for example the solutions of fenoxycarb are quite viscous due to the extremely high concentrations, which may help explain the low values of  $A$  for fenoxycarb. Furthermore, as has already been suggested in the literature (Jiang and ter Horst 2010), low values of  $\nu^*$  could be caused by solute molecules being strongly solvated, or by energetically difficult conformational changes being involved in the formation of the stable nucleus. Indeed, evidence for the influence of conformational transformations and/or solvation on the nucleation of organic systems is growing (Derdour and Skliar 2014). More specifically, as is discussed in the following section, there is strong evidence that in the case of fenoxycarb and tolbutamide solvent-solute interactions affect nucleation.

The number of fenoxycarb and tolbutamide molecules in the critical nucleus,  $n^*$ , are quite small, ranging from 20 to just under 1 (Table 7 and Table 9). For the highest  $S$  of fenoxycarb in ethyl acetate  $n^*$  appears to have reached unity, implying the solution-crystal spinodal has been reached, where  $\Delta G^*$  is less than the thermal energy of the molecules (Vekilov 2010d). If this were correct, further increasing  $S$  would result in a change in the observed dependence of  $t_{ind}$  on  $S$  and  $T_{cry}$ . Unfortunately, we did not obtain any relevant data to test this. Such low numbers of  $n^*$  have recently been found in several similar studies of medium-sized organic molecules, though unfortunately also in these cases no induction times were collected beyond the implied spinodal (Yang *et al.* 2014, Mealey *et al.* 2015a, Mealey *et al.* 2015f).

### **4.3.5 Solvent Influence on Ease of Nucleation**

Overall, the order of interfacial energies and ease of nucleation in terms of required driving force to achieve similar induction times of the different solvents is similar for both fenoxycarb and tolbutamide form I<sup>L</sup>, namely nucleation from ethyl acetate is easier than from toluene or the alcohols (see summary in Table 11). For fenoxycarb, nucleation from toluene is easier than from the alcohols, while for tolbutamide form I<sup>L</sup>

### Influence of Solvent on Nucleation of Tolbutamide and Fenoxycarb

nucleation from toluene may be slightly more difficult than from n-propanol (more difficult according to RTlnS, but easier according to interfacial energy; though the latter difference is not significant, see discussion in section 4.2). The order between isopropanol and ethanol for fenoxycarb is similarly ambiguous. Thus, it is most difficult to nucleate from alcohols, and nucleation of fenoxycarb occurs with similar difficulty from both ethanol and isopropanol.

**Table 11: Ranking (1 = lowest/easiest, 4 = highest/most difficult) for fenoxycarb and tolbutamide of interfacial energies from CNT and thermodynamic driving forces (RTlnS) required to achieve induction times of 2.06 h (fenoxycarb) and 2 h (tolbutamide).**

	Fenoxycarb		Tolbutamide	
	$\gamma$ ( $\text{mJ m}^{-2}$ )	Driving force, RTlnS ( $\text{kJ mol}^{-1}$ )	$\gamma$ ( $\text{mJ m}^{-2}$ )	Driving force, RTlnS ( $\text{kJ mol}^{-1}$ )
<b>Acetonitrile</b>			1	1
<b>Ethyl acetate</b>	1	1	2	2
<b>Toluene</b>	2	2	3	4
<b>Isopropanol</b>	3	4		
<b>N-propanol</b>			4	3
<b>Ethanol</b>	4	3		

The ease of nucleation cannot be correlated for both solutes to the same basic property such as dipole moment (not shown), boiling point, solvent density or solubility (Figure 19). In the case of fenoxycarb,  $\gamma$  and RTlnS seem to follow the trend often observed and also justifiable assuming regular solution theory (Bennema and Söhnel 1990) of being inversely proportional to solubility, while no such correlation appears for tolbutamide (Figure 19 left; RTlnS is not shown but is similar). Solvent boiling point has been found to correlate for other molecules, and Yang (2013) postulates this is due to boiling point being a measure of the solvent cohesiveness, and the formation of an interface requiring the breaking of some solvent-solvent bonds. We find a weak correlation in the case of tolbutamide (Figure 19 bottom right), while no such correlation is apparent for fenoxycarb. Accordingly, this may suggest the nucleation of tolbutamide is somewhat

## Influence of Solvent on Nucleation of Tolbutamide and Fenoxycarb

related to solvent-solvent interactions. Strangely, we found a strong correlation with solvent density for fenoxycarb (Figure 19 top right).

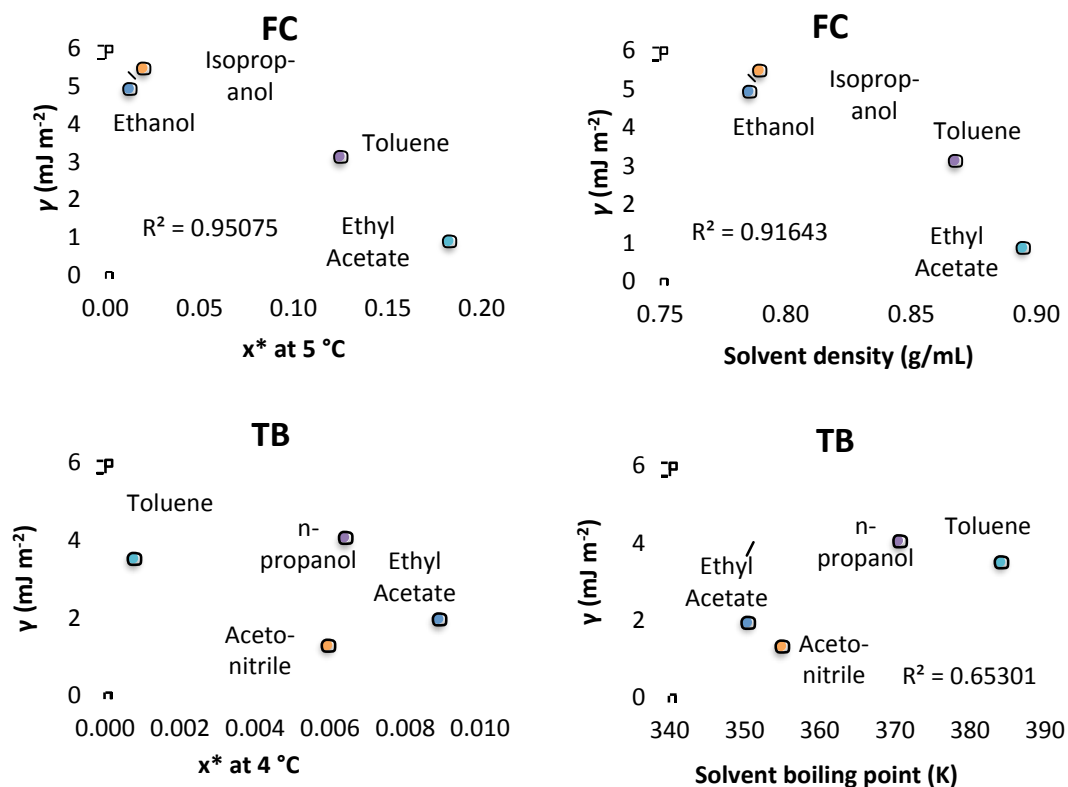


**Figure 19: Interfacial energy compared to mole fraction solubility for both fenoxycarb and tolbutamide (top and bottom left, respectively), to solvent density for fenoxycarb (top right), and to solvent boiling point for tolbutamide (bottom right). Lines are linear fits for checking direct proportionality.**

It is also interesting to note that fenoxycarb's solubility in toluene is between those of the alcohols and ethyl acetate (Table 3), while tolbutamide's solubility in toluene is far less than in all other measured solvents (Table 5). Yet despite this significant difference, fenoxycarb and tolbutamide both nucleate with comparative ease from toluene, namely between ethyl acetate and the alcohols (Table 11).

That nucleation from alcohol is more difficult than from ethyl acetate has been observed in several other studies of organic molecules (Yang and Rasmuson 2013, Yang *et al.* 2014, Mealey *et al.* 2015a, Mealey *et al.* 2015f). One of these studies also tested

## Influence of Solvent on Nucleation of Tolbutamide and Fenoxycarb

toluene, and, unlike for fenoxycarb and tolbutamide, found nucleation from toluene significantly easier than from both alcohols and ethyl acetate (Mealey *et al.* 2015f).

Recent work on salicylic acid and risperidone found that nucleation from 8 and 6 organic solvents, respectively, became more difficult as the solvent-solute interactions became stronger (Khamar *et al.* 2014, Mealey *et al.* 2015f). This was based on nucleation, spectroscopic, calorimetric and modelling work, and the correlation was rationalised by the hypothesis that the more the solvent binds the solute, the more difficult the nucleation becomes.

Thus, to further rationalise the influence of solvent in the case of fenoxycarb and tolbutamide, solvent-solute interaction enthalpies determined by co-authors from molecular modelling and calorimetrically measured solution enthalpies (see Appendices A & B) are compared to the nucleation results. Both calorimetric and molecular modelling derived solvent-solute interactions have been cross-validated against each other, and found to agree substantially. Both methods have also been successfully cross-validated against FTIR frequencies of the solvent-solute carbonyl bands which are indicative of the strength of solvent-solute interactions (see Appendices A & B). In general, solvent-solute interactions are reported to decrease in the order n-propanol > acetonitrile > ethyl acetate > toluene with tolbutamide, and ethanol > isopropanol > ethyl acetate > toluene with fenoxycarb.

In the case of fenoxycarb, an overall trend similar to that reported for salicylic acid and risperidone of increasing nucleation difficulty with increasing solvent-solute interaction is discovered quantitatively (Figure 20), and qualitatively in the order between the solvents, especially when considering that the difference in nucleation difficulty between the alcohols is ambiguous. A significant exception to this trend is toluene. Despite having a slightly weaker solvent-solute interaction than ethyl acetate, it is far more difficult to nucleate from.

## Influence of Solvent on Nucleation of Tolbutamide and Fenoxycarb

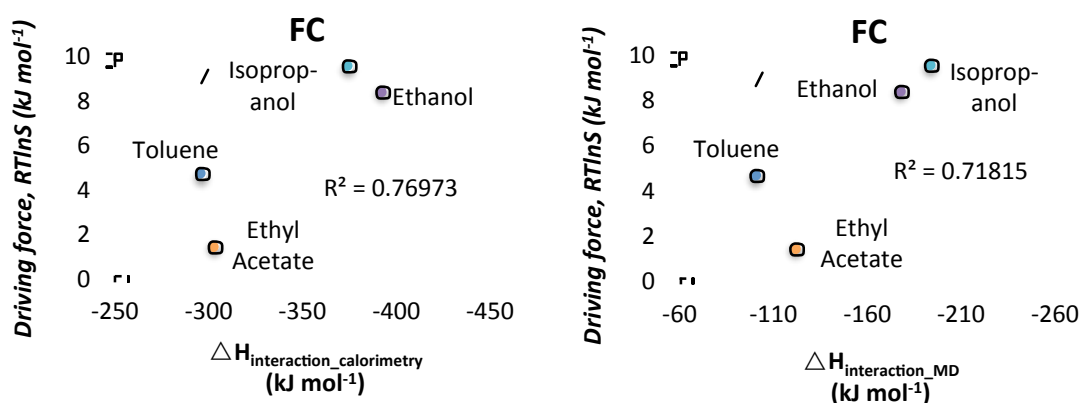


**Figure 20: Fenoxycarb thermodynamic driving force,  $RT\ln S$ , required to reach median induction times of 2.06 h, correlated to calorimetric (left) and molecular dynamics (MD, right) solvent-solute interaction enthalpies determined by co-authors. Source of enthalpies: Appendix A.**

In the case of tolbutamide a similar overall trend does not appear, either quantitatively (Figure 21), or qualitatively in the order between the solvents. Interestingly, as in the case of fenoxycarb, toluene fits the trend least of all, since it is very difficult for tolbutamide to nucleate from this solvent despite having by far the weakest solvent-solute interactions. On the other hand, the relative difficulty of nucleation from ethyl acetate and acetonitrile is the reverse of their solvent-solute interactions. However, tolbutamide is easier to nucleate from these than from n-propanol, which has much higher solvent-solute interaction enthalpies, in agreement with the general trend previously reported.

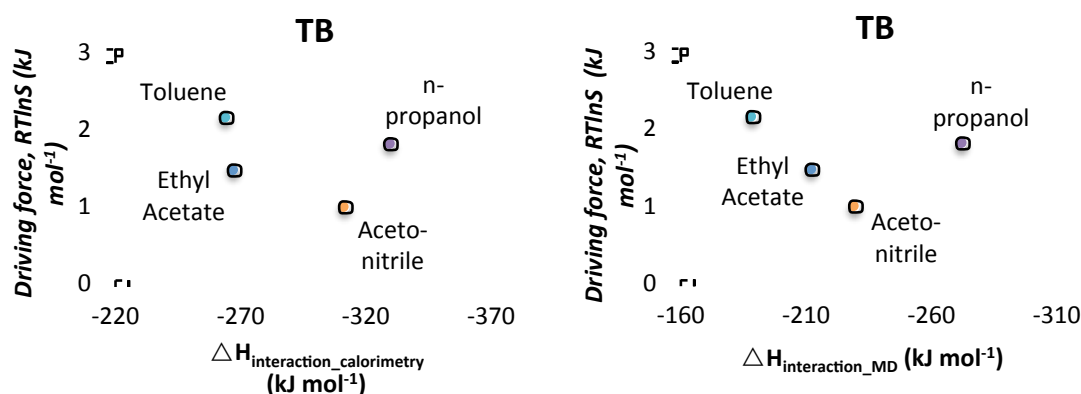


**Figure 21: Tolbutamide nucleation difficulty as driving force required to reach  $t_{\text{ind}} = 2$  h correlated to calorimetric (left) and molecular dynamics (right) solvent-solute interaction enthalpies as determined by co-authors. Source of enthalpies: Appendix B.**

## Influence of Solvent on Nucleation of Tolbutamide and Fenoxycarb

The spectroscopic, calorimetric and modelling investigations carried out by co-authors (Appendix B) may offer an explanation, especially keeping in mind that the evidence for the sensitivity of nucleation to the conformer population in the solution is growing (Derdour and Skliar 2014). Radial distribution functions from the MD trajectories of intra-molecular O-H distances of tolbutamide molecules in solution have been reported (see Appendix B). It suggests that only in toluene does tolbutamide exist as a conformer with intra-molecular hydrogen bonding (Figure 22c), and that all tolbutamide molecules transform to this conformer in toluene. This observation matches results of the DFT conformational analysis (see Appendix B), where it was predicted that intramolecularly hydrogen-bonded conformations of tolbutamide are more stable by 4 - 14 kJ mol<sup>-1</sup> than the form II conformer, which in turn is around 20 kJ mol<sup>-1</sup> more stable than the form I<sup>L</sup> conformer. In order to nucleate form I<sup>L</sup>, the tolbutamide molecules would have to transform to the form I<sup>L</sup>-like conformer, and this transformation could be quite difficult with intra-molecular hydrogen-bonded conformers possibly present in toluene solutions. Reported conformational analysis indicates that such a transformation can be a multistage process and the energy barrier for interconversion between the non-intramolecularly-H-bonded and the intramolecularly-H-bonded conformations can be as high as 42 kJ mol<sup>-1</sup> (see Appendix B), which according to recent findings (Derdour *et al.* 2011) may be of sufficient magnitude to influence the overall nucleation process. This could explain why nucleation of tolbutamide from toluene is very difficult despite weak solvent-solute interactions.

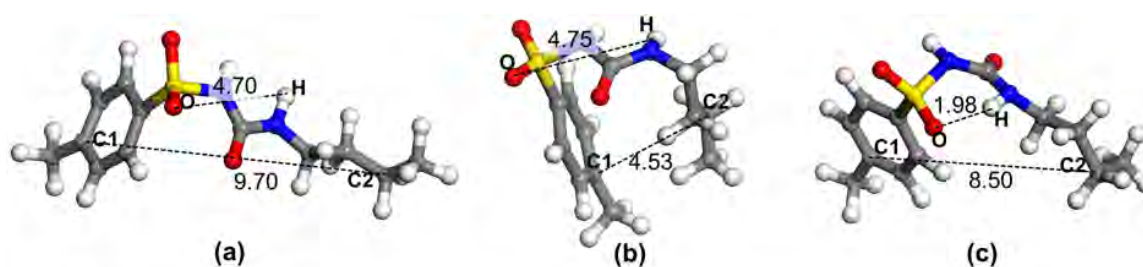


**Figure 22: Representative conformations of tolbutamide in n-propanol (a and b), and in toluene (c), for which co-authors have calculated radial distribution functions (RDF) to illustrate how different solvents influence conformational changes. Source: Appendix B.**

## Influence of Solvent on Nucleation of Tolbutamide and Fenoxycarb

The discrepancy in the nucleation order between acetonitrile and ethyl acetate could also be related to the presence of crystal-like and non-crystal-like conformers of tolbutamide in their respective solutions and the energy barriers associated with their interconversion. The radial distribution functions of the C1-C2 distances have been reported (Figure 22 right), and suggest that in acetonitrile tolbutamide may exist as both a linear-like molecule, similar to that of form II, and a U-shaped conformer similar to tolbutamide form I<sup>L</sup> (Figure 22a and b, respectively). However, in ethyl acetate tolbutamide only appears to exist as the linear conformer similar to form II (cf. Figure 22a). Thus the nucleation of the metastable form I<sup>L</sup>, which was found to preferentially nucleate from both acetonitrile and ethyl acetate solutions under experimental conditions, could be more difficult from ethyl acetate than from acetonitrile from a conformational point of view.

Furthermore, the stronger solvent-solvent interactions in acetonitrile compared to ethyl acetate (see Appendix B) could allow more clustering of tolbutamide molecules in acetonitrile solutions, which in turn could facilitate easier nucleation. Indeed, reported spectroscopic data shows the relative height of the C=O shoulder peak, indicative of solute-solute interactions, rising more quickly with concentration in acetonitrile compared to ethyl acetate (see Appendix B).

Lastly, in the case of fenoxycarb in isopropanol, reported modelling also suggests that the structure of fenoxycarb solute clusters may influence the nucleation (see 5.3.3). Though we have not yet tested whether this effect is solvent-dependent, this could be another mechanism whereby the solvent influences nucleation.

In summary, it has been demonstrated that in the case of fenoxycarb the previously-reported trend of stronger solvent-solute binding leading to more difficult nucleation from solution is also observed, with the exception of nucleation from toluene, which is difficult despite weak solvent-solute interaction. In the case of tolbutamide, this relationship appears to be complimented by significant differences in the identity of tolbutamide conformers present in the solutions. For example, modelling gives a possible explanation why the weak solvent-solute interactions of tolbutamide and toluene does not lead to easy nucleation: tolbutamide may be assuming an

## Influence of Solvent on Nucleation of Tolbutamide and Fenoxycarb

intramolecularly hydrogen-bonded conformation not found in the crystal structures which has a very high transformation barrier.

# V

## **5 Influence of History of Solution in Crystal Nucleation of Fenoxycarb**

## Influence of History of Solution in Crystal Nucleation of Fenoxycarb

*The history of solution work presented below has been published in modified form in a peer-reviewed journal (Kuhs et al. 2014).*

While collecting induction times of fenoxycarb in isopropanol for section 4.1, it was discovered that increasing pretreatment time and temperature increased the subsequent induction time. The systematic study of this history of solution effect on nucleation is reported below.

### **5.1 Validation**

The simplest explanation for any observed thermal history effect on induction times is incomplete dissolution of the crystal material. We offer the following evidence that this is highly unlikely to be the case here:

- Visual observation of the nucleation event shows that the appearance of the first crystal in a supersaturated solution is immediately followed by further nucleation and crystal growth. As such, if undissolved fenoxycarb were present in the solution, we would expect the nucleation to become visible shortly after achieving supersaturation, which is not the case (average induction times are several hours).
- Crystallised vials contain so much solid that the entire vial appears filled with the solid when crystallised at 5 °C, yet when exposed to even minor undersaturation temperatures of 25 °C (5 C° above saturation), dissolution appears complete to the naked eye after less than 5 minutes (i.e. no more solids are visible). Furthermore, varying pretreatment (i.e. dissolution) time from 24 to 72 *hours* at the same temperature still results in a significant difference in subsequent induction times.
- Concentration measured in the vials both at the beginning of the pretreatment stage (after 10 minutes) and immediately before dissolution show no noticeable difference (although admittedly the inaccuracy of our concentration measurements in this case is around 5-6%).

## Influence of History of Solution in Crystal Nucleation of Fenoxycarb

Assuming then that simple incomplete dissolution of the solute is not the explanation, before analysing the effect of the thermal history of solution on crystallization, the following must be validated:

1. All vials must behave identically – no vials must have a systematic tendency to nucleate faster or slower than other vials.
2. Since vials are reused over a period of more than 5 months, there must be no significant solvent evaporation or decomposition.
3. Runs must be independent of previous runs – the induction times of a run must depend solely on the pretreatment condition of that run.

Because of the spread of induction times that occurs at the scale of these experiments, identical vials are not expected to have the same induction time every time they nucleate; rather, the *spread* of induction times for every vial should be identical. However, because the different induction times for a particular vial correspond to different pretreatment conditions, it is not possible to simply compare the spread of induction times. Instead, for each experiment in which all vials nucleate under the same pretreatment conditions, each vial can be assigned a nucleation rank, specifying when in relation to the other vials nucleation takes place, e.g. rank 4 means that this vial was the 4<sup>th</sup> to nucleate in that experiment. This should give a discrete uniform distribution of ranks for each vial if the vials are identical and sufficient experiments have been performed. A 2 sample Kolmogorov-Smirnov test was carried out, comparing the rank distribution of each individual vial to the relevant discrete uniform distribution (each vial had 62 rank values). At a 95% confidence level, the null hypothesis that the rank distribution of vials 15, 16, 24 and 25 is the same as the uniform discrete distribution is rejected, while for all other vials it is not rejected (see Table 12). As such, it appears that 4 out of 29 vials do not behave randomly and consequently these are ignored in the following sections (although we confirmed that even including these the results remain substantially the same).

## Influence of History of Solution in Crystal Nucleation of Fenoxycarb

**Table 12: Results of 2 sample Kolmogorov-Smirnov tests of the rank distribution of each vial against the uniform discrete distribution which is expected if all vials are identical.**

<b>Vial #</b>	<b>p value*</b>	<b>Vial #</b>	<b>p value*</b>	<b>Vial #</b>	<b>p value*</b>
<b>10</b>	1.0000	<b>9</b>	0.5953	<b>23</b>	0.2135
<b>1</b>	0.9985	<b>8</b>	0.4426	<b>7</b>	0.1397
<b>12</b>	0.9985	<b>5</b>	0.3139	<b>13</b>	0.1397
<b>18</b>	0.9985	<b>20</b>	0.3139	<b>19</b>	0.1397
<b>4</b>	0.9750	<b>22</b>	0.3139	<b>3</b>	0.0535
<b>11</b>	0.9750	<b>29</b>	0.3139	<b>15</b>	0.0313
<b>28</b>	0.9750	<b>2</b>	0.2135	<b>16</b>	0.0313
<b>26</b>	0.8935	<b>6</b>	0.2135	<b>25</b>	0.0096
<b>14</b>	0.7558	<b>17</b>	0.2135	<b>24</b>	0.0050
<b>27</b>	0.7558	<b>21</b>	0.2135		

\* *p* values below 0.05 mean there is a 95% likelihood that these vials are biased towards either shorter or longer induction times compared to the remainder of the vials.

The solutions were used for a total of 225 days. Solvent evaporation and fenoxycarb decomposition over time were examined by regularly obtaining solution <sup>1</sup>H NMR spectra from 2 vials. In no cases were new organic species detected, and the concentration results are shown in Figure 23. The Pearson's correlation coefficient's *p* value of 0.5342 means there is no evidence that concentration changed systematically with time, and the 6% variation, though large, is similar to the variation we found when repeatedly measuring the same solution, and is most likely due to inaccuracies inherent in measuring concentration using NMR (inaccurate integration, peak overlapping, etc.).

## Influence of History of Solution in Crystal Nucleation of Fenoxycarb

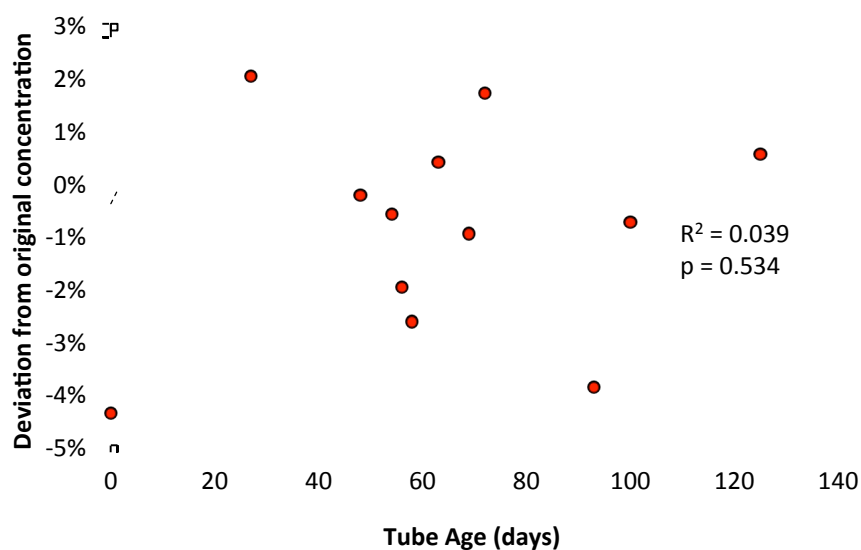


**Figure 23: Solution concentration in g fenoxycarb / g isopropanol over vial age determined by solution  $^1\text{H}$  NMR. Solid line is the best straight line fit, for which Pearson's correlation parameters  $R^2$  and  $p$  are shown.**

The third is considerably more difficult to investigate. A run might be affected by the combined effect of all preceding ones. Even assuming that only the experiment immediately preceding is significant, 3 runs of each pair of run/preceding run conditions would need to be performed to obtain statistically significant results, which would mean at least 6 runs for each pretreatment condition. This is not feasible, however. Therefore, we simply analysed the relationship between induction time and preceding induction time by calculating the Pearson's correlation coefficient of the relationship between the two, reasoning that the preceding induction time is the best single measure of the effect of the preceding cycle on the solution history. The results are shown in Table 13. At a 95% confidence level, only the results for pretreatment conditions of 24 h 35 °C show significant correlation with the pretreatment of the previous experiment, while the rest appear unaffected.

**Table 13: Relationship between induction time and immediately preceding induction time.**

Pretreatment Conditions			Pearson's Correlation Coefficient	
Time (h)	Temp (°C)	# of runs	r	p-value
24	35	3	0.997	0.049
2	25	3	0.980	0.126
2	30	3	0.9717	0.1518
6	35	3	-0.921	0.255
2	35	3	0.900	0.287
18	30	3	-0.8343	0.3718
24	40	3	-0.747	0.463
2	45	3	0.617	0.577
12	35	3	-0.419	0.725
4	45	4	0.181	0.819
18	35	5	-0.142	0.820
6	30	3	-0.1679	0.8926
24	45	3	0.072	0.954

Although there is some indication that all aspects of the validation are not entirely satisfactory, overall the validation analysis does give us confidence to proceed with reporting and analysing the experimental results and drawing the conclusions made.

## 5.2 Induction Times

The relationship between pretreatment time,  $t_{PT}$ , and the nucleation induction time,  $t_{ind}$ , was measured at different preheating temperatures,  $T_{PT}$ , and the results are reported in Figure 24. The induction time consistently increases with increasing preheating time, except in the 45 °C experiments, where an end point appears to be reached after which there is no clear increase in  $t_{ind}$  with increasing  $t_{PT}$  (see especially Figure 24 (d) right-hand side). Since the distributions in some cases show overlap, we performed 2-sample Kolmogorov-Smirnov tests to determine if they can be treated as being statistically different. At 95% significance, only the distributions at 45 °C with pretreatment time > 0.66 h were found to be non-distinguishable.

### Influence of History of Solution in Crystal Nucleation of Fenoxycarb

The right hand graphs of Figure 24 suggest an overall behaviour where the inverse of the geometric mean of the induction time decays exponentially with increasing preheating time at all preheating temperatures, except at 45 °C. At this temperature there is an initial rapid increase in the induction time at short preheating times, consistent with the behaviour at the other temperatures (though admittedly we do not have induction times for the other pretreatment temperatures at  $t_{PT}$  of 0.33 and 0.66 h). However, this is followed by behaviour where the induction time changes are much slower or perhaps entirely non-existent. This result is consistent with the view that the changes that take place during the pretreatment eventually terminate into a “steady-state” situation.

Describing the relationship of the inverse geometric means with  $t_{PT}$  as an exponential decay was statistically investigated through the calculation of Pearson’s correlation coefficients for fits. These were found to be statistically significant in all cases, though with varying significance (see  $p$  values on right side in Figure 24).

## Influence of History of Solution in Crystal Nucleation of Fenoxycarb

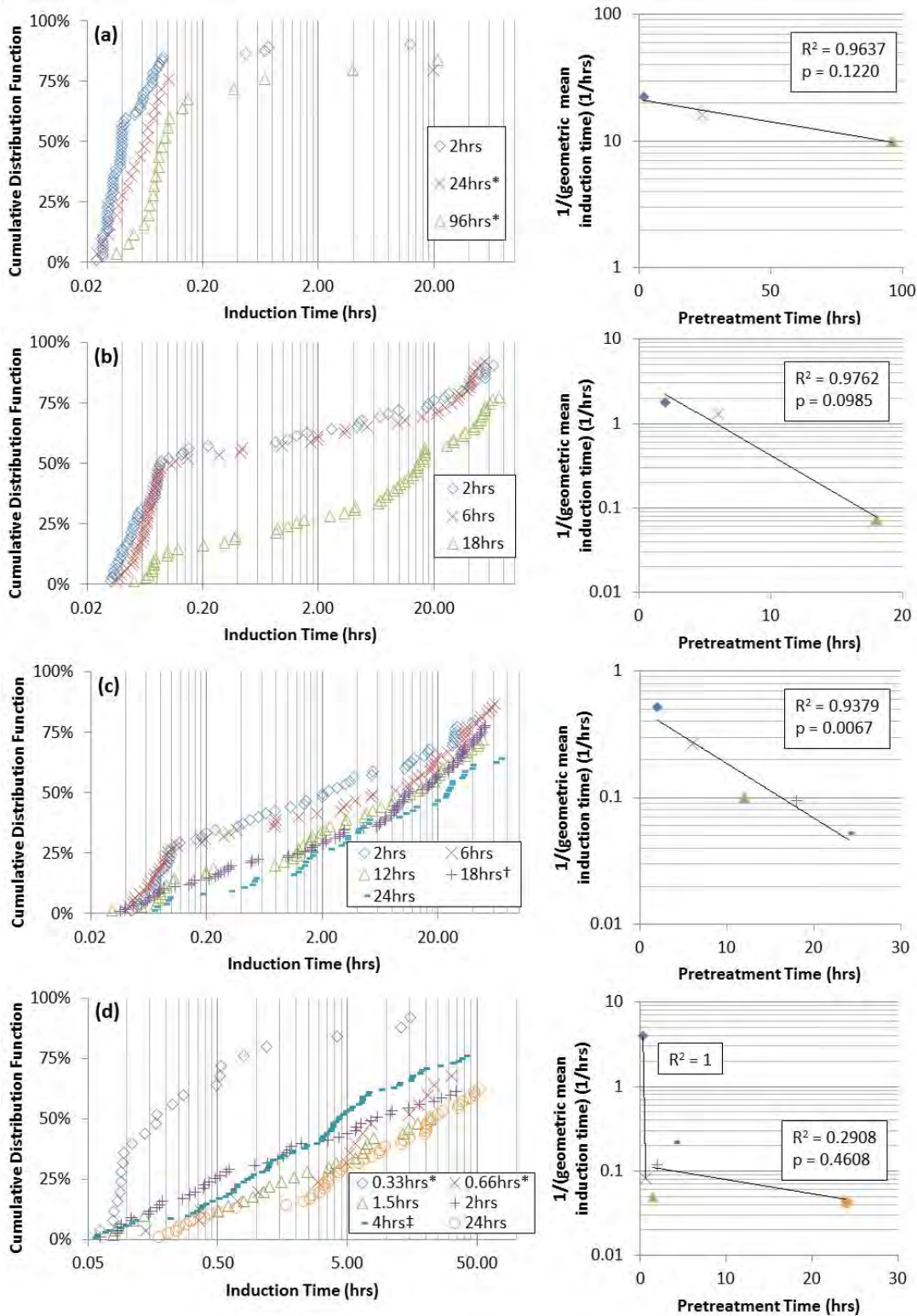


**Figure 24: Effect of pretreatment time on induction time at (a) 25 °C, (b) 30 °C, (c) 35 °C and (d) 45 °C pretreatment temperature. Left: Cumulative distribution curves; right: point estimates of each distribution as geometric mean. Pretreatment conditions marked with \*, † and ‡ were iterated 1, 5 and 4 times, respectively, compared to the normal 3 times, with the set of 25 validated solutions.**

## Influence of History of Solution in Crystal Nucleation of Fenoxycarb

At constant pretreatment time, the induction time is substantially influenced by the pretreatment temperature, as is shown in Figure 25. At 2 h pretreatment, the dependence of the inverse of the induction time on the pretreatment temperature can be well represented by an exponential relationship (with 94% confidence). However, this relationship is not found at  $t_{PT} = 24$  h, where 35, 40 and 45 °C experiments have reached roughly the same induction time (Figure 25).

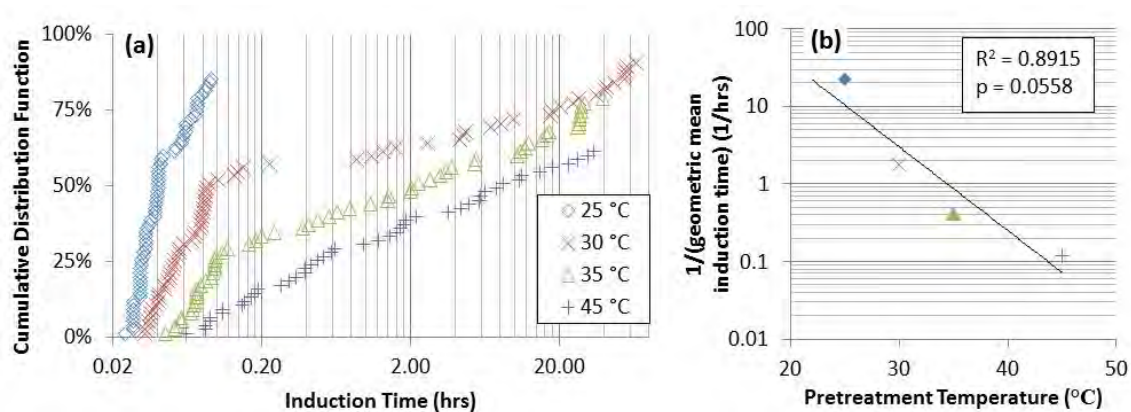


**Figure 25: Effect of pretreatment temperature on induction time for a pretreatment time of 2 h. (a) is raw data for all 3 runs per pretreatment condition set; (b) induction time geometric mean vs pretreatment temperature.**

Accordingly, there appears to be an end point for the transformation during the pretreatment period where there is no more noticeable effect of thermal history on the nucleation. This end point position appears to be independent of pretreatment temperature, though the higher the pretreatment temperature the faster this steady state is approached.

The very first time the solutions in the vials were exposed to nucleation, the induction time distribution is clearly different from all following nucleation experiments. Figure 26 shows the induction time distribution of this very first nucleation experiment with 25 different vials (vials giving accepted randomness, see the validation), *viz.* that immediately following the filtration and aliquoting into the vials of the stock solution dissolved at pretreatment conditions of 24 h at 25 °C. The results are compared with the induction times obtained subsequently for experiments heated at different preheating temperatures for 24 h. The induction time distributions for 24 hours pretreatment time at

## Influence of History of Solution in Crystal Nucleation of Fenoxycarb

35 and 45 °C pretreatment temperature represent the longest induction times achieved under any conditions after the first nucleation (compare with Figure 24). Note that these distributions correspond to the “steady state” induction times discussed previously, where the history of solution effect has vanished.

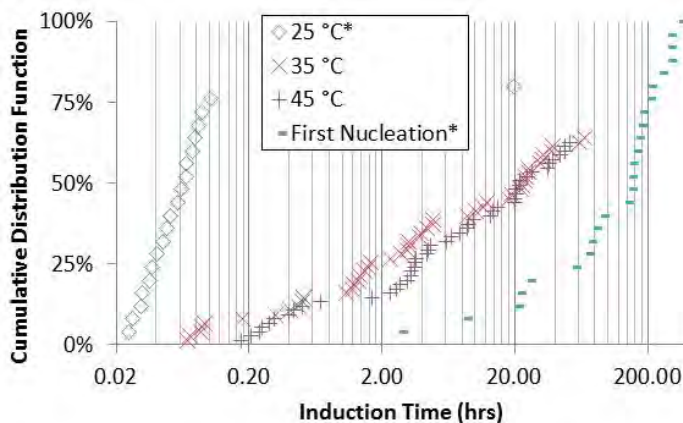


**Figure 26:** Nucleation induction time distribution of the “first nucleation” compared to the distributions obtained at subsequent experiments at the same preheating time of 24 h. Pretreatment conditions marked with \* only have 25 data points (from a single iteration of 25 solutions), compared to the normal 75 (from 3 iterations).

A 2 sample Kolmogorov-Smirnov test comparing the distributions of the first nucleation to all 24 h distributions (i.e. 25, 35 and 45 °C) gives  $p < 0.005$  in each case, meaning that the induction time distribution of the first nucleation experiment significantly exceeds all subsequent induction time distributions irrespective of pretreatment conditions.

### **5.3 Discussion**

For discussion of the method and general features of induction time distributions obtained in this thesis, see sections 4.3.1 and 4.3.2.

#### **5.3.1 First Nucleation**

The very first nucleation experiment exhibited induction times significantly longer than any that could subsequently be achieved regardless of pretreatment conditions (Figure 26 and discussion). This suggests a principal difference between the nucleation

## Influence of History of Solution in Crystal Nucleation of Fenoxycarb

mechanism of the very first experiment in the vial and subsequent experiments. Thus an irreversible change (under the present conditions) must have occurred in the solutions during or after the first nucleation event subsequent to filtration and aliquoting. The following mechanisms could be envisaged:

1. The 0.2  $\mu\text{m}$  filtration step removed undissolved or thermodynamically-stable prenucleation clusters of fenoxycarb (which would have resulted in increased nucleation rate had they remained in the solution). Following the first nucleation event, they re-formed and never dissolved again, effectively seeding all subsequent nucleation events.
2. Following the first nucleation event, some fenoxycarb crystals were lodged in crevices in the glass walls of the vials, where they never dissolved again and also seeded all subsequent nucleation events.

However, as discussed in during validation, observation of the nucleation events show that the nucleation is very fast once supersaturation is created, rendering the second possibility highly unlikely.

On the other hand, a recent study on prenucleation clusters of glycine in aqueous solutions reveals a mechanism whereby the first possibility can occur (Jawor-Baczynska *et al.* 2013). It was found that dissolution of glycine crystals produced glycine-rich nanodroplets with diameter greater than 750 nm, the presence of which increased nucleation rates by an order of magnitude. These nucleation-inducing droplets, which were found to be stable even in undersaturated solutions, were removable by filtration but reformed during dissolution of glycine crystals following nucleation. Thus, if the same phenomena were occurring in the present work, the filtration could remove fenoxycarb-rich nucleation-inducing nanodroplets, leading to the observed slow nucleation rate in the first nucleation experiment. Only following recrystallization and subsequent dissolution do these nanodroplets re-form. Thus all subsequent nucleation experiments are effectively seeded by the previous dissolution process, preventing the slow nucleation rate from being observed again.

### Influence of History of Solution in Crystal Nucleation of Fenoxycarb

This raises the interesting question whether this phenomena of stable prenucleation clusters does not occur in many other cases. It is well known that filtration, by removing impurities, can significantly reduce the nucleation rate; perhaps it is not only impurities that are being removed but also large prenucleation clusters or “nanodroplets”?

Unfortunately for induction times of fenoxycarb in other solvents (section 4.1) only 6 vials were used per solvent. The resultant maximum 6 first nucleation induction times were not enough to demonstrate any clear difference between the first and subsequent nucleation experiments. In the case of tolbutamide (section 4.2), 30 vials were used for each solvent, which is sufficient to gain statistically significant induction time distributions for the first nucleation event. Interestingly, the first nucleation of tolbutamide in the different solvents did not exhibit a different induction time distribution than subsequent nucleation events. This suggests that, under the present conditions, tolbutamide does not form prenucleation clusters or nanodroplets larger than 0.2  $\mu\text{m}$ , or that if these are removed, they do not re-form during subsequent nucleation or dissolution.

#### **5.3.2 Rate of Change of Solution State**

In heterogeneous nucleation, which can reasonably be assumed to be the effective mechanism under these experimental conditions (Mullin 2001), the rate of nucleation depends on the concentration of nucleation-promoting species. A lower rate of nucleation at a higher temperature of pretreatment reflects a lower number of such species in solution. At conditions at which the solution history is affecting the nucleation rate, the rate of nucleation can be used as a measure of the concentration of the species responsible for the solution history effect. Under the assumption that nucleation is related to the presence of pre-nucleation clusters in the solution, the rate of nucleation may depend on the concentration and properties (size, structure, etc.) of these clusters. The kinetic analysis below is valid whether these clusters are crystalline sub-critical clusters in the sense of the classical nucleation theory, more amorphous or liquid-like entities in the sense of the two-step theory, or just a particular bonding between a few fenoxycarb molecules. If the rate of nucleation is assumed to be proportional to the inverse of the induction time, the higher induction time after a longer

## Influence of History of Solution in Crystal Nucleation of Fenoxycarb

pretreatment would then reflect a lower number of such species in solution. Indeed, the relationship of the inverse of the induction time with time of pretreatment is well described by an exponential decay (see Figure 24). Thus, if the inverse of the induction time is directly proportional to the concentration of these nucleation-promoting clusters, we may surmise that the concentration of these clusters decays according to a first order reaction. By fitting a first order rate equation, Equation (28), to  $1/t_{ind}$  against  $t_{PT}$  from the second column in Table 14, we can calculate a rate constant  $k$  at different  $T_{PT}$ . Similarly, the intercept of the exponential fit gives us the induction time corresponding to the conditions at the start of the pretreatment.

$$\frac{1}{t_{ind}} = \frac{1}{t_{ind}^0} e^{-kt_{PT}} \quad (28)$$

**Table 14: Rate of change of solution structure at different pretreatment temperatures.**

$T_{PT}$ (°C)	$k$ (h <sup>-1</sup> )	$1/t_{ind}^0$ (h <sup>-1</sup> )
<b>25</b>	0.0081	21.3
<b>30</b>	0.21	3.39
<b>35</b>	0.092	0.438
<b>45</b>	11.8	195.0

It is customary to measure the temperature dependence of any process by calculating an activation energy ( $E_A$ ). This is done, using the Arrhenius equation, not only for reaction rates, but also for a variety of different physical transformation processes such as dissolution (Thomas *et al.* 1971, Jordan and Rammensee 1996):

$$k = Ae^{-E_A/RT} \quad (29)$$

A plot of  $\ln k$  vs  $1/T$  will then allow calculation of  $E_A$  for the process. Here, we apply a similar approach to the temperature-dependence of the influence of the pretreatment on the primary nucleation of fenoxycarb, without limiting ourselves with respect to the detailed mechanism behind this effect, simply denoting it “solution restructuring” or transformation. In Figure 27, the values for the rate constant  $k$  are plotted against the

## Influence of History of Solution in Crystal Nucleation of Fenoxycarb

inverse of  $T_{PT}$  (from Table 14). The data fits Equation (28) with over 93% certainty (1-p), although it only accounts for 88% of the variation ( $R^2$ ). The resultant  $E_A$  is 262 kJ/mol, reflecting the strong temperature dependence that is observed in the experiments. This value must be regarded as approximate because of the uncertainties underlying each point on the right hand graphs of Figure 2, and the limited number of data points used to obtain each  $k$  value.

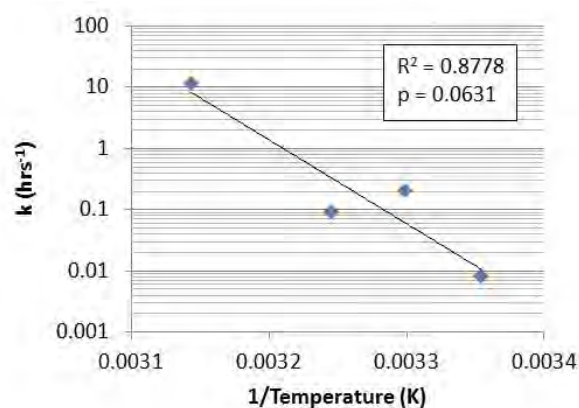


**Figure 27: Rate of change of  $1/t_{ind}$  against  $1/T$  according to the Arrhenius plot.**

According to Arrhenius' rationalization of the activation energy (collision theory), the activation energy is the minimum kinetic energy required for a collision to result in a reaction, while according to van't Hoff's explanation (transition-state theory) it is the enthalpy of activation, i.e. the enthalpy change upon formation of the activated complex.

In our case, the activation energy appears to be a measure of the stability of the prenucleation clusters, impurities, undissolved solute, or whatever species is responsible for the thermal history effect. To our knowledge, no activation energy has been reported previously for the kinetics of the restructuring responsible for history of solution effects. As to dissolution, activation energies less than 30 kJ mol<sup>-1</sup> are generally considered to indicate diffusion-controlled dissolution, while greater values are indicative of surface-control (Jordan and Rammensee 1996). Even though there are similarly-high values reported in the literature for crystal dissolution in organic solvents (Thomas *et al.* 1971), we do find our value of 262 kJ mol<sup>-1</sup> at first quite large. However, as reported in our

## Influence of History of Solution in Crystal Nucleation of Fenoxycarb

publication, molecular modelling suggests that the intermolecular bonding between just two solute molecules amounts to 60 kJ/mol. Hence if the cluster involves many molecules, restructuring of these through a transition state could very well involve enthalpies of activation of the same order of magnitude as that obtained experimentally.

The relationship between pretreatment temperature and the inverse of the inferred initial induction time is plotted in Figure 28. Again with reference to the uncertainties involved in the evaluation of  $\frac{1}{t_{ind}^0}$ , these data can only be taken as approximate.

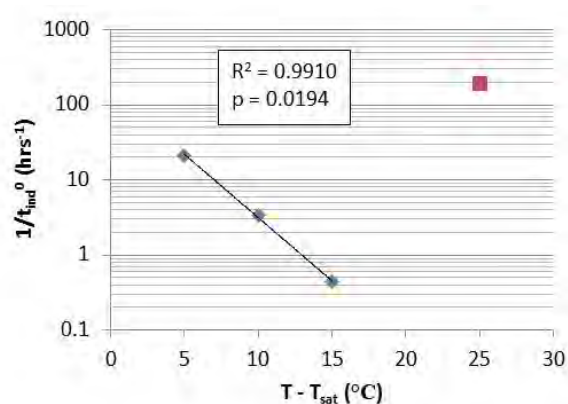


**Figure 28: Relationship between inferred initial induction time and pretreatment temperature.**

Ignoring for the moment the clear outlier corresponding to the 45 °C data, a surprisingly strong correlation is found between the logarithm of the intercept and the level of overheating. According to Equation (28),  $\frac{1}{t_{ind}^0}$  is the extrapolated induction time that would correspond to the original state of nucleation promoting clusters at negligible preheating time. This initial concentration appears to decay significantly with increasing superheating, which is in general agreement with the remainder of our results according to which these species are more unstable at higher temperatures. At present we do not have a rational explanation for why the 45 °C data deviates from this trend, but it should be noted that the value is obtained by extrapolation of a very steep line drawn from two points only. However, even if the line is based on merely the first three values in the right side of Figure 24 (d), the 45 °C point in Figure 5 remains a clear outlier.

## Influence of History of Solution in Crystal Nucleation of Fenoxycarb

According to the previously-made assumption that  $\frac{1}{t_{ind}}$  is directly proportional to the concentration of nucleation-promoting clusters,  $\frac{1}{t_{ind}^0}$  should be directly proportional to their initial concentration,  $c_0$ . As such, it appears that increasing the pretreatment temperature decreases the initial concentration of the solution history species; this trend is in general agreement with the remainder of our results, which suggest that these species are more unstable at higher temperatures. It is, however, difficult to conceive a mechanism whereby  $T_{PT}$  could influence  $c_0$ , since  $c_0$  is the concentration of solution history species when  $t = 0$ , at which point no pretreatment heating has been applied since the solutions are all still at 5 °C. Thus, considering that  $c_0$  is an extrapolated value, it seems most likely that the variation in  $c_0$  with  $T_{PT}$  is an artefact of the equilibration time period at the beginning of the pretreatment stage, during which the solutions approach, but are not actually at,  $T_{PT}$ .

### **5.3.3 Hypothesised Mechanism**

The majority of reported cases of a solution history effect are either of highly concentrated solutions or of melts. Similarly, in our case we have a very high concentration, which corresponds to only around 19 solvent molecules per fenoxycarb molecule. Molecular mechanics modelling by a co-author (Kuhs *et al.* 2014) suggests that this concentration is insufficient to form even the first solvation shell around dimers. Thus, the presence of solute clusters is a realistic possibility owing merely to the high concentration.

Modelling by a co-author of the relative stability of two different fenoxycarb dimers gave further insights (Kuhs *et al.* 2014), and it is interesting to note that nucleation initiated specifically by dimers (admittedly covalently bonded) has been reported by Furuta *et al.* (2007). The structure of the first modelled fenoxycarb dimer is similar to that found in the fenoxycarb crystal, whereby the aromatic ends of both fenoxycarb molecules are above each other, which we call a head-by-head dimer (dimer (1) in Figure 29). In the other dimer (dimer (2) in Figure 29), the position is reversed, with the aliphatic end of one being above the aromatic end of another, giving a head-by-tail

## Influence of History of Solution in Crystal Nucleation of Fenoxycarb

dimer. Molecular dynamics found that the head-by-tail dimer is slightly more stable than the crystal-like head-by-head dimer (Kuhs *et al.* 2014).

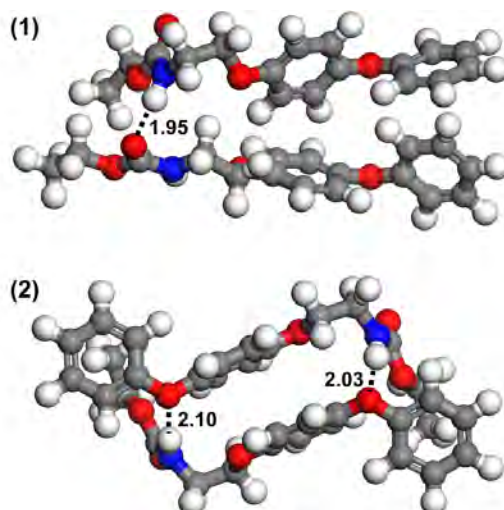


**Figure 29: Optimized structures of fenoxycarb dimers: (1) fenoxycarb dimer in geometry close to that in the crystal, (2) fenoxycarb dimer with aliphatic-to-aromatic orientation of end-groups. Numeric values are hydrogen bond distances in Å. Work done by a co-author (Kuhs *et al.* 2014).**

As the crystals dissolve, it can be envisioned that the dissolved clusters initially retain a crystal-like head-by-head structure. If, as this molecular dynamics modelling suggests, there is a more stable structure, the head-by-head clusters could slowly re-orientate to the more stable structure, such as the hypothesised head-by-tail orientation. In order for nucleation to occur, the clusters must first re-form the head-by-head orientation of the crystal. Thus, solutions in which more head-by-tail clusters have formed will be more difficult to nucleate. According to this hypothesis, the  $\sim 260 \text{ kJ mol}^{-1} E_A$  would be the  $E_A$  of the transformation of head-by-head clusters to head-by-tail clusters. This hypothesized mechanism is schematized in Figure 30. Of course the chief weakness of this hypothesis is the lack of any direct evidence of the existence of any such pre-nucleation clusters.

## Influence of History of Solution in Crystal Nucleation of Fenoxycarb

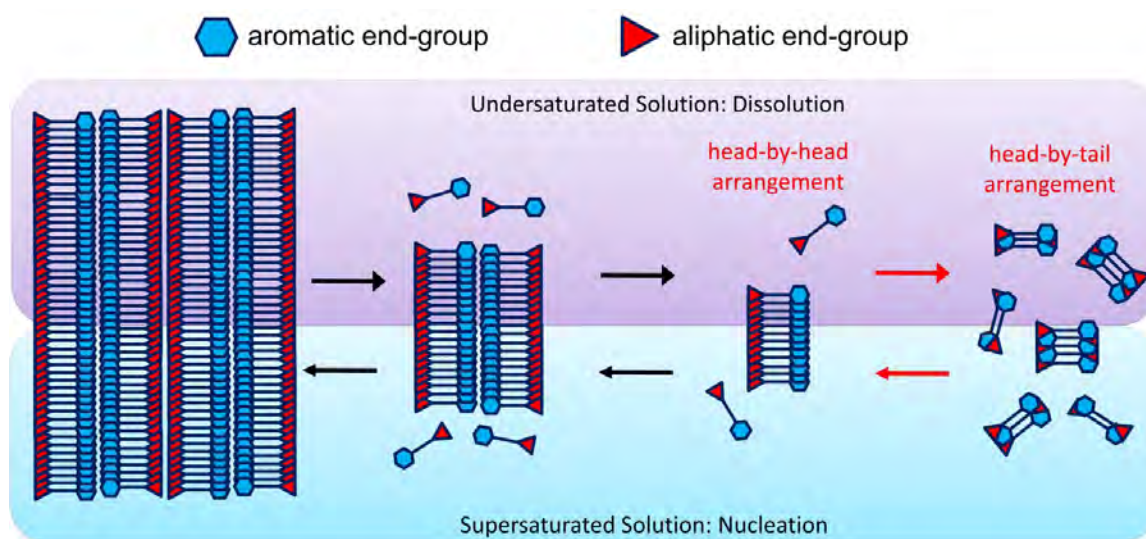


**Figure 30: Schematic description of the hypothesized history of solution mechanism.**

# VI

## **6 Conclusion**

## Conclusion

The interaction of solvent and solute was found to be a decisive factor in the nucleation of tolbutamide and fenoxycarb from solution. In general, the stronger the solvent binds the solute molecules, the more difficult the subsequent nucleation becomes. The same correlation has recently been found for salicylic acid (Khamar *et al.* 2014) and risperidone (Mealey *et al.* 2015f). This suggests that desolvation of the solute molecules may play a significant role in nucleation from solution. However, in the case of tolbutamide this appears to be complicated by a second mechanism, whereby the solvent environment causes the solute molecules to assume conformations and/or cluster structures that are different to those found in the crystal and which have high energy barriers for transforming to those corresponding to the crystal structure. Consequently a solvent that only weakly binds the solute can still make nucleation difficult by “trapping” the solute molecules in conformations or structured clusters dissimilar to the crystal. Furthermore, if, following crystal dissolution, the initial transformation to these conformers or cluster structures is sufficiently slow, a history of solution effect can occur whereby the extent of pretreatment will affect the subsequent ease of nucleation.

More specifically, for two medium-sized organic molecules, tolbutamide and fenoxycarb, the ease of nucleation measured in terms of thermodynamic driving force required to reach similar induction times, as well as the interfacial energy calculated from the CNT, were found to depend strongly on the solvent choice. Both driving force and interfacial energy were found to decrease in the order ethanol > isopropanol > toluene > ethyl acetate for fenoxycarb, and [n-propanol & toluene] > ethyl acetate > acetonitrile for tolbutamide. Thus they exhibited a similar dependence of nucleation difficulty on solvent choice, namely that nucleation from ethyl acetate is easier than from toluene and alcohols, and that nucleation from different alcohols happens with similar difficulty. It was not possible to correlate this behaviour to the same basic solvent property or solubility for both solutes, though a correlation to solubility (decreasing with nucleation difficulty) was found for fenoxycarb, and to solvent boiling point (increasing with nucleation difficulty) for tolbutamide. Both of these relationships have at times been observed for other organic systems. However, they do not appear to be generally applicable to medium-sized organic molecules. The ease of nucleation

## Conclusion

correlated well to solvent-solute interaction enthalpies of fenoxycarb from the different solvents, whereby stronger binding of the solute by the solvent increased the nucleation difficulty, with the exception of toluene from which nucleation was difficult despite weak solvent-solute interactions. However, the nucleation of tolbutamide did not appear to follow this trend, with the exception of n-propanol in which it was difficult to nucleate and accordingly had very strong solvent-solute interactions. The reported conformational identities of tolbutamide molecules in the different solutions and their respective rotation barriers for transforming to the molecular conformation found in the crystal, as predicted by modelling, were able to provide an explanation for tolbutamide's behaviour. For example, nucleation of tolbutamide from toluene is very difficult despite weak solvent-solute interactions. However, in toluene molecular dynamics modelling predicts that tolbutamide assumes a highly stable intramolecularly hydrogen bonded conformer with a large rotational barrier for transforming to the crystal conformer. It remains to experimentally confirm the existence of these conformers, and to investigate the existence of this mechanism in other systems.

Furthermore, a history of solution effect on the nucleation of fenoxycarb from isopropanol also pointed to the importance of solution structure leading up to and influencing the nucleation. A solution restructuring process during pretreatment that affects the subsequent nucleation mechanism has been hypothesised, whereby fenoxycarb clusters in solution that initially retain molecular structuring similar to the crystal slowly rearrange to clusters that are more stable but whose structure is unlike that of the crystal. According to our analysis, this restructuring appears to follow first order reaction kinetics with strong temperature dependence expressed as an activation energy of over  $200 \text{ kJ mol}^{-1}$ . Once again, it remains to directly verify the existence and structural identity of these clusters.

Solubilities of fenoxycarb in different organic solvents were an order of magnitude higher than tolbutamide solubilities, likely due to tolbutamide having a greater stability as reflected in a higher melting point. Solubility trends were quite similar for both solutes, both being most soluble in ethyl acetate and slightly less soluble in alcohols. In toluene, however, fenoxycarb is highly soluble, while tolbutamide is almost insoluble.

## Conclusion

The order of solubilities was rationalised by considering a combination of hydrogen bonding capabilities and structural similarities. In particular, the difference between the solubility of tolbutamide and fenoxycarb in toluene was hypothesised as arising from toluene being the only non-polar solvent and consequently being unable to compete with tolbutamide's six intermolecular hydrogen bonds in the crystal compared to fenoxycarb's four.

Finally, as outlined in Appendix C, microfluidics did not prove to be a feasible tool for measuring induction times of the nucleation of medium-sized organic molecules from organic solvents. This was due to a combination of the complexity involved in achieving stable and independent solution droplets, and the long induction times observed at such a small scale, which make this method unfeasible as a general tool for measuring nucleation kinetics of medium-sized molecules in various solvents.

**B**

**Bibliography**

## Bibliography

- Bennema, P. and Söhnel, O. (1990) 'Interfacial surface tension for crystallization and precipitation from aqueous solutions', *Journal of Crystal Growth*, 102(3), 547-556.
- Bernstein, J. (2002) *Polymorphism in Molecular Crystals*, Oxford: Oxford University Press.
- Boistelle, R. and Astier, J. P. (1988) 'Crystallization mechanisms in solution', *Journal of Crystal Growth*, 90(1-3), 14-30.
- Boon, J., Challa, G. and van Krevelen, D. W. (1968) 'Crystallization kinetics of isotactic polystyrene. II. Influence of thermal history on number of nuclei', *Journal of Polymer Science Part A-2: Polymer Physics*, 6(11), 1835-1851.
- Bowen, K. R., Stephens, T. W., Lu, H., Satish, K., Shan, D., Acree, W. E. and Abraham, M. H. (2013) 'Experimental and predicted solubilities of 3,4-dimethoxybenzoic acid in select organic solvents of varying polarity and hydrogen-bonding character', *European Chemical Bulletin*, 2(9).
- Buchanan, P., Soper, A. K., Thompson, H., Westacott, R. E., Creek, J. L., Hobson, G. and Koh, C. A. (2005) 'Search for memory effects in methane hydrate: structure of water before hydrate formation and after hydrate decomposition', *J Chem Phys*, 123(16), 164507.
- Burke, M. W., Judge, R. A. and Pusey, M. L. (2001) 'The effect of solution thermal history on chicken egg white lysozyme nucleation', *Journal of Crystal Growth*, 232(1-4), 301-307.
- Chen, J. and Trout, B. L. (2008) 'Computational Study of Solvent Effects on the Molecular Self-Assembly of Tetrolic Acid in Solution and Implications for the Polymorph Formed from Crystallization', *The Journal of Physical Chemistry B*, 112(26), 7794-7802.
- Davey, R. J., Dent, G., Mughal, R. K. and Parveen, S. (2006) 'Concerning the Relationship between Structural and Growth Synthons in Crystal Nucleation: Solution and Crystal Chemistry of Carboxylic Acids As Revealed through IR Spectroscopy', *Crystal Growth & Design*, 6(8), 1788-1796.
- Derdour, L., Pack, S. K., Skliar, D., Lai, C. J. and Kiang, S. (2011) 'Crystallization from solutions containing multiple conformers: A new modeling approach for solubility and supersaturation', *Chemical Engineering Science*, 66(1), 88-102.

## Bibliography

- Derdour, L. and Skliar, D. (2014) 'A review of the effect of multiple conformers on crystallization from solution and strategies for crystallizing slow inter-converting conformers', *Chemical Engineering Science*, 106(0), 275-292.
- Di, Y.-Y., Tan, Z.-C., Wu, X.-M., Meng, S.-H. and Qu, S.-S. (2000) 'Heat capacity and thermochemical study of trifluoroacetamide (C<sub>2</sub>H<sub>2</sub>F<sub>3</sub>NO)', *Thermochimica Acta*, 356(1-2), 143-151.
- Dixit, N. M., Kulkarni, A. M. and Zukoski, C. F. (2001) 'Comparison of experimental estimates and model predictions of protein crystal nucleation rates', *Colloids and Surfaces A: Physicochemical and Engineering Aspects*, 190(1-2), 47-60.
- Dombrowski, R. D., Litster, J. D., Wagner, N. J. and He, Y. (2007) 'Crystallization of alpha-lactose monohydrate in a drop-based microfluidic crystallizer', *Chemical Engineering Science*, 62(17), 4802-4810.
- Dunitz, J. D. and Bernstein, J. (1995) 'Disappearing Polymorphs', *Accounts of Chemical Research*, 28(4), 193-200.
- Farkas, L. (1927) 'Keimbildungsgeschwindigkeit in übersättigten dampfen', *Z. Phys. Chem.*, 125, 236.
- Forster, A., Hempenstall, J. and Rades, T. (2001) 'Characterization of glass solutions of poorly water-soluble drugs produced by melt extrusion with hydrophilic amorphous polymers', *Journal of Pharmacy and Pharmacology*, 53(3), 303-315.
- Furuta, K., Okutsu, T., Sazaki, G., Yoshizaki, I., Horiuchi, H., Shimizu, T., Yamamoto, M., Tanaka, Y. and Hiratsuka, H. (2007) 'Detection of Covalent-bonded Dimer in Photochemically Induced Crystallization of Protein', *Chemistry Letters*, 36(6), 714-715.
- Galkin, O. and Vekilov, P. G. (1999) 'Direct Determination of the Nucleation Rates of Protein Crystals', *The Journal of Physical Chemistry B*, 103(49), 10965-10971.
- Gerdts, C. J., Sharoyan, D. E. and Ismagilov, R. F. (2004) 'A Synthetic Reaction Network: Chemical Amplification Using Nonequilibrium Autocatalytic Reactions Coupled in Time', *Journal of the American Chemical Society*, 126(20), 6327-6331.
- Gerdts, C. J., Tereshko, V., Yadav, M. K., Dementieva, I., Collart, F., Joachimiak, A., Stevens, R. C., Kuhn, P., Kossiakoff, A. and Ismagilov, R. F. (2006) 'Time-Controlled Microfluidic Seeding in nL-Volume Droplets To Separate Nucleation and Growth Stages of Protein Crystallization', *Angewandte Chemie International Edition*, 45(48), 8156-8160.

## Bibliography

- Gerson, A. R., Counter, J. A. and Cookson, D. J. (1996) 'Influence of solution constituents, solution conditioning and seeding on the crystalline phase of aluminium hydroxide using in situ X-ray diffraction', *Journal of Crystal Growth*, 160(3-4), 346-354.
- Gibbs, J. W. (1876) 'On the equilibrium of heterogeneous substances', *Trans. Connect. Acad. Sci.*, 3, 108-248.
- Gibbs, J. W. (1878) 'On the equilibrium of heterogeneous substances', *Trans. Connect. Acad. Sci.*, 16, 343-524.
- Goh, L., Chen, K., Bhamidi, V., He, G., Kee, N. C. S., Kenis, P. J. A., Zukoski, C. F. and Braatz, R. D. (2010) 'A Stochastic Model for Nucleation Kinetics Determination in Droplet-Based Microfluidic Systems', *Crystal Growth & Design*, 10(6), 2515-2521.
- Graber, T. A., Taboada, M. E., Alvarez, M. N. and Schmidt, E. H. (1999) 'Determination of Mass Transfer Coefficients for Crystal Growth of Nitrate Salts', *Crystal Research and Technology*, 34(10), 1269-1277.
- Gracin, S. and Rasmuson, Å. C. (2004) 'Polymorphism and Crystallization of p-Aminobenzoic Acid', *Crystal Growth & Design*, 4(5), 1013-1023.
- Hasegawa, G., Komasa, T., Bando, R., Yoshihashi, Y., Yonemochi, E., Fujii, K., Uekusa, H. and Terada, K. (2009) 'Reevaluation of solubility of tolbutamide and polymorphic transformation from Form I to unknown crystal form', *International Journal of Pharmaceutics*, 369(1-2), 12-18.
- Hinshelwood, C. N. and Hartley, H. (1922) 'VII. The probability of spontaneous crystallization of supercooled liquids', *Philosophical Magazine Series 6*, 43(253), 78-94.
- Hodate, Y., Ueno, S., Yano, J., Katsuragi, T., Tezuka, Y., Tagawa, T., Yoshimoto, N. and Sato, K. (1997) 'Ultrasonic velocity measurement of crystallization rates of palm oil in oil-water emulsions', *Colloids and Surfaces A: Physicochemical and Engineering Aspects*, 128(1-3), 217-224.
- Hollenbeck, R. G. (1980) 'Determination of differential heat of solution in real solutions from variation in solubility with temperature', *Journal of Pharmaceutical Sciences*, 69(10), 1241-2.

## Bibliography

- Ildefonso, M., Candoni, N. and Veessler, S. (2011) 'Using Microfluidics for Fast, Accurate Measurement of Lysozyme Nucleation Kinetics', *Crystal Growth & Design*, 11(5), 1527-1530.
- Izmailov, A. F., Myerson, A. S. and Arnold, S. (1999) 'A statistical understanding of nucleation', *Journal of Crystal Growth*, 196(2-4), 234-242.
- Jawor-Baczynska, A., Sefcik, J. and Moore, B. D. (2013) '250 nm Glycine-Rich Nanodroplets Are Formed on Dissolution of Glycine Crystals But Are Too Small To Provide Productive Nucleation Sites', *Crystal Growth & Design*, 13(2), 470-478.
- Jiang, S. and ter Horst, J. H. (2010) 'Crystal Nucleation Rates from Probability Distributions of Induction Times', *Crystal Growth & Design*, 11(1), 256-261.
- Jordan, G. and Rammensee, W. (1996) 'Dissolution rates and activation energy for dissolution of brucite (001) : A new method based on the microtopography of crystal surfaces', *Geochimica et Cosmochimica Acta*, 60(24), 5055-5062.
- Judge, R. A., Johns, M. R. and White, E. T. (1995) 'Protein purification by bulk crystallization: The recovery of ovalbumin', *Biotechnology and Bioengineering*, 48(4), 316-323.
- Kadam, S. S., Kulkarni, S. A., Coloma Ribera, R., Stankiewicz, A. I., ter Horst, J. H. and Kramer, H. J. M. (2012) 'A new view on the metastable zone width during cooling crystallization', *Chemical Engineering Science*, 72(0), 10-19.
- Karpinska, J., Kuhs, M., Rasmuson, A., Erxleben, A. and McArdle, P. (2012) 'Ethyl N-[2-(4-phenoxyphenoxy)ethyl]carbamate', *Acta Crystallographica Section E*, 68(10), o2834-o2835.
- Kashchiev, D. (2000) *Nucleation: Basic Theory with Applications*, Boston, MA: Butterworth-Heinemann.
- Kashchiev, D. and Rosmalen, G. M. v. (2003) 'Review: Nucleation in solutions revisited', *Crystal Research and Technology*, 38(7-8), 555-574.
- Khamar, D., Zeglinski, J., Mealey, D. and Rasmuson, Å. C. (2014) 'Investigating the role of solvent-solute interaction in crystal nucleation of salicylic acid from organic solvents', *Journal of the American Chemical Society*, 163(33), 11664-11673.

## Bibliography

- Kitamura, M., Umeda, E. and Miki, K. (2012) 'Mechanism of Solvent Effect in Polymorphic Crystallization of BPT', *Industrial & Engineering Chemistry Research*, 51(39), 12814-12820.
- Kuhs, M., Svärd, M. and Rasmuson, Å. C. (2013) 'Thermodynamics of fenoxycarb in solution', *The Journal of Chemical Thermodynamics*, 66(0), 50-58.
- Kuhs, M., Zeglinski, J. and Rasmuson, Å. C. (2014) 'Influence of History of Solution in Crystal Nucleation of Fenoxycarb: Kinetics and Mechanisms', *Crystal Growth & Design*, 14(3), 905-915.
- Kulkarni, S. A., Kadam, S. S., Meekes, H., Stankiewicz, A. I. and ter Horst, J. H. (2013) 'Crystal Nucleation Kinetics from Induction Times and Metastable Zone Widths', *Crystal Growth & Design*, 13(6), 2435-2440.
- Kulkarni, S. A., McGarrity, E. S., Meekes, H. and ter Horst, J. H. (2012) 'Isonicotinamide self-association: the link between solvent and polymorph nucleation', *Chemical Communications*, 48(41), 4983-4985.
- Lancia, A., Musmarra, D. and Prisciandaro, M. (1999) 'Measuring induction period for calcium sulfate dihydrate precipitation', *AIChE Journal*, 45(2), 390-397.
- Laval, P., Crombez, A. and Salmon, J.-B. (2008) 'Microfluidic Droplet Method for Nucleation Kinetics Measurements', *Langmuir*, 25(3), 1836-1841.
- Laval, P., Salmon, J.-B. and Joanicot, M. (2007) 'A microfluidic device for investigating crystal nucleation kinetics', *Journal of Crystal Growth*, 303(2), 622-628.
- Leng, J. and Salmon, J.-B. (2009) 'Microfluidic crystallization', *Lab on a Chip*, 9(1), 24-34.
- Liang, R., Bao, Z., Su, B., Xing, H. and Ren, Q. (2012) 'Solubility of Vitamin D3 in Six Organic Solvents at Temperatures from (248.2 to 273.2) K', *Journal of Chemical & Engineering Data*, 57(8), 2328-2331.
- Limpert, E., Stahel, W. A. and Abbt, M. (2001) 'Log-normal Distributions across the Sciences: Keys and Clues', *BioScience*, 51(5), 341-352.
- Lindenberg, C. and Mazzotti, M. (2009) 'Effect of temperature on the nucleation kinetics of [alpha] l-glutamic acid', *Journal of Crystal Growth*, 311(4), 1178-1184.

## Bibliography

- Liu, J. and Rasmuson, Å. C. (2013) 'Influence of Agitation and Fluid Shear on Primary Nucleation in Solution', *Crystal Growth & Design*, 13(10), 4385-4394.
- Liu, J., Svärd, M. and Rasmuson, Å. C. (2014) 'Influence of Agitation and Fluid Shear on Nucleation of m-Hydroxybenzoic Acid Polymorphs', *Crystal Growth & Design*, 14(11), 5521-5531.
- Maggioni, G. M. and Mazzotti, M. (2015) 'Modelling the stochastic behaviour of primary nucleation', *Faraday Discussions*, DOI: 10.1039/C4FD00255E.
- Maher, A., Croker, D., Rasmuson, Å. C. and Hodnett, B. K. (2010) 'Solubility of Form III Piracetam in a Range of Solvents', *Journal of Chemical & Engineering Data*, 55(11), 5314-5318.
- Maher, A., Rasmuson, Å. C., Croker, D. M. and Hodnett, B. K. (2012) 'Solubility of the Metastable Polymorph of Piracetam (Form II) in a Range of Solvents', *Journal of Chemical & Engineering Data*, 57(12), 3525-3531.
- Masner, P., Angst, M. and Dorn, S. (1987) 'Fenoxycarb, an insect growth regulator with juvenile hormone activity: A candidate for *Heliothis virescens* (F.) control on cotton', *Pesticide Science*, 18(2), 89-94.
- McKinley, M. (2012) *Irish pharmaceutical sector overview* [online], available: <http://www.morganmckinley.ie/article/irish-pharmaceutical-sector-overview> [accessed 2015-02-25].
- Mealey, D., Croker, D. M. and Rasmuson, A. (2015a) 'Crystal nucleation of salicylic acid in organic solvents.', *CrystEngComm*, DOI: 10.1039/C4CE01428F.
- Mealey, D., Svärd, M. and Rasmuson, Å. C. (2014) 'Thermodynamics of risperidone and solubility in pure organic solvents', *Fluid Phase Equilibria*, 375(0), 73-79.
- Mealey, D., Zeglinski, J., Khamar, D. and Rasmuson, A. (2015f) 'Influence of Solvent on Crystal Nucleation of Risperidone', *Faraday Discussions*, DOI: 10.1039/C4FD00223G.
- Mirmehrabi, M., Rohani, S., Murthy, K. S. K. and Radatus, B. (2004) 'Solubility, dissolution rate and phase transition studies of ranitidine hydrochloride tautomeric forms', *International Journal of Pharmaceutics*, 282(1-2), 73-85.

## Bibliography

- Mitchell, N. A., Frawley, P. J. and Ó'Ciardhá, C. T. (2011) 'Nucleation kinetics of paracetamol-ethanol solutions from induction time experiments using Lasentec FBRM<sup>®</sup>', *Journal of Crystal Growth*, 321(1), 91-99.
- Mullin, J. W. (2001) *Crystallization, Fourth Edition*, Butterworth-Heinemann.
- Munroe, A. (2010) *Polymorphic Transformation of Sulphathiazole*, unpublished thesis (PhD), University of Limerick.
- Muschol, M. and Rosenberger, F. (1995) 'Interactions in undersaturated and supersaturated lysozyme solutions: Static and dynamic light scattering results', *The Journal of Chemical Physics*, 103(24), 10424-10432.
- Nakai, T. (1972) 'Effects of the thermal history of a solution to nucleation', *Journal of the Chinese Institute of Chemical Engineers*, 3(2), 83-93.
- Nangia, A. and R. Desiraju, G. (1999) 'Pseudopolymorphism: occurrences of hydrogen bonding organic solvents in molecular crystals', *Chemical Communications*, (7), 605-606.
- Nath, N. K. and Nangia, A. (2011) 'Novel form V of tolbutamide and a high Z[prime or minute] crystal structure of form III', *CrystEngComm*, 13(1), 47-51.
- Nordström, F. L. and Rasmuson, Å. C. (2006a) 'Phase equilibria and thermodynamics of p-hydroxybenzoic acid', *Journal of Pharmaceutical Sciences*, 95(4), 748-760.
- Nordström, F. L. and Rasmuson, Å. C. (2006b) 'Solubility and Melting Properties of Salicylic Acid', *Journal of Chemical & Engineering Data*, 51(5), 1668-1671.
- Nordström, F. L. and Rasmuson, Å. C. (2009) 'Prediction of solubility curves and melting properties of organic and pharmaceutical compounds', *European Journal of Pharmaceutical Sciences*, 36(2-3), 330-344.
- Nordström, F. L., Svärd, M., Malmberg, B. and Rasmuson, Å. C. (2012) 'Influence of Solution Thermal and Structural History on the Nucleation of m-Hydroxybenzoic Acid Polymorphs', *Crystal Growth & Design*, 12(9), 4340-4348.
- Nordstrom, F. L., Svard, M. and Rasmuson, A. C. (2013) 'Primary nucleation of salicylamide: the influence of process conditions and solvent on the metastable zone width', *CrystEngComm*, 15(36), 7285-7297.

## Bibliography

- Nyvt, J. (1963) 'Crystallization. IV. Crystal nucleation in solutions', *Collection of Czechoslovak Chemical Communications*, 28, 2269-79.
- Omar, W., Mohnicke, M. and Ulrich, J. (2006) 'Determination of the solid liquid interfacial energy and thereby the critical nucleus size of paracetamol in different solvents', *Crystal Research and Technology*, 41(4), 337-343.
- Ostwald, W. Z. (1897) 'Studies on the formation and transformation of solid compounds: Report I. Supersaturation and practicing cooling. [machine translation]', *Z. physik. Ch.*, 22, 289-330.
- Parveen, S., Davey, R. J., Dent, G. and Pritchard, R. G. (2005) 'Linking solution chemistry to crystal nucleation: the case of tetrolic acid', *Chemical Communications*, (12), 1531-1533.
- Petit, S., Coquerel, G. and Hartman, P. (1994) 'Nucleation and crystal growth of molecular solvates with several conformations both in solution and in solid state; application to some hydrated copper(II) sulfoxinates', *Journal of Crystal Growth*, 137(3-4), 585-594.
- Reichardt, C. and Welton, T. (2011) *Solvents and Solvent Effects in Organic Chemistry*, John Wiley & Sons.
- Revalor, E., Hammadi, Z., Astier, J.-P., Grossier, R., Garcia, E., Hoff, C., Furuta, K., Okustu, T., Morin, R. and Veessler, S. (2010) 'Usual and unusual crystallization from solution', *Journal of Crystal Growth*, 312(7), 939-946.
- Rodríguez-Hornedo, N. and Murphy, D. (1999) 'Significance of controlling crystallization mechanisms and kinetics in pharmaceutical systems', *Journal of Pharmaceutical Sciences*, 88(7), 651-660.
- Schaum, K. and Schoenbeck, F. (1902) 'Unterkühlung und Krystallisation von Schmelzflüssen polymorpher Stoffe', *Annalen der Physik*, 313(7), 652-662.
- Schwartz, A. M. and Berglund, K. A. (1999) 'The use of Raman spectroscopy for in situ monitoring of lysozyme concentration during crystallization in a hanging drop', *Journal of Crystal Growth*, 203(4), 599-603.
- Sear, R. P. (2006) 'Heterogeneous and Homogeneous Nucleation Compared: Rapid Nucleation on Microscopic Impurities', *The Journal of Physical Chemistry B*, 110(10), 4985-4989.

## Bibliography

- Spracklen, D. V., Carslaw, K. S., Kulmala, M., Kerminen, V. M., Mann, G. W. and Sihto, S. L. (2006) 'The contribution of boundary layer nucleation events to total particle concentrations on regional and global scales', *Atmos. Chem. Phys.*, 6(12), 5631-5648.
- Sullivan, R. A., Davey, R. J., Sadiq, G., Dent, G., Back, K. R., ter Horst, J. H., Toroz, D. and Hammond, R. B. (2014) 'Revealing the Roles of Desolvation and Molecular Self-Assembly in Crystal Nucleation from Solution: Benzoic and p-Aminobenzoic Acids', *Crystal Growth & Design*, 14(5), 2689-2696.
- Teychené, S. and Biscans, B. (2008) 'Nucleation Kinetics of Polymorphs: Induction Period and Interfacial Energy Measurements', *Crystal Growth & Design*, 8(4), 1133-1139.
- Thirunahari, S., Aitipamula, S., Chow, P. S. and Tan, R. B. H. (2010) 'Conformational polymorphism of tolbutamide: A structural, spectroscopic, and thermodynamic characterization of Burger's forms I-IV', *Journal of Pharmaceutical Sciences*, 99(7), 2975-2990.
- Thirunahari, S., Chow, P. S. and Tan, R. B. H. (2011) 'Quality by Design (QbD)-Based Crystallization Process Development for the Polymorphic Drug Tolbutamide', *Crystal Growth & Design*, 11(7), 3027-3038.
- Thomas, J. M., Evans, E. L. and Clarke, T. A. (1971) 'Activation energy of dissolution at emergent dislocations', *Journal of the Chemical Society A: Inorganic, Physical, Theoretical*, 2338-2341.
- Threlfall, T. L. (2009) 'Turning DSC Charts of Polymorphs into Phase Diagrams: A Tutorial Paper†', *Organic Process Research & Development*, 13(6), 1224-1230.
- Tsekova, D., Dimitrova, S. and Nanev, C. N. (1999) 'Heterogeneous nucleation (and adhesion) of lysozyme crystals', *Journal of Crystal Growth*, 196(2-4), 226-233.
- Valder, C. and Merrifield, D. (1996) 'Pharmaceutical Technology', *SmithKline Beecham R&D News*, 32.
- Vekilov, P. G. (2010a) 'Nucleation', *Crystal Growth & Design*, 10(12), 5007-5019.
- Vekilov, P. G. (2010d) 'The two-step mechanism of nucleation of crystals in solution', *Nanoscale*, 2(11), 2346-2357.

## Bibliography

- Vekilov, P. G., Monaco, L. A., Thomas, B. R., Stojanoff, V. and Rosenberger, F. (1996) 'Repartitioning of NaCl and Protein Impurities in Lysozyme Crystallization', *Acta Crystallographica Section D*, 52(4), 785-798.
- Vincze, J., Valiskó, M. and Boda, D. (2010) 'The nonmonotonic concentration dependence of the mean activity coefficient of electrolytes is a result of a balance between solvation and ion-ion correlations', *The Journal of Chemical Physics*, 133(15), 154507.
- Volmer, M. (1939) *Kinetik der Phasenbildung*, Dresden: Steinkopff.
- Webster, W. L. (1933) 'Phenomena Occurring in the Melting of Metals', *Proceedings of the Royal Society of London. Series A*, 140(842), 653-660.
- Wood, G. R. and Walton, A. G. (1970) 'Homogeneous Nucleation Kinetics of Ice from Water', *Journal of Applied Physics*, 41(7), 3027-3036.
- Xiao-Hong, S., Yuan-Fa, L., Zhi-Cheng, T., Ying-Qi, J., Jian-Wu, Y. and Mei-Han, W. (2005) 'Heat Capacity and Enthalpy of Fusion of Fenoxycarb', *Chinese Journal of Chemistry*, 23(5), 501-505.
- Yang, H. and Rasmuson, Å. C. (2013) 'Nucleation of Butyl Paraben in Different Solvents', *Crystal Growth & Design*, 13(10), 4226-4238.
- Yang, H., Svärd, M., Zeglinski, J. and Rasmuson, Å. C. (2014) 'Influence of Solvent and Solid-State Structure on Nucleation of Parabens', *Crystal Growth & Design*, 14(8), 3890-3902.
- Yang, J., Wu, H., Wang, Y., Luan, Q., Zhang, J., Wang, G. and Hao, H. (2015) 'Thermodynamics of 4'-bromomethyl-2-cyanobiphenyl in different solvents', *The Journal of Chemical Thermodynamics*, 83(0), 77-84.
- Yang, W., Hu, Y., Chen, Z., Jiang, X., Wang, J. and Wang, R. (2012) 'Solubility of itaconic acid in different organic solvents: Experimental measurement and thermodynamic modeling', *Fluid Phase Equilibria*, 314(0), 180-184.
- Zeglinski, J., Khamar, D., Kuhs, M. and Rasmuson, A. (2014) 'Analysis of the structure and morphology of fenoxycarb crystals', *Journal of Molecular Graphics and Modelling*, 53, 92-99.

# A

## **Appendix A – Paper Draft: Solvent Effects on Nucleation Kinetics and Thermodynamics of Fenoxycarb**

## **Probing Crystal Nucleation from Solution through the effect of Solvent: Fenoxycarb**

---

Manuel Kuhs<sup>a</sup>, Dikshitkumar Khamar<sup>a</sup>, Jacek Zeglinski<sup>a</sup>, Damien Thompson<sup>b</sup> and Åke C. Rasmuson<sup>a,c,\*</sup>

<sup>a</sup> Materials and Surface Science Institute, Chemical and Environmental Science, University of Limerick, Limerick, Ireland

<sup>b</sup> Department of Physics & Energy, University of Limerick, Limerick, Ireland

<sup>c</sup> Department of Chemical Engineering and Technology, KTH Royal Institute of Technology, Stockholm, Sweden

\* Corresponding author: ake.rasmuson@ul.ie

### **Abstract**

Induction time experiments, spectroscopic and calorimetric analysis, and molecular modelling were used to probe the influence of solvent on the crystal nucleation of fenoxycarb (FC), a medium-sized, flexible organic molecule. 800 induction times covering a range of supersaturations and crystallisation temperatures in four different solvents were measured to elucidate the relative ease of nucleation. To achieve similar induction times, the required thermodynamic driving force,  $RT\ln S$ , increases in the order ethyl acetate < toluene < ethanol < isopropanol. This is roughly matched by the order of interfacial energies calculated using the Classical Nucleation Theory, which was found to well describe the relationship between supersaturation, crystallisation temperature and induction times. Solvent-solute interaction strengths were estimated using three methods: solvent-solute enthalpies derived from calorimetric solution enthalpies, solvent-solute interactions from molecular modelling, and the FTIR shifts in the carbonyl stretching corresponding to the solvent-solute interaction. The three methods gave an overall order of solvent-solute interactions increasing in the order toluene < ethyl acetate < alcohols. Thus, with the exception of FC in toluene, it is found that the nucleation difficulty increases the more the solvent binds the solute.

## 1 Introduction

Crystallization is heavily used in various manufacturing industries, ranging from the production of salt to silicon wafers. The process is also used in the pharmaceutical industry, where over 90% of all pharmaceutical products contain crystalline ingredients<sup>1</sup>, and where crystallisation is considered the single most important unit operation.<sup>2</sup>

However, there is insufficient understanding of crystallization, and the fundamental theory is insufficiently developed to replace empirical approaches.<sup>3</sup> The first step in crystallisation, nucleation, is particularly problematic. Nucleation is instrumental in determining critical parameters such as crystal morphology, size, size distribution and polymorphic form, but its mechanism is still debated (as discussed below). This fundamental lack of understanding was epitomised by the famous shortage of the HIV protease inhibitor Norvir in the 1990s due to the sudden formation of a different polymorph than the one produced for months<sup>4</sup>. In general, poor yields and the presence of undesirable or unpredictable polymorphs continue to plague crystallization processes at both a lab and industrial scale.<sup>4</sup>

Symptomatic of the unsolved nature of nucleation science is the continued use of the Classical Nucleation Theory (CNT). Developed over 100 years ago, and admitted to have several serious flaws not much later, it remains the default model for analysing experimental results. Only in recent years have alternative models been receiving wider acceptance, chief of which is the Two Step Theory.<sup>5</sup>

The difficulty in studying nucleation arises from a combination of its stochastic nature, the miniscule size of the smallest stable nuclei (which are typically in the order of 10 to 1,000 molecules), and the great speed at which nuclei form. Thus, it is very difficult to directly observe nucleation, from both a temporal and a spatial perspective.<sup>6</sup>

One promising approach to understanding nucleation is studying its dependence on the solute-solvent interaction for nucleation from solution. The sensitivity of nucleation to solution chemistry has been known over 100 years.<sup>7</sup> According to CNT, the interfacial energy between the solute and the solution,  $\gamma$ , represents the solvent-specific contribution to the solute's thermodynamic barrier to nucleation. Thus, it is common practice to calculate  $\gamma$  using CNT. A general inverse proportionality between solubility and interfacial energy has been found for aqueous solutions of inorganic salts.<sup>8</sup> In individual cases interfacial energies have been correlated with intrinsic solvent properties such as solvent boiling points<sup>9</sup> and solvent-solute interaction properties such as solvation and deformation energies.<sup>10</sup> Recent studies have demonstrated solvent-induced self-assembly of solvate molecules prior to nucleation, as well as implicit<sup>11</sup> and explicit<sup>9, 12</sup> relationships between solution structure and polymorphic outcome.

Our group has recently shown that the nucleation of salicylic acid, a small inflexible organic molecule, and risperidone, a medium-sized flexible API, may depend on the strength with which the solvent binds the molecule in solution.<sup>13, 14</sup> This was deduced from positive linear correlation between the ease of nucleation from induction times and

## Appendix A – Paper Draft: Solvent Effects on Nucleation Kinetics and Thermodynamics of Fenoxycarb

several other experimental and modelled variables: at salicylic acid's carboxyl group, both the frequency in the Raman spectrum for the monomer and the DFT-derived 1:1 binding energy; at risperidone's carbonyl group the FTIR peak frequency; the calorimetrically-derived enthalpy of solvent-solute interaction (salicylic acid); and the DFT-derived solvation (salicylic acid) and 1:1 binding (risperidone) energy.

To further probe the relationship between solvent and nucleation, we measure the effect of four different solvents on the nucleation of a medium-sized flexible organic molecule, FC, and compare the results with various experimental and modelled thermodynamic quantities of the solvents and solutions.

Fenoxycarb (FC) has chemical formula  $C_{17}H_{19}NO_4$ , systematic name *2-(p-phenoxyphenoxy)ethylcarbamate*, and is shown in Figure 1. It is a flexible organic molecule that exhibits conformational isomerism in its single reported crystal form.<sup>15</sup> It is produced industrially as an insect growth regulator since it prevents the production of insect growth hormones.<sup>16</sup> Its melting temperature and enthalpy are reported as  $53.16 \pm 0.14$  °C and  $26.98 \pm 0.04$  kJ mol<sup>-1</sup>, respectively.<sup>17</sup> It is practically insoluble in water but highly soluble in alcohols, ethyl acetate and toluene, with solubilities at 25 °C ranging from 266 to 1,660 g per kg organic solvent.<sup>18</sup> Recrystallization leads to platelets regardless of solvent used.<sup>18</sup> Recrystallisation from isopropanol was found to exhibit a history of solution effect on the nucleation kinetics, whereby longer pretreatment at higher pretreatment temperatures increases the induction time.<sup>11</sup>

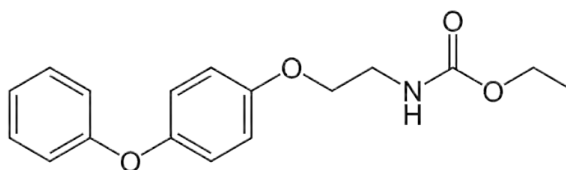


Figure 1: Molecular structure of FC.

## 2 Methodology

### 2.1 Induction Times

The procedure used for measuring induction times is almost identical to that reported in our previous work on this compound.<sup>11</sup> The chief differences are the use of multiple solvents (unmixed), constant pretreatment conditions, and variable crystallisation temperature ( $T_{cry}$ ). The differences are outlined in detail below.

FC was added, as received, to several organic solvents, to give solutions with known saturation temperatures ( $T_{sat}$ , see Table 1).

Except for the isopropanol solution, these were dissolved for 20 hours in sealed vessels with large magnetic stir bars spinning at 400 rpm, and the vessels submersed in a 45 °C water bath (all water baths used throughout this study are Grant GR150, stability  $\pm 0.005$  °C and uniformity  $\pm 0.02$  °C at 36.85 °C). The isopropanol solution was dissolved for 24 hours at 25 °C. All solutions were filtered and divided into 20 mL portions to

Appendix A – Paper Draft: Solvent Effects on Nucleation Kinetics and  
Thermodynamics of Fenoxycarb

give 15 identical solutions each of ethanol and ethyl acetate, 6 of toluene, and 29 of isopropanol.

To measure induction times, the vials were placed in a water bath set to a certain crystallization temperature,  $T_{cry}$ , and the time to first appearance of crystals in each vial, the induction time ( $t_{ind}$ ), recorded with a video camera. The values of  $T_{cry}$  and the corresponding supersaturation ratios ( $S$ ) for each solvent are shown in Table 6. To scan the different  $T_{cry}$  values, the solutions were redissolved between each induction time experiment at 45 °C for 24 hrs. Such a harsh pretreatment was chosen in an attempt to preclude the possibility of solution history effects which we have reported for FC in isopropanol.<sup>11</sup>

For the solution in the vials, the time to reach a temperature deviating by 1 °C from the final value was measured to be approximately 1 minute (Dostmann P750 with Pt100 immersion probe, accuracy 0.03 °C). It took about 7 minutes to reach deviations < 0.03 °C.

Multiple iterations of induction time experiments were performed at each  $T_{cry}$  in order to capture stochastic variation, such that at least 30 induction times are obtained for each solvent at each  $T_{cry}$ . The median value was calculated for each resultant distribution of induction times through the use of lognormal fitting for data smoothing. If all vials did not nucleate after 24 h, the experiment was stopped at the earliest once more than 50% of vials had nucleated. Crystallization was induced in any remaining homogeneous solutions by vigorous manual shaking to ensure all solutions had crystallised prior to redissolving. Induction times were only measured at 3 thermodynamic driving forces per solvent due to the length of time required for collecting sufficient data at each driving force per solvent (around 2 weeks on average).

The Classical Nucleation Theory (assuming the initial nucleus to be cubic in shape) postulates the influence of  $S$  and  $T_{cry}$  on the nucleation rate,  $J$ , as:<sup>5</sup>

$$J = A \exp \left( - \frac{32\Omega^2 \gamma_{eff}^3}{\mathbf{R}^3 T_{cry}^3 \ln^2 S} \right) \quad (1)$$

where  $A$  is the pre-exponential factor,  $\Omega$  the volume occupied by a molecule in the crystal (calculated as the unit cell volume from the published crystal structure<sup>15</sup> divided by the number of FC molecules in the cell),  $\mathbf{R}$  the universal gas constant, and  $\gamma_{eff}$  the interfacial energy between the crystal, the solution, and, in the case of heterogeneous nucleation, the surface on which nucleation occurs.

According to the CNT,  $\gamma_{eff}$  is related to the Gibbs free energy of the critical nucleus,  $\Delta G^*$ , and to the number of nuclei in the critical nucleus,  $n^*$ , by:<sup>5</sup>

$$\Delta G^* = \frac{32\Omega^2 \gamma_{eff}^3}{(\mathbf{R} T_{cry} \ln S)^2} \quad (2)$$

$$n^* = \frac{2\Delta G^*}{\mathbf{R} T_{cry} \ln S} \quad (3)$$

## Appendix A – Paper Draft: Solvent Effects on Nucleation Kinetics and Thermodynamics of Fenoxycarb

Assuming that impurities (which provide surfaces for heterogeneous nucleation and can thus modify  $\gamma_{eff}$ ) are constant,  $\gamma_{eff}$  can be used to compare the effect of solvent on the thermodynamic barrier to nucleation of the solute.

The time to the first appearance of crystals,  $t_{ind}$ , is usually assumed to be related to  $J$  as follows:<sup>19</sup>

$$J \approx 1/Vt_{ind} \quad (4)$$

where  $V$  is the volume of the reactor.

By combining equations (1) and (4),  $\gamma_{eff}$  can be calculated by measuring the effect of  $T_{cry}$  and  $S$  on  $t_{ind}$ .

### 2.2 Calorimetry

Solution calorimetry has been used to determine the enthalpy of solution of FC in the four solvents that were used in nucleation experiments as well as methanol. A Precision Solution Calorimeter (TA Instruments, USA) along with Thermal Activity Monitor (TAMIII) was used in semi adiabatic mode. In each experiment, about 326-330 mg of Fenoxycarb was dissolved in 100 mL of solvent. The variation among multiple runs was  $\leq 0.1$  kJ mol<sup>-1</sup>. A detailed experimental method is described elsewhere.<sup>13</sup> From the experimentally determined enthalpy of solution,  $\Delta H_{solution}$ , the enthalpy of solvation,  $\Delta H_{solvation}$ , can be calculated provided the enthalpy of sublimation,  $\Delta H_{sublimation}$  is known:

$$\Delta H_{solvation} = \Delta H_{solution} - \Delta H_{sublimation} \quad (5)$$

The enthalpy of sublimation for fenoxycarb is not reported in the literature; however the lattice energy,  $E_{lattice}$ , is reported: -175.9 kJ mol<sup>-1</sup>.<sup>Jacek paper ref</sup> From the lattice energy, the enthalpy of sublimation can be calculated as follows<sup>Ouvrard and Mitchell Acta Cryst B 2003</sup>:

$$\Delta H_{sublimation} = -E_{lattice} - 2RT \quad (6)$$

according to which  $\Delta H_{sublimation}$  is 170.94 kJ mol<sup>-1</sup>.

Use of scaled particle theory on experimental enthalpy of solution data allowed calculation of enthalpy of cavity formation and from that the enthalpy of solvent-solute interaction was determined in these 5 solvents. In addition to SPT theory, an alternate approach as described in Kuhs, et al.<sup>20</sup> is used for cavity calculation. A detailed account on the calculation of cavity formation with the two methods and the parameters used for these calculations are shown in supporting information file.

### 2.3 IR Spectroscopy

IR spectra were collected using a Mettler Toledo ReactIR 10 fitted with a silver halide probe composed of diamond composite and an MCT (mercury cadmium telluride) detector cooled with liquid nitrogen. In total, 167 scans were collected for each spectrum with a resolution of 4 cm<sup>-1</sup> in the spectral region of 2000-650 cm<sup>-1</sup> using iC IR software version 4.3. Solution IR spectra were collected at ambient conditions (18-20 °C) and 40 °C. Due to the nature of fibre optic probes, it was not possible to obtain the

## Appendix A – Paper Draft: Solvent Effects on Nucleation Kinetics and Thermodynamics of Fenoxycarb

spectra in the functional group region. For collection of melt spectra, the IR probe was inserted into a glass vial containing crystalline material and sealed with a tight cap. This glass vial was then kept in a copper block to minimize sublimation during heat-cool cycles (54 – 20 °C) and provide uniform heating.

### **2.4 Computational**

Energy barriers to conformational rotation were calculated with density functional theory (DFT) at selected single bonds of the FC molecule. For each of the rotational centres, a relaxed potential energy surface (PES) scan over 360 ° was performed. In this approach, four atoms forming a dihedral angle of interest are fixed at each step of rotation (with the step interval of 5°), while the remaining atoms are allowed to adjust their positions to reach a new energy minimum. The optimised geometries and relevant energies are calculated with a B97-D Grimme's functional,<sup>ref.</sup> which includes a long-range dispersion correction, and a 6-31G(d,p) basis set.<sup>ref.</sup> A molecule of FC, extracted from the FC crystal and optimised in vacuum, served as the starting geometry for the PES scans. Calculations were performed using the GAUSSIAN 09 code.<sup>ref.</sup>

Molecular dynamics (MD) simulations were employed to model both diluted and concentrated solutions of FC in the different solvents used in experiment, i.e. ethanol (ET), isopropanol (IP), ethyl acetate (EA), and toluene (TL). Eight FC model solutions (four diluted and four concentrated) were constructed. The number of molecules in a simulation box was set to achieve comparable volumes for all the modelled solutions. To simulate diluted solutions, the following compositions were applied: 1 FC + 2000 ET, 1 FC + 1500 IP, 1 FC + 1280 EA, and 1 FC + 1200 TL. For concentrated solutions, the compositions were set as follows: 160 FC + 1848 ET, 71 FC + 1207 IP, 242 FC + 673 EA, 250 FC + 665 TL.

Appendix A – Paper Draft: Solvent Effects on Nucleation Kinetics and Thermodynamics of Fenoxycarb

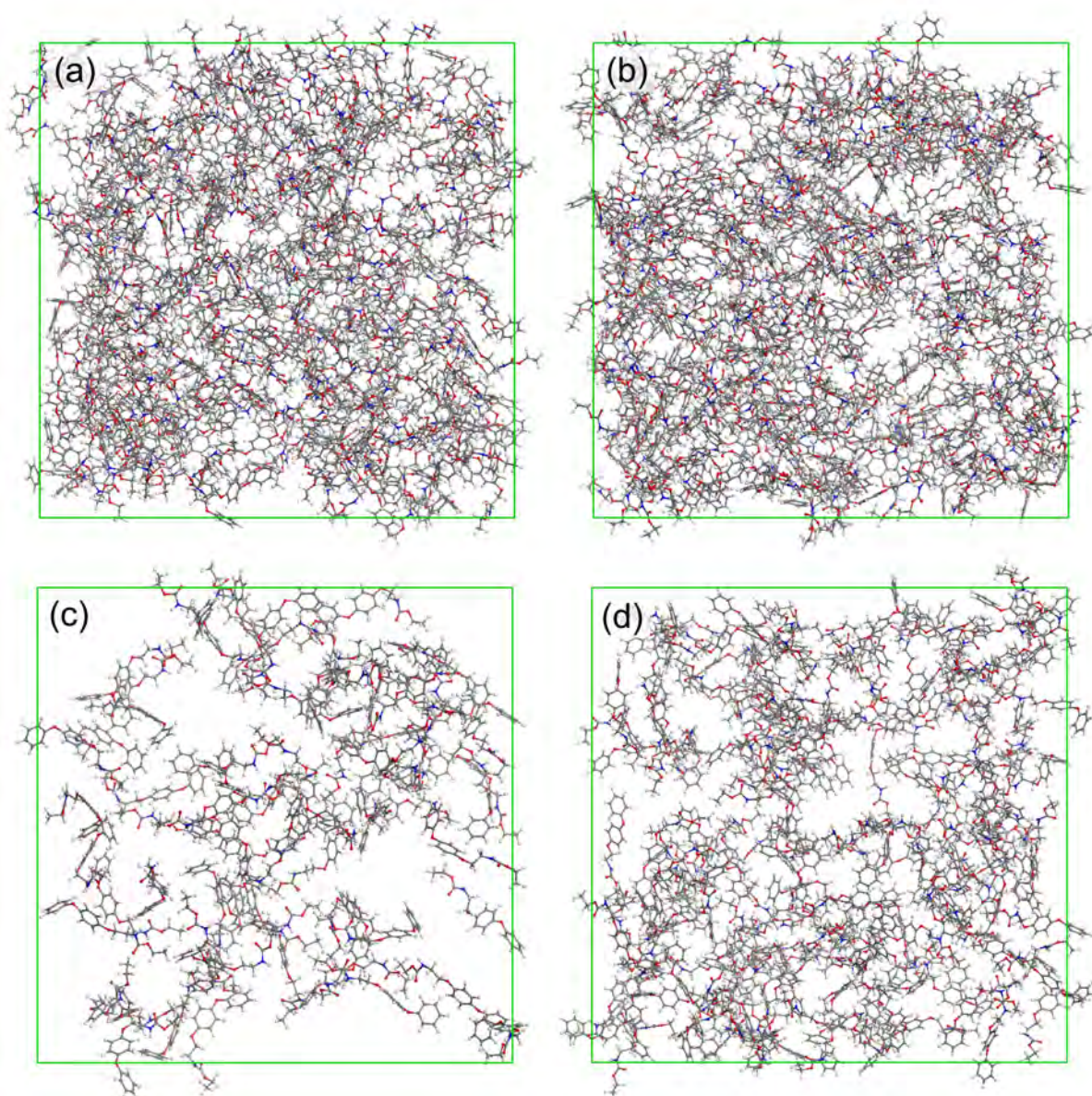


Fig. 2 MD models of FC solutions (concentrated) in different solvents: (a) 242 FC + 673 ethyl acetate molecules, (b) 250 FC + 665 toluene molecules, (c) 71 FC + 1207 isopropanol molecules, (d) 160 FC + 1848 ethanol molecules. To improve clarity, molecules of solvent are not shown. Snapshots are taken after running simulations for 100 ns at 2 °C.

The models of the concentrated solutions match compositions and concentrations of our experimental solutions. Each model was relaxed using 1000 steps of steepest descent minimization and then brought to 25 °C over 1 ns of dynamics. Eight well-equilibrated stable cubic boxes were formed of edge length  $58.9 \pm 1.9$  Å, following 15 ns (diluted solutions) and 65-100 ns (concentrated solutions) of constant pressure (1 atm) and temperature (2 °C) dynamics with periodic boundary conditions; four of those systems are shown in Fig. 2. Molecular Langevin dynamics were performed using the NAMD

program<sup>ref</sup> with Ewald summation used to calculate the electrostatic interactions. Solvent-solute binding energies were calculated using the NAMDenergy suite of the VMD program<sup>ref</sup> as follows: for dilute solutions and pure solvents, by selecting configurations/frames generated during 10 ns of dynamics, after the initial 5 ns of a simulation; for concentrated systems, by selecting the frames generated for 50 ns, after the initial 10 ns.

All the molecules used in the MD simulations were parametrized with Charmm General Force Field (CGenFF) v. 2b7. The FC molecule was built by bridging with an oxygen atom two residues available in the CGenFF parameters and topology files, i.e. a biphenyl (C37) and diethylcarbamate (DECB).

### 3 Results & Discussion

#### 3.1 Induction Times and Interfacial Energies

Induction times were recorded at a combination of different  $S$  and  $T_{cry}$  for four different organic solvents (ethyl acetate, toluene, isopropanol and ethanol, Figure 2).

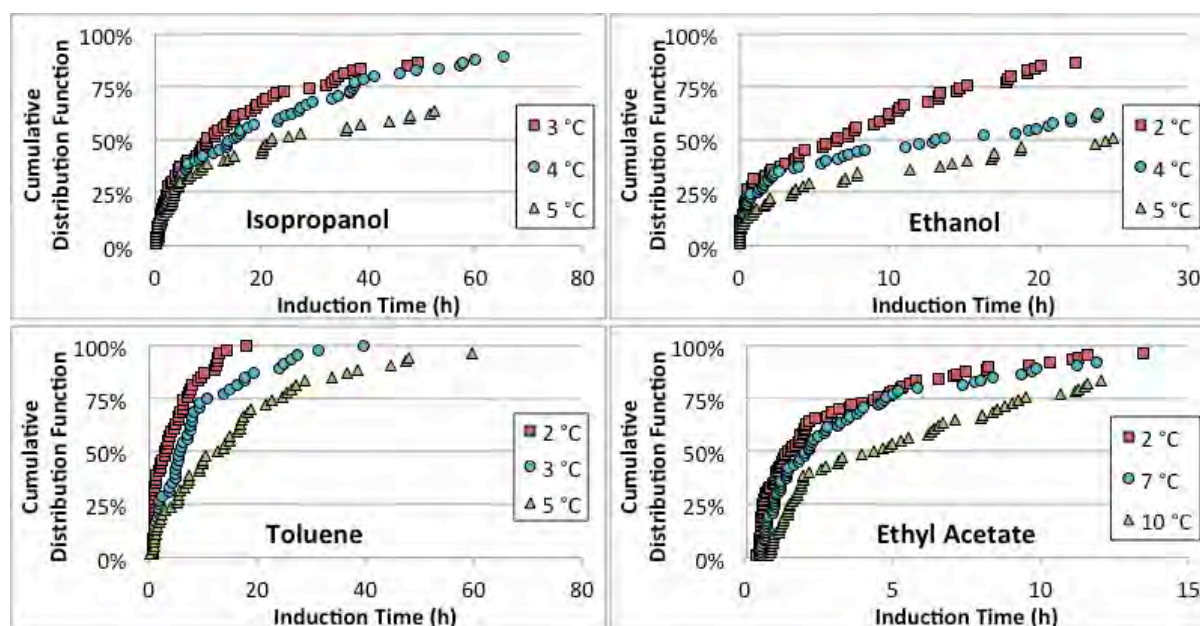


Figure 2: Induction time distributions of FC in different solvents. Temperatures are  $T_{cry}$ .

Appendix A – Paper Draft: Solvent Effects on Nucleation Kinetics and  
Thermodynamics of Fenoxycarb

**Table 1: Solutions and induction time results.**  $S = x/x^*$ , where  $x$  is the actual mole fraction of FC in the solution, and  $x^*$  the equilibrium mole fraction at  $T_{cry}$  from<sup>18</sup>;  $n$  is the number of induction times measured for each condition; *Logn.  $t_{ind}$*  is the median of the lognormal fit to the experimental  $t_{ind}$  distributions (Figure 2).

Solvent	Appr $T_{sat}$ (°C)	Mass ratio (g FC/g solvent)	# 20mL vials	$T_{cry}$ (°C)	S	RTlnS (kJ/mol)	n	Logn. $t_{ind}$ (h)
Ethyl Acetate	15	1.2307	15	8.0	1.33	<b>1.32</b>	41	2.1
				7.0	1.38	<b>1.49</b>	55	2.0
				2.1	1.68	<b>2.36</b>	74	1.4
Tolu-ene	20	1.2295	6	5.1	2.19	<b>3.59</b>	51	10.5
				3.1	2.44	<b>4.08</b>	48	5.5
				2.1	2.59	<b>4.33</b>	54	2.8
Isopro- panol	20	0.2633	30	5.1	4.58	6.98	65	23.5
				4.0	5.19	7.53	65	12.1
				3.1	5.74	7.98	65	8.9
Ethanol	20	0.5706	15	5.1	4.18	<b>6.56</b>	38	31.7
				4.0	4.66	<b>7.04</b>	56	11.8
				2.1	5.64	<b>7.88</b>	65	4.3

The range of distributions as well as the medians (identical to the geometric means in the case of the lognormal distributions used) are compared using the fitted lognormal distributions in Figure 3.

Appendix A – Paper Draft: Solvent Effects on Nucleation Kinetics and Thermodynamics of Fenoxycarb

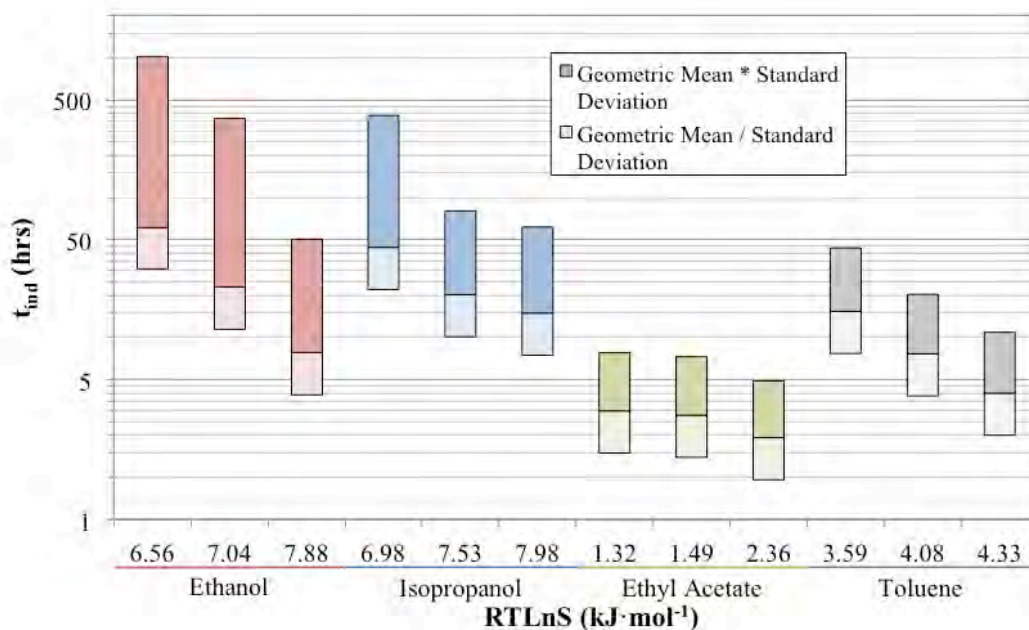
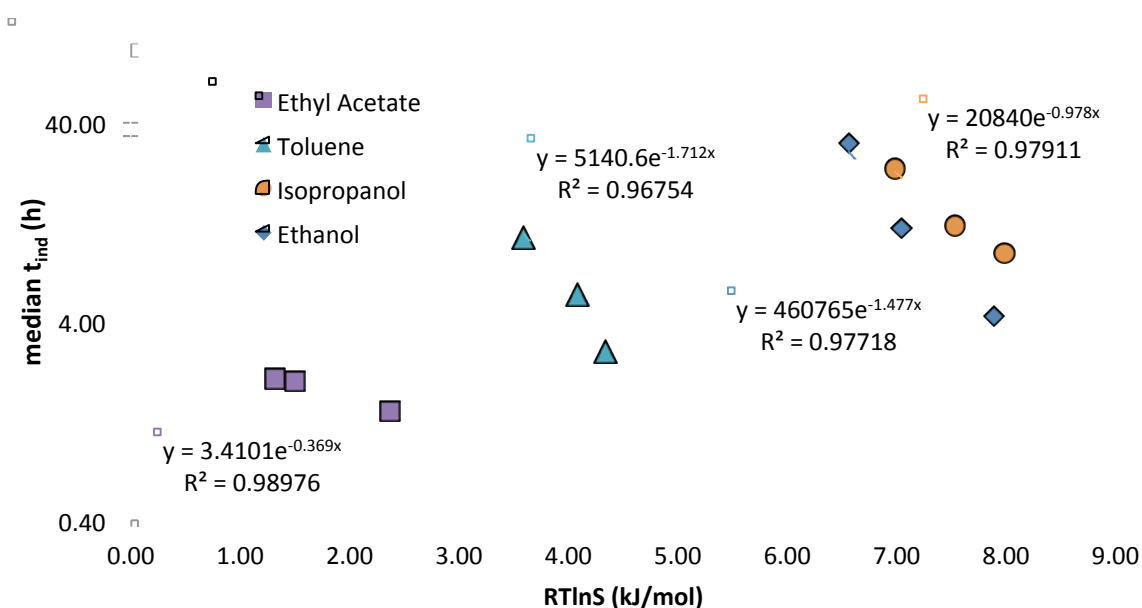


Figure 3: Lognormal fits of the induction time distributions. The centres of the box plots are the geometric means of the fitted lognormal distributions (identical to the medians); the shaded regions represent one geometric standard deviation from the mean.

The medians of the lognormal fits are plotted directly against the thermodynamic driving force of nucleation,  $RT_{cry} \ln S$ ,<sup>8</sup> in Figure 4.

Appendix A – Paper Draft: Solvent Effects on Nucleation Kinetics and Thermodynamics of Fenoxycarb



**Figure 4: The relationship between median induction time and thermodynamic driving force of nucleation of FC in different solvents. Lines are guides for the eyes only.**

From this plot an approximate order of ease of nucleation can be established in the range of the examined  $RTlnS$  (extrapolation of exponential fits suggests this order changes at higher and lower  $RTlnS$ , especially for the alcohols). Ethyl acetate clearly requires the lowest thermodynamic driving force for nucleation, toluene is an intermediate, and the alcohols require the highest, with isopropanol being slightly higher.

In order to compare the ease of nucleation at the same driving force, the fits from Figure 14 were extrapolated to  $t_{ind}$  of 2.06 h (the highest recorded  $t_{ind}$  for ethyl acetate). This gives the following values for  $RTlnS$ : 1.4 (ethyl acetate), 4.6 (toluene), 9.4 (isopropanol) and 8.3 (ethanol) kJ/mol. This matches the order previously mentioned, and is well correlated to solubility and solvent density (Figure 5).

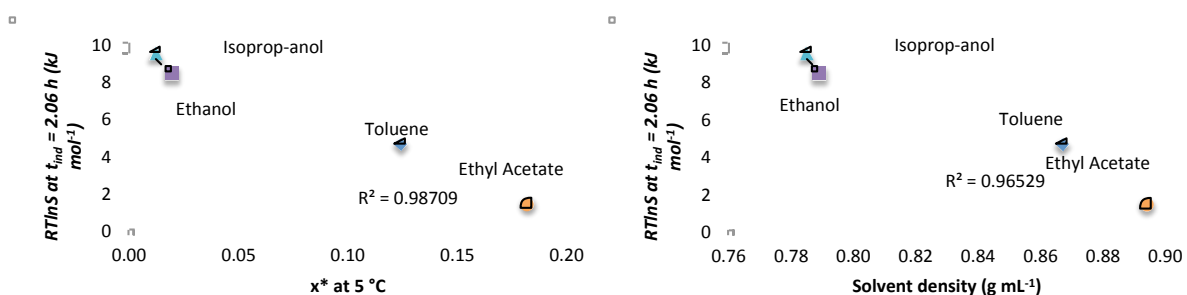


**Figure 5:  $RTlnS$  required to reach similar induction times compared to mole fraction solubility (left) and solvent density (right).**

Appendix A – Paper Draft: Solvent Effects on Nucleation Kinetics and  
Thermodynamics of Fenoxycarb

For further evaluation, the results are plotted according to the CNT by combining equations (1) and (4):

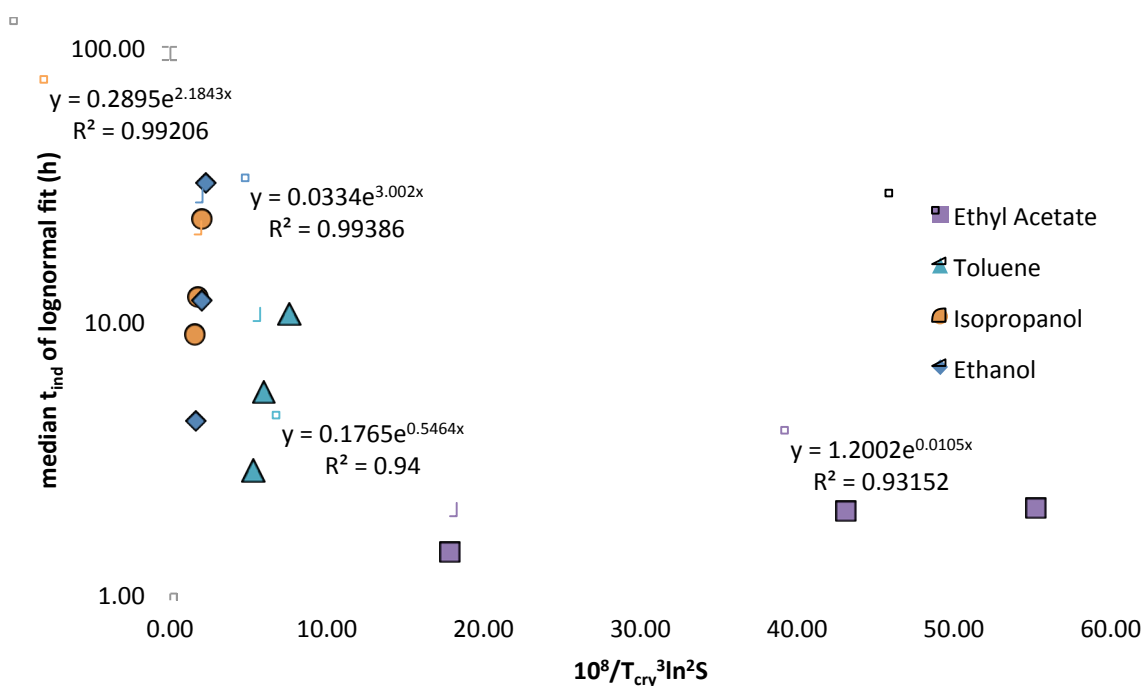


**Figure 6: The relationship between  $T_{cry}$ ,  $S$  and  $t_{ind}$  plotted according to the Classical Nucleation Theory. Lines are exponential fits.  $A$  and  $\gamma$  in Table 6 are calculated from the intercepts and slopes, respectively, according to Equations (1) and (4).**

From this,  $\gamma_{eff}$  and  $A$  were calculated for each solvent (Table 2) from the slopes and intercepts, respectively, of the exponential fits of Figure 15. Although  $\gamma_{eff}$  is temperature-dependent,<sup>8</sup> the variation in  $T_{cry}$  is quite low (5 K), and more importantly, the ability of the CNT to account for the data suggests the effect of  $T_{cry}$  on  $\gamma_{eff}$  is negligible under the narrow investigated temperature range. A negligible variance in  $\gamma_{eff}$  over temperature ranges of 65 °C have been reported.<sup>21</sup> The absolute values of  $\gamma_{eff}$  are of the same order of magnitude as similar studies for similar compounds.<sup>9, 10</sup>

**Table 2: Parameters calculated from CNT according to Equations (1), (3) and (4).**

Solvent	$A$ ( $m^{-3} s^{-1}$ )	$\gamma$ ( $mJ m^{-2}$ )	$n^*$	$\Delta G^*$ ( $kJ mol^{-1}$ )
Ethyl Acetate	16.67	0.82	4.1	2.68
			2.8	2.09
			0.7	0.86
Toluene	2.45	3.06	10.6	19.0
			7.3	14.9
			6.1	13.2
Isopropanol	4.02	4.86	5.7	20.1
			4.6	17.3

Appendix A – Paper Draft: Solvent Effects on Nucleation Kinetics and Thermodynamics of Fenoxycarb

			3.9	15.5
<b>Ethanol</b>	0.46	5.40	9.5	31.2
			7.7	27.3
			5.6	22.0

As can be seen from their slopes in Figure 2,  $\gamma_{eff}$  of ethanol and isopropanol may not be significantly different. The ease of nucleation according to  $\gamma_{eff}$  follows the general order of ease of nucleation from Figure 14 with only the order of the alcohols switched, and is (from low to high  $\gamma_{eff}$ ) ethyl acetate < toluene < isopropanol < ethanol. Only the order of the alcohols is switched. Since in both cases the differences between the alcohols is not very significant, this could explain the discrepancy. Alternatively it could be due to the absence of any direct theoretical relationship between  $RT_{cry}\ln S$  and  $t_{ind}$ .

Quantitatively,  $\gamma_{eff}$  seems to follow the trend often observed and also predicted by regular solution theory<sup>8</sup> of being inversely proportional to solubility (Figure 19). Unlike other molecules,<sup>9</sup> we found no correlation with solvent boiling point. Strangely, we found a strong correlation with solvent density (Figure 7).

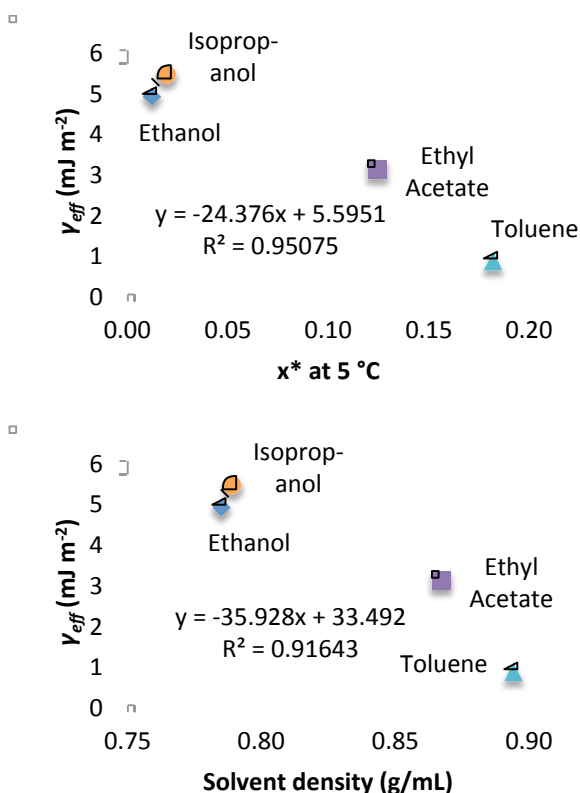


**Figure 7: Interfacial energy compared to mole fraction solubility (left) and solvent density (right).**

The number of FC molecules in the critical nucleus,  $n^*$ , are quite small, ranging from 10 to just under 1. For the highest  $S$  of ethyl acetate  $n^*$  appears to have reached unity, implying the solution-crystal spinodal has been reached, where  $\Delta G^*$  is less than the

thermal energy of the molecules.<sup>22</sup> If this is correct, further increasing  $S$  would result in a change in the observed dependence of  $t_{ind}$  on  $S$  and  $T_{cry}$ . Unfortunately, we did not obtain any such data to test this. Such low numbers of  $n^*$  have recently been found in several similar studies of medium-sized organic molecules, though unfortunately also in these cases no induction times were collected beyond the supposed spinodal.<sup>10, 14, 23</sup>

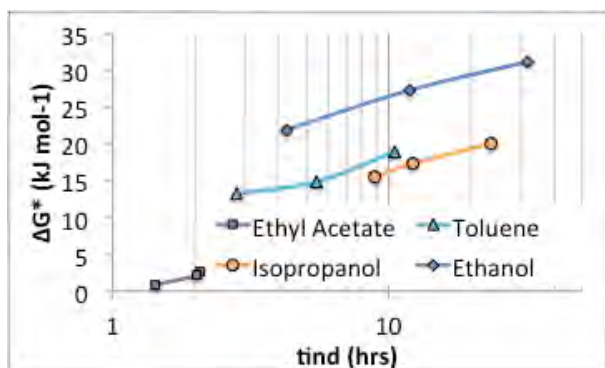


Figure 8: The nucleation work according to the CNT calculated from Equations (1) and (3) compared to the corresponding median induction times.

For median induction times of around 10 h, the largest amount of nucleation work would be required by ethanol and the least by ethyl acetate, as can be seen from Figure 8. Considering that ethanol has the smallest interfacial energy and the highest pre-exponent, while ethyl acetate has the highest interfacial energy and the lowest pre-exponent, this makes sense. On the other hand, isopropanol and toluene require almost identical nucleation work to achieve similar induction times despite the former having a significantly larger interfacial energy than the latter. Toluene, however, has a much smaller pre-exponent, and these two factors appear to have a similar but inverse effect to yield the similarity in relationship between nucleation work and induction time.

### 3.2 Spectroscopy

Figure 9 shows the IR spectra for solid, crystalline FC material. Peaks in the region  $1750\text{-}1630\text{ cm}^{-1}$  (amide I) can be attributed to arise primarily from the carbonyl stretching and a peak at  $1549\text{ cm}^{-1}$  (amide II) arises the combination of N-H in-plane bending and C-N stretching. These peaks correspond to C=O---N-H type hydrogen bonded motif as observed in the crystal structure of fenoxycarb (Figure 13).

Appendix A – Paper Draft: Solvent Effects on Nucleation Kinetics and Thermodynamics of Fenoxycarb

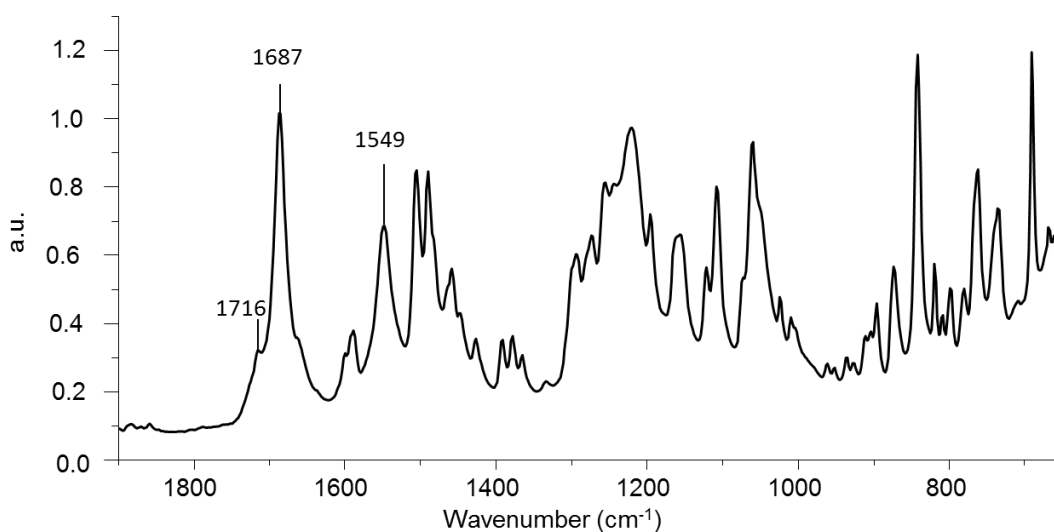
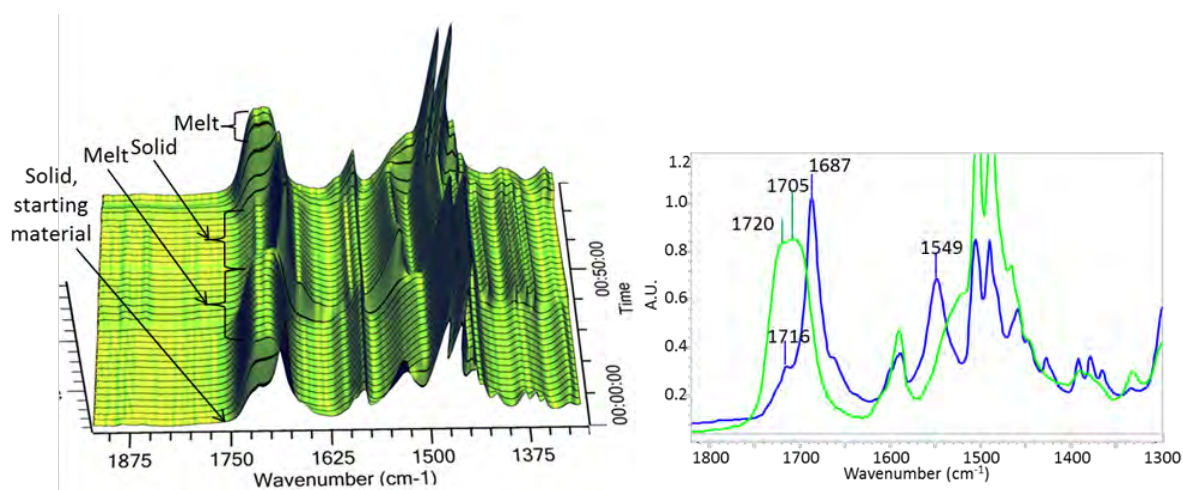


Figure 9: IR spectra of crystalline FC.

Figure 10 shows the change in the IR spectra during heat-cool cycles. Upon heating the material melted above 54 °C and during the cooling cycle it was possible to supercool the melt to about 30 °C before it crystallized; there was no change observed in the spectra from melting point to 30 °C. Upon melting, the major changes were observed in the carbonyl peak; a mixture of two peaks at 1720 and 1705 cm<sup>-1</sup> can be seen in the carbonyl region. Hydrogen bonding moves carbonyl stretching to a lower wavenumber and it appears that the peak at 1705 cm<sup>-1</sup> corresponds to the strongly bound carbonyl species compared to the bulk structure corresponding to the peak at 1720 cm<sup>-1</sup>. The melt phase can have different conformations and hydrogen bonding motifs of FC molecules, including the motif that is observed in the crystal structure. For the -C=O group, the strongest donor in FC molecule is -N-H and the crystal structure of FC exhibits the -C=O---N-H motif. Hence it is likely that in the melt spectra the strongly bound carbonyl at 1705 cm<sup>-1</sup> corresponds to this hydrogen bonding motif. Another clear change in the melt spectra was observed for the amide II peak region; a clear peak at 1549 cm<sup>-1</sup> in the crystalline material becomes less clear in the melt spectra.



Appendix A – Paper Draft: Solvent Effects on Nucleation Kinetics and  
Thermodynamics of Fenoxycarb

Figure 10: IR spectra (a) snapshot of heat-cool cycles (54-20 °C) over a period of time, showing solid-melt-solid-melt transition and (b) comparison of super-cooled melt with crystalline material

Solution spectra collected for solutions with different concentrations are shown in Figure 11a. No clear difference appeared between solution spectra of the alcohols, methanol, ethanol and isopropanol, and for that reason only one alcohol, isopropanol, is shown here. Detailed solution spectra for different solvents are shown in the supporting information file. It was possible to differentiate and subtract ethyl acetate carbonyl information from the solute carbonyl as ethyl acetate, being an ester, shows carbonyl at a higher wavenumber (due to the inductive effect) while the solute carbonyl, being a secondary amide, shows carbonyl at a lower wavenumber (due to the resonance effect).

At ambient temperature, the dilute solutions of FC prepared in ethyl acetate and toluene show only one dominant peak for carbonyl stretching at 1721 and 1725  $\text{cm}^{-1}$  respectively. With increasing solute concentration in ethyl acetate and toluene, the carbonyl peak shows a shoulder at a lower wavenumber which continually increases with concentration. A rise of this peak at lower frequency in the carbonyl region suggests an increase in strongly bound carbonyl species with increase in the concentration of solute. Interestingly, with increasing concentration this shoulder grows quite rapidly in the case of toluene solutions compared to solutions in ethyl acetate. On the other hand, solutions of isopropanol showed no such concentration effects at room temperature.

Appendix A – Paper Draft: Solvent Effects on Nucleation Kinetics and Thermodynamics of Fenoxycarb

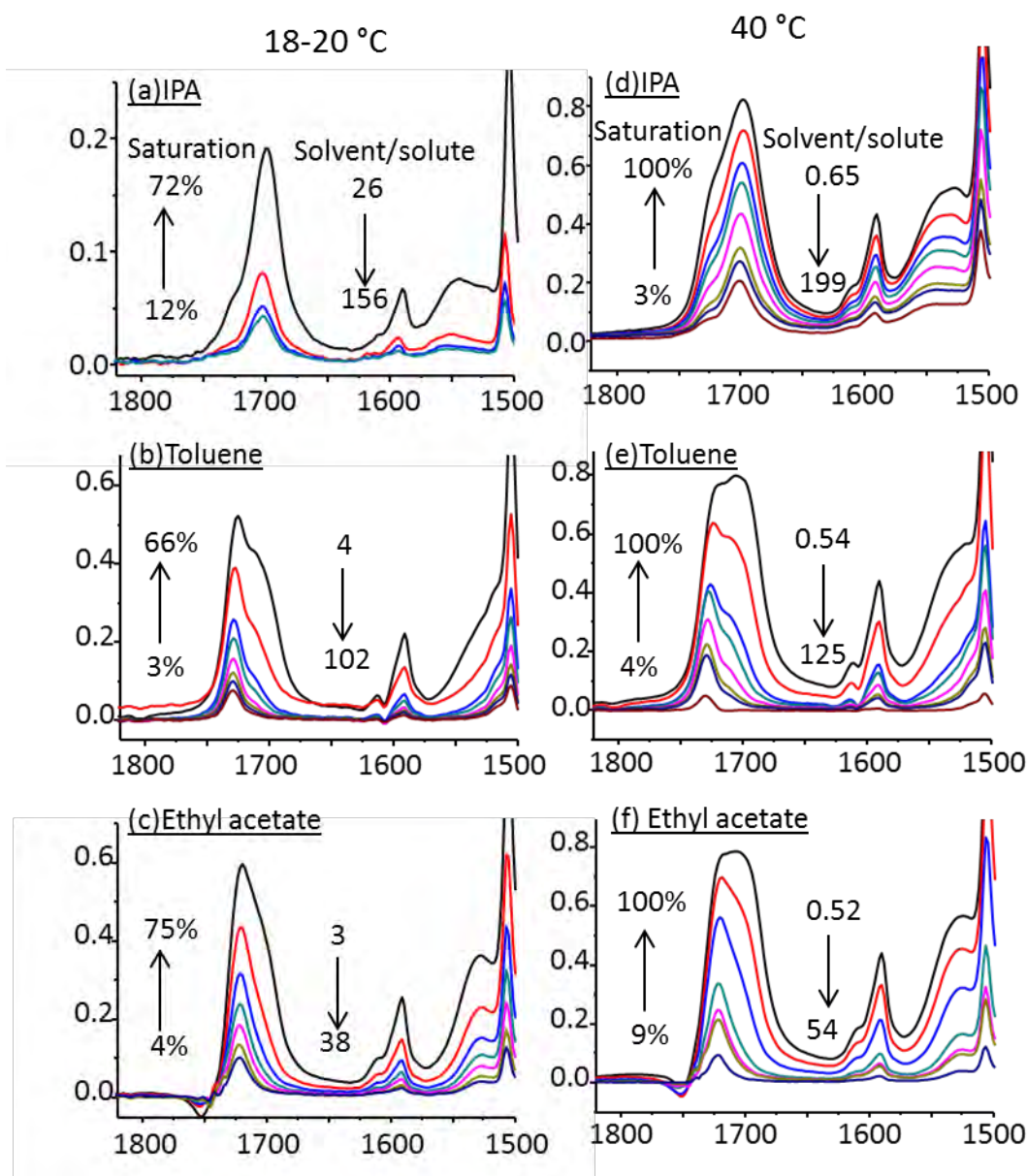


Figure 11: IR spectra of FC solutions at room temperature (a, b and c) and 40 °C (d, e and f), saturation and the number of solvent molecules per solute molecule (calculated from the mole fraction concentration) are shown for the lowest and the highest concentrations in each case.

In order to study the concentration effect for a wider concentration range and to aid interpretation of spectral changes, solution spectra were collected at 40 °C (Figure 11b). FC is highly soluble in all the solvents at 40 °C, and saturated solutions of FC at this temperature lead to compositions of solutions with less than one molecule of solvent per one molecule of solute. Considering the large size of the FC molecule compared to the smaller size of solvent molecules, it is expected that the solution is actually very similar to the melt phase. Indeed, the saturated solutions of FC at 40°C show similar spectra to that of the melt (Figure 10). At 40°C, carbonyl peaks in solutions of toluene and ethyl

Appendix A – Paper Draft: Solvent Effects on Nucleation Kinetics and  
Thermodynamics of Fenoxycarb

acetate show a similar trend to that observed at room temperature; with increasing concentration the shoulder at lower wavenumbers increases. Again, the rise in shoulder as a peak was quite rapid in the case of solutions in toluene compared to solutions in ethyl acetate. This could be generalized in terms of hydrogen bonding characteristics of these two solvents. Toluene can only very weakly interact with a carbonyl group via hydrogen bonding and it is reasonable that the solute-solute aggregation involving the carbonyl group is quite rapid for toluene. Ethyl acetate is a strong hydrogen bond acceptor and amongst many other possible sites of interactions with the solute, it would certainly interact with N-H. If the N-H is blocked by solvent, it creates an additional barrier to solute aggregation involving strongly bound carbonyl, i.e.  $-C=O\cdots N-H$ .

It is difficult to interpret the solute-solute aggregation information in alcohol solutions as alcohol can act as both hydrogen bond donor and acceptor, which poses difficulty in differentiating solvent-solute and solute-solute interactions. There was no concentration effect observed for solutions in alcohols at room temperature. However, with further increase in concentration at 40 °C, the shoulder at the higher wavenumber increases. It is expected that the alcohol would strongly interact with the carbonyl site and the major peak in carbonyl region could be mainly due to the solvent-solute interactions. With decreasing amounts of alcohol molecules (at very high solute concentration), there is a rise in some relatively free or loosely bound carbonyl species in solutions. The summary of peaks observed for different solvents in the carbonyl region is shown in Table 3.

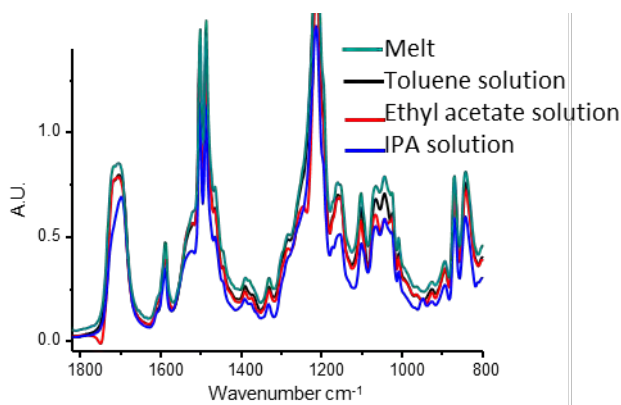


Figure 12: IR spectra of melt in comparison with saturated solutions at 40 °C

Table 3: Summary of peaks in the carbonyl region. s = strong peak, sh = shoulder.

Samples	Amide I , $cm^{-1}$
Solid	1716(sh) 1687(s)
Melt	1720 and 1705
E. acetate solution	1721(s) 1704(sh)

Appendix A – Paper Draft: Solvent Effects on Nucleation Kinetics and Thermodynamics of Fenoxycarb

Toluene solution	1725(s)	1710-1706(sh)
IPA solution	1725(sh)	1702(s)

It should be noted here that the nucleation experiments were carried out on solutions saturated at 15 and 20 °C. From the solution IR spectroscopy at room temperature, it was observed that in the concentrated solutions in ethyl acetate and toluene, there is an increased aggregation of strongly bound (solute-like) carbonyl species. On the other hand, the alcohol solutions at room temperature do not show any changes at the carbonyl site, appearing to be involved in strong solvent-solute interactions at this site.

### 3.3 Calorimetry

Experimentally determined enthalpies of solution,  $\Delta H_{\text{solution}}$ , for FC in five different solvents are given in Table 4. Since these values correspond to dissolution of only a small quantity of solute in a large quantity of solvent, the values can be interpreted as essentially being infinite dilution values,  $\Delta H_{\text{solution}}^{\infty}$ . In addition, the table shows calculated values of enthalpy of solvation ( $\Delta H_{\text{solvation}}$ ), enthalpy of cavity formation ( $\Delta H_{\text{cavity}}$ ) and enthalpy of solvent-solute interactions ( $\Delta H_{\text{interaction}}$ ) calculated from two approaches.

**Table 4: Enthalpies of solution, solvation, cavity, interaction at 25°C.**

Solvent	Solubility	$\Delta H_{\text{solution}}^{\infty}$ (kJ mol <sup>-1</sup> )	$\Delta H_{\text{solvation}}$ (kJ mol <sup>-1</sup> )	SPT approach		Alternative approach	
				$\Delta H_{\text{cavity}}$ (kJ mol <sup>-1</sup> )	$\Delta H_{\text{interaction}}$ (kJ mol <sup>-1</sup> )	$\Delta H_{\text{cavity}}$ (kJ mol <sup>-1</sup> )	$\Delta H_{\text{interaction}}$ (kJ mol <sup>-1</sup> )
Ethyl Acetate	0.3927	24.300 ± 0.063	-146.6	101.1	-246.4	156.3	-301.5
Toluene	0.3537	30.477 ± 0.011	-140.5	84.4	-223.2	294.4	-294.4
Ethanol	0.578	32.599 ± 0.106	-138.3	110.6	-247.3	253.9	-390.6
Isopropanol	0.1081	38.608 ± 0.009	-132.3	88.5	-219.1	242.1	-372.7

Table 4 shows that the calorimetric  $\Delta H_{\text{solution}}$  decreases with increasing solubility. It was interesting to see this correlation between  $\Delta H_{\text{solution}}$  and solubility as the solubility is an equilibrium-related thermodynamic quantity, whereas the values of  $\Delta H_{\text{solution}}$  are obtained by measuring the heat involved in dissolving a small quantity of solute to prepare dilute, undersaturated solutions. Since at the same temperature  $\Delta H_{\text{solvation}}$  is correlated with  $\Delta H_{\text{solution}}$  by equation (5),  $\Delta H_{\text{solvation}}$  increases with increasing solubility.

The  $\Delta H_{\text{interaction}}$  term obtained from the  $\Delta H_{\text{solvation}}$  term after cavity correction overall shows a similar trend to that of solvent-solute interaction obtained from MD calculation (cf. Table 5).

### 3.4 Computational molecular level analysis

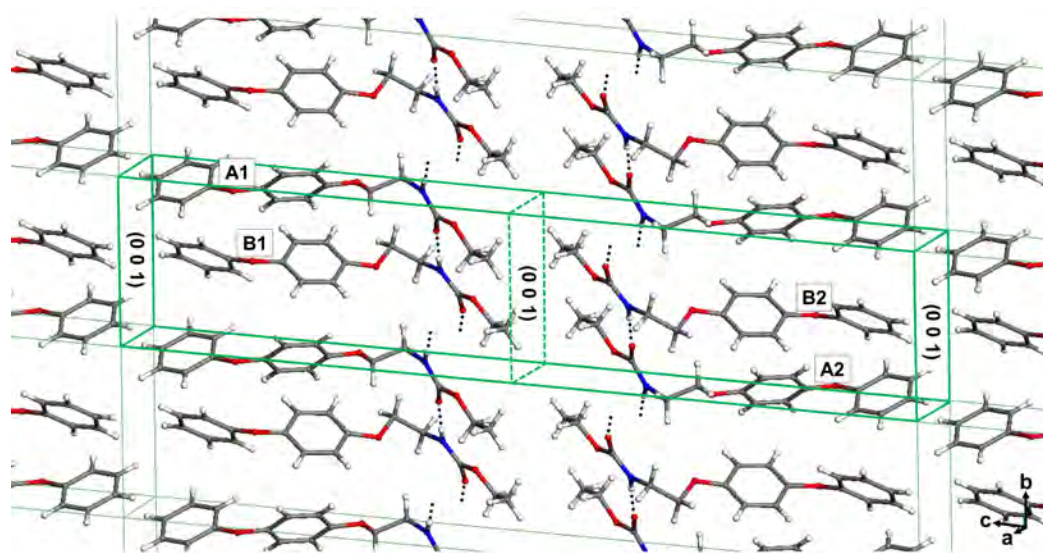


**Figure 13: Molecular arrangement in the crystal lattice of FC. Highlighted is a unit cell occupied by four FC molecules having distinct conformations, where A1 – A2 and B1 – B2 are non-superimposable mirror images.**

In the FC crystal, there are four distinct molecular conformations, which, in theory, can be interconverted by rotating particular segments around particular single bonds of the FC molecule (Figure 13). We identified three centres of rotation allowing for such an interconversion. DFT calculations of gas-phase energy barriers to rotation around those three single bonds, namely (i) C(ring)–O(ether) (in dihedral angle denoted as D1), (ii) C(aliphatic)–C(aliphatic) (D2), and C(aliphatic) –N(amide) (D3), are presented in Figure 14. It appears that flipping over one of the benzene rings around a C(ring)-O(ether) bond requires crossing an energy barrier of 5 kJ mol<sup>-1</sup>. On the other hand, rotation around dihedrals D2 and D3 require overcoming much higher energy barriers of about 25 and 30 kJ mol<sup>-1</sup>, respectively. Those energy barriers are typical for flexible organic molecules, and according to available experimental data, such barriers should not prevent a molecule from changing a conformation in solution.<sup>24</sup>

Appendix A – Paper Draft: Solvent Effects on Nucleation Kinetics and Thermodynamics of Fenoxycarb

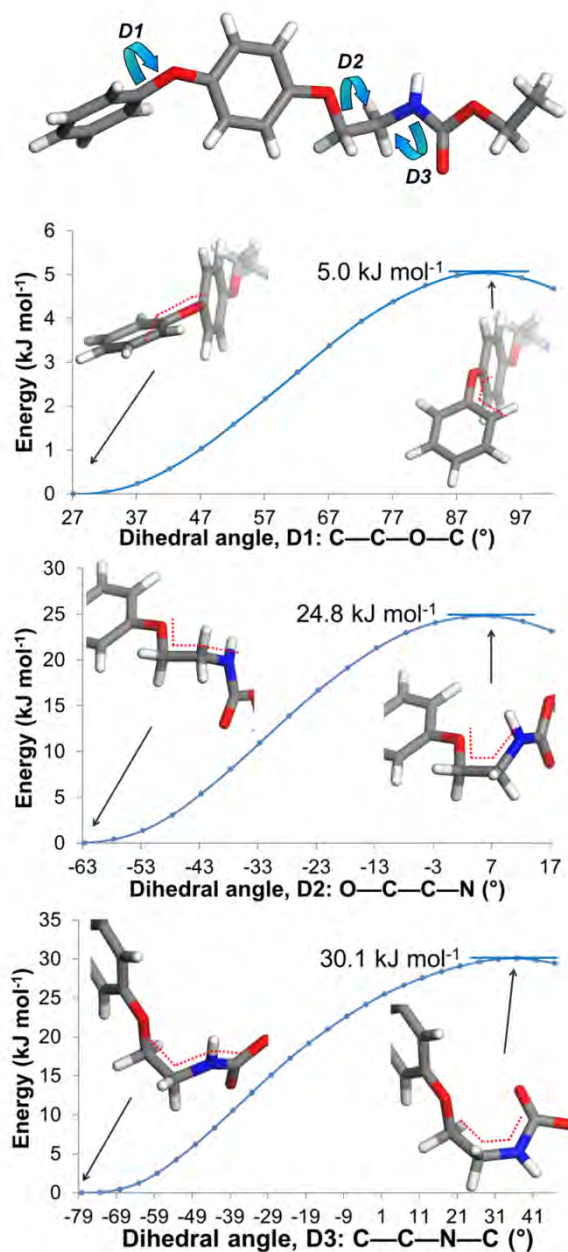
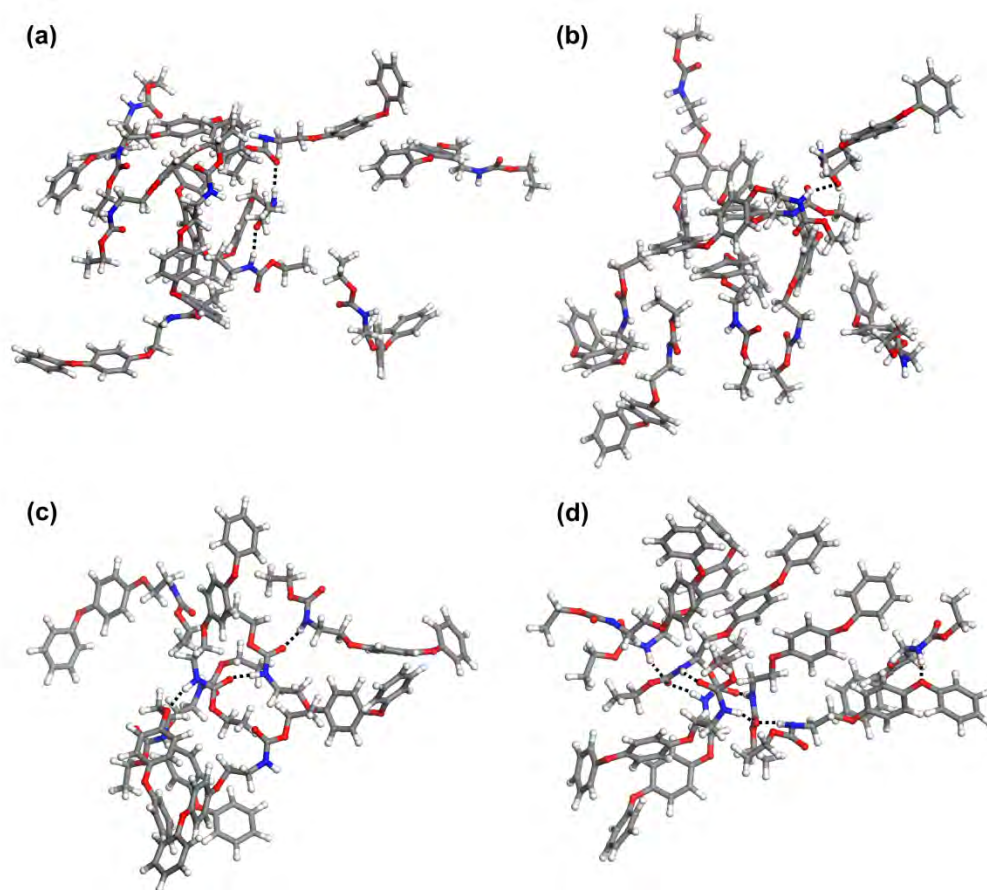


Figure 14: Energy barriers to rotation for selected single bonds of the FC molecule calculated with DFT. Top: the optimized FC molecule with the rotational centres highlighted with arrows.

FC exhibits very high solubility in ethyl acetate and toluene, and significantly lower, though still relatively high, solubility in ethanol and isopropanol. This is clearly reflected in our MD simulation snapshots (Figure 15b-c). Due to the high solute-to-solvent ratios, clustering of FC molecules is observed in all solvents at high concentration. At such a high concentration, the aggregates of FC molecules are largely interconnected and form three-dimensional gel-like structure in ethyl acetate and toluene. In the least concentrated isopropanol solution the clustering is less pronounced, but it is still obvious.

## Appendix A – Paper Draft: Solvent Effects on Nucleation Kinetics and Thermodynamics of Fenoxycarb

Conditions of our MD simulations were set to emulate the experimental conditions, i.e. the solution concentrations and temperatures were similar to those of the experimental supersaturated states. The simulations were performed at the crystallization temperature of 2 °C, and we aimed to observe how the different solvents affect cluster size, cluster shape, and chief intermolecular interactions governing growth of pre-nucleation clusters. Examples of pre-nucleation clusters extracted from the respective solvent boxes after 100 ns simulations at 2 °C are shown in Figure 15.



**Figure 15: Examples of FC pre-nucleation clusters formed in supersaturated solutions of (a) ethanol, (b) isopropanol, (c) ethyl acetate, and (d) toluene. H-bonds are indicated by black dotted lines. Molecules of solvent are not shown. Simulations were performed at 2 °C for 100 ns employing a Charmm General Force Field.**

The MD simulations confirm the high flexibility of FC molecules. The FC molecules adapt a variety of conformations in solution, where most geometries are quite different from those of the four crystal lattice conformers. This observation is in line with the relatively low energy barriers to rotation predicted with our DFT computations (Figure 14). It also appears that the molecular geometries/conformations in solution are not specific to the solvent. Comparing pre-nucleation clusters (Figure 15) suggests that most FC molecules in the clusters formed in ethanol and isopropanol are associated together only by a fraction of their interaction surface, such that the outer molecules of a

## Appendix A – Paper Draft: Solvent Effects on Nucleation Kinetics and Thermodynamics of Fenoxycarb

cluster are separated from one another and are, to a great extent, solvated (Figure 15a and b). On the other hand, the cluster forming in toluene (Figure 15d) appears to be more compact, with the FC molecules overlapping significantly. This cluster seems to be more stable than those from other solvents as, besides the significant overlapping of the FC molecules, its structure is strengthened by the highest number of hydrogen bonds (seven).

The MD simulations, regardless of the solvent used, reveal formation in solution of crystal-like H-bonds, (amide)N–H...O=C(carbonyl), and to a lesser extent (amide)N–H...O–C(ether) – the latter not existing in the FC crystal structure. As the former is a feature of the FC crystal, we calculated the radial distribution function (RDF) of interatomic distances of H (amide) and O (carbonyl) for the four considered solvents (Figure 16).

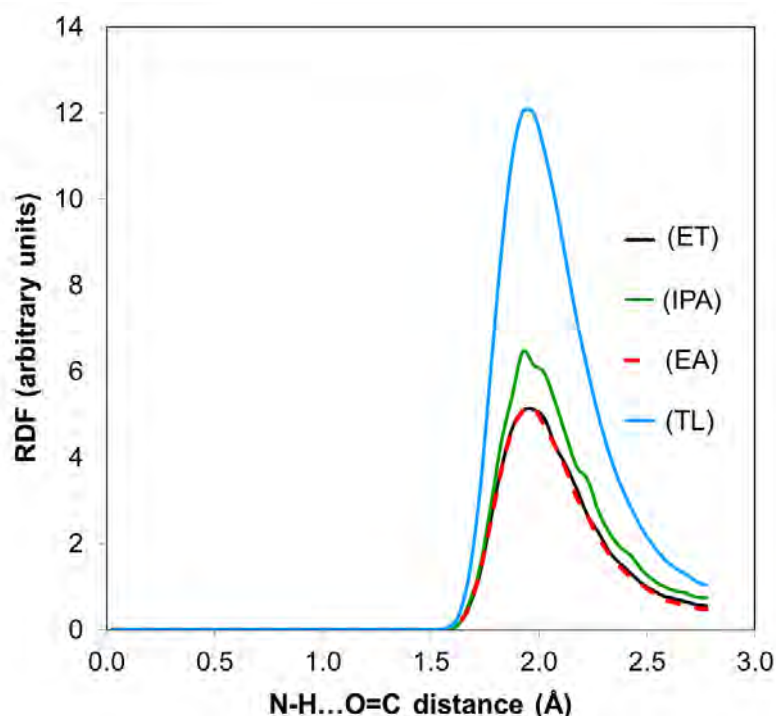


**Figure 16: Radial distribution function (RDF) plot for amide hydrogen...carbonyl oxygen hydrogen bonding established by FC molecules in ethanol (ET), isopropanol (IPA), ethyl acetate (EA), and toluene (TL).**

RDF is a pair correlation function, and describes how, on average, the atoms in a system are radially packed around each other. Our results indicate that most of the H (amide) and O (carbonyl) H-bonds are formed at a distance of ca. 1.9 Å, i.e. at a comparable distance as in the crystal (1.95 Å).<sup>15</sup> Based on the RDF values, the probability of finding two atoms forming this H-bond type is joint lowest in ethanol and ethyl acetate, slightly higher in isopropanol and the highest in toluene. This indicates that (crystal-like) H-bond formation is more facilitated in toluene than in the other solvents. Thus, the efficiency of hindering the formation of the crystal-like H-bond by the four solvents can

Appendix A – Paper Draft: Solvent Effects on Nucleation Kinetics and  
Thermodynamics of Fenoxycarb

be set in the order (from low to high): toluene << isopropanol < [ethyl acetate = ethanol].

Our recent work on the nucleation of salicylic acid<sup>13, 23</sup> and risperidone<sup>14</sup> suggest that the influence of the solvent on the crystal nucleation is related to the desolvation of a solute molecule. It stands to reason that the stronger solvent and solute molecules bind to each other in solution, the more difficult the desolvation, and consequently we hypothesise that this slows the nucleation becomes. To validate this hypothesis further, we have calculated the solvent–solute binding energies for both dilute and concentrated solutions of FC (Table 5).

**Table 5: Solvent–solute interaction/solvation enthalpy (per molecule of FC) from the MD simulations.**

System	$\Delta E_{\text{solvent-solute}}$ (kJ mol <sup>-1</sup> )			
	FC–Ethyl Acetate	FC–Toluene	FC–Isopropanol	FC–Ethanol
Diluted <sup>a</sup>	-221.4 ± 15.2	-208.2 ± 13.6	-243.7 ± 23.2	-248.5 ± 23.3
Concentrated <sup>b</sup>	-121.8 ± 1.9	-100.6 ± 1.6	-193.6 ± 4.5	-177.7 ± 2.7

<sup>a</sup>A single FC molecule in a box of solvent  
<sup>b</sup>molecular composition of 160 FC + 1848 ET, 71 FC + 1207 IP, 242 FC + 673 EA, and 250 FC + 665 TL.  
 Standard deviation (±) shown for each energy value.

As expected, the solvation enthalpies for the diluted solutions are higher than those of the concentrated solutions regardless of solvent. For the diluted system, the energies reflect binding of one FC molecule placed in a cavity surrounded by bulk solvent molecules. In the case of the concentrated solutions, the solute molecules are highly agglomerated, such that certain fractions of strongly binding polar groups are already engaged in solute-solute bonding. This can explain why the binding energies for the concentrated solutions are lower than those for the diluted systems. Following this reasoning, lower (less negative) solvation energies of the concentrated solutions indicate more pronounced clustering of the solute molecules. This is corroborated by the calculated solute-solute interaction enthalpies (Table 6). The results show that toluene and ethyl acetate create an environment where the FC molecules cluster significantly stronger as compared to the solute molecules assembling in ethanol and isopropanol.

Appendix A – Paper Draft: Solvent Effects on Nucleation Kinetics and  
Thermodynamics of Fenoxycarb

**Table 6: Solute–solute interaction enthalpy (kJ mol<sup>-1</sup>) at 2°C between all the solute molecules present in a simulation box averaged per a molecule of fenoxycarb (MD simulations (CGenFF)).**

FC–FC in Ethyl Acetate	FC–FC in Toluene	FC–FC in Isopropanol	FC–FC in Ethanol
-204.6 ± 1.2	-216.5 ± 1.2	-168.4 ± 2.5	-181.7 ± 1.6

Molecular composition of 160 FC + 1848 ET, 71 FC + 1207 IP, 242 FC + 673 EA, and 250 FC + 665 TL. Standard deviation (±) shown for each energy value.

**Table 7: Solvent-solvent interaction enthalpy (kJ mol<sup>-1</sup>) at 2°C between one solvent molecule and bulk solvent from MD simulations (CGenFF).**

Toluene	Ethyl Acetate	Isopropanol	Ethanol
-71.2 ± 6.2	-71.1 ± 8.2	-91.8 ± 11.8	-84.3 ± 12.9

Number of molecules in a box: 2000 ET, 1500 IP, 1280 EA, and 1200 TL

### 3.5 Discussion

In this work, the strength of solvent-solute interactions were calculated by two different methods – calorimetrically determined enthalpies of interaction ( $\Delta H_{\text{interaction}}$ ) and the solvent-solute interaction energies derived from the molecular dynamics work ( $E_{\text{solvent-solute}}$ ). Both methods account for solvent-solvent interaction as well as solute-solute interactions while deriving the values for solvent-solute interactions and there should be a good correlation for the solvent-solute interaction obtained by two methods. Indeed the correlation is strong (Figure 17 left), and it follows the decreasing order of ethanol > isopropanol > ethyl acetate > toluene. Furthermore, IR spectra allow estimating the strength of solvent-solute binding at the carbonyl site by probing the shift in the carbonyl stretching corresponding to the solvent-solute interaction. Spectroscopy data suggests that alcohols are strongly interacting at the carbonyl site, followed by ethyl acetate, and toluene is only weakly interacting at this site. Thus, the interaction order obtained from calorimetric, MD calculations and spectroscopic data (for the C=O site) all agree on the order of solvent-solute interactions, with the exception of a clear order between two alcohols. In case of MD calculations for concentrated solutions, the order of the alcohols is reversed and in case of spectroscopic data it was difficult to differentiate the shifts between two alcohols. Overall, this gives evidence of the validity of all three methods as measurements for the strength of the solvent-solute interactions.

Appendix A – Paper Draft: Solvent Effects on Nucleation Kinetics and  
Thermodynamics of Fenoxycarb

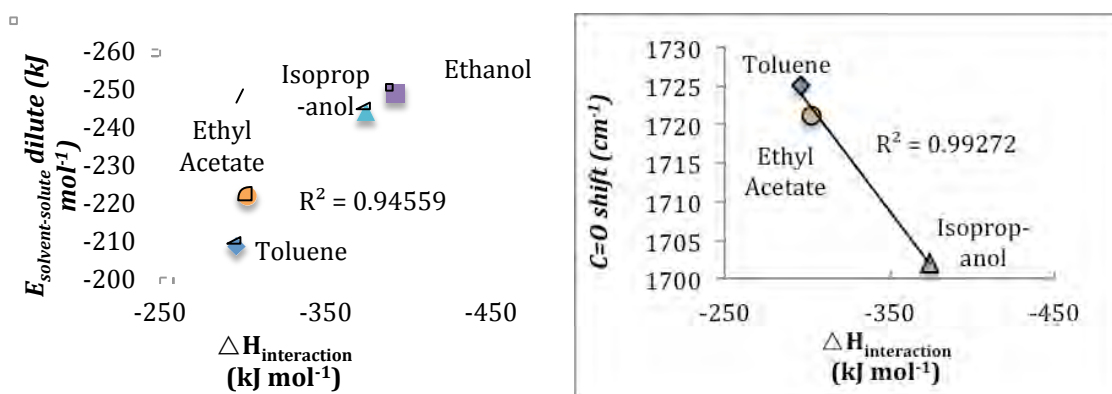


Figure 17: Cross-validating the spectroscopic, calorimetric and modelling investigations into the solvent-solute interactions.

Table 8: Solvents ranked (1 = lowest, 4 = highest) according to different properties.

Solvent	Ease of Nucleation		Solvent-Solute Interaction			
	$\gamma$ ( $\text{mJ m}^{-2}$ )	$RT \ln S$ for $t_{\text{ind}} = 2.06 \text{ h}$ ( $\text{kJ/mol}$ )	Calorimetric $\Delta H_{\text{interaction}}$ ( $\text{kJ mol}^{-1}$ )	Spectroscopic C=O ( $\text{cm}^{-1}$ )	MD dilute $E_{\text{interaction}}$ ( $\text{kJ mol}^{-1}$ )	MD conc. $E_{\text{interaction}}$ ( $\text{kJ mol}^{-1}$ )
Toluene	2	2	1	1	1	1
Ethyl Acetate	1	1	2	2	2	2
Isopropanol	3	4	3	3	3	4
Ethanol	4	3	4	4	4	3

In recent work on salicylic acid and risperidone we found that nucleation from 8 and 6 organic solvents, respectively, became more difficult as the solvent-solute interactions became stronger.<sup>13, 14</sup> This was based on similar nucleation, spectroscopic, calorimetric and modelling work, and the correlation was rationalised by the hypothesis that the more the solvent binds the solute, the more difficult the nucleation becomes.

In the case of FC we only have 4 datapoints (i.e. solvents), so it is more difficult to find significant trends. Furthermore, unlike salicylic acid, fenoxycarb is a flexible molecule with several conformers present in the single reported crystal structure.<sup>15</sup> Nevertheless, a similar overall trend is discovered quantitatively (Figure 20), and qualitatively in the order between the solvents (Table 8), especially when considering that the difference in nucleation difficulty between the alcohols is ambiguous (see 3.1).

## Appendix A – Paper Draft: Solvent Effects on Nucleation Kinetics and Thermodynamics of Fenoxycarb

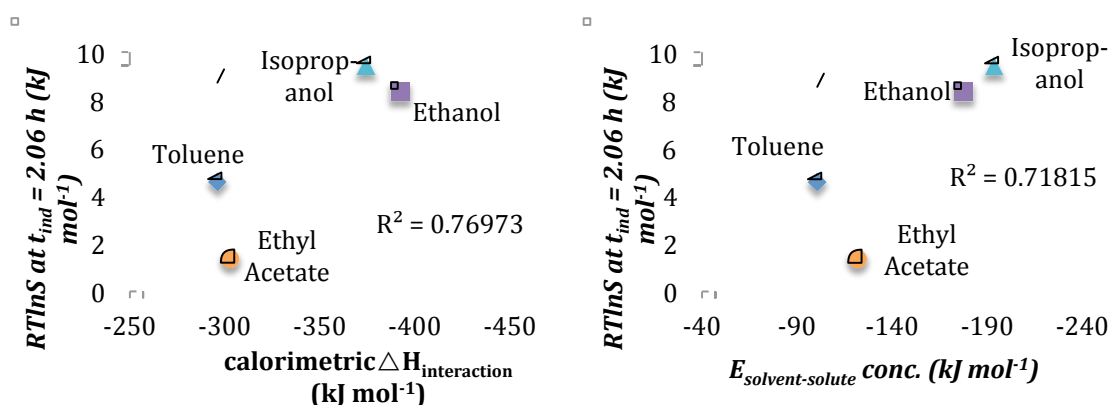


Figure 18: Nucleation difficulty correlated to calorimetric and molecular dynamics solvent-solute interaction.

A significant exception to this trend is toluene. Despite having a slightly weaker solvent-solute interaction than ethyl acetate, it is far more difficult to nucleate from.

## 4 Conclusion

The influence of solvent on the nucleation of FC, measured both as thermodynamic driving force (RTlnS) required to achieve similar induction times, and as the interfacial energy estimated using CNT, was found to be reasonably described by the relative prominence of solvent-solute interactions from spectroscopic, calorimetric and molecular dynamics investigations, whereby stronger binding of the solute by the solvent makes nucleation more difficult. The exception to this trend is toluene, which despite having the weakest solvent-solute interaction exhibits medium nucleation difficulty. It seems that the previously-found trend of stronger binding of the solute by the solvent leading to more difficult nucleation is somewhat complicated in the case of more flexible molecules such as FC.

## Acknowledgements

The financial support of Science Foundation Ireland (SFI, grant numbers 10/IN.1/B3038 and 11/SIRG/B2111) and the donation of fenoxycarb material by Syngenta, Switzerland are gratefully acknowledged. In addition, the SFI and Higher Education Authority funded Irish Centre for High End Computing is acknowledged for access to computational facilities.

## Bibliography

- (1) Valder, C.; Merrifield, D., Pharmaceutical Technology. *SmithKline Beecham R&D News* **1996**, 32.
- (2) Bernstein, J., *Polymorphism in Molecular Crystals*. ed.; Oxford University Press: Oxford, 2002.
- (3) Leng, J.; Salmon, J.-B., Microfluidic crystallization. *Lab on a Chip* **2009**, 9, (1), 24-34.

Appendix A – Paper Draft: Solvent Effects on Nucleation Kinetics and  
Thermodynamics of Fenoxycarb

- (4) Rodríguez-hornedo, N.; Murphy, D., Significance of controlling crystallization mechanisms and kinetics in pharmaceutical systems. *Journal of Pharmaceutical Sciences* **1999**, 88, (7), 651-660.
- (5) Vekilov, P. G., Nucleation. *Crystal Growth & Design* **2010**, 10, (12), 5007-5019.
- (6) Revalor, E.; Hammadi, Z.; Astier, J.-P.; Grossier, R.; Garcia, E.; Hoff, C.; Furuta, K.; Okustu, T.; Morin, R.; Veessler, S., Usual and unusual crystallization from solution. *Journal of Crystal Growth* **2010**, 312, (7), 939-946.
- (7) Ostwald, W. Z., Studies on the formation and transformation of solid compounds: Report I. Supersaturation and practicing cooling. [machine translation]. *Z. physik. Ch.* **1897**, 22, 289-330.
- (8) Mullin, J. W., *Crystallization, Fourth Edition*. ed.; Butterworth-Heinemann: 2001.
- (9) Yang, H.; Rasmuson, Å. C., Nucleation of Butyl Paraben in Different Solvents. *Crystal Growth & Design* **2013**, 13, (10), 4226-4238.
- (10) Yang, H.; Svärd, M.; Zeglinski, J.; Rasmuson, Å. C., Influence of Solvent and Solid-State Structure on Nucleation of Parabens. *Crystal Growth & Design* **2014**.
- (11) Kuhs, M.; Zeglinski, J.; Rasmuson, Å. C., Influence of History of Solution in Crystal Nucleation of Fenoxycarb: Kinetics and Mechanisms. *Crystal Growth & Design* **2014**.
- (12) Gracin, S.; Rasmuson, Å. C., Polymorphism and Crystallization of p-Aminobenzoic Acid. *Crystal Growth & Design* **2004**, 4, (5), 1013-1023.
- (13) Khamar, D.; Zeglinski, J.; Mealey, D.; Rasmuson, Å. C., Investigating the role of solvent-solute interaction in crystal nucleation of salicylic acid from organic solvents. *Journal of the American Chemical Society* **2014**.
- (14) Mealey, D.; Zeglinski, J.; Khamar, D.; Rasmuson, A., Influence of Solvent on Crystal Nucleation of Risperidone. *Faraday Discussions* **2015**.
- (15) Karpinska, J.; Kuhs, M.; Rasmuson, A.; Erxleben, A.; McArdle, P., Ethyl N-[2-(4-phenoxyphenoxy)ethyl]carbamate. *Acta Crystallographica Section E* **2012**, 68, (10), o2834-o2835.
- (16) Masner, P.; Angst, M.; Dorn, S., Fenoxycarb, an insect growth regulator with juvenile hormone activity: A candidate for *Heliothis virescens* (F.) control on cotton. *Pesticide Science* **1987**, 18, (2), 89-94.
- (17) Xiao-Hong, S.; Yuan-Fa, L.; Zhi-Cheng, T.; Ying-Qi, J.; Jian-Wu, Y.; Mei-Han, W., Heat Capacity and Enthalpy of Fusion of Fenoxycarb. *Chinese Journal of Chemistry* **2005**, 23, (5), 501-505.
- (18) Kuhs, M.; Svärd, M.; Rasmuson, Å. C., Thermodynamics of fenoxycarb in solution. *The Journal of Chemical Thermodynamics* **2013**, 66, (0), 50-58.
- (19) Kashchiev, D.; Rosmalen, G. M. v., Review: Nucleation in solutions revisited. *Crystal Research and Technology* **2003**, 38, (7-8), 555-574.
- (20) Kuhs, M.; Zeglinski, J.; Khamar, D.; Rasmuson, A., Influence of Solvent in Crystal Nucleation of Tolbutamide. **in preparation**.
- (21) Lancia, A.; Musmarra, D.; Prisciandaro, M., Measuring induction period for calcium sulfate dihydrate precipitation. *AIChE Journal* **1999**, 45, (2), 390-397.
- (22) Vekilov, P. G., The two-step mechanism of nucleation of crystals in solution. *Nanoscale* **2010**, 2, (11), 2346-2357.
- (23) Mealey, D.; Croker, D. M.; Rasmuson, A., Crystal nucleation of salicylic acid in organic solvents. *CrystEngComm* **2015**.
- (24) Derdour, L.; Pack, S. K.; Skliar, D.; Lai, C. J.; Kiang, S., Crystallization from solutions containing multiple conformers: A new modeling approach for solubility and supersaturation. *Chemical Engineering Science* **2011**, 66, (1), 88-102.

# B

**Appendix B – Paper Draft: Tolbutamide  
nucleation dependence on solvent**

## Influence of Solvent in Crystal Nucleation of Tolbutamide

---

Manuel Kuhs<sup>a</sup>, Jacek Zeglinski<sup>a</sup>, Dikshitkumar Khamar<sup>a</sup> and Åke C. Rasmuson<sup>a,b,\*</sup>

<sup>a</sup> Materials and Surface Science Institute, Chemical and Environmental Science, University of Limerick, Limerick, Ireland.

<sup>b</sup> Department of Chemical Engineering and Technology, KTH Royal Institute of Technology, Stockholm, Sweden

\* Corresponding author: ake.rasmuson@ul.ie

### Abstract

The influence of solvent and solution structure on the nucleation of a medium-sized organic molecule has been studied by measuring induction times, estimating solvent-solute interaction energies using modelling and calorimetric data, probing interactions and clustering with spectroscopy, and modelling solvent-dependence of conformational behaviour.

Over 1,100 induction time experiments were performed to measure the effect of solvent on the nucleation rate of tolbutamide form I<sup>L</sup>. A range of crystallisation temperatures and supersaturations were explored in toluene, acetonitrile, ethyl acetate and n-propanol to elucidate the relative ease of nucleation. Since different forms nucleated nonconcomitantly in n-propanol, careful monitoring of the nucleating form was required to isolate the induction times corresponding only to form I<sup>L</sup>. Both the thermodynamic driving force required to achieve median induction times of 2 hours, and the interfacial energies calculated using the Classical Nucleation Theory, were found to decrease in the order [n-propanol & toluene] > ethyl acetate > acetonitrile. To rationalise this order, solvent-solute interactions, which have been found to increase with increasing nucleation difficulty in the case of salicylic acid and risperidone, were estimated by molecular modelling and by using calorimetric enthalpies of solution. The two methods were successfully cross-validated against each other, and against the FTIR frequency of the tolbutamide carbonyl band indicative of solvent-solute bonding. The consensus solvent-solute interactions decrease in the order n-propanol > acetonitrile > ethyl acetate > toluene, which does not correlate to the nucleation order, with the exception of n-propanol, from which nucleation is difficult and interactions are strong. However, conformational identities of tolbutamide molecules in the different solutions and their respective rotation barriers for transforming to the molecular conformation found in the crystal, as predicted by modelling, were able to provide an explanation for the lack of correlation. For example, nucleation from toluene is very difficult despite weak solvent-solute interactions. However, in toluene molecular dynamics modelling predicts that tolbutamide assumes an intramolecularly hydrogen bonded conformer with a very high rotational barrier for transforming to the crystal conformer.

## 1 Introduction

Crystallization is heavily used in various manufacturing industries, ranging from the production of salt to silicon wafers. The process is also used in the pharmaceutical industry, where over 90% of all pharmaceutical products contain crystalline ingredients,<sup>1</sup> and where it is considered the single most important unit operation.<sup>2</sup>

However, there is insufficient understanding of crystallization, and the fundamental theory is insufficiently developed to replace empirical approaches.<sup>3</sup> The first step in crystallisation, nucleation, is particularly problematic. Though instrumental in determining critical parameters such as crystal morphology, size, size distribution and polymorphic form, its mechanism is still unclear. This fundamental lack of understanding was epitomised by the famous shortage of the HIV protease inhibitor Norvir in the 1990s due to the sudden formation of a different polymorph than the one produced for months.<sup>4</sup> In general, poor yields and the presence of undesirable or unpredictable polymorphs continue to plague crystallization processes at both a lab and industrial scale.<sup>4</sup>

Symptomatic of the unsolved nature of nucleation science is the continued use of the Classical Nucleation Theory (CNT). Developed over 100 years ago, and admitted to have several serious flaws not much later, it remains the default model for analysing experimental results. Only in recent years have alternative models been receiving wider acceptance, chief of which is the Two Step Theory.<sup>5</sup>

The difficulty in studying nucleation arises from a combination of its stochastic nature, the miniscule size of the smallest stable nuclei (which are typically in the order of 10 to 1,000 molecules), and the great speed at which nuclei form. Thus, it is very difficult to directly observe nucleation, both from a temporal and a spatial perspective.<sup>6</sup>

One promising approach to understanding nucleation is studying its dependence on the solute/solvent interaction for nucleation from solution. The sensitivity of nucleation to solution chemistry has been known over 100 years.<sup>7</sup> According to CNT, the interfacial energy between the solute and the solution,  $\gamma$ , represents the solvent-specific contribution to the solute's thermodynamic barrier to nucleation. Thus, it is common practice to calculate  $\gamma$  using CNT. A general inverse proportionality between solubility and interfacial energy is well established for aqueous solutions of inorganic salts.<sup>8</sup> In individual cases interfacial energies have been correlated with intrinsic solvent properties such as solvent boiling points<sup>9</sup> and solvent-solute interaction properties such as solvation and deformation energies.<sup>10</sup> Recent studies have demonstrated solvent-induced self-assembly of solute molecules prior to nucleation, as well as implicit<sup>11</sup> and explicit<sup>9, 12</sup> relationships between solution structure and polymorphic outcome.

After statistically measuring the induction time in several organic solvents,<sup>13</sup> our group has recently shown that the nucleation of salicylic acid, a small inflexible organic molecule, may depend on the strength with which the solvent binds the molecule in solution.<sup>14</sup> This was deduced from strong positive linear correlation between the interfacial energy calculated from induction times and several other experimental and modelled variables at SA's carboxyl group, both the carbonyl peak shift in the Raman

spectrum for the salicylic acid monomer and the DFT-derived 1:1 binding energy; the calorimetrically-derived enthalpy of solvent-solute interaction; and the DFT-derived solvation energy. In a similar study using risperidone, we also found evidence suggesting the nucleation of this compounds depends on the inability of the solvent to bind the risperidone molecules in solution.<sup>15</sup> On the other hand, our most recent study on fenoxycarb found the opposite relationship, namely a negative correlation between interfacial energy and enthalpy of solvation.<sup>16</sup>

To further probe the complex relationship between solvent and nucleation, we measure the effect of four different solvents on the nucleation of a medium-sized API, tolbutamide, and compare the results with various experimental and modelled thermodynamic quantities of the solvents and solutions.

Tolbutamide is a first-generation oral anti-diabetic drug that stimulates the secretion of insulin in the pancreas and is used in managing type II diabetes.<sup>17</sup> It has chemical formula  $C_{12}H_{18}N_2O_3S$ , systematic name *n*-[(Butylamino)carbonyl]-4-methylbenzenesulfonamide, and is shown in Figure 1. A flexible organic molecule, it has six reported crystal forms. These have a complex relationship, with some disagreement in published studies, which was recently resolved; we use the naming convention from that study.<sup>17</sup> The stability order below 38 °C is Form II > I<sup>L</sup> > III > IV, where II is most stable and melts at 117 °C;<sup>17, 18</sup> form I<sup>H</sup> is inaccessible below 38 °C;<sup>19</sup> the exact relative stability of form V has not yet been determined, although it is highly unstable at room temperature, transforming to form I within several hours.<sup>18</sup> Cooling crystallisation from pure solvents have only been reported in ethanol, where forms II, I<sup>L</sup> and III can all nucleate as follows:<sup>20</sup> for long induction times ( $t_{ind}$ ) form II nucleates, otherwise forms I<sup>L</sup> and III nucleate at low and high cooling rates and supersaturations ( $S$ ), respectively. Though poorly water-soluble,<sup>21</sup> solubilities for pure non-aqueous solvents are only reported for ethanol and above 15 °C.<sup>17</sup>

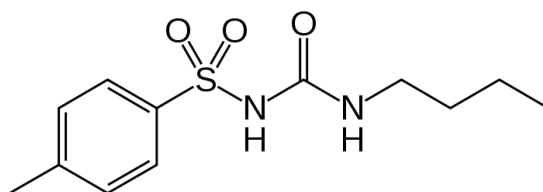


Figure 1: Molecular structure of tolbutamide.

## 2 Methodology

All chemicals (Table 1) were used as-received.

**Table 1: Suppliers and purities of materials.**

<b>Solvent</b>	<b>Supplier</b>	<b>Purity</b>
<b>Tolbutamide Form I<sup>L</sup>*</b>	Sigma-Aldrich	0.997
<b>N-propanol</b>	VWR International	0.995
<b>Acetonitrile</b>	VWR International	0.999
<b>Toluene</b>	Sigma-Aldrich	0.999
<b>Ethyl Acetate</b>	Sigma-Aldrich	0.997

\* Powder XRD showed only peaks corresponding to Form I<sup>L</sup>.

## 2.1 Solubility

The as-received tolbutamide was confirmed to be the metastable form I<sup>L</sup> by PXRD. Solubilities for the as-received metastable form I<sup>L</sup> were measured similar to a previous publication by us<sup>22</sup> with only minor modifications chiefly to ensure transformation to the stable form II had not occurred.

Vials were duplicated instead of duplicating samples from vials, and slurries were allowed to equilibrate for only 1 h. For each solvent, the time to reach equilibrium concentration was measured at the lowest  $T_{cry}$  (see Table 2), where this process is presumably the slowest, by taking samples after 3 successive 1 h equilibration cycles and after a final 12 h equilibration. In all cases there was no significant variation in concentration after the first measurement (i.e. after 1 h), and the crystal form of the slurry was verified to still be pure form I<sup>L</sup> by PXRD. This is in keeping with literature reports of transformation times in ethanol of around 2-3 h, which were measured at room temperature.<sup>17, 20</sup> The absence of transformation was also confirmed by PXRD for slurries of each solvent at their respective highest  $T_{cry}$  (see Table 2) after 1 h equilibration.

## 2.2 Induction Times

The procedure used for measuring induction times in different solvents is almost identical to that used previously.<sup>16</sup> Minor deviations are outlined below.

Since precise saturation temperatures ( $T_{sat}$ ) for the solutions were not known (in the absence of relevant solubility data), the following steps were taken to ensure complete dissolution prior to entering supersaturation. Rough solubility measurements (not reported) indicated all  $T_{sat}$  were less than 20 °C for the range of solvents employed. After mixing of solute powder and solvent, stock solutions (see Table 2 for concentrations) were dissolved with stirring at 25 °C for at least 12 h (visual homogeneity was achieved after several minutes). After aliquoting and filtering as outlined previously, vials were heated to 35 °C prior to crystallisation at  $T_{cry}$ , and were subsequently kept at 35 °C for at least 3 h between successive crystallisation cycles.

This filtration at 25 °C followed by heating to 35 °C ensured complete dissolution despite the absence of precise  $T_{sat}$  data.

The only other deviations from the previously-published protocol are the usage of median  $t_{ind}$  values directly from experimental data without fitting, experiments often being stopped after 7 h instead of 24 h (since nucleation for these experiments was significantly faster), 600 mL of stock solution being used for all solvent to give 30 vials per solvent, and solid state monitoring for polymorphism as explained further below.

The Classical Nucleation Theory (assuming the initial nucleus to be cubic in shape) postulates the influence of  $S$  and  $T_{cry}$  on the nucleation rate,  $J$ , as:<sup>8</sup>

$$J = A \exp \left( - \frac{32\Omega^2 \gamma_{eff}^3}{\mathbf{R}^3 T_{cry}^3 \ln^2 S} \right) \quad (1)$$

where  $A$  is the pre-exponential factor,  $\Omega$  the volume occupied by a molecule in the crystal,  $\mathbf{R}$  the universal gas constant, and  $\gamma_{eff}$  the interfacial energy between the crystal, the solution, and, in the case of heterogeneous nucleation, the surface on which nucleation occurs.

According to the CNT,  $\gamma_{eff}$  is related to the Gibbs free energy of the critical nucleus,  $\Delta G^*$ , and to the number of molecules in the critical nucleus,  $n^*$ , as:

$$\Delta G^* = \frac{32\Omega^2 \gamma_{eff}^3}{(\mathbf{R} T_{cry} \ln S)^2} = 0.5 n^* \mathbf{R} T_{cry} \ln S \quad (2)$$

Assuming that impurities (which provide surfaces for heterogeneous nucleation and can thus modify  $\gamma_{eff}$ ) are the same in different solvents,  $\gamma_{eff}$  can be used to compare the effect of solvent on the thermodynamic barrier to nucleation of the solute.

The time to the first appearance of crystals,  $t_{ind}$ , is usually assumed to relate to the nucleation rate,  $J$ , as:<sup>23</sup>

$$J = 1/V t_{ind} \quad (3)$$

By combining equations (1) and (3),  $\gamma_{eff}$  can be calculated by measuring the effect of  $T_{cry}$  and  $S$  on  $t_{ind}$ . However, as  $\Omega$ ,  $S$ ,  $\gamma_{eff}$  and thus  $J$  are polymorph-specific, the nucleating crystal form must be identified.

### 2.3 Solid Phase Characterisation

Tolbutamide is reported to nucleate during cooling crystallisations in pure ethanol as either form II, I<sup>L</sup> or III, depending on  $t_{ind}$ ,  $S$  and cooling rate.<sup>20</sup> Absolute values of these conditions, however, cannot be compared to our work, since our work was carried out at 20 mL compared to over 400 mL, and we did not measure meta-stable zone widths but  $t_{ind}$ . We performed preliminary induction time experiments under experimental conditions and analysed the crystallised form using powder X-ray Diffraction (PXRD). This was done within several minutes after crystallisation to minimise the likelihood of polymorphic transformation. Transmission PXRD was performed with an Empyrean diffractometer (PANalytical, Phillips) with Cu K $\alpha$  radiation ( $\lambda = 1.5406 \text{ \AA}$ ) at room temperature. Data were recorded at a tube voltage of 40 kV and a tube current of 35

mA, applying a step size of  $0.0131^\circ$  ( $2\theta$ ) and a scan speed of  $0.164^\circ$  ( $2\theta$   $s^{-1}$ ) in the angular range of 5 to  $35^\circ$  in  $2\theta$  with 4 revolutions per minute. These spectra were compared to theoretical powder spectra calculated using the software package Mercury (CSD System) from the crystal structures found in the Cambridge Crystal Structure Database. In these exploratory experiments, all recrystallised tolbutamide was found to be form I<sup>L</sup>. We decided to carry out spot-checks on the final  $t_{ind}$  experiments to verify the crystallisation of form I<sup>L</sup> by similarly analysing the crystal form of a vial with a short and a long  $t_{ind}$  of each of the lowest and highest  $S$  experiment performed last for each solvent (see stars in Figure 7) This was done during the last iteration of the respective crystallising conditions because extraction of slurry renders a vial unusable (the concentration, and thus  $S$ , having changed). In acetonitrile, ethyl acetate and toluene, form I<sup>L</sup> was found in each case. However, in n-propanol two vials contained pure form I<sup>L</sup> and the other two pure form II. Repeating these experiments and checking further vials found that both forms nucleated non-concomitantly at either short or long  $t_{ind}$  and at either low or high  $S$  in n-propanol.

The nucleation of multiple forms of tolbutamide in n-propanol renders the  $t_{ind}$  data collected for this solvent unusable for calculating  $\gamma_{eff}$  since we do not know which form nucleated for the majority of induction times collected. Thus it was determined to repeat n-propanol  $t_{ind}$  experiments while monitoring the crystal form nucleating in each case using Raman spectroscopy *without opening the vials to allow re-using them* as follows.

A non-contact probe attached to a Kaiser RamanRxn2 Analyzer with an Invictus 785 nm NIR laser set to 200 mW was used to obtain the Raman IR spectra of slurries of both pure form II and pure form I<sup>L</sup> tolbutamide (as determined by PXRD) in n-propanol by standing the non-contact probe upright and placing the sealed vial containing the slurry directly on top of the sampling window. iC Raman software, version 4.1, was used to collect the spectra from  $150 - 3,400$   $cm^{-1}$  with an exposure time of 15 s, 3 accumulations, a resampling interval of  $1$   $cm^{-1}$ , cosmic ray removal, and intensity correction. Similarly, the Raman spectra of pure powders of both forms were obtained by placing the probe facing down about 20 mm above the powder. Comparing the four spectra (Figure 2), the peaks at  $1160$  and  $1165$   $cm^{-1}$  were found to be unique to forms I<sup>L</sup> and II in n-propanol slurries, respectively. In the repeat n-propanol  $t_{ind}$  experiments, the Raman spectrum for each vial was obtained less than 8 h after crystallisation in the same manner as for the slurries of known polymorphic form (under experimental conditions no trace of form II was detected by either PXRD or Raman in slurries of form I<sup>L</sup> after 8 h). About 60% of vials at each condition were found to be form I<sup>L</sup> without a form II peak and 30% form II without a form I<sup>L</sup> peak, both types of Raman spectra being identical to those of their respective slurries of known, pure forms. The remaining 10% were inconclusive. Only the induction times corresponding to the 60% of confirmed form I<sup>L</sup> were kept for subsequent analysis. Interestingly, each vial usually nucleated only a single form, i.e. if a vial nucleated form II in the first iteration, it also nucleated form II in all following iterations. Furthermore, the  $t_{ind}$  distributions at each  $T_{cry}$  for both forms I<sup>L</sup> and II were mostly indistinguishable (Figure 7), though insufficient data for form II at 6 and 7 °C were collected for these conclusion to be statistically significant.

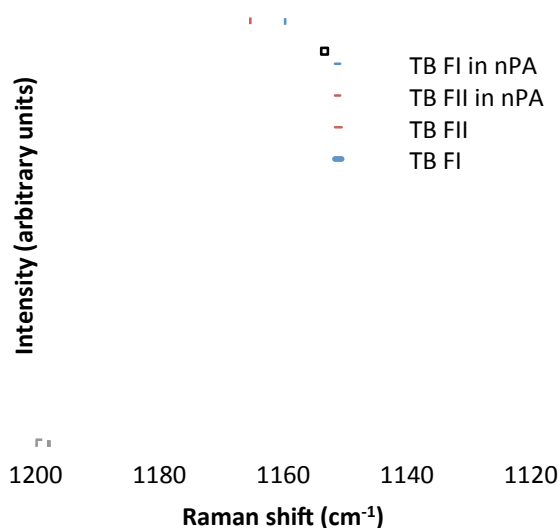


**Figure 2: Raman shifts distinguishing between forms I<sup>L</sup> and II. Vertical lines indicate peaks unique to forms I<sup>L</sup> (blue) and II (red).**

## 2.4 IR Spectroscopy

IR spectra of the solid forms were collected using a Perkin Elmer spectrum 100 spectrometer fitted with universal ATR accessory and lithium tantalite detector. The spectral data were collected in the region of 4000-400 cm<sup>-1</sup> with resolution of 4 cm<sup>-1</sup>. For solution IR spectroscopy, Mettler Toledo ReactIR 10 fitted with silver halide probe and liquid nitrogen cooled MCT detector was used. The solution IR data were collected from 2000-650 cm<sup>-1</sup> with 4 cm<sup>-1</sup> resolution. To collect solution IR spectra of varied concentrations, for each solvent the saturated solution was prepared first at ambient temperature (20-22 °C) and scanned. Dilute solutions were then prepared by adding, in series, pure solvent to the concentrated solution and the IR spectra were collected for each of these diluted solutions.

## 2.5 Calorimetry

A Precision Solution Calorimeter from TA Instruments, USA along with Thermal Activity Monitor (TAMIII) was used in semi adiabatic mode. A small quantity of (0.347-0.349 g for measurements in acetonitrile, ethyl acetate and n-propanol and 0.100g for experiments in toluene) Tolbutamide was dissolved in 100 mL of pure solvent and the corresponding temperature change was measured to determine the enthalpy of solution,  $\Delta H_{\text{solution}}$ . The detailed experimental method was described previously.<sup>14</sup> The experimentally determined  $\Delta H_{\text{solution}}$  allows calculation of the enthalpy of solvation,  $\Delta H_{\text{solvation}}$  using the relationship:

$$\Delta H_{\text{solvation}} = \Delta H_{\text{solution}} - \Delta H_{\text{sublimation}} \quad (4)$$

The enthalpy of sublimation was not reported in the literature; however the lattice energy for tolbutamide is reported to be -168.22°C<sup>ref</sup>. Using the lattice energy value, the enthalpy of sublimation was determined as:

$$\Delta H_{\text{sublimation}} = -E_{\text{lattice}} - 2RT \quad (5)$$

The solvation term ( $\Delta H_{\text{solvation}}$ ) relates to transferring gas phase solute molecule into the solution state and requires cavity formation values as well as solvent-solute interaction as outlined below.

$$\Delta H_{\text{solvation}} = \Delta H_{\text{cavity}} + \Delta H_{\text{interaction}} + \alpha RT^2 - RT \quad (6)$$

In our previous work,<sup>14</sup> we used the Scaled Particle Theory (SPT) approach to determine the cavity formation contribution and using that the enthalpy of solvent-solute interaction,  $\Delta H_{\text{interaction}}$  was determined. A detailed account of the SPT theory, its origin, application and limitations can be found in the literature. Some of the major issues with the SPT approach are: (a) the approach is extremely sensitive to the values of solvent and solute diameters; (b) originally the theory was developed on simple, small, spherical solute molecules and application to large, flexible molecules may not be appropriate; (c) solvents which involve strong, directional and non-additive interactions such as alcohols may lead to high inaccuracy in the values; (d) when there is strong, directional interaction between solute and solvent the additivity of the cavity calculation is questionable.

In this work, we estimate the cavity values by two methods: using the SPT approach and also by an alternative approach where we calculate strength of solvent-solvent interactions using MD calculation. It is assumed that for a given molecule, the higher the strength of solvent-solvent interaction, the higher the work required to create a cavity and incorporate a solute molecule. In this alternative approach, to account for molecular shape and volume of tolbutamide molecule, we normalised MD-predicted solvent-solvent interaction enthalpies by normalising accessible surface areas of the four solvents for the equivalent surface area of the tolbutamide molecule. A detailed account on the calculation of cavity formation with the two methods and the parameters used for these calculations are shown in the supporting information file.

## 2.6 Computational Methods

Molecular dynamics (MD) simulations were employed to quantify the solvent–solute and solvent–solvent interaction enthalpies in bulk solutions of four different solvents, i.e. n-propanol, toluene, ethyl acetate, and acetonitrile. In addition, interactions of a tolbutamide molecule within bulk crystals of both form I<sup>L</sup> and form II were calculated. The simulations were performed using COMPASS II force field along with the force field assigned charges as implemented in the Forcite module of the Materials Studio software package.

By multiplying a single unit cell of the most stable tolbutamide form II (ZZZPUS05), a periodic supercell containing 128 tolbutamide molecules has been constructed, with the cell dimensions of  $a = 36.35 \text{ \AA}$ ;  $b = 34.46 \text{ \AA}$ ;  $c = 35.90 \text{ \AA}$ ,  $\alpha = 90.0^\circ$ ;  $\beta = 95.0$ ;  $\gamma = 90.0^\circ$ . It was observed that after initial optimisation/energy minimisation and subsequent equilibrating with molecular dynamics for 100 ps at 298 K and standard pressure (1 atm), the shape of the simulation box has been preserved while it expanded slightly, giving  $a = 36.80 \text{ \AA}$ ,  $b = 34.88 \text{ \AA}$ , and  $c = 36.34 \text{ \AA}$ ; this negligible change in the volume

and shape of the crystal supercell upon MD equilibration indicates suitability of the force field used. In the same way, we have constructed a supercell of the metastable form I<sup>L</sup> (ZZZPUS04) also containing 128 tolbutamide molecules. In addition, four periodic boxes with approx. dimensions of 40 x 40 x 40 Å have been constructed, each filled with molecules of the respective solvent and containing one tolbutamide molecule. Four boxes of similar size, containing only solvent molecules have also been constructed. All simulation cells were equilibrated for 50-100 ps (solutions) and 100 ps (crystals) at 298 K and 1 atm, using NPT ensemble, Nose thermostat and Berendsen barostat. Ewald summation was used to calculate the electrostatic interactions. At these conditions, uniform molecular densities and constant energies have been achieved. We have found that the densities calculated for pure solvents reproduced the equivalent experimental densities with high accuracy; this further confirms suitability and robustness of the force field used.

The interaction energies have been calculated for the MD-equilibrated systems by considering three types of interaction: (i) between the tolbutamide molecule and the surrounding molecules of bulk solvent (solvent–solute), (ii) between a solvent molecule interacting with bulk solvent (solvent–solvent), and (iii) between the tolbutamide molecule interacting in its crystal lattice (solute–solute). To calculate the solvent-solute interaction, the force field total energy is calculated for the three following components/structures: (1) the MD–equilibrated box of solvent + solute, (2) the box containing only solvent molecules, with a cavity left after removal of the tolbutamide molecule, and (3) the removed solute molecule in its constrained geometry. The calculated energies are temperature dependent, thus the interaction energies are referred here as interaction enthalpies and have been computed according to Equation (7) and Figure 3:

$$\Delta H_{\text{interact}} = E_{(1)} - (E_{(2)} + E_{(3)}) \quad (7)$$

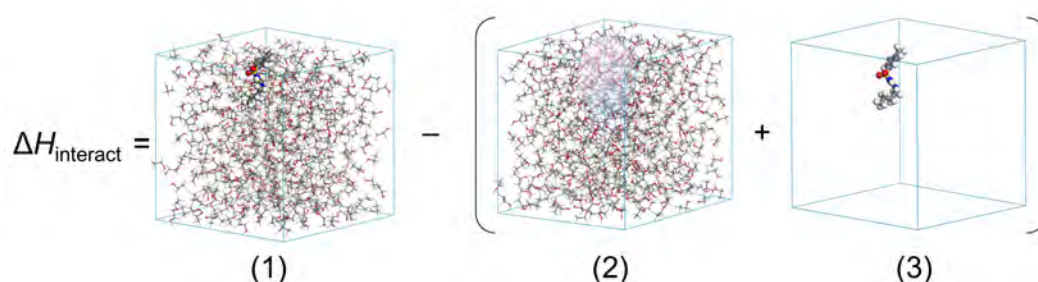


**Figure 3: A method for quantifying interaction enthalpy in MD-equilibrated solution between a solute molecule and bulk solvent.**

The solvent-solvent interaction enthalpies are calculated in a similar manner by considering an MD-equilibrated box of pure solvent as (1) and the extracted solvent molecule as (3). To quantify the solute-solute interactions, an MD-equilibrated box of the tolbutamide crystal has been used. The solvent–solute, and solvent-solvent interaction enthalpies are shown as mean values ( $n=5$ )  $\pm$  standard deviation (SD), by calculating energies for structures equilibrated at 5 ps time intervals over the last 20 ps

of simulation. The solute–solute interactions are quantified by calculating interaction enthalpies for two random molecules at five time intervals, giving mean values for 10 configurations ( $n=10 \pm \text{SD}$ ).

Conformational analysis of the tolbutamide molecule has been carried out at the DFT B97-D3/6-31G(d,p)//B2PLYP-D3/def2-QZVP level (gas-phase, 0K), with energy barriers to rotation calculated for five rotational centres (single bonds) of the solute molecule, denoted as R1-R5. A relaxed potential energy surface (PES) scan over  $360^\circ$ , with the step interval of  $5^\circ$ , has been performed for the respective dihedral angles. Six new conformers were identified and their stabilities have been compared relative to the relaxed crystal-like conformation of form II. Calculations were performed using the GAUSSIAN 09 package,<sup>24</sup> and the electrostatic potential maps were generated with the MOLEKEL 5.4 software.<sup>R9</sup>

## 3 Results & Discussion

### 3.1 Solubility

The solubilities of tolbutamide metastable form I<sup>L</sup> were determined for each combination of solvent and  $T_{cry}$  used in the induction time experiments (see Table 2). At the low temperatures and small temperature ranges for which solubilities were measured, the solubilities are highly linear (Figure 4), which is not unusual far from the melting point. Solubilities in ethanol at similar temperatures were also measured to allow some comparison to published solubility data for this solvent.<sup>17</sup> Using a van't Hoff plot (Figure 5), our solubility data for ethanol seems to be somewhat higher than expected from the literature data, though it is well within the possible deviations from linearity.<sup>22</sup>

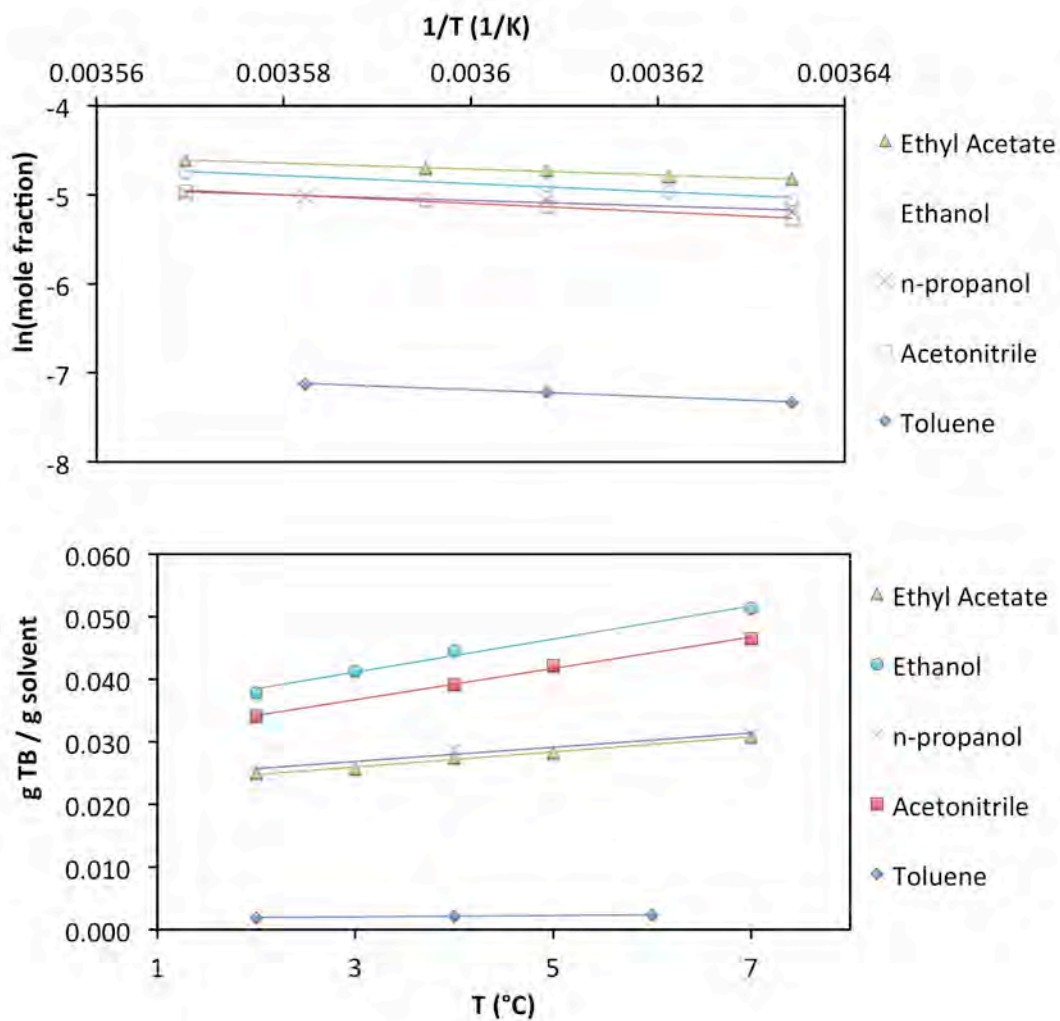


Figure 4: Tolbutamide form I<sup>L</sup> solubilities in various solvents as g/g (bottom) and van't Hoff (top). Lines are guides for the eye only.

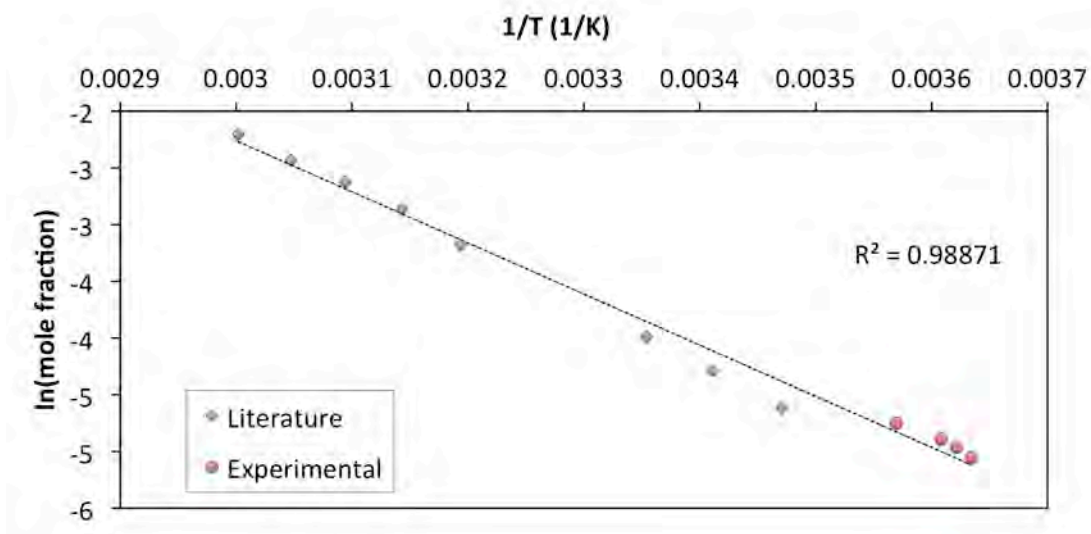
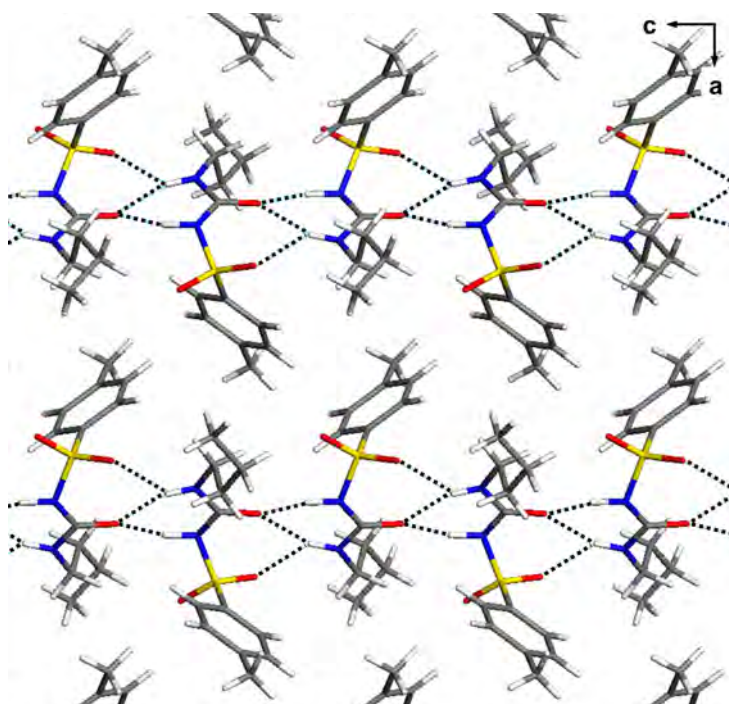


Figure 5: Van't Hoff plot of ethanol solubility compared with literature values.<sup>17</sup>

Tolbutamide is a highly polar molecule with two strongly positive protons liable to be donated to form hydrogen bonds, as well as three highly negative oxygens capable of receiving such protons. The crystal structure of form I<sup>L</sup> has also been analysed.<sup>17</sup> The molecules form chains in the Form I<sup>L</sup> crystal (see Figure 6), where each molecule is held in place by six hydrogen bonds perpendicular to the chain. Thus, tolbutamide form I<sup>L</sup> could be quite dependent on the hydrogen bonding ability of a solvent in order to be dissolved.



**Figure 6: Molecular packing in unit cell of tolbutamide crystal (form I<sup>L</sup>, ref. code ZZZPUS04). H-bonds shown as black dots.**

All utilised solvents are capable of accepting a hydrogen bond, though the  $\pi$ -electron system of toluene's aromatic ring can only act as a weak hydrogen bond acceptor<sup>25</sup>. Ethyl acetate and toluene are incapable of hydrogen bond donation, while the alcohols can both donate and accept. Hence, neither ethyl acetate nor toluene can hydrogen bond internally, which may indicate that they have weaker solvent-solvent interaction than the alcohols. However, it also implies that hydrogen bonding with molecules that both donate and accept hydrogen bonds, such as tolbutamide, would be weaker. Though toluene is the weakest in terms of hydrogen bonding, it is the only solvent that has an aromatic ring. Since tolbutamide has aromatic rings, this may help toluene in terms of "like dissolves like". Among the solvents, ethyl acetate has a unique similarity to tolbutamide, in that its polar group is in the centre, surrounded by non-polar regions. The only difference between the alcohols is the length of the aliphatic chain, whereby a longer chain decreases the solvent's polarity.

The solubility decreases in the order ethyl acetate > ethanol > n-propanol > acetonitrile >> toluene, where tolbutamide is the most soluble in ethyl acetate and by far the least in toluene. That ethyl acetate exhibits the greatest solubility appears to suggest that ethyl acetate's structural similarity to tolbutamide previously outlined is more significant than the alcohols' greater ability to form hydrogen bonds with tolbutamide, at least when offset against the alcohols' greater solvent-solvent interaction due to their internal hydrogen bonding ability. The decreasing solubility of the alcohols with increasing alkyl chain length is as expected, since the alkyl chain decreases polarity. Toluene, the only non-polar solvent, is almost an entire order of magnitude less soluble. Most likely

its inability to create strong hydrogen bonds renders it incapable of competing with tolbutamide's strong internal bonding.

### 3.2 Induction Times and Interfacial Energies

Induction times were recorded at a combination of different  $S$  and  $T_{cry}$  for four different organic solvents (n-propanol, acetonitrile, ethyl acetate and toluene, Figure 7).

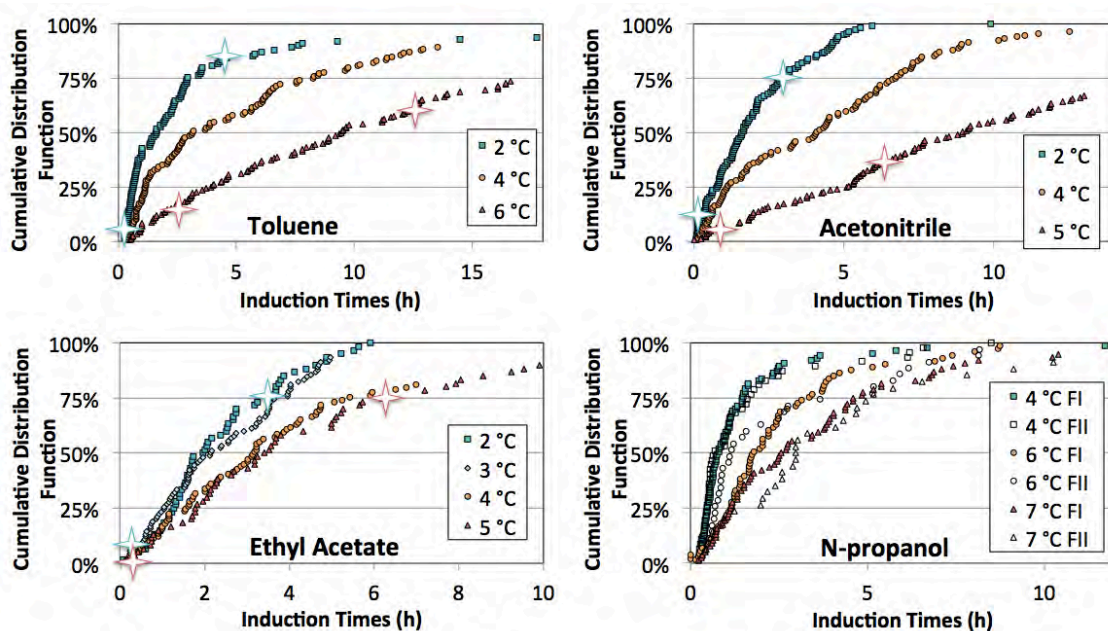


Figure 7: Induction time distributions of tolbutamide in different solvents. Temperatures are  $T_{cry}$  and stars indicate sampling of slurry for PXRD analysis, which always gave a form  $I^L$  diffraction pattern.

Appendix B – Paper Draft: Tolbutamide nucleation dependence on solvent

**Table 2: Solutions and induction time results. # expts is the number of induction times recorded and  $S = c/c^*$ , where  $c$  is the actual concentration of tolbutamide, and  $c^*$  the equilibrium concentration (i.e. solubility) at  $T_{cry}$ .**

Solvent	$c$ (g tolbutamide / g solvent)	$T_{cry}$ (°C)	$c^*$ (Form I <sup>l</sup> )	$S$	$RT \ln S$ (kJ/mol)	# expts	median $t_{ind}$ (h)
<b>Toluene</b>	0.0050	2	0.0019	2.60	2.19	104	1.60
		4	0.0022	2.33	1.95	130	3.15
		6	0.0024	2.12	1.74	106	9.45
<b>Acetonitrile</b>	0.0534	2	0.0341	1.57	1.03	118	1.62
		4	0.0391	1.36	0.72	113	4.08
		5	0.0422	1.27	0.55	97	8.97
<b>Ethyl Acetate</b>	0.0471	2	0.0250	1.89	1.45	60	1.97
		3	0.0257	1.83	1.39	84	2.15
		4	0.0275	1.71	1.24	72	3.15
		5	0.0282	1.67	1.18	60	3.42
<b>n-propanol (Form I<sup>l</sup> only)</b>	0.0655	4	0.0288	2.27	1.89	87	0.78
		6	0.0302	2.17	1.80	73	1.78
		7	0.0312	2.10	1.73	76	2.55
<b>Ethanol</b>		2	0.0379				
		3	0.0413				
		4	0.0446				
		7	0.0514				

The medians of the lognormal fits are plotted against the thermodynamic driving force of nucleation,  $RT_{cry} \ln S$ ,<sup>8</sup> in Figure 8.

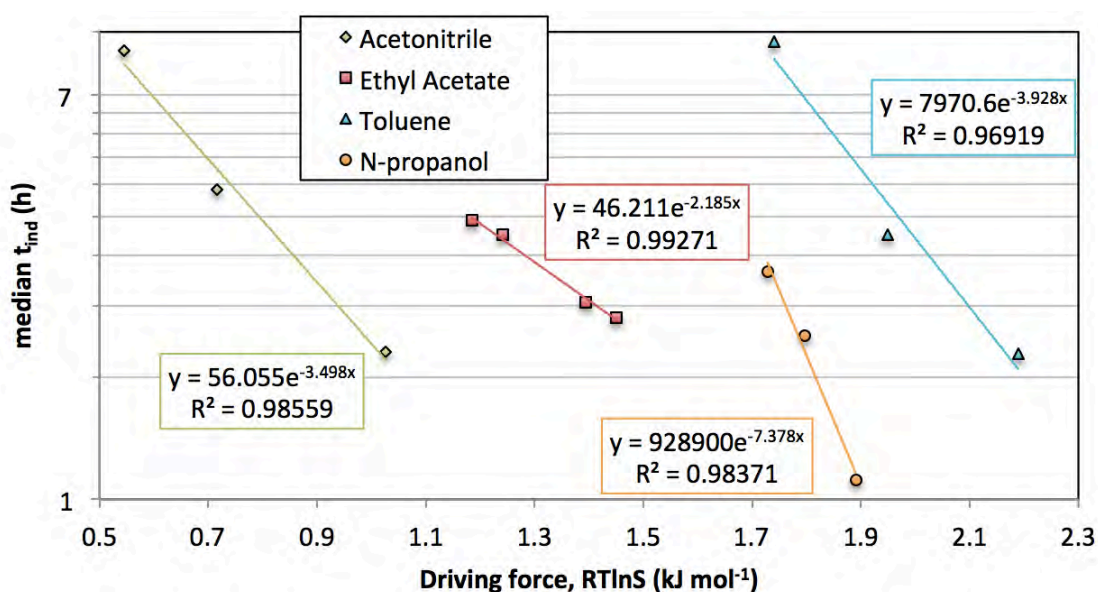


Figure 8: The relationship between median induction time and thermodynamic driving force of nucleation of tolbutamide in different solvents. Lines are exponential fits.

$t_{ind}$  seems to exponentially decay with increasing driving force. From this plot an approximate order of ease of nucleation can be established without assuming a particular theory of nucleation. However, this order is only valid at the examined  $RT\ln S$  (extrapolation of exponential fits suggests this order changes at higher and lower  $RT\ln S$ , especially reversing the order between n-propanol and toluene). Comparing similar  $t_{ind}$  values, acetonitrile clearly requires the lowest thermodynamic driving force for nucleation, followed by ethyl acetate, n-propanol, and finally toluene as requiring the highest driving force.

For further evaluation, the results are plotted according to the CNT by combining equations (1) and (3):

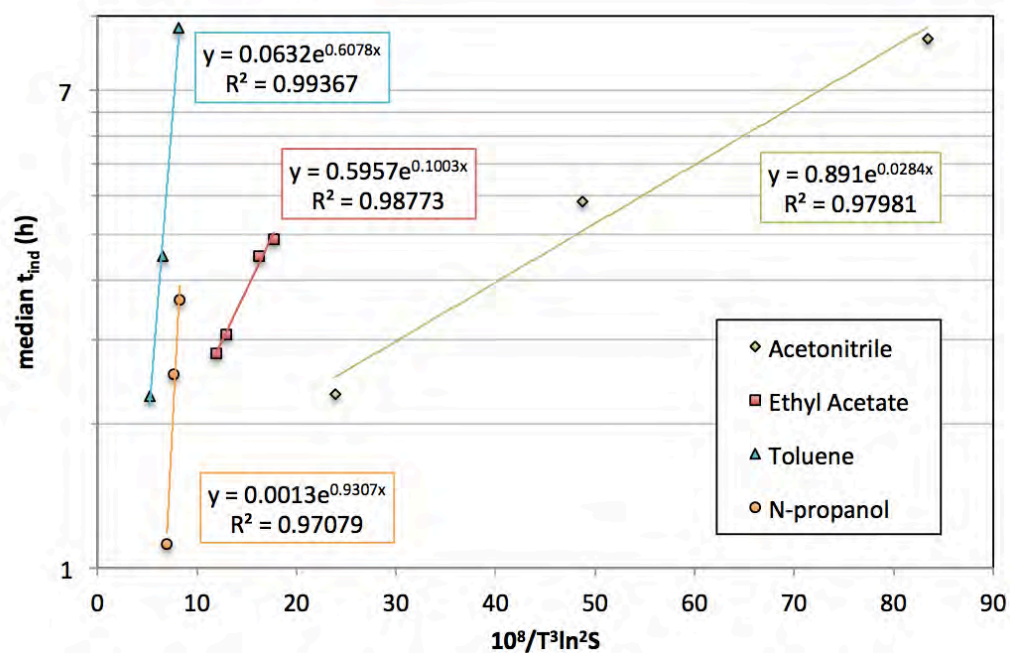


Figure 9: The relationship between  $T_{cry}$ ,  $S$  and  $t_{ind}$  plotted according to the Classical Nucleation Theory. Lines are exponential fits from which  $A$  and  $\gamma$  in Table 3 are calculated according to Equations (1) and (3).

From this,  $\gamma_{eff}$  was calculated for each solvent (Table 3). Although  $\gamma_{eff}$  is technically temperature-dependent,<sup>8</sup> the variation in  $T_{cry}$  is quite low ( $\sim 5$  K), and more importantly, the ability of the CNT to account for the data (as evidenced by the high  $R^2$  values in Figure 9) suggests the effect of  $T_{cry}$  on  $\gamma_{eff}$  is negligible under the narrow investigated temperature range. A negligible variance in  $\gamma_{eff}$  over temperature ranges of 65 °C have been reported.<sup>26</sup> The absolute values of  $\gamma_{eff}$  are the same order of magnitude as similar studies for similar compounds.<sup>9, 10, 27</sup>

Table 3: Calculated parameters of the CNT for form I<sup>L</sup> according to equations (1), (2) and (3).

Solvent	$\gamma$ (mJ m <sup>-2</sup> )	$A$ (m <sup>-3</sup> s <sup>-1</sup> )	$\Delta G^*$ (kJ mol <sup>-1</sup> )	$n^*$
Toluene	3.46	0.88	7.29	6.7
			9.20	9.4
			11.54	13.3
Acetonitrile	1.25	12.38	1.55	3.0
			3.19	8.9
			5.48	20.1
Ethyl Acetate	1.90	8.27	2.74	3.8
			3.74	6.0
			4.11	6.9
n-propanol (Form I <sup>L</sup> only)	3.99	0.02	14.97	15.8
			16.57	18.4
			17.90	20.7

As can be seen from their slopes in Figure 9,  $\gamma_{eff}$  of n-propanol and toluene are not sufficiently different to be distinguished. As expected, the order of  $\gamma_{eff}$  inversely follows the general order of ease of nucleation from Figure 8, and is [n-propanol & toluene] > ethyl acetate > acetonitrile.

Quantitatively,  $\gamma_{eff}$  does not seem to follow the trend often observed and also predicted by regular solution theory<sup>8</sup> of being inversely proportional to solubility (Figure 10). In particular, n-propanol's  $\gamma_{eff}$  is surprisingly high, even higher than that of the almost insoluble toluene. However, we found some correlation with solvent boiling point, which has been observed, though more strongly, for other molecules.<sup>9</sup> Since boiling point is indicative of the strength of solvent-solvent interaction, this suggests the interfacial barrier is related more to such solvent-solvent interactions than to solvent-solute interactions or a combination of both.

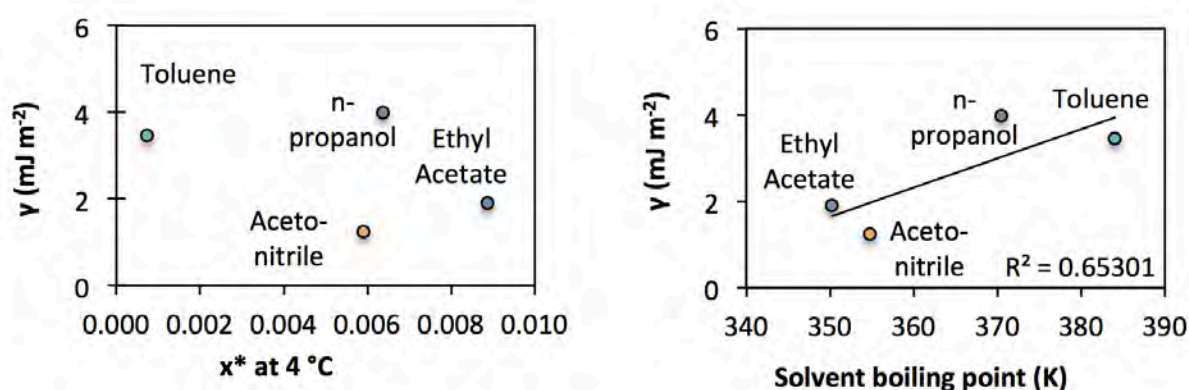


Figure 10: Interfacial energy correlated with solubility (left) and solvent boiling point (right). Line is a straight line fit for direct proportionality.

$\gamma$  and  $A$  were found to be inversely proportional (Figure 11).

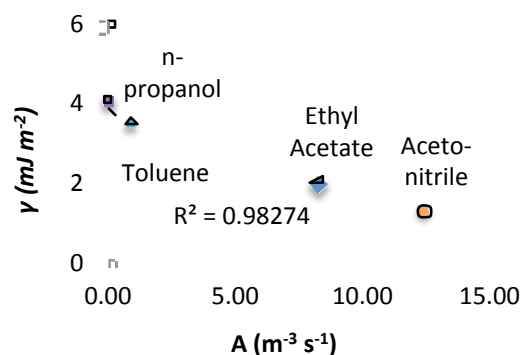


Figure 11: The relationship between  $\gamma$  and  $A$ .

### 3.3 IR Spectroscopy

Solid state IR spectra of three solid forms in comparison with solution IR spectra are shown in Figure 12 in the selected region. The carbonyl region ( $1720\text{-}1640 \text{ cm}^{-1}$ ) in the solid forms shows two peaks, and the peak in  $1560\text{-}1520 \text{ cm}^{-1}$  is attributed to the N-H functional group. The crystal structures of forms I<sup>L</sup>, II and III (ZZZPUS04 to 06) show complex carbonyl interactions. Each of the crystal structures show multiple interactions of carbonyl with the N-H site and the bond length varies in such multiple interactions. Also the vicinal  $\text{SO}_2$  group influences the carbonyl interactions and this could be the region for these multiple carbonyl peaks.

Solution state IR spectra in n-propanol shows predominantly one carbonyl peak at  $1703 \text{ cm}^{-1}$  and a tiny shoulder at around  $1725 \text{ cm}^{-1}$ . There was no clear effect of concentration changes in this carbonyl peak and this suggests that the carbonyl peak is most likely due to the solvent-solute interaction. The dilute solutions in acetonitrile and ethyl acetate shows only one carbonyl peak at  $1718 \text{ cm}^{-1}$ , and as the concentration rises the shoulder at lower wavenumber grows. The rise in the carbonyl peak at lower wavenumber is relatively rapid in acetonitrile compared to ethyl acetate. This indicates that with increase in concentration the solvated species of tolbutamide tend to aggregate more readily in acetonitrile and also in ethyl acetate. The carbonyl region in toluene solutions is similar to solid forms, although the two carbonyl peaks are shifted to higher wavenumbers. The solubility of tolbutamide in toluene is relatively less and that is why the solution spectra show more noise in comparison to other solution spectra. The solution spectra from toluene indicate that the carbonyl group is not as well solvated by toluene.

From the solution spectroscopy, it is clear that the carbonyl site of tolbutamide is strongly solvated in n-propanol. The dilute solutions in acetonitrile and ethyl acetate show solvated carbonyl species which tend to aggregate with increase in concentration and the growth of the new peak suggests solute-solute interactions at higher concentration. In the case of toluene even the dilute solutions show solvent-solute as

well as some solute-solute aggregation, and with increase in concentration the solute-solute aggregation increases rapidly. Table 4 shows carbonyl frequencies observed in different solutions.

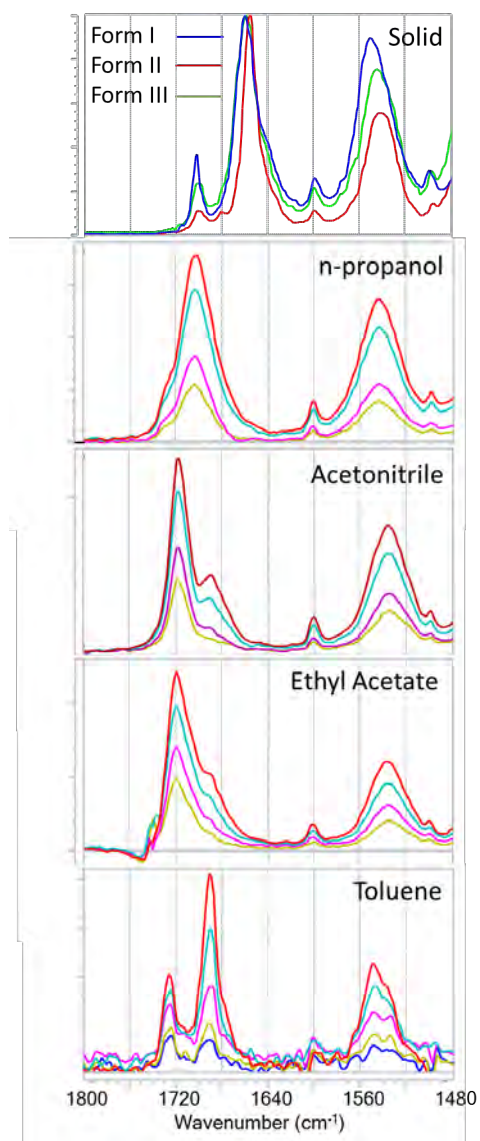


**Figure 12: IR spectroscopy showing carbonyl and N-H related region in the three solid forms of tolbutamide in comparison with the solution spectra for different concentrations. Solvent spectra are subtracted from the solution spectra.**

**Table 4: Frequency for the carbonyl peak from IR spectroscopy.**

Samples	Amide I, $\text{cm}^{-1}$	
Solid, Form I	1702(s)	1660(vs)
n-propanol	1730(sh)	1703(vs)
Acetonitrile	1717 (vs)	1689(sh)
Ethyl acetate	1719(vs)	1690-1689(sh)
Toluene	1726-1724(s)	1690-1689(vs)

### 3.4 Solution Calorimetry

Experimentally determined  $\Delta H_{\text{solution}}$  relates to dissolution of only a small quantity of solid in a large quantity of solvent and the values can be interpreted as essentially being close to infinite dilution values,  $\Delta H_{\text{solution}}^{\infty}$ . Table 5 shows various thermodynamic quantities obtained from calorimetric work.

**Table 5: Enthalpies of solution, solvation, cavity, and interaction at 25°C.**

Solvent	$\Delta H_{\text{solution}}$ ( $\text{kJ mol}^{-1}$ )	$\Delta H_{\text{solvation}}$ ( $\text{kJ mol}^{-1}$ )	SPT approach		Alternative approach	
			$\Delta H_{\text{cavity}}$ ( $\text{kJ mol}^{-1}$ )	$\Delta H_{\text{interaction}}$ ( $\text{kJ mol}^{-1}$ )	$\Delta H_{\text{cavity}}$ ( $\text{kJ mol}^{-1}$ )	$\Delta H_{\text{interaction}}$ ( $\text{kJ mol}^{-1}$ )
<b>n-propanol</b>	$31.175 \pm 0.036$	-132.1	86.2	-216.5	197.3	-327.6
<b>Acetonitrile</b>	$29.755 \pm 0.052$	-133.5	104.9	-236.9	177.9	-309.9
<b>Ethyl Acetate</b>	$25.220 \pm 0.010$	-138.0	93.1	-229.7	129.0	-265.6
<b>Toluene</b>	$32.942 \pm 0.159$	-130.3	77.7	-206.3	133.5	-262.2

The cavity formation was estimated from the two different methods and this allowed obtaining two values for  $\Delta H_{\text{interaction}}$ . It must be noted here that when deriving solvent-solute interaction values from calorimetry data using estimated cavity formation, it is the order between solvents that is important more than the absolute values. A major discrepancy was observed for n-propanol. Otherwise both methods agree that the exothermic solvent-solute interaction increases in the order of toluene < ethyl acetate < acetonitrile. The  $\Delta H_{\text{interaction}}$  obtained here can also be compared with MD calculated solvent-solute interaction (Figure 13 a and b). Again, n-propanol seems to be the biggest discrepancy here. As mentioned earlier in the experimental section, the SPT approach may not be appropriate with a solvent system that involves strong, directional interactions with itself as well as with the solute. This is because in this condition the additivity of the cavity formation is inappropriate. Henceforth, the values from the alternative approach will be used for further discussion and correlation purposes.

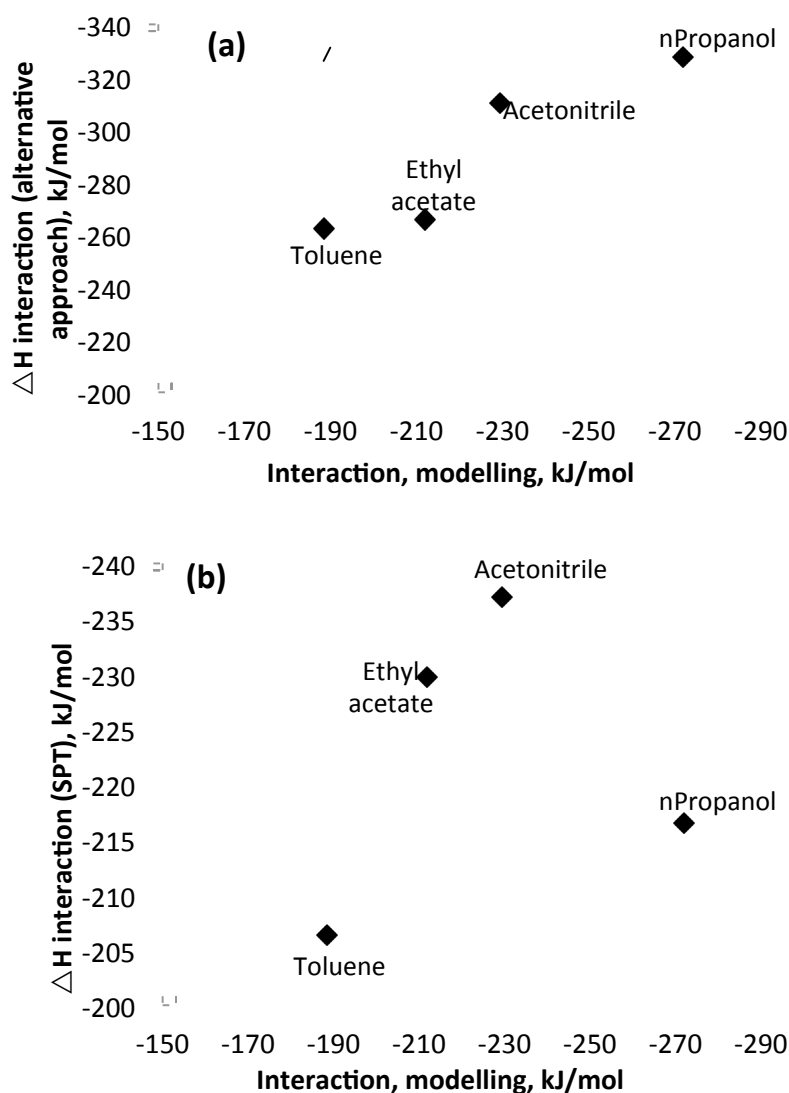
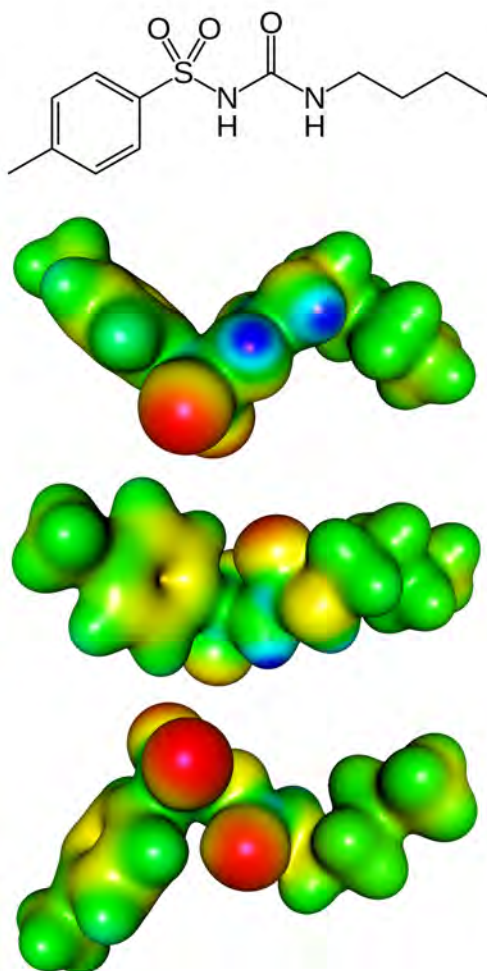


Figure 13: Comparison of solvent-solute interaction obtained from MD calculation with the same derived from calorimetry data using (a) the alternative approach and (b) the SPT approach.

### 3.5 Computational

A tolbutamide molecule has an amphiphilic character. This is clearly indicated by the distribution of the electrostatic potential (Figure 14). The centre of the molecule features a sulfonylurea unit that combines two sulfone oxygens and one carbonyl oxygen, being negatively charged (red colour), and two amide hydrogens being positively charged (blue colour). These five atoms are easily accessible for H-bonding and as is shown in Figure 6, a single tolbutamide molecule in the crystal lattice of form I<sup>L</sup> creates six intermolecular H-bonds. On the other hand, the sides of the molecule, i.e. the toluene and the n-butane end-groups have predominantly hydrophobic character, and thus are expected to yield much weaker intermolecular interactions.



**Figure 14: The electrostatic potential maps of the tolbutamide form II (three different projections) (red – negative, yellow – weakly negative, blue – positive, and green – neutral potential).**

The tolbutamide molecule adopts different conformations in each of its three known polymorphs. Form I<sup>L</sup> and form III feature U-shaped conformations, being stabilised by intramolecular binding of the benzene ring  $\pi$ -electrons and aliphatic hydrogens. On the other hand, the form II crystal structure is created by a Z-shaped conformation (Figure 15). Interestingly, when we consider the three different conformations as single molecules in isolation (gas-phase) and allow for their full relaxation, it appears that the most stable is the Z-shaped conformation of F II. This suggests that the mentioned stabilization through benzene ring  $\pi$ -electrons in the U-shaped conformations is overcome by an energetic penalty due to unfavourable geometry and non-optimum distances between atoms.

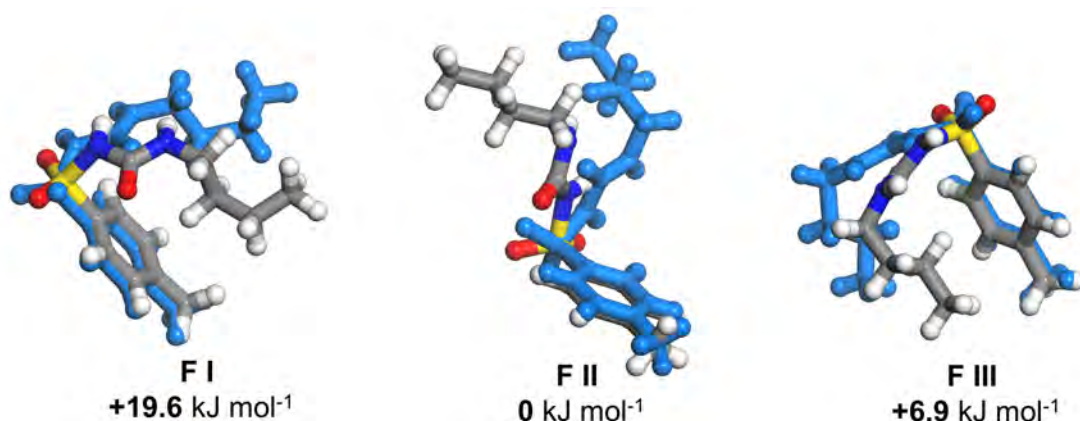


**Figure 15: Relative stability of different tolbutamide conformations constituting the respective crystal forms of F I<sup>L</sup>, F II, and F III, after optimisation in vacuum. Non-optimised crystal lattice geometries (in blue) shown for comparison. Calculations performed at B97-D3/ 6-31++G(3df,2p) (geometry) and B2PLYP-D3/def2-QZVP (energy).**

We chose the most stable Z-like conformation of tolbutamide as a starting geometry in our MD simulations and have placed one solute molecule in a periodic box filled with solvent molecules. With this approach, we were able to emulate diluted solutions and gain molecular level insights into energetics and conformational changes of tolbutamide in the different solvents. For the four respective solvents we have calculated the interaction enthalpy of the tolbutamide molecule in equilibrium with bulk solvent (solute-solvent interaction). In addition, we have quantified interaction enthalpy of a solvent molecule in equilibrium with bulk solvent (solvent-solvent), and interaction enthalpy of the tolbutamide molecule in crystal lattice of form I and form II (solute-solute) (Table 6).

Table 6: Interaction enthalpies at 298 K (in kJ mol<sup>-1</sup> ± SD) of a tolbutamide molecule in bulk solvent (solute-solvent), a solvent molecule interacting with bulk solvent (solvent-solvent), and a tolbutamide molecule interacting within the crystal lattice of form I and form II (solute-solute). Simulation boxes were equilibrated for 100 ps at 298 K using a COMPASS II force field.

Interaction type	Tolbutamide crystal	n-Propanol	Acetonitrile	Ethyl acetate	Toluene
Solute–solvent (kJ mol <sup>-1</sup> )	–	<b>-272.0 ± 20.6</b>	<b>-229.3 ± 15.7</b>	<b>-211.9 ± 17.7</b>	<b>-188.4 ± 5.1</b>
Solvent–solvent (kJ mol <sup>-1</sup> )	–	<b>-87.7 ± 4.5</b>	<b>-62.7 ± 4.2</b>	<b>-67.8 ± 6.4</b>	<b>-70.7 ± 8.0</b>
Solvent–solvent normalised <sup>b</sup> (kJ mol <sup>-1</sup> )	–	<b>-197.3</b>	<b>-177.9</b>	<b>-129.0</b>	<b>-133.5</b>
Solute–solute (F I <sup>L</sup> ) (kJ mol <sup>-1</sup> )	<b>-387.6 ± 14.8</b> (1.270 ± 0.003) <sup>a</sup>	–	–	–	–
Solute–solute (F II) (kJ mol <sup>-1</sup> )	<b>-375.3 ± 16.6</b> (1.237 ± 0.003) <sup>a</sup>	–	–	–	–

<sup>a</sup> Density (g cm<sup>-3</sup>) at 298 K calculated for the MD-equilibrated models

<sup>b</sup> Normalised by considering accessible solvent surface area equivalent to the surface area of the tolbutamide molecule

The solute-solvent interaction enthalpies resulting from our MD simulations range from -272 kJ mol<sup>-1</sup> in n-propanol to -188 kJ mol<sup>-1</sup> in toluene and decrease in the order n-propanol > acetonitrile > ethyl acetate > toluene. If comparing the strength of the intermolecular binding within the form I<sup>L</sup> and II crystals (solute-solute interaction), it appears that the cohesive strength in the tolbutamide crystal is higher by ca. 12 kJ mol<sup>-1</sup> for the F I<sup>L</sup> polymorph with  $\Delta H_{\text{solute-solute}} = -387.6$  kJ mol<sup>-1</sup>. From the comparison of the solute-solute and the solute-solvent interaction values, it appears that the net energy gain due to complete desolvation of one tolbutamide molecule, i.e. breaking the solute-solvent bonding and subsequent establishing an ideal solute-solute bonding as in tolbutamide crystal form I<sup>L</sup>, is quite substantial and depends on the solvent, increasing in the order 116 kJ mol<sup>-1</sup> (n-propanol) < 158.3 kJ mol<sup>-1</sup> (acetonitrile) < 175.7 kJ mol<sup>-1</sup> (ethyl acetate) < 199 kJ mol<sup>-1</sup> (toluene). The higher energy gain suggests that the formation of tolbutamide crystal-like particles (nuclei) would be energetically more favourable in toluene than in the other solvents, being the least favourable in n-propanol.

To assess energy barriers to rotation and the relative stability of any resulting conformations, we have done conformational analysis of the tolbutamide molecule by employing high-level quantum-chemical calculations. This level of theory is computationally very demanding, therefore we limited our simulations to a single tolbutamide molecule in isolation (gas-phase) and have considered five rotational centres over the sulfonylurea unit of the molecule (Figure 16). By performing potential energy scans over the respective single bonds we have identified a number of new conformers (local energy minima) being separated from the initial crystal F II conformation by energy barriers (energy maxima) of 21–72 kJ mol<sup>-1</sup>. These barriers are substantially larger than those for risperidone (10–26 kJ mol<sup>-1</sup>). A full (360°) scan over the rotational centre R1 yields an energy barrier of 22.5 kJ mol<sup>-1</sup> and results in the same conformation as the starting tolbutamide geometry (Figure 16a). The potential energy

landscape is much more complex when considering the R2 centre of rotation. Here we observe a three-step interconversion over the 360° scan, with three energy barriers and two intermediate conformations. In the other cases (rotations over R3-R5 centres) we observe only one barrier and one new conformational minimum, all being different from the starting form II conformation. The first intermediate conformer resulting from the R2 rotation (Figure 16b) and another conformer from the rotation over the R5 centre (Figure 16e), are both U-shaped, similar to the conformers present in the form I<sup>L</sup> and form III polymorphs (cf. Figure 14). Interestingly three of the new conformers are substantially different from their crystal counterparts as they feature intramolecular H-bonding between the sulfonyl oxygen and the amide hydrogen (S=O···H-N) (cf. Fig. 14 (b) and (c)). They are energetically more stable by 4–14 kJ mol<sup>-1</sup> compared to the crystal-like F II conformation.

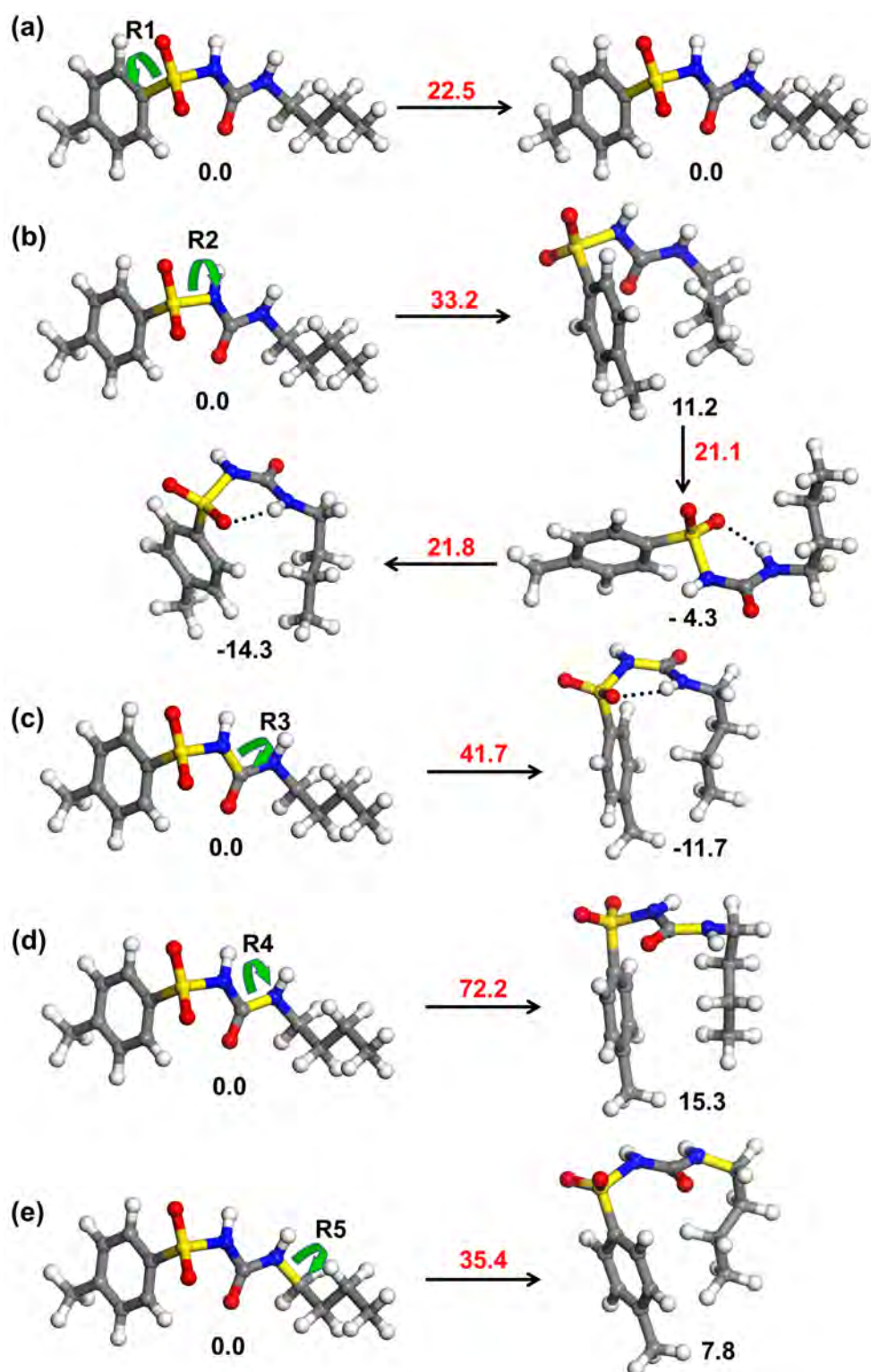
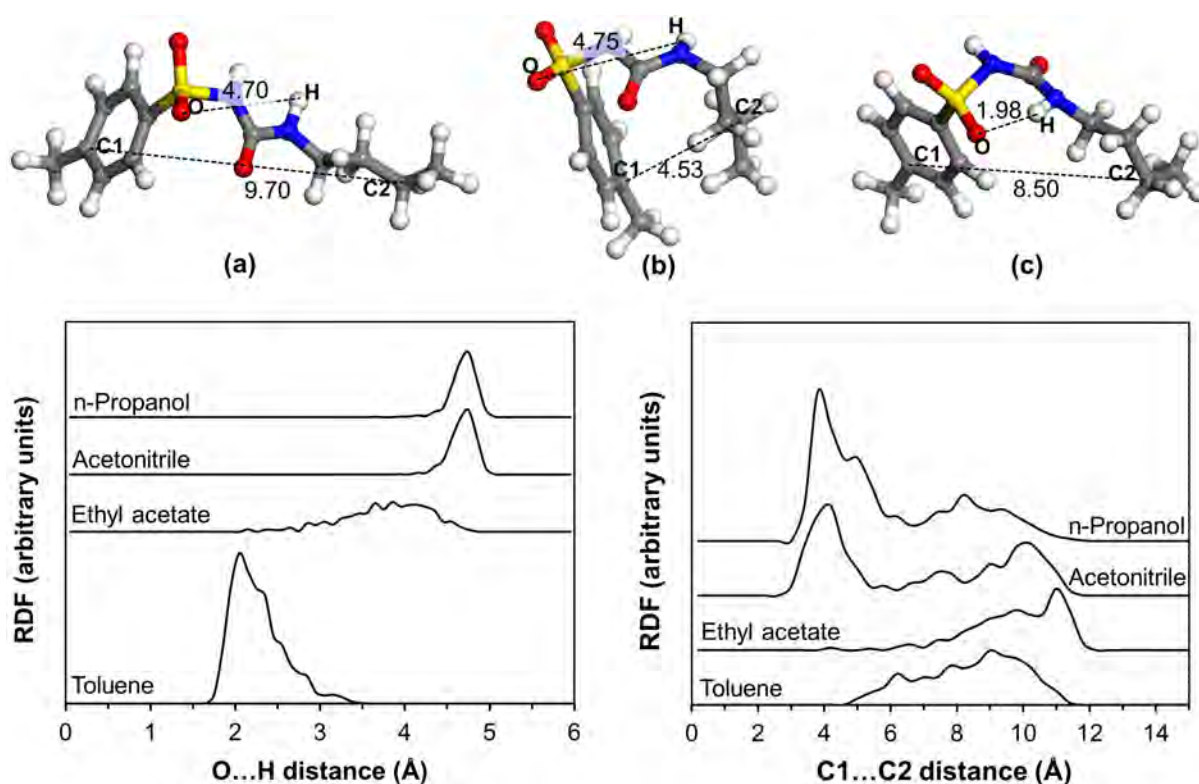


Figure 16: Energy barriers to rotation (kJ mol<sup>-1</sup>, red numbers) in the gas-phase for five rotational centres R1-R5 (single bonds highlighted in yellow) of the tolbutamide molecule. The new conformers (local energy minima) resulting from the rotation, with their relative energies (kJ mol<sup>-1</sup>, black numbers) calculated as a difference between the conformer energy and the relaxed

conformation of the tolbutamide form II. Calculations performed at B97-D3/6-31G(d,p) (geometry) and B2PLYP-D3/def2-QZVP (energy).

The conformational analysis presented above predicts a range of alternative conformations of tolbutamide, from which the most intriguing is the prediction of the intramolecularly H-bonded conformations, being also energetically favourable over the known crystal-like equivalents. The gas-phase DFT calculations do not account for interactions with solvent. To overcome this limitation we have employed MD simulations to investigate if the solvent can induce/mediate conformational changes of the tolbutamide molecule.



**Figure 17: MD-derived representative conformations of tolbutamide in n-propanol (a and b), and in toluene (c). Radial distribution function (RDF) plots illustrate how different solvents influence conformational changes as reflected by fluctuations of selected interatomic pair distances: sulfone oxygen – amide hydrogen (O...H) and carbon – carbon (C1...C2). MD simulations performed with COMPASS II force field at 298 K for ca. 1 ns; distances in angstroms.**

Figure 17 shows the radial distribution functions (RDF) for two pair distances: (1) O...H, which reflects the propensity for formation of intramolecular H-bonding, and (2) C1...C2, which indicates the extent of the U-shape-like bending in the tolbutamide molecule. The results show that the different solvents indeed influence conformational changes, as the probability for a particular interatomic pair distance, which is related to a certain geometrical feature, strongly depends on the solvent environment. Three types

of conformers are derived from the MD simulations: (1) linear (Z-shaped), (2) U-shaped, and (3) intramolecularly H-bonded. These are shown along with their relevant interatomic distances in Figure 17 (a), (b) and (c), respectively. The RDFs in n-propanol and acetonitrile are quite similar for both the pair distances with clear maxima at ca. 4.75 Å for the O...H pair. The distribution of the C1...C2 pair distances in n-propanol features a clear maximum at ca. 4 Å and broad lower intensity band spanning 7-11 Å; this suggests predominance of the U-shaped conformation as in Figure 17 (b), but also the presence of linear conformations being similar to that in Figure 17 (a). In acetonitrile there are also both the U-shaped and the linear conformations; however, the former seems to be less pronounced than in n-propanol. The distribution of the O...H and C1...C2 distances in ethyl acetate suggests predominance of the linear to subtly bent type of tolbutamide conformers. It appears that the O...H distance of ca. 2 Å, being associated with the intramolecular H-bond is pronounced only in toluene (cf. Figure 17c). Regarding the C1...C2 distances, the range of 4.5-11 Å with the maximum at ca. 9 Å suggests that in toluene the intramolecularly H-bonded tolbutamide molecule would prefer to adopt a more open conformation to facilitate solvent interactions with the nonpolar parts of the solute.

### 3.6 Discussion

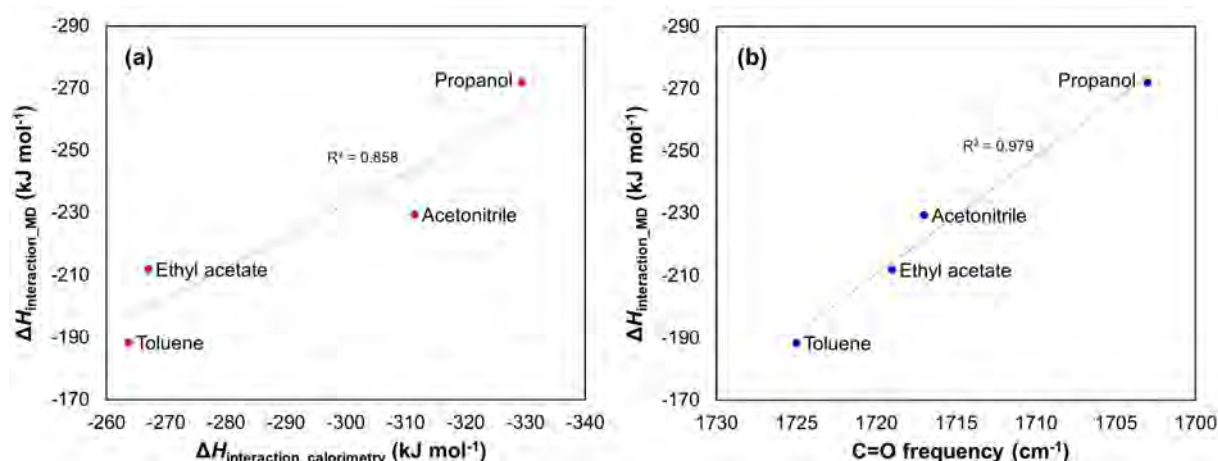


**Figure 18: The solute-solvent interaction enthalpy of tolbutamide in four different solvents calculated with MD and COMPASS II force field vs. (a) enthalpy of interaction derived from experimental enthalpy of solution and (b) FTIR frequency (cm<sup>-1</sup>) of the tolbutamide carbonyl band in diluted solutions of the respective solvents.**

The solvent-solute interaction energies from the molecular dynamics modelling should correlate with the calorimetrically-derived enthalpies of interaction, and the correlation is indeed quite strong (Figure 18a). Furthermore, in the IR spectra the position of the carbonyl stretching peak reflects the strength in the solute-solvent binding and thus should correlate with both calorimetric and MD solvent-solute interactions, which is also the case (Figure 18b, shown only for MD interactions). Finally, spectroscopic, calorimetric and modelled values of solvent-solute interactions all agree on the order of solvent-solute interaction strength (Table 7). This gives evidence of the validity of all three methods as measurements for the strength of the solvent-solute interactions.

**Table 7: Solvents ranked (1 = lowest, 4 = highest) according to different properties. Driving force for achieving  $t_{ind} = 2$  h.**

Solvent	Solvent-Solute Interaction			Ease of Nucleation	
	<i>Calorimetric</i> $\Delta H_{interaction}$ (kJ mol <sup>-1</sup> )	<i>Spectroscopic</i> C=O frequency (cm <sup>-1</sup> )	<i>MD</i> $\Delta E_{interaction}$ (kJ mol <sup>-1</sup> )	$\gamma$ (mJ m <sup>-2</sup> )	Driving force, RTlnS (kJ/mol)
<b>Toluene</b>	1	1	1	3	4
<b>Ethyl Acetate</b>	2	2	2	2	2
<b>Acetonitrile</b>	3	3	3	1	1
<b>N-propanol</b>	4	4	4	4	3

In our previous nucleation study on salicylic acid<sup>14</sup> and risperidone<sup>15</sup> we have observed that the difficulty of nucleation is directly related to the strength of solvent-solute interaction such that the stronger solvent molecules bind to a solute molecule in solution the more difficult is the nucleation process. According to this hypothesis we could expect that nucleation of tolbutamide should follow the order of solvent-solute interaction, i.e. be the easiest in toluene, more difficult in ethyl acetate and acetonitrile and the most difficult in n-propanol. Though the nucleation of tolbutamide is indeed the most difficult in n-propanol, the second longest induction times are recorded in toluene, and the order between ethyl acetate and acetonitrile is the reverse of that expected (Table 7 and Figure 18). This clearly does not follow our proposed desolvation mechanism and suggests that in case of tolbutamide the nucleation process is more complex than that observed for salicylic acid and risperidone.

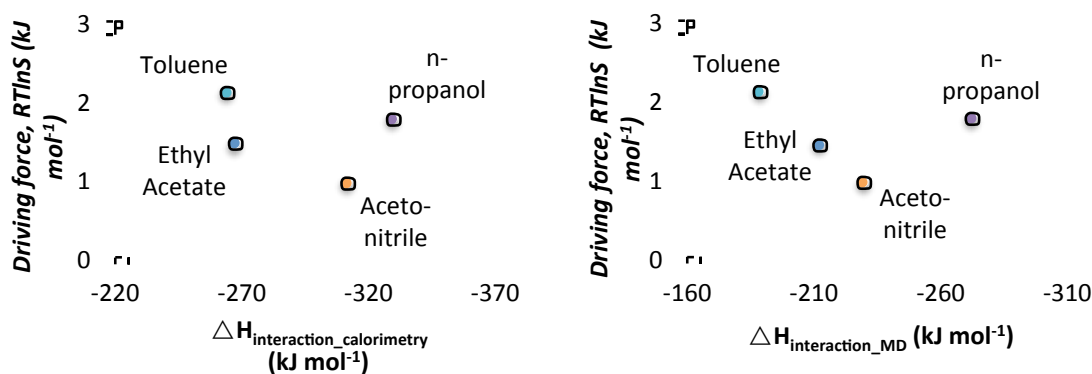


**Figure 19: Nucleation difficulty as driving force required to reach  $t_{\text{ind}} = 2$  h correlated to calorimetric (left) and molecular dynamics (right) solvent-solute interaction.**

Salicylic acid ( $M_w = 138 \text{ g mol}^{-1}$ ) is a relatively simple and rigid molecule, i.e. does not demonstrate conformational flexibility. Risperidone, on the other hand, is a much larger ( $M_w = 410 \text{ g mol}^{-1}$ ) and highly flexible molecule as indicated by calculated relatively low energy barriers (10 - 26 kJ mol<sup>-1</sup>) to interconversion between its different conformations.<sup>15</sup> These low barriers indicate a lack of kinetically stable conformations in solution that could affect the nucleation process. Indeed, in the case of risperidone we do observe, without any deviations, that the nucleation difficulty correlates to the strength of solute-solvent interaction.

Tolbutamide with  $M_w = 270 \text{ g mol}^{-1}$  is between salicylic acid and risperidone in terms of molecular mass. It can both donate and accept H-bonding, and in the crystalline phase it tends to form chains of intermolecular H-bonds, what makes it different from the other two compounds. From the tolbutamide structure (Fig. 1) it is clear that the molecule possesses a number of single bonds that can serve as rotational centres, where rotation about a single bond may lead to a different molecular conformation(s). Indeed, our molecular modelling suggests that energy barriers to rotation are significantly larger than for risperidone (21–72 kJ mol<sup>-1</sup>), which according to recent findings<sup>29</sup> is of sufficient magnitude to influence the overall nucleation process.

Thus, the spectroscopic, calorimetric and modelling investigations may offer an explanation for why tolbutamide does not follow the trend of easier nucleation with weaker solvent-solute interaction, especially keeping in mind that the evidence for the sensitivity of nucleation to the conformer population in the solution is growing.<sup>28</sup> The radial distribution functions of O-H distances calculated from the MD trajectories suggest that only in toluene does tolbutamide exist as a conformer with intra-molecular hydrogen bonding, and that all tolbutamide molecules transform to this conformer in toluene (left). This observation matches results of the DFT conformational analysis, where we have in fact predicted intramolecularly H-bonded conformations of tolbutamide. The DFT calculations also indicate that the formation of the intramolecular H-bond gives between 4 - 14 kJ mol<sup>-1</sup> of additional stabilisation to the ground-state energy of the tolbutamide molecule. In order to nucleate form I<sup>L</sup>, the tolbutamide

molecules would have to transform to the crystal-like conformer, and with the presence of intra-molecular hydrogen bonding in the conformer possibly present in toluene solutions, this transformation could be quite difficult. In fact, our conformational analysis indicate that such a transformation can be a multistage process and the energy barrier for interconversion between the non-intramolecularly-H-bonded and the intramolecularly-H-bonded conformations can be as high as 42 kJ mol<sup>-1</sup>, which according to recent findings<sup>29</sup> is of sufficient magnitude to influence the overall nucleation process. This could explain why nucleation from toluene is very difficult despite weak solvent-solute interactions.

The discrepancy in the nucleation order between acetonitrile and ethyl acetate could also be related to the presence of crystal-like and non-crystal-like conformers of tolbutamide in their respective solutions and the energy barriers associated with their interconversion. According to the order of solvent–solute interactions, ethyl acetate would be expected to yield the second easiest environment for tolbutamide nucleation. However, nucleation of tolbutamide is the easiest in acetonitrile, despite having the second highest strength of solvent-solute interactions (cf. Table 7). The radial distribution functions of the C1-C2 distances (Figure 17) suggest that in acetonitrile tolbutamide may exist as both a conformer similar to tolbutamide form I<sup>L</sup> (U-shaped), and as a linear-like molecule, similar to that of form II (a and b in Figure 17, respectively). However, in ethyl acetate tolbutamide only appears to exist as the linear conformer similar to form II (Figure 17a). Thus the nucleation of the metastable form I<sup>L</sup>, which was found to preferentially nucleate from both acetonitrile and ethyl acetate solutions under experimental conditions, would be more difficult from ethyl acetate than from acetonitrile from a conformational point of view.

Furthermore, the stronger solvent-solvent interactions in acetonitrile compared to ethyl acetate (cf. Table 6) could allow more clustering of tolbutamide molecules in acetonitrile solutions, which in turn could facilitate easier nucleation. Indeed, the spectroscopic data shows the relative height of the C=O shoulder peak, indicative of solute-solute interactions, rising more quickly with concentration in acetonitrile than in ethyl acetate (cf. Figure 12).

## 4 Conclusion

The nucleation of tolbutamide metastable form I<sup>L</sup> shows a clear dependence on the solvent choice, with nucleation becoming more difficult in the order acetonitrile < ethyl acetate < [toluene & n-propanol]. The solvent-solute interactions were characterised by solution FTIR spectroscopy, solution calorimetry and molecular dynamics simulations, and unanimously found to increase in the order toluene < ethyl acetate < acetonitrile < n-propanol. The trend of increasing nucleation difficulty with increasing interaction, which we recently found for several other organic molecules, does not describe these findings, especially for toluene, in which solvent nucleation is far more difficult than predicted by its weak solvent-solute interactions. However, solvent-dependent evidence of difference in clustering and conformational populations can provide an explanation for the deviations from the trend previously established. Our DFT conformational

analysis reveals the presence of energetically preferred non-crystal-like conformations of tolbutamide which feature an intramolecular S-O...H-N H-bond, separated by a quite large energy barrier of ca. 42 kJ mol<sup>-1</sup> from the crystal-like conformations. This finding is further corroborated by MD simulations, where we observe transformation to such intramolecularly bound tolbutamide molecule in toluene only. Our experimental nucleation data in combination with the modelling results overall suggest that in case of tolbutamide the previously observed influence of desolvation on the nucleation process is complemented by an alternative mechanism, i.e. the formation of crystal-incompatible conformers in solution, in particular, the intramolecularly H-bonded conformation of tolbutamide.

## Acknowledgements

The financial support of the Science Foundation Ireland (10/IN.1/B3038) is gratefully acknowledged. In addition, the Science Foundation Ireland (SFI) and Higher Education Authority funded Irish Centre for High End Computing (ICHEC) is acknowledged for access to computational facilities.

## Bibliography

- (1) Valder, C.; Merrifield, D., Pharmaceutical Technology. *SmithKline Beecham R&D News* **1996**, 32.
- (2) Bernstein, J., *Polymorphism in Molecular Crystals*. ed.; Oxford University Press: Oxford, 2002.
- (3) Leng, J.; Salmon, J.-B., Microfluidic crystallization. *Lab on a Chip* **2009**, 9, (1), 24-34.
- (4) Rodríguez-hornedo, N.; Murphy, D., Significance of controlling crystallization mechanisms and kinetics in pharmaceutical systems. *Journal of Pharmaceutical Sciences* **1999**, 88, (7), 651-660.
- (5) Vekilov, P. G., Nucleation. *Crystal Growth & Design* **2010**, 10, (12), 5007-5019.
- (6) Revalor, E.; Hammadi, Z.; Astier, J.-P.; Grossier, R.; Garcia, E.; Hoff, C.; Furuta, K.; Okustu, T.; Morin, R.; Veessler, S., Usual and unusual crystallization from solution. *Journal of Crystal Growth* **2010**, 312, (7), 939-946.
- (7) Ostwald, W. Z., Studies on the formation and transformation of solid compounds: Report I. Supersaturation and practicing cooling. [machine translation]. *Z. physik. Ch.* **1897**, 22, 289-330.
- (8) Mullin, J. W., *Crystallization, Fourth Edition*. ed.; Butterworth-Heinemann: 2001.
- (9) Yang, H.; Rasmuson, Å. C., Nucleation of Butyl Paraben in Different Solvents. *Crystal Growth & Design* **2013**, 13, (10), 4226-4238.
- (10) Yang, H.; Svärd, M.; Zeglinski, J.; Rasmuson, Å. C., Influence of Solvent and Solid-State Structure on Nucleation of Parabens. *Crystal Growth & Design* **2014**.
- (11) Kuhs, M.; Zeglinski, J.; Rasmuson, Å. C., Influence of History of Solution in Crystal Nucleation of Fenoxycarb: Kinetics and Mechanisms. *Crystal Growth & Design* **2014**.
- (12) Gracin, S.; Rasmuson, Å. C., Polymorphism and Crystallization of p-Aminobenzoic Acid. *Crystal Growth & Design* **2004**, 4, (5), 1013-1023.
- (13) Mealey, D.; Croker, D. M.; Rasmuson, A., Crystal nucleation of salicylic acid in organic solvents. *CrystEngComm* **2015**.

## Appendix B – Paper Draft: Tolbutamide nucleation dependence on solvent

- (14) Khamar, D.; Zeglinski, J.; Mealey, D.; Rasmuson, Å. C., Investigating the role of solvent-solute interaction in crystal nucleation of salicylic acid from organic solvents. *Journal of the American Chemical Society* **2014**.
- (15) Mealey, D.; Zeglinski, J.; Khamar, D.; Rasmuson, A., Influence of Solvent on Crystal Nucleation of Risperidone. *Faraday Discussions* **2015**.
- (16) Zeglinski, J.; Khamar, D.; Kuhs, M.; Rasmuson, A., Analysis of the structure and morphology of fenoxycarb crystals. *Journal of Molecular Graphics and Modelling* **2014**, 53, 92-99.
- (17) Thirunahari, S.; Aitipamula, S.; Chow, P. S.; Tan, R. B. H., Conformational polymorphism of tolbutamide: A structural, spectroscopic, and thermodynamic characterization of Burger's forms I–IV. *Journal of Pharmaceutical Sciences* **2010**, 99, (7), 2975-2990.
- (18) Nath, N. K.; Nangia, A., Novel form V of tolbutamide and a high Z[prime or minute] crystal structure of form III. *CrystEngComm* **2011**, 13, (1), 47-51.
- (19) Hasegawa, G.; Komasa, T.; Bando, R.; Yoshihashi, Y.; Yonemochi, E.; Fujii, K.; Uekusa, H.; Terada, K., Reevaluation of solubility of tolbutamide and polymorphic transformation from Form I to unknown crystal form. *International Journal of Pharmaceutics* **2009**, 369, (1–2), 12-18.
- (20) Thirunahari, S.; Chow, P. S.; Tan, R. B. H., Quality by Design (QbD)-Based Crystallization Process Development for the Polymorphic Drug Tolbutamide. *Crystal Growth & Design* **2011**, 11, (7), 3027-3038.
- (21) Forster, A.; Hempenstall, J.; Rades, T., Characterization of glass solutions of poorly water-soluble drugs produced by melt extrusion with hydrophilic amorphous polymers. *Journal of Pharmacy and Pharmacology* **2001**, 53, (3), 303-315.
- (22) Kuhs, M.; Svärd, M.; Rasmuson, Å. C., Thermodynamics of fenoxycarb in solution. *The Journal of Chemical Thermodynamics* **2013**, 66, (0), 50-58.
- (23) Kashchiev, D.; Rosmalen, G. M. v., Review: Nucleation in solutions revisited. *Crystal Research and Technology* **2003**, 38, (7-8), 555-574.
- (24) frisch, t. e. a., **2009**.
- (25) Reichardt, C.; Welton, T., *Solvents and Solvent Effects in Organic Chemistry*. ed.; John Wiley & Sons: 2011.
- (26) Lancia, A.; Musmarra, D.; Prisciandaro, M., Measuring induction period for calcium sulfate dihydrate precipitation. *AIChE Journal* **1999**, 45, (2), 390-397.
- (27) Kuhs, M.; Zeglinski, J.; Khamar, D.; Rasmuson, A., Solvent Effects on Nucleation Kinetics and Mechanics of Fenoxycarb. *in preparation* **2014**.
- (28) Derdour, L.; Skliar, D., A review of the effect of multiple conformers on crystallization from solution and strategies for crystallizing slow inter-converting conformers. *Chemical Engineering Science* **2014**, 106, (0), 275-292.
- (29) Derdour, L.; Pack, S. K.; Skliar, D.; Lai, C. J.; Kiang, S., Crystallization from solutions containing multiple conformers: A new modeling approach for solubility and supersaturation. *Chemical Engineering Science* **2011**, 66, (1), 88-102.

# C

## **Appendix C – Droplet Microfluidics**

# 1 Droplet Microfluidics Theory

Growing single crystals to solve protein structures through x-ray diffraction requires high-throughput crystallisation setups utilising as little of the costly and rare protein as possible (Nguyen 2002, van der Woerd *et al.* 2003, Sauter *et al.* 2007). This is traditionally performed by robotic platforms using micro wells. Such rigs are, however, far too costly for most laboratories, limiting it to those with sizeable funding sources such as large international pharmaceutical companies (Willneff *et al.* 2006).

In the past decade, microfluidics or “lab-on-a-chip” technology has become a possible low-cost alternative to robotics for high-throughput crystallization screening, as well as a platform for the study of fundamental nucleation theories (van der Woerd *et al.* 2003, Leng and Salmon 2009).

## 1.1 Microfluidics

Microfluidics is an interdisciplinary science referring to the manipulation of miniscule amounts of fluid (in general, at least one dimension being less than a millimeter) and the utilization of the unique behaviour of fluids at such scales (Nguyen 2002). Microfluidics has its origin in the miniaturization of gas chromatography equipment around 1975 (Tabeling 2005).

Besides the apparent cost-saving benefits of using less volumes for reactions (microfluidics is already able to accurately dispense discrete volumes as low as 10 pL (Teh *et al.* 2008)), the behaviour of matter at the micro scale is very different from what we perceive and work with in everyday life. Whereas at the macroscale the effects of inertia and gravity dominate, these factors play a nearly insignificant role at the microscale and are replaced in importance by such effects as diffusion, surface tension and viscosity (Atencia and Beebe 2005). For example, flow is usually laminar, leading to a nearly unparalleled control over mass and energy transfer. Also, there is a large surface area to volume ratio, allowing excessively large heat transfer rates between the system and its surroundings (Squires and Quake 2005).

Furthermore, the specific sub-set of microfluidics that this review is concerned with, droplet microfluidics, has not only been successfully applied to the study of crystallization, but also to assays (Srinivasan *et al.* 2004, Zheng *et al.* 2004) and chemical synthesis (Shestopalov *et al.* 2004).

## 1.2 Droplet Microfluidics Basics

Microfluidic technologies to study crystallization can, with some exceptions (e.g. Sanjoh and Tsukihara 1999, Leng *et al.* 2006)), be divided into two groups (Li and Ismagilov 2010). The first simply uses microfluidic tools to replace the robotic aspects of high-throughput crystallization experiments in microwells (e.g. Hansen *et al.* 2002, Thorsen *et al.* 2002)). These tools can be subdivided into complicated networks of valves, and a technology known as SlipChip (Li and Ismagilov 2010). The second creates microreactors in the form of droplets (the discrete phase) separated from each other by immiscible oil (the continuous phase). It is the latter, “droplet microfluidics”, which is reviewed here.

Furthermore, since our interest is not in protein study but studying the nucleation kinetics of organic pharmaceutical compounds, we will limit ourselves to studies relevant to this.

### 1.3 Device Material

Initially, the material that made up the microfluidic channels through which fluid was conveyed were mainly fabricated using silicon, glass and quartz via photolithography, etching and micromachining. These techniques are very costly and require highly specialized procedures and working environments. As a result, an alternative was developed in the form of soft lithography, the most common soft material used being poly(dimethylsiloxane) (PDMS) (Kim *et al.* 2009). This has the advantage of being cheap, having a simple and fast manufacturing procedure (at least comparatively, since access to the relevant workshop and expertise is still required) and being transparent (Whitesides *et al.* 2001). Most of the studies reviewed in this chapter use PDMS. However, PDMS is permeable or at least semi-permeable to gas and many liquids including water (Leng and Salmon 2009) and also swells with common organic solvents (Lee *et al.* 2003). Although water permeability is sufficiently low to allow short-term experiments, as seen in most of the studies reviewed, the swelling caused by organic solvents is of such a magnitude that droplets of organic solvents, with the exception of hexadecene, have been formed only in devices made from etched silicon (Cygan *et al.* 2005). As such, work has been done very recently to alleviate this issue. The results can be classified into two groups: Those that demonstrate soft materials (usually fluorinated polymers) without these issues (Rolland *et al.* 2004, Cygan *et al.* 2005, Begolo *et al.* 2011) and those that modify the surface of PDMS (Kim *et al.* 2009).

Another solution is using standard micro-sized tubing also made of various fluorinated polymers such as PTFE, Teflon, etc. (Dombrowski *et al.* 2007). This requires no manufacturing, as all the tubing and connectors can be ordered from numerous suppliers and can then simply be connected in the laboratory. The obvious limitation of this solution is that more elaborate lab-on-a-chip functions such as valves and complex geometries are more difficult to implement.

### 1.4 Droplet Generation

One of the main strengths of droplet microfluidics is the consistency with which it can produce droplets. Whereas traditional top-down methods of droplet-creation result in highly polydisperse droplets (Xu *et al.* 2006b), microfluidics can produce droplets with less than 2% volume dispersity (Nisisako *et al.* 2006). This is due to the laminar flow conditions prevalent in microflows, which lead to highly predictable and regular flow conditions (Thorsen *et al.* 2001). It must, however, be kept in mind, that the ability to form droplets can be greatly influenced by the ingredients of the discrete phase, which can alter the surface tensions in the system and prevent droplet formation without the addition of a surfactant (Zheng *et al.* 2003).

The simplest device to produce such droplets is the T-junction (Nisisako *et al.* 2002, Xu *et al.* 2006a). As the name implies, the continuous phase flow is intersected perpendicularly by the discrete phase flow. As the discrete phase enters the flow of the continuous phase, the shear force of the latter and the resultant pressure gradient cause

the former to elongate and stretch until it breaks off to form a discrete droplet. The factors that control the size of the droplets are the relative flow rates and viscosities of the two phases as well as the channel dimensions. A recent paper developed a simple formula for *a priori* prediction of droplet size via these factors (van Steijn *et al.* 2010).

The other major microfluidic method of creating monodisperse droplets is flow-focusing (Anna *et al.* 2003, Yobas *et al.* 2006). In this case, both the continuous and the discrete phase are forced through a narrow region *together*. Symmetric shearing by the continuous phase causes monodisperse emulsion of the discrete (Teh *et al.* 2008). Droplet size ranges as well as factors affecting droplet size are similar to those for the T-junction method.

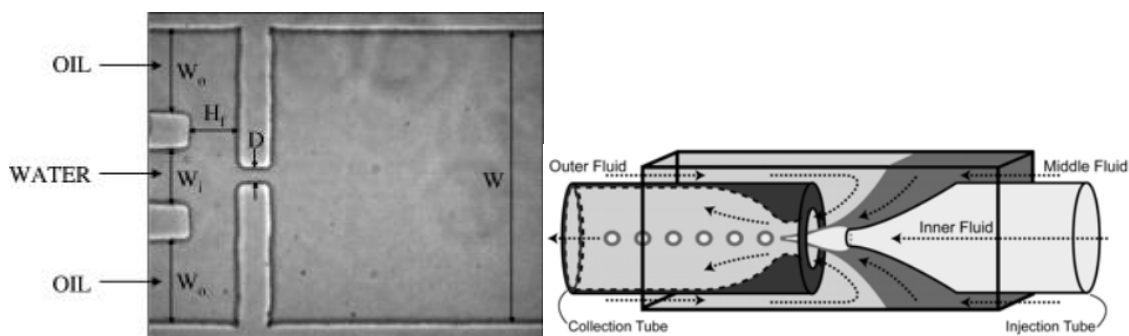


**Figure 1:** Left: Capillary version of the flow-focussing device. Source: (Utada *et al.* 2005). Right: The geometry of a flow-focussing device. Source: (Anna *et al.* 2003)

## 1.5 Measuring Nucleation Kinetics

DMC can be used to measure nucleation kinetics using both the induction time and the two-step method (see Section 1.2.2 of the main text). Droplet microfluidics is also of special interest in nucleation studies because it is a very promising method for implementing the “droplet method” (Laval *et al.* 2007b), a technique to measure true homogenous nucleation kinetics. To date, it has been nearly impossible to measure true homogenous nucleation in solutions (Galkin and Vekilov 1999).

In droplet microfluidics, there is only one feasible way to detect the crystals due to the fact that hundreds of separate reactors are to be monitored simultaneously: The visual method, aided with recording from a high-quality camera (Ataka and Tanaka 1986, Svärd *et al.* 2009), where the smallest crystal detectable is determined by magnification and camera resolution. The detection limit can be drastically lowered using microscopy (Dombrowski *et al.* 2007, Laval *et al.* 2008a, Ildefonso *et al.* 2011).

The following is the basic procedure for both methods using DMC. Hundreds of monodisperse droplets of a solution to be studied are formed via one of the previously-described methods at an elevated temperature above the saturation point, and either stored in or flowed continuously through a channel cooled below the saturation temperature. The large surface area to volume ratio will allow large temperature quenches to be achieved almost instantaneously (e.g. 50 °C in 10s (Laval *et al.* 2007b)). This is necessary because the low reactor volume can result in very long induction time,

## Appendix C – Droplet Microfluidics

which must be counteracted by achieving high supersaturation so that crystallization occurs within a feasible timeframe. Furthermore, hundreds of droplets must be formed, because at the low reactor volumes used (less than 1  $\mu\text{L}$ ) the stochasticity of nucleation becomes evident and must be accounted for statistically (see Section 1.2.4 of the main text). Temperature variation is then performed, and results (i.e. qualitative or quantitative presence of crystals) recorded visually via a microscope and camera.

Gong et al (Gong *et al.* 2007) reported the nucleation kinetics measurement of thermoresponsive colloids via droplet microfluidics, and concluded that they probably observed homogenous nucleation, but this has yet to be verified.

Litster's group (Dombrowski *et al.* 2007) studied the crystallization of alpha-lactose in microfluidic droplets for the purpose of investigating the feasibility of droplet microfluidics for industrial production of pharmaceutical compounds, with the purpose of achieving very small and accurate crystal size distribution. Using a T-junction, they filled a PTFE tube with aqueous lactose droplets separated by oil, which was initially saturated at 80  $^{\circ}\text{C}$ . The tube ("crystallizer") was then immersed in a cold water bath (repeated for several temperatures between 20 and 40  $^{\circ}\text{C}$ ) to apply a temperature. After 24 hours, the tube was removed and the crystals per droplet and droplet size examined under a microscope. The nucleation kinetics were estimated from the statistical results by assuming a Poisson distribution.

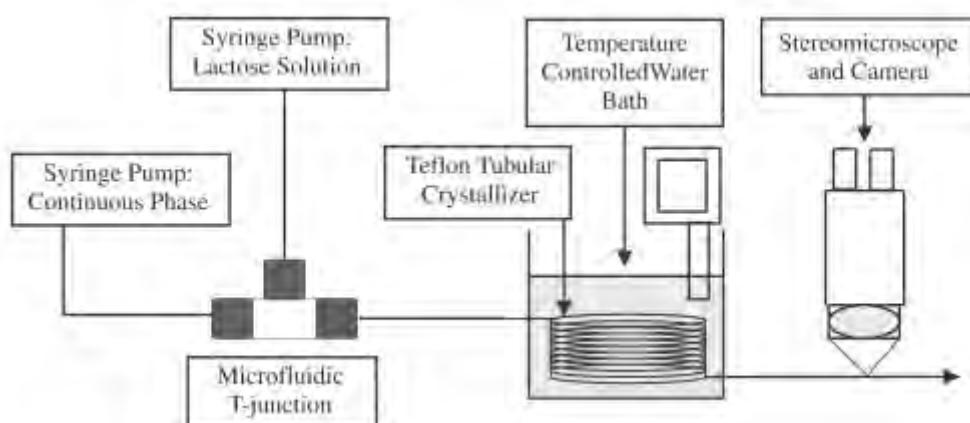


**Figure 2: Litster et al's simple experimental set-up for nucleation kinetics and CSD estimation of alpha-lactose using droplet microfluidics. Source: (Dombrowski *et al.* 2007)**

Laval's group (Laval *et al.* 2007b) developed a device for *continuous* production, crystallization and observation of aqueous potassium nitrate droplets using a slight adaptation of the T-junction. Using soft lithography and PDMS, they created a microfluidic chip capable of creating droplets of  $\sim 100$  nL and collecting induction time statistics using a microscope and camera. They collected much more data than the previous authors by monitoring crystallization of droplets at many different positions simultaneously (corresponding to different "reaction" times). Nucleation was found to always be heterogeneous, and they estimated that droplets of 10 nL volume or less were required to observe true homogenous nucleation.

## Appendix C – Droplet Microfluidics

Veesler's group (Ildefonso *et al.*) used the same to study the nucleation kinetics of aqueous lysozyme solutions. They determined the metastable zone width and the temperature conditions under which mononuclear nucleation occurs without varying reactor volume (i.e. a degree of supersaturation sufficiently high to cause nucleation, yet sufficiently low such that all supersaturation is consumed by the growth of the first nucleus before a second can be formed).

A paper published by Veesler's group in 2011 (Ildefonso *et al.*) represents, to our knowledge, the first application of the double-pulse method in microfluidics to study nucleation kinetics. They determined the steady-state nucleation rate of lysozyme in water using the same device as in the previous paragraph, and results corresponded to homogenous rates reported in the literature.

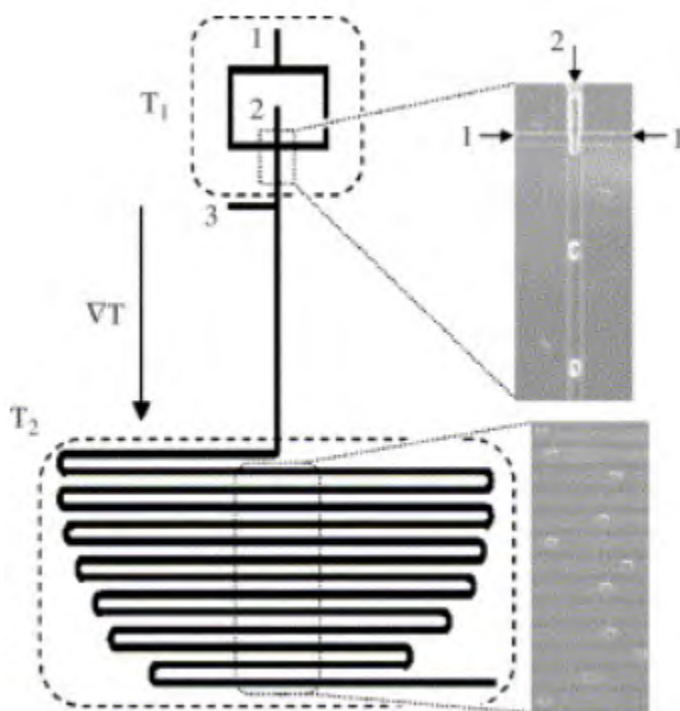


Figure 3: A PDMS microfluidic chip for the continuous production and monitoring of crystallization in aqueous droplets. A simple modification to the T-junction can be seen. The smaller highlighted area of the serpentine-shape marks the observation window of the microscope. Source: (Laval *et al.* 2007b)

## 2 Methodology

### 2.1 Materials & Equipment

All materials were used as-received without further processing.

Table 1. Source and mass fraction purity of chemicals.

Chemical Name	Abbreviation	Source	Purity
---------------	--------------	--------	--------

### Appendix C – Droplet Microfluidics

<b>Fenoxycarb</b>	FC	Syngenta,	0.986
<b>Tolbutamide</b>	TB	Sigma-Aldrich	0.997
<b>Isopropanol</b>	IPA	VWR	0.997
<b>N-propanol</b>	nPA	VWR	0.995
<b>Methanol</b>	MeOH	Sigma-Aldrich	0.999
<b>Ethanol</b>	EtOH	Sigma-Aldrich	0.998
<b>Ethyl Acetate</b>	EtOAc	Sigma-Aldrich	0.997
<b>Toluene</b>	TL	Sigma-Aldrich	0.999
<b>Acetonitrile</b>	ACN	VWR	0.999
<b>Acetone</b>	ACE	VWR	0.999
<b>Acetic Acid</b>		Sigma-Aldrich	0.997
<b>Deuterated Chloroform (0.03% TMS)</b>	CDCl <sub>3</sub>	VWR	0.998
<b>Potassium Nitrate</b>	KNO <sub>3</sub>	Fisher Scientific	0.95
<b>Benzoic Acid</b>	BA	Sigma-Aldrich	0.995
<b>Salicylic Acid</b>	SA	Sigma-Aldrich	0.99
<b>Carbamazepine</b>		Polpharma	0.98
<b>Salicylamide</b>		VWR	0.98
<b>Paracetamol</b>		Sigma-Aldrich	0.99
<b>Piracetam</b>		Axo Industry	0.983
<b>Silicone Oil 47 V 50 Rhodorsil</b>	Sil	VWR	Not given
<b>Paraffin Oil</b>	Par	Sigma-Aldrich	0.985
<b>Perfluoro-n-octane</b>	PFnO	VWR	1.00

The microfluidic device-type and technique chosen to perform induction time experiments using droplet microfluidics is a modification of that developed by (Dombrowski *et al.* 2007).

A Chemyx Nexus 3000 and a Chemyx Fusion 200 syringe pump were purchased from KR Analytical, the Nexus for the faster oil flows and the Fusion for the slower solution flows. Transparent microfluidic tubing (PFA and ETFE, 0.5, 1.55 and 3.2mm inner diameter, by Upchurch), T-junctions (0.5 and 3.2mm internal diameter, by Upchurch) as well as relevant accessories were purchased from Presearch. Various dimensions of gas-tight glass syringes were purchased from K R Analytical (ILS Gastight) and from VWR (Hamilton Gastight). A flexible heater (Thermalfoil), miniature thermostat (Thermal tab) and controller (CT16A) were purchased from Minco. A variable DC power supply (Thurlby Thandar EL183R) was purchased from Imex Instruments. An aluminium plate to hold the tubing was custom-made in the University of Limerick materials workshop. The waterbaths used consisted of a Grant GR150 stainless steel tank with immersion thermostat and a Grant C2G cooling unit. PFA or ETFE tubing was used depending on solvent compatibility (Table 2).

## Appendix C – Droplet Microfluidics

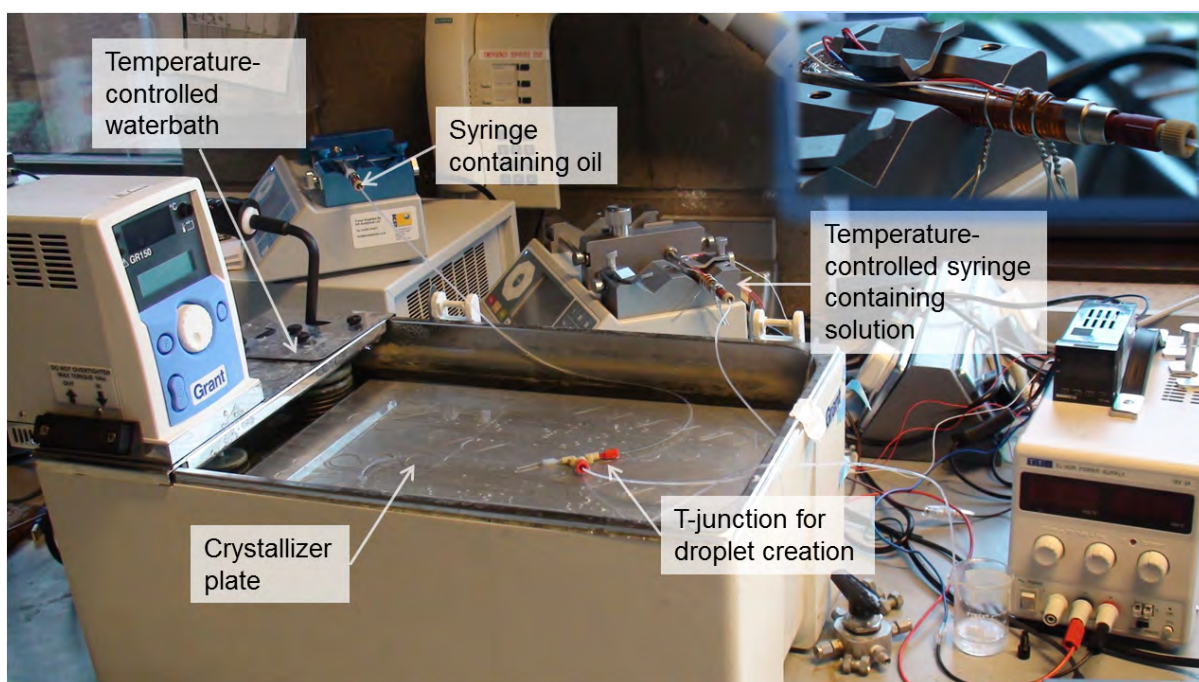


**Figure 4:** Experimental set-up for induction time measurements using droplet microfluidics. Inset: Close-up of the syringe containing the solution, showing the flexible heater and miniature thermostat attached using metal wires.

**Table 2:** Tubing compatibility of relevant solvents.

Solvent	PFA Compatible?*	ETFE Compatible?*
Acetic Acid	Yes	Yes
Toluene	Yes	Yes
Ethanol	Yes†	
Ethyl Acetate	Yes	Yes (up to 60 °C)
Acetonitrile	No‡	Yes
Methanol	Yes	
Isopropanol	Yes§	
N-propanol	No§	Yes (McKeen and Knoel 2006)
Acetone	Yes	Yes

\* Unless otherwise stated, source:

<http://webstore.idexhs.com/TechInfo/chemMatList.asp?vChem=Ethanol>

† <http://www.coleparmer.com/techinfo/ChemComp.asp>

‡ <http://www.agrenetics.com/page11.html>

§ [http://www.efunda.com/designstandards/oring/oring\\_chemical.cfm](http://www.efunda.com/designstandards/oring/oring_chemical.cfm)

## 2.2 Experimental Methodology

### 2.2.1 Chemicals Testing

In order for the droplets to act as independent crystallizers, the following conditions must be met:

1. The solution and oil must be immiscible in order for stable droplets to form.
2. The solute must have negligible solubility in the oil; otherwise, solute will diffuse into the oil, changing its concentration in the solution and allowing crystallization in the oil phase and thus cross-contamination between droplets.
3. The oil must preferentially wet the tube walls, to prevent the solution wetting the walls and thus allowing cross-contamination between droplets.

Simple immiscibility tests were performed by adding ~2 mL of each of the two liquids to be tested into a small glass container which was then sealed and shaken. The only two observed outcomes were interpreted as follows (partial miscibility was ignored for the sake of simplicity):

- a) Immiscible: A cloudy or bubbly mixture was created by shaking, and after being allowed to settle the mixture was separated again into two clearly distinct phases.
- b) Miscible: A single clear phase resulted which did not separate even after several days.

Due to their high viscosities and boiling temperatures, it is somewhat more cumbersome to determine solubilities in oils; as such, very simple semi-quantitative solubility tests were performed as follows:

1. Less than 5 tiny crystals were added to a small glass container and about 1 mL of oil added (all quantities were weighed).
2. After being sealed, the container was placed into a high-temperature water bath and kept there for several hours (without stirring), while regularly checking for any visible dissolution. The extent of dissolution was measured visually (“much”, “little”, “none”) and recorded.
3. The container was then placed into a very cold water bath for several hours, again regularly checking for any visible dissolution.

Which of two immiscible liquids preferentially wets a surface can be determined simply by simultaneously placing both in contact with that surface and observing which liquid will touch the surface (presuming no gravity effect). At no time during the lab work was it observed that liquid in the 0.5 mm inner diameter tubing flowed simply due to the force of gravity. Therefore, it can be presumed that there is no appreciable effect of gravity.

Preferential tube wall wetting was determined by filling a tube with solvent droplets separated by the oil and checking the shape of the droplets: If the solvent droplets were rounded into themselves at the edge (i.e. has a contact angle less than 90°, see (a) in Figure 5), the oil preferentially wets the tube wall; if the droplets are spread out at the

## Appendix C – Droplet Microfluidics

edges (i.e. a contact angle greater than  $90^\circ$ , see (b) in Figure 5), then the solvent preferentially wets the tube walls.

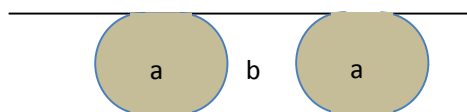


**Figure 5:** Demonstration of preferential tube wall wetting. That (b) preferentially wets the tube wall can be seen from its shape, which shows that it is more attracted to the tube wall than (a).

### 2.2.2 Solution Preparation

Solutions were prepared according to published solubility data and, in cases where solubility data was not available for the desired temperatures, the published data was extrapolated (see Table 3).

**Table 3:** Sources of solubility data for compounds used.

Compound	Solvent	Solubility Source
Potassium Nitrate (KNO <sub>3</sub> )	Water	(Laval <i>et al.</i> 2007a)
Benzoic Acid	Acetic Acid	(Wang <i>et al.</i> 2007)*
	Toluene	(Thati <i>et al.</i> 2010)
Salicylic Acid	Ethanol	(Shalmashi and Eliassi 2007)
	Ethyl Acetate	(Shalmashi and Eliassi 2007)*
	Acetonitrile	(Nordström and Rasmuson 2006)*
	Acetic Acid	(Nordström and Rasmuson 2006)*

\* via extrapolation from literature values.

To make up a solution saturated at  $T_{sat}$ , an exact amount of solute was weighed out in a gas-tight container and the amount of solvent needed to make a solution saturated at  $T_{sat}$  was added by mass. After adding clean stirrer bar and sealing the container, the container was placed in a waterbath at  $T_{sat} + 5^\circ\text{C}$  and set stirring. At least 4 hours following complete dissolution (checked visually), the solution was filtered into another gas-tight container with plastic syringes and filters ( $0.2\ \mu\text{m}$ ) of appropriate material for the different solvents. A stirrer bar was added to the filtered solution, the container sealed tightly, placed back in the  $T_{sat} + 5^\circ\text{C}$  waterbath and set stirring. At least 4 hours following complete dissolution (to allow for crystallization occurring during the filtration step), the solution was considered ready for experimentation.

### 2.2.3 Induction Times using Droplet Microfluidics

The experimental set-up for the induction time measurements using droplet microfluidics adopted in this study is shown in .

## Appendix C – Droplet Microfluidics

The gas-tight syringe initially used (ILS) had a maximum operation temperature of 60 °C. Thus, considering that the solution syringe would have to be held 5 °C above  $T_{sat}$ , 50 °C was chosen as the maximum  $T_{sat}$ . The minimum operation temperature of the used water baths is 5 °C. It was decided to utilise the maximum temperature drop (50 to 5 °C) in order to minimize induction times.

The following two criteria were used to determine which solvents were used for a certain compound:

1. Is solubility data available?
2. Is the excess solid at  $T_{cry}$  (i.e. the amount of solute above the solubility line at  $T_{cry}$ ) sufficiently large so that if it crystallizes it will be visible in the small droplet to the naked eye? This limit was arbitrarily set at 0.1 g solute per g solvent.

The following is the procedure for carrying out induction time estimates using droplet microfluidics:

1. Following on from step (7) of the previous section, the filtered solution to be studied was carefully and quickly loaded into a gas-tight 1 mL syringe pre-heated to  $T_{sat} + 5$  °C and the syringe immediately sealed, taking care to prevent air being trapped in the syringe.
2. After much experimentation, it was determined that the most efficient way to connect the syringe to the tubing without sample loss was as follows:
  - a. The syringe, while sealed, was allowed to cool until crystallization occurred and equilibrium was achieved (i.e. no more crystallization occurs once the syringe has reached room temperature, checked visually). At this stage, opening the syringe should lead to minimal solvent evaporation and prevent further crystallization.
  - b. During (a), the flexible heater and miniature thermostat were attached to the syringe using metal wire (see Inset, ). These were both attached to the controller, and the heater was powered by the variable DC power supply.
  - c. The syringe was then opened and the tubing, pre-filled with the oil to prevent the solution from travelling into the tubing too early, connected as fast as feasible.
3. The other end of this tube was connected to a T-junction, to which the syringe containing the oil was also connected. The exit of the T-junction was connected with the “crystallizer” tube, which was a long piece of tubing placed into the crystallizer plate (see ), the other end of which was placed above a waste container. The crystallizer plate was used to enable easy observation of many droplets at once, as without it the long tubing would have formed coils and made it quite difficult to observe all the droplets at once.
4. At this stage, the flexible heater was turned on and set to heat to  $T_{sat} + 5$  °C. Due to minor evaporation occurring after several hours, the next step was performed roughly 1 hour (and not 4 hours, as previously) after complete (visible) dissolution.
5. The oil syringe pump was turned on to fill the T-junction and a little of the crystallizer tube with oil. Then the solution syringe pump was also turned on and

## Appendix C – Droplet Microfluidics

left on until the desired number of droplets of solution, separated by oil, were filled into the crystallizer tubing. At this point, the flow was stopped. Typical flow rates are shown in Table 4.

**Table 4:** Typical flow rates used to fill crystallizer tubing with solution droplets.

Tubing inner diameter (mm)	Oil flow rate (mL/hr)	Solution flow rate (mL/hr)
0.5	4	2
3.2	20	8

6. The crystallizer tubing was disconnected from the T-junction and then sealed at both ends. Then the crystallizer plate was lifted out of the hot water bath and placed into a second water bath set at the (lower) crystallization temperature  $T_{cry}$ . A high-definition video camera was placed vertically above the plate looking down on it and set to record.
7. Once all the droplets had crystallized or too much time had passed, recording was stopped and induction time data extracted from the video.

### 2.2.4 Rough Nucleation Kinetics Screening

According to Equation (23) in the main body, the induction time is approximately inversely proportional to the reactor volume if all other variables remain unchanged (which is practically impossible, see next paragraph). Thus, by carrying out crystallization experiments at a larger scale, even organic compounds with very slow nucleation kinetics should nucleate. This principle is demonstrated in Table 5.

**Table 5:** Theoretical examples of effect on changing reactor volume on  $t_{ind}$  if all other factors remain unchanged.

Supersaturation	Reactor Volume	$t_{ind}$
$S_1$	100nL ( $1 \times 10^{-7}$ L)	24hrs
$S_1$	1mL ( $1 \times 10^{-3}$ L)	0.001 sec
$S_1$	1L	$1 \times 10^{-6}$ seconds
$S_2$	1L	1 sec
$S_2$	1mL ( $1 \times 10^{-3}$ L)	16 minutes
$S_2$	100nL ( $1 \times 10^{-7}$ L)	320 years

However, it is practically impossible for all other factors to remain unchanged. For one, the time taken for  $T_{cry}$  to be reached increases as reactor volume increases, and therefore

## Appendix C – Droplet Microfluidics

systems which nucleate quickly are actually not giving induction time values but rather metastable zone widths. Furthermore, nucleation is extremely sensitive to changes in hydrodynamics, and hydrodynamics is dramatically affected by reactor scaling. Therefore, it is practically impossible to use the proportionality of induction time and reactor volume to estimate the induction time of a system at microfluidic scales (e.g. 100 nL) from its induction time at macroscopic volumes (e.g. 2 mL).

As such, instead of mathematically estimating the microscopic induction times, the macroscopic nucleation times, under identical temperature drops and reactor volumes, of the organic compounds to be screened are simply compared to the induction times of compounds whose microscopic induction times are known (e.g.  $\text{KNO}_3$  and BA). Thus, it can be assumed that any system which has induction times similar to these “references” will be suitable candidates for DMC.

To very roughly screen the nucleation kinetics of various compounds, the following procedure was carried out for each compound:

1. Following from step (7) of Section 2.2.2, around 2mL were placed into another gas-tight container along with a magnetic stirrer bar, tightly sealed, placed into a water bath and allowed to equilibrate at  $T_{sat} + 5\text{ }^\circ\text{C}$  as described previously.
2. The container was then placed into a second water bath set at the (lower) crystallization temperature  $T_{cry}$  and visually checked for crystallization within a reasonable time frame.
3. Then the container was placed back into the hot water bath and allowed to equilibrate, after which step (2) was carried out again.
4. Step (3) was repeated 2 or 3 times.

## 3 Results & Discussion

### 3.1 Independent Microreactors

To test the ability of the droplets to act as independent reactors,  $\text{KNO}_3$  in water was used as a model compound since it has very fast nucleation kinetics and has already been used in droplet microfluidic nucleation kinetic studies (Laval *et al.* 2007a, Laval *et al.* 2007b, Laval *et al.* 2008a, Laval *et al.* 2008b).

Crystallization occurred roughly within the same time-scale for the same  $T_{sat}$  (50 °C), similar  $T_{cry}$  (this study: 22 °C) and same droplet volume (~100 nL) as reported in the literature (Laval *et al.* 2007b), namely around 1 minute (see Figure 6). More importantly, no cross-communication between droplets was observed and the droplets seemed to act as independent crystallizers.



**Figure 6:**  $\text{KNO}_3$  crystals visible in water droplets separated by paraffin oil.

## Appendix C – Droplet Microfluidics

Thus, it was concluded that, according to these preliminary tests, our device is able of carrying out droplet microfluidics induction time determination using the model  $\text{KNO}_3$ /water/oil system.

### 3.2 Immiscibility

The results of the immiscibility tests are shown in the table below.

**Table 6:** Results of miscibility experiments, along with solvent dipole moments and dielectric constants. “i” represents immiscible and “m” miscible.

	Water	ACN	MeOH	EtOH	ACE	Acetic Acid	EtOAc	Tol
Dipole Moment (D)*	1.85	3.92	1.7	1.69	2.88	1.74	1.78	0.375
Dielectric Constant*	80	36.6	33	24.3	20.7	6.715	6.02	2.38
Paraffin oil	i	i	i	i	i	i	m	m
Silicone oil	i	i	i	i	i	i	m	m
Water	-	m†	m†	m†	m†	m†	i†	i
Perfluoro-n-octane	i	i	i	i	i	i	i	i

\* Source: [http://www.usm.maine.edu/~newton/Chy251\\_253/Lectures/Solvents/Solvents.html](http://www.usm.maine.edu/~newton/Chy251_253/Lectures/Solvents/Solvents.html)

† Not tested; common knowledge.

Dipole moment and dielectric constant are considered quantitative measurements of polarity. As can be seen from the table above, the results follow the expected pattern of “like dissolves like” in that only the weakly-polar EtOAc and the non-polar Tol dissolve in the non-polar paraffin and silicone oils.

As expected, PFnO was immiscible with all solvents. Consisting only of carbon and fluorine atoms, it is really only miscible with other fluorinated compounds.

As such, it can be seen that all solvents tested were immiscible with at least one of the oils, and can thus be used for droplet experiments.

### 3.3 Compound Solubilities in Oil

The following results were obtained for the compound solubilities in the various oils.

**Table 7:** Results of semi-quantitative tests for solubility of organic compounds in oils.

Compound	Oil	Crystal % wt.	Temp.	Solubility (wt)*	Details
<b>BA</b>	Par	0.15%	70 °C	>0.15%	Completely dissolved (<24 hrs)
	Sil	0.35%	70 °C	>0.35%	Completely dissolved (<72 hrs)
	PFnO	0.84%	60 °C	<<0.84%	No visible dissolution but faint crystallization visible upon cooling to -15 °C
<b>SA</b>	Par	0.24%	70 °C	<0.24%	Partially dissolved (24 hrs)
	Sil	0.42%	70 °C	<<0.42%	No visible dissolution but crystallization visible upon cooling to room temperature
	PFnO †	2.05%	60 °C	~0%	No visible dissolution or crystallization at room temperature (RT)
<b>Salicylamide</b>	Par	0.01%	75 °C	~0%	No visible dissolution after 3 days nor crystallization after 3 days at RT
	Sil	0.01%	75 °C	~0%	No visible dissolution after 3 days nor crystallization after 3 days at RT

\* These values are *not* absolute solubilities, see explanation below.

These solubilities are not absolute values, but merely reflect the presence or absence of visible dissolution (or crystallization) at certain temperatures. As such, they serve merely as semi-quantitative indications of the extent of solubility.

As can be seen from this data, solubility appears to be negligible (indicated by “~”) or very small (“<<”) in all cases except for BA in Par and Sil oil, although BA is barely soluble in PFnO. Thus, all examined organic compounds seem to have negligible solubility in at least one oil.

### 3.4 Preferential Tube Wall Wetting

Preferential tube wall wetting was determined as follows.

**Table 8:** Test results for preferential tube wall wetting. The phase that preferentially wets the tube walls is indicated. Tube material and size is PFA and 0.5 mm, respectively.

	Water	Acetone	Ethanol	Methanol	Acetic Acid	Acetonitrile	Toluene	Ethyl Acetate
<b>Parafin</b>	Oil	Oil	*	Solvent	Oil	Oil	n/a†	n/a†

## Appendix C – Droplet Microfluidics

<b>Oil</b>								
<b>Silicone Oil</b>	_____	_____	*	Oil	_____	Oil	n/a†	n/a†
<b>Water</b>	_____	_____	_____	_____	_____	_____	Solvent	_____
<b>Perfluorooctane</b>	_____	_____	_____	Oil	Oil	Oil	Oil	Oil

\* It proved impossible to form visible droplets for this combination.

† Miscible

As can be seen, in most cases the oils preferentially wet the tube wall. This is understandable since the tube wall material, PFA (perfluoroalkoxyalkane) is extremely hydrophobic (Ha *et al.* 2005) – Teflon (polytetrafluoroethylene), famous as a hydrophobic material, is a PFA. That PFnO always preferentially wets the tube wall is due to the fact that both the tube wall and PFnO are fluorinated compounds.

### 3.5 Initial Droplet Microfluidic Crystallization Experiments

Over 30 induction time experiments were carried out using KNO<sub>3</sub>, SA and BA in various organic solvents. The results are summarised in the table below.

**Table 9:** Initial DMC induction time experimental results. Tubing material: PFA; tubing inner diameter: 0.5 mm; droplet volume: ~100 nL.

_____	Solvent	Oil	$T_{sat}$	$T_{cry}$	Super-saturation (c/c*)	Crystallization?	Time	Independent?	
<b>KNO<sub>3</sub></b>	Water	Sil	50	RT	2.43	yes	1min*	yes	
				15	5	1.51	no	24hrs	-
			Par	15	5	1.51	no	24hrs	-
				15	10	1.23	no	3days	-
				45	5	4.21	yes	<5sec*	yes
				45	10	3.42	yes	15sec*	yes
<b>SA</b>	MeOH	Par &† Sil	50	5	2.37	no	30hrs	-	
	ACE	Paraffin	45	5	1.84	no	12hrs	-	
	ACN	Par &†	50	5	3.73	no	36 &	-	

## Appendix C – Droplet Microfluidics

		PFnO					12hrs	
	EtOAc	PFnO	50	5	3.65	no	3days	-
<b>B</b>	Tol	Water	50	RT	3.02	yes	3min*	no‡
<b>A</b>		PFnO	50	5	5.92	yes	<10sec*	no§
	Acetic	Sil	50	5	4.89	yes	1min*	no§
	Acid	Par	50	10	3.41	no	3days	-

\* The induction times for KNO<sub>3</sub> and BA are most likely underestimated since the droplets take at least 3 minutes to actually reach the set point temperature.

† Experiment was repeated with both, without any difference in result.

‡ Solution preferentially wet the tube wall; travel of crystallization from a droplet to its neighbour clearly visible in video (see Figure 8).

§ Crystal has non-negligible solubility in oil; travel of crystallization from a droplet to its neighbour via crystallization in the oil was clearly visible in video (see Figure 9).

### 3.5.1 KNO<sub>3</sub> and Interfacial Tension

The KNO<sub>3</sub>/water system was the only one that gave meaningful induction time data. The literature indicates that for our conditions  $t_g$  is negligible. (Laval *et al.* 2007b) Thence, for this dataset,  $t_{ind} \approx t_n = 1/VJ$ .

The results were thus plotted below according to the CNT as set forth in Section 1.2.2.2 of the main body.

The good fit demonstrates that the results follow the predictions of the CNT to a reasonable degree. Some loss in quality doubtlessly resulted from the fact that supersaturations and induction times were not measured with a great degree of accuracy, which could easily be done if required.

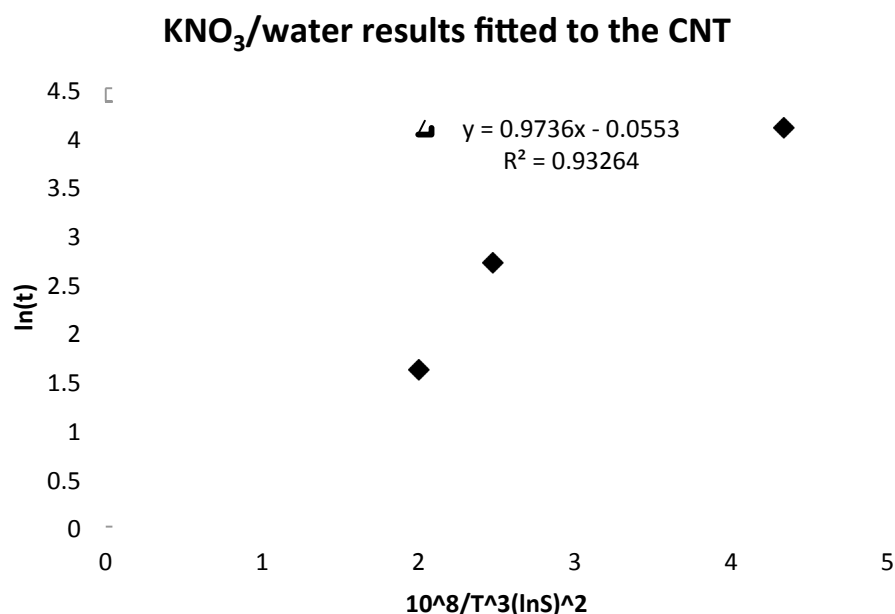


**Figure 7:** The results from the KNO<sub>3</sub>/water droplet microfluidic induction time experiments fitted to the CNT.

## Appendix C – Droplet Microfluidics

### 3.5.2 Cross-Communication – Benzoic Acid

BA, unlike SA, gave crystallization within experimentally-feasible timeframes. However, in all cases there was clear cross-communication between neighbouring droplets, such that crystallization in one induced it in the other. This was clearly visible in the videos.

In the case of Tol/water, where Tol preferentially wetted the tube walls, crystallization in the water was not visible (see Figure 8) and cross-communication presumably occurred via a film of solution covering the tubing even where there is water, connecting neighbouring droplets, such that there really is one elongated reactor which gets very thin where there is some water. This problem is easily alleviated by choosing a separating phase which preferentially wets the tube wall and is still immiscible with Tol, such as PFnO.



**Figure 8:** Still images from a video showing cross-communication due to preferential wall wetting of the solution (in this case,  $\text{KNO}_3$ /toluene) separated by water (droplet-shaped). Time progresses left-to-right at a rate of approximately 1 second per image. Tubing inner diameter = 0.5 mm.

However, in this case, as well as the other cases, cross-communication still occurred. This time, however, via a different mechanism: the BA dissolving in PFnO in the hot water bath and then crystallizing there in the cold water bath (see Figure 9). The oil solubility data in Section 3.3 confirms that BA is somewhat soluble in all three oils. Crystal growth seemed to occur at a faster linear rate in the droplets than in the oil.

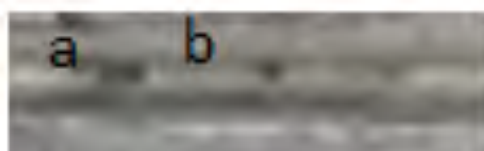


**Figure 9:** Still image from a video showing cross-communication due to solute dissolving in PFnO and crystallizing there. The area beneath (a) is the clear oil before any crystallization; beneath (b) the oil has darkened due to crystallization; the very dark patch between (a) and (b) is a crystallised droplet. Tubing inner diameter = 0.5 mm.

That BA dissolves even in PFnO, which, due to consisting only of carbon and fluorine atoms, is known to be immiscible with nearly all non-fluorinated materials, does not bode well for BA. It will be very difficult to find a replacement separating liquid which will meet all 3 requirements enumerated in Section 2.2.1.

### 3.5.3 Nucleation Kinetics – Salicylic Acid

SA, unlike BA, seems to be practically insoluble in the oils, especially in PFnO (see Section 3.3) and hence should not suffer from cross-communication.

## Appendix C – Droplet Microfluidics

However, SA completely fails to crystallize within experimentally-feasible timeframes.

Although the supersaturations used in the SA experiments are slightly below those of BA, they are the same as  $\text{KNO}_3$  which nucleated far faster than BA. This confirms that the key factor in a system's ability to nucleate in a timely manner is not supersaturation, but nucleation kinetics in general. It also explains why  $\text{KNO}_3$  nucleates significantly faster than BA, since it is generally known that larger compounds have slower nucleation kinetics.

Thus, these preliminary results already suggest that the limiting factor in the applicability of DMC to medium-sized organic compounds is their slow nucleation kinetics.

### 3.6 Screening for Fast Nucleation Kinetics

#### 3.6.1 Testing the Theory

To examine the validity of this hypothesis, the suggested experiments were carried out as set forth in Section 2.2.4 using  $\text{KNO}_3$ , BA and SA.

**Table 10:** Induction times of initial rough nucleation kinetics screening. All results are in seconds, the average of at least 2 iterations with small standard deviation (<4 sec). >60 indicates no crystallization was observed after 60 seconds, when the experiment was stopped.

Compound	Solvent	$T_{\text{sat}} = 50\text{ }^\circ\text{C}$ , $T_{\text{cry}} = 5\text{ }^\circ\text{C}$	$T_{\text{sat}} = 50\text{ }^\circ\text{C}$ , $T_{\text{cry}} = -15\text{ }^\circ\text{C}^*$	$T_{\text{sat}} = 70\text{ }^\circ\text{C}$ , $T_{\text{cry}} = -15\text{ }^\circ\text{C}^*$
$\text{KNO}_3$	Water	16	5	2
Benzoic acid	Acetic acid	>60	20	
	Toluene	22	8	
Salicylic acid	Ethanol			7
	Ethyl Acetate	>60	>60	6
	Acetonitrile	>60	>60	9
	Acetic Acid			20
	Acetone			20

\* Temperatures below freezing point were reached using a specialised oil cooling system.

These results indicate an order of nucleation kinetics, from fastest to slowest, as follows:  $\text{KNO}_3/\text{water} > \text{BA}/\text{Tol} > \text{BA}/\text{acetic acid} > \text{SA}$ . This is identical to the pattern observed in the microfluidics experiments in Table 9. Therefore, it was concluded that this technique is able to find organic compounds with sufficiently-fast nucleation kinetics for the droplet microfluidic experimental conditions used previously.

#### 3.6.2 Screening Other Organic Compounds

Having established the validity of the technique, some other organic compounds were screened. The results are presented in the table below.

## Appendix C – Droplet Microfluidics

**Table 11:** Induction times of initial rough nucleation kinetics screening. All results are in seconds, the average of at least 2 iterations with small standard deviation (<4 sec). >60 indicates no crystallization was observed after 60 seconds, when the experiment was stopped.

Compound	Solvent	$T_{\text{sat}} = 50\text{ }^{\circ}\text{C}$ ,	$T_{\text{sat}} = 50\text{ }^{\circ}\text{C}$ ,	$T_{\text{sat}} = 70\text{ }^{\circ}\text{C}$ ,
		$T_{\text{cry}} = 5\text{ }^{\circ}\text{C}$	$T_{\text{cry}} = 15\text{ }^{\circ}\text{C}^*$	$T_{\text{cry}} = 15\text{ }^{\circ}\text{C}^*$
Carbamazepine	EtOH	>60	>60	>60
	nPA		>60	>60
	EtOAc			6
Paracetamol	EtOH	>60	>60	>60
	nPA	>60	>60	>60
	EtOAc	>60	>60	†
Piracetam	EtOH			20
	IPA			4
Salicylamide	ACE	>60‡		†
	ACN			13‡

\* Temperatures below freezing point were reached using a cryo-oil bath.

†  $T_{\text{sat}}$  too close/above solvent boiling point

‡  $T_{\text{cry}} = 10\text{ }^{\circ}\text{C}$

These results indicate that carbamazepine/EtOAc, piracetam/EtOH, piracetam/IPA and salicylamide/ACN are suitable compounds for the conditions used so far in the droplet microfluidic experiments. Paracetamol, on the other hand, seems to have far too slow nucleation kinetics in all solvents tested.

### 3.6.3 Testing the Potential Candidates

Some of these have already been tested using DMC, and the results are presented below.

**Table 12:** Results of DMC experiments performed on some of the systems identified as potentially suitable in Table 11. Tubing material: PFA; tubing inner diameter: 0.5 mm; droplet volume: ~100 nL.

Compound	Solvent	Oil	$T_{\text{sat}}$	$T_{\text{cry}}$	Super-saturation (c/c*)	Crystallization?	Time	Independent?
Piracetam	IPA	PFnO	70	5	23.7	no	48hrs	-
Salicylamide	ACN	Par	70	5	4.87	no	48hrs	-

Disappointingly, there was no crystallization in both tested systems. Salicylamide solubility in paraffin oil was already tested and found to be negligible (see Section 3.3), so the explanation is likely not found here, but rather in that salicylamide's nucleation kinetics are simply too slow. It is probably the same for piracetam, though it is possible

that some piracetam dissolved in the PFnO, since the solubility for this has not yet been tested.

## 4 Conclusion

Droplet microfluidics was found not to be a suitable method for measuring the induction times of medium-sized organic molecules. First, it appears that most medium-sized and above molecules do not have sufficiently fast nucleation kinetics to crystallise in feasible timeframes. And second, the one found to crystallise sufficiently fast (BA) dissolved in all oils and thus caused cross-contamination between droplets, invalidating the results.

One way forward is to move towards larger tubing and droplets in order to significantly decrease induction times.

**Table 13:** Different inner diameter tubing and its effect on droplet volume and estimated effect on induction time.

<b>Tubing inner diameter (mm)</b>	<b>Droplet volume (nL)*</b>	<b>Volume increase (=induction time increase?)</b>
<b>0.5</b>	65	
<b>1.55</b>	1,900	x30
<b>3.2</b>	17,100	x260

\* Assuming droplet diameter = tubing inner diameter

As can be seen, using larger tubing could drastically decrease induction time, far more than increasing the supersaturation via temperature could hope to achieve. The feasibility of using larger diameter tubing depends on whether flow remains laminar; if flow becomes turbulent, it will be very difficult or even impossible to produce monodisperse and stable droplets. A recent publication indicates that stable, monodisperse droplets can be formed in 1.55 mm tubing. (Lorber *et al.* 2011)

Another solution could be the use of ultrasonic vibration to increase nucleation rates similar to stirring in larger reactor volumes.

The primary aim of the PhD is measuring the influence of solvent on nucleation kinetics. Since over 18 months had been expended on microfluidics already without any relevant results, and since the success of further experiments was uncertain, it was decided not to pursue droplet microfluidics any further.

## Bibliography

- Anna, S. L., Bontoux, N. and Stone, H. A. (2003) 'Formation of dispersions using "flow focusing" in microchannels', *Applied Physics Letters*, 82(3), 364-366.
- Ataka, M. and Tanaka, S. (1986) 'The growth of large single crystals of lysozyme', *Biopolymers*, 25(2), 337-350.
- Atencia, J. and Beebe, D. J. (2005) 'Controlled microfluidic interfaces', *Nature*, 437(7059), 648-655.
- Begolo, S., Colas, G., Viovy, J.-L. and Malaquin, L. (2011) 'New family of fluorinated polymer chips for droplet and organic solvent microfluidics', *Lab on a Chip*, 11(3), 508-512.
- Cygan, Z. T., Cabral, J. T., Beers, K. L. and Amis, E. J. (2005) 'Microfluidic Platform for the Generation of Organic-Phase Microreactors', *Langmuir*, 21(8), 3629-3634.
- Dombrowski, R. D., Litster, J. D., Wagner, N. J. and He, Y. (2007) 'Crystallization of alpha-lactose monohydrate in a drop-based microfluidic crystallizer', *Chemical Engineering Science*, 62(17), 4802-4810.
- Galkin, O. and Vekilov, P. G. (1999) 'Are Nucleation Kinetics of Protein Crystals Similar to Those of Liquid Droplets?', *Journal of the American Chemical Society*, 122(1), 156-163.
- Gong, T., Shen, J., Hu, Z., Marquez, M. and Cheng, Z. (2007) 'Nucleation Rate Measurement of Colloidal Crystallization Using Microfluidic Emulsion Droplets', *Langmuir*, 23(6), 2919-2923.
- Ha, J.-W., Park, I. J. and Lee, S.-B. (2005) 'Hydrophobicity and Sliding Behavior of Liquid Droplets on the Fluorinated Latex Films', *Macromolecules*, 38(3), 736-744.
- Hansen, C. L., Skordalakes, E., Berger, J. M. and Quake, S. R. (2002) 'A robust and scalable microfluidic metering method that allows protein crystal growth by free interface diffusion', *Proceedings of the National Academy of Sciences of the United States of America*, 99(26), 16531-16536.
- Ildefonso, M., Candoni, N. and Veessler, S. (2011) 'Using Microfluidics for Fast, Accurate Measurement of Lysozyme Nucleation Kinetics', *Crystal Growth & Design*, null-null.
- Ildefonso, M., Revalor, E., Punniam, P., Salmon, J. B., Candoni, N. and Veessler, S. 'Nucleation and polymorphism explored via an easy-to-use microfluidic tool', *Journal of Crystal Growth*, In Press, Corrected Proof.
- Kim, B.-Y., Hong, L.-Y., Chung, Y.-M., Kim, D.-P. and Lee, C.-S. (2009) 'Solvent-Resistant PDMS Microfluidic Devices with Hybrid Inorganic/Organic Polymer Coatings', *Advanced Functional Materials*, 19(23), 3796-3803.
- Laval, P., Crombez, A. and Salmon, J.-B. (2008a) 'Microfluidic Droplet Method for Nucleation Kinetics Measurements', *Langmuir*, 25(3), 1836-1841.
- Laval, P., Giroux, C., Leng, J. and Salmon, J.-B. (2008b) 'Microfluidic screening of potassium nitrate polymorphism', *Journal of Crystal Growth*, 310(12), 3121-3124.
- Laval, P., Lisai, N., Salmon, J.-B. and Joanicot, M. (2007a) 'A microfluidic device based on droplet storage for screening solubility diagrams', *Lab on a Chip*, 7(7), 829-834.
- Laval, P., Salmon, J.-B. and Joanicot, M. (2007b) 'A microfluidic device for investigating crystal nucleation kinetics', *Journal of Crystal Growth*, 303(2), 622-628.

## Appendix C – Droplet Microfluidics

- Lee, J. N., Park, C. and Whitesides, G. M. (2003) 'Solvent Compatibility of Poly(dimethylsiloxane)-Based Microfluidic Devices', *Analytical Chemistry*, 75(23), 6544-6554.
- Leng, J., Lonetti, B., Tabeling, P., Joanicot, M. and Ajdari, A. (2006) 'Microevaporators for Kinetic Exploration of Phase Diagrams', *Physical Review Letters*, 96(8), 084503.
- Leng, J. and Salmon, J.-B. (2009) 'Microfluidic crystallization', *Lab on a Chip*, 9(1), 24-34.
- Li, L. and Ismagilov, R. F. (2010) 'Protein Crystallization Using Microfluidic Technologies Based on Valves, Droplets, and SlipChip', *Annual Review of Biophysics*, 39(1), 139-158.
- Lorber, N., Sarrazin, F., Guillot, P., Panizza, P., Colin, A., Pavageau, B., Hany, C., Maestro, P., Marre, S., Delclos, T., Aymonier, C., Subra, P., Prat, L., Gourdon, C. and Mignard, E. (2011) 'Some recent advances in the design and the use of miniaturized droplet-based continuous process: Applications in chemistry and high-pressure microflows', *Lab on a Chip*, 11(5), 779-787.
- McKeen, L. W. and Knovel (2006) *Fluorinated coatings and finishes handbook : the definitive user's guide and databook*, Norwich, NY: William Andrew Pub.
- Nguyen, N.-T. (2002) *Fundamentals and Applications of Microfluidics*, Norwood, MA: Artech House.
- Nisisako, T., Torii, T. and Higuchi, T. (2002) 'Droplet formation in a microchannel network', *Lab on a Chip*, 2(1), 24-26.
- Nisisako, T., Torii, T., Takahashi, T. and Takizawa, Y. (2006) 'Synthesis of Monodisperse Bicolored Janus Particles with Electrical Anisotropy Using a Microfluidic Co-Flow System', *Advanced Materials*, 18(9), 1152-1156.
- Nordström, F. L. and Rasmuson, Å. C. (2006) 'Solubility and Melting Properties of Salicylic Acid', *Journal of Chemical & Engineering Data*, 51(5), 1668-1671.
- Rolland, J. P., Van Dam, R. M., Schorzman, D. A., Quake, S. R. and DeSimone, J. M. (2004) 'Solvent-Resistant Photocurable "Liquid Teflon" for Microfluidic Device Fabrication', *Journal of the American Chemical Society*, 126(8), 2322-2323.
- Sanjoh, A. and Tsukihara, T. (1999) 'Spatiotemporal protein crystal growth studies using microfluidic silicon devices', *Journal of Crystal Growth*, 196(2-4), 691-702.
- Sauter, C., Dhouib, K. and Lorber, B. (2007) 'From Macrofluidics to Microfluidics for the Crystallization of Biological Macromolecules†', *Crystal Growth & Design*, 7(11), 2247-2250.
- Shalmashi, A. and Eliassi, A. (2007) 'Solubility of Salicylic Acid in Water, Ethanol, Carbon Tetrachloride, Ethyl Acetate, and Xylene', *Journal of Chemical & Engineering Data*, 53(1), 199-200.
- Shestopalov, I., Tice, J. D. and Ismagilov, R. F. (2004) 'Multi-step synthesis of nanoparticles performed on millisecond time scale in a microfluidic droplet-based system', *Lab on a Chip*, 4(4), 316-321.
- Squires, T. M. and Quake, S. R. (2005) 'Microfluidics: Fluid physics at the nanoliter scale', *Reviews of Modern Physics*, 77(3), 977.
- Srinivasan, V., Pamula, V. K. and Fair, R. B. (2004) 'Droplet-based microfluidic lab-on-a-chip for glucose detection', *Analytica Chimica Acta*, 507(1), 145-150.

## Appendix C – Droplet Microfluidics

- Svärd, M., Nordström, F. L., Jasnobulka, T. and Rasmuson, Å. C. (2009) 'Thermodynamics and Nucleation Kinetics of m-Aminobenzoic Acid Polymorphs', *Crystal Growth & Design*, 10(1), 195-204.
- Tabeling, P. (2005) *Introduction to microfluidics*, Oxford University Press.
- Teh, S.-Y., Lin, R., Hung, L.-H. and Lee, A. P. (2008) 'Droplet microfluidics', *Lab on a Chip*, 8(2), 198-220.
- Thati, J., Nordström, F. L. and Rasmuson, Å. C. (2010) 'Solubility of Benzoic Acid in Pure Solvents and Binary Mixtures', *Journal of Chemical & Engineering Data*, 55(11), 5124-5127.
- Thorsen, T., Maerkl, S. J. and Quake, S. R. (2002) 'Microfluidic Large-Scale Integration', *Science*, 298(5593), 580-584.
- Thorsen, T., Roberts, R. W., Arnold, F. H. and Quake, S. R. (2001) 'Dynamic Pattern Formation in a Vesicle-Generating Microfluidic Device', *Physical Review Letters*, 86(18), 4163.
- Utada, A. S., Lorenceau, E., Link, D. R., Kaplan, P. D., Stone, H. A. and Weitz, D. A. (2005) 'Monodisperse Double Emulsions Generated from a Microcapillary Device', *Science*, 308(5721), 537-541.
- van der Woerd, M., Ferree, D. and Pusey, M. (2003) 'The promise of macromolecular crystallization in microfluidic chips', *Journal of Structural Biology*, 142(1), 180-187.
- van Steijn, V., Kleijn, C. R. and Kreutzer, M. T. (2010) 'Predictive model for the size of bubbles and droplets created in microfluidic T-junctions', *Lab on a Chip*, 10(19), 2513-2518.
- Wang, Q., Hou, L., Cheng, Y. and Li, X. (2007) 'Solubilities of Benzoic Acid and Phthalic Acid in Acetic Acid + Water Solvent Mixtures', *Journal of Chemical & Engineering Data*, 52(3), 936-940.
- Whitesides, G. M., Ostuni, E., Takayama, S., Jiang, X. and Ingber, D. E. (2001) 'SOFT LITHOGRAPHY IN BIOLOGY AND BIOCHEMISTRY', *Annual Review of Biomedical Engineering*, 3(1), 335-373.
- Willneff, E. A., Davey, R. J., Richards, C. L., Burton, R. C. and Cilliers, J. J. (2006) 'Development and applications of an inexpensive and modular medium-throughput microcrystalliser for the preparation and characterisation of solid phases', *Journal of Crystal Growth*, 294(1), 29-34.
- Xu, J. H., Li, S. W., Tan, J., Wang, Y. J. and Luo, G. S. (2006a) 'Preparation of highly monodisperse droplet in a T-junction microfluidic device', *AIChE Journal*, 52(9), 3005-3010.
- Xu, J. H., Luo, G. S., Li, S. W. and Chen, G. G. (2006b) 'Shear force induced monodisperse droplet formation in a microfluidic device by controlling wetting properties', *Lab on a Chip*, 6(1), 131-136.
- Yobas, L., Martens, S., Ong, W.-L. and Ranganathan, N. (2006) 'High-performance flow-focusing geometry for spontaneous generation of monodispersed droplets', *Lab on a Chip*, 6(8), 1073-1079.
- Zheng, B., Roach, L. S. and Ismagilov, R. F. (2003) 'Screening of Protein Crystallization Conditions on a Microfluidic Chip Using Nanoliter-Size Droplets', *Journal of the American Chemical Society*, 125(37), 11170-11171.

## Appendix C – Droplet Microfluidics

Zheng, B., Tice, J. D. and Ismagilov, R. F. (2004) 'Formation of Droplets of Alternating Composition in Microfluidic Channels and Applications to Indexing of Concentrations in Droplet-Based Assays', *Analytical Chemistry*, 76(17), 4977-4982.